Author:
Young, Megan E

Title:
Cardiac remodelling following myocardial infarction and the cardioprotective efficacy of adrenergic stimulation against reperfusion injury in healthy and failing hearts

Cardiac remodelling following myocardial infarction and the cardioprotective efficacy of adrenergic stimulation against reperfusion injury in healthy and failing hearts

Megan Young

Supervisors: Professor Massimo Caputo, Professor Saadeh Suleiman and Dr Andrew James

A dissertation submitted to the University of Bristol in accordance with the requirements of the degree of Doctor of Philosophy in the Faculty of Health Sciences, Bristol Medical School

December 2022

Word count: 39,331

Abstract

Introduction:

Following myocardial infarction (MI) a process of adverse cardiac remodelling occurs leading to impaired function and eventually heart failure. Improving understanding of cardiac remodelling progression will aid in identifying targets for therapeutic intervention. Additionally, there is a need to design cardioprotective interventions against ischemia reperfusion (I/R) injury in failing hearts. Strategies targeting the adrenergic receptor (AR) signalling pathways are cardioprotective, whether such interventions are protective in the failing heart or in combination with cardioplegic arrest is not presently known.

Methods:

MI was induced in Wistar rats by occlusion of the left anterior descending coronary artery. Animals were recovered for 3-days, 2-weeks, or 4 weeks. Cardiac function was assessed by echocardiography. Blood and tissue samples were collected for metabolomics, histology, electron microscopy (EM) and proteomics. Cardioprotection against I/R injury was assessed ex-vivo in healthy and failing hearts. Pre-conditioning drugs targeting AR pathways were given prior to I/R, with or without cardioplegic arrest.

Results:

Functional impairment was evident at 3-days, with further deterioration at later time-points. Cardiomyocyte loss alongside increased collagen deposition occurred over-time in the infarct area, with subtle changes in remote areas. EM showed a time-dependent increase in telocytes within the extracellular matrix of the infarcted area. There were extensive cardiac proteome changes during early remodelling which markedly decreased during the later stages. Interestingly, there were changes in cardiac proteome and blood metabolites in response to sham surgery. Targeting the α1A-ARs conferred protection against I/R injury in healthy and failing hearts. Targeting β-ARs pathways provided additional protection to cardioplegic arrest, the underlying mechanism(s) involving modulation of the mitochondrial permeability transition pore.

Conclusion:

This work comprehensively characterised the cardiac remodelling process over-time following MI, providing new insights into disease progression. It has also shown the potential of targeting AR pathways to protect the heart against I/R injury as occurs in cardiac surgery.

Acknowledgements

I would like to acknowledge my supervisors, Professor Caputo, Professor Suleiman and Dr James for their support and encouragement throughout my PhD. I would like to thank Prof Caputo for securing the studentship to support me. Prof Suleiman has given me endless support throughout my time as a student at the University of Bristol. He has always been available to discuss my work and encouraged me to travel to international conferences to share my research. Dr Andrew James for his great help and supervision especially during the difficult periods of Covid to establish our heart failure model.

I would like to thank members of the Caputo and Suleiman research groups who have given me guidance, helped me problem solve and taught me experimental techniques. Particularly Dr Katie Skeffington who helped with the in vivo work, both establishing the LAD occlusion model and teaching me echocardiography. I would also like to acknowledge Dr Svetlana Mastitskaya whom gave us the initial training in LAD occlusion. I would also like to thank the research project students whom I supervised that contributed to some of the work in this thesis, Amy Harris with the control A61603 experiments, Jorge De La Fuente Martinez to the cardioplegia I/R experiments and Joseph Carr to the mitochondrial swelling work.

Thanks to my fellow students on the 4-year BHF programme who have been there to share the ups and downs of PhD research, particularly during the frustrations of Covid. To my friends and family who have always supported me, thanks for giving me a place to escape the world of research. Finally, thanks to Adam for his endless support and encouragement throughout the last 4-years.

Covid-19 impact statement

The Covid-19 pandemic hit during the first year of my PhD project and impacted my ability to complete experimental research throughout the course of my PhD.

This was largely due to the closure/restrictions especially during the onset of the pandemic. The research laboratories and the Animal Services Unit (ASU) were closed completely, preventing any experimental work. My project involves a large amount of animal work, performing surgery on rodents, which cannot be completed when the ASU is closed. The animal unit then remained closed due to refurbishments taking place. When the unit was reopened in the autumn it was a phased return and I was unable to restart any animal work until late November 2020. Furthermore, the financial impact of Covid resulted in the university not being able to commit to funding promised to buy an echocardiography machine until February 2021. The echo machine is essential to assess cardiac function post-MI.

We were able to adapt the project plan to focus on adult hearts only and investigate cardiac remodelling changes over time and to investigate potential cardioprotection strategies against I/R.

Author’s declaration

I declare that the work in this dissertation was carried out in accordance with the requirements of the University's *Regulations and Code of Practice for Research Degree Programmes* and that it has not been submitted for any other academic award. Except where indicated by specific reference in the text, the work is the candidate's own work. Work done in collaboration with, or with the assistance of, others, is indicated as such. Any views expressed in the dissertation are those of the author.

SIGNED:  DATE: 04/01/23

Conference presentations and awards

Poster presentations

- BHF 4-year PhD student conference, April 2019, London, UK
  β-adrenergic stimulation and the cardiac mitochondrial permeability transition pore – Megan Young, Martin Lewis, Saadeh Suleiman
- BSCR Autumn meeting, September 2022, Belfast, UK
  Preconditioning with alpha-1A receptor agonist A61603 is cardioprotective against global ischemia and reperfusion injury in healthy hearts, but not in failing rat hearts – Megan Young, A Harris, K Skeffington, MS Suleiman, M Caputo
- IACS-ES meeting, September 2022, Szeged, Hungary
  The cardioprotective efficacy of drugs targeting adrenergic receptor pathways when added prior to cardioplegic ischaemic arrest – Megan Young, Jorge de La Fuente Martinez, Saadeh Suleiman

Prizes

Poster prize at IACS-ES 2022, Szeged, Hungary – September 2022

Contents

List of figures

List of tables

Abbreviations

8-Br – 8- Bromoadenosine- 3', 5'- cyclic monophosphate

AC – Adenylyl Cyclase

AR – Adrenergic Receptor

ATP – Adenosine Triphosphate

AUC – Area Under the Curve

BCCA – Branched chain amino acid

BPM – Beats Per Minute

cAMP – Cyclic adenosine 3′,5′-monophosphate

CPB – Cardiopulmonary Bypass

CPT – Carnitine-palmitoyl transferase

CsA – Cyclosporin A

DAG – Diacylglycerol

DEP – Differentially Expressed Protein

ECC – Excitation-Contraction Coupling

ECM – Extracellular Matrix

EDTA – Ethylenediaminetetraacetic acid

EDP – End Diastolic Pressure

EM – Electron Microscopy

Epac – Exchange Protein directly activated by cAMP

ERK – Extracellular signal-related kinase

ETC – Electron Transport Chain

EVG – Elastic Verhoeff-Van Gieson

FAD – Flavin Adenine Dinucleotide

FC – Fold Change

GPCR – G-Protein Coupled Receptor

H^+ – Hydrogen

H+E – Haematoxylin and Eosin

HR – Heart Rate

IMM – Inner Mitochondrial Membrane

IP – Intraperitoneal

IP_3 - Inositol Triphosphate

IPA – Ingenuity Pathway Analysis

IPC – Ischemic Preconditioning

I/R – Ischemia Reperfusion

LAD – Left Anterior Descending

LDH – Lactate Dehydrogenase

LTCC – L-Type Calcium Channels

LV – Left Ventricle

LVDP – Left Ventricular Developed Pressure

MI – Myocardial Infarction

MMP – Matrix Metalloproteinase

MPO – Myeloperoxidase

MPTP – Mitochondrial Permeability Transition Pore

Na^+ – Sodium

NAD - Nicotinamide Adenine Dinucleotide

NCX – Sodium Calcium Exchanger

PBS – Phosphate Buffered Saline

PFA – Paraformaldehyde

PKA – Protein Kinase A

PKC – Protein Kinase C

PLC – Phospholipase C

ROS – Reactive Oxygen Species

RPP – Rate Pressure Product

RV – Right Ventricle

RYR – Ryanodine Receptor

SERCA – Sarcoplasmic Reticulum Calcium ATPase

SOD – Superoxide dismutase

SR – Sarcoplasmic Reticulum

TCA – Tricarboxylic acid

TMT – Tandem Mass Tagging

TTC – Triphenyltetrazolium Chloride

1 Introduction

This thesis investigates the functional, structural, metabolic, and molecular changes over time that occur following myocardial infarction (MI). In addition, it looks at cardioprotective strategies, involving adrenergic signalling pathways in the heart, against global ischemia reperfusion (I/R) injury with a focus on their potential to work in failing hearts. This introduction will give an overview of cardiac physiology before discussing the detrimental impact of ischemia on the heart, and the current understanding of the subsequent remodelling process into heart failure. It will also cover the clinical relevance of this work in the context of cardioplegic arrest and cardiopulmonary bypass (CPB) surgery and attempts to design cardioprotective interventions by targeting adrenergic receptor (AR) pathways.

1.1 Cardiac physiology

The heart, (Figure 1-1A), comprised of four chambers, two atria and two ventricles, provides a constant blood supply to the body, delivering oxygen and nutrients to allow for normal physiological function. The heart contracts during systole, expelling blood from the ventricles, and relaxes during diastole allowing passive filling of the ventricles from the atria ready for the next cardiac cycle. The right side of the heart receives deoxygenated blood from the systemic circulation into the right atria, during diastole the blood moves through the tricuspid valve into the right ventricle (RV) and upon systole is ejected into the pulmonary circulation. The left side of the heart deals with oxygenated blood, received from the pulmonary circulation into the left atria, oxygenated blood moves through the mitral valve during diastole into the left ventricle (LV), and is ejected into the systemic circulation during systole. The blood supply to the heart itself is supplied by the coronary arteries. The coronary arteries branch from the aortic root, just above the aortic valve taking oxygenated blood ejected from the LV. There are two coronary branches serving the left and right sides of the heart (Figure 1-1B). To maintain sufficient cardiac output for normal physiological function the hearts must succinctly contract and relax to allow efficient ventricular filling and ejection.

1.1.1 Cardiac structure

The heart is comprised of various cell types, the main type being cardiomyocytes which occupy the largest volume within the heart. Cardiomyocytes are the contractile cells within the heart, located within the muscular layer termed the myocardium. Other cell types in the heart include cardiac fibroblasts, smooth muscle cells and endothelial

cells. Cardiac fibroblasts are the most abundant cell type in the heart, responsible for regulation of the extracellular matrix (ECM) (Bai et al. 2020; Baudino et al. 2006). The ECM surrounds the cellular structures providing a mechanical scaffold, as well as contributing to signal transduction. The ECM is comprised of collagen and glycoproteins as well as containing growth factors and proteases (Baudino et al. 2006; Frangogiannis 2017).

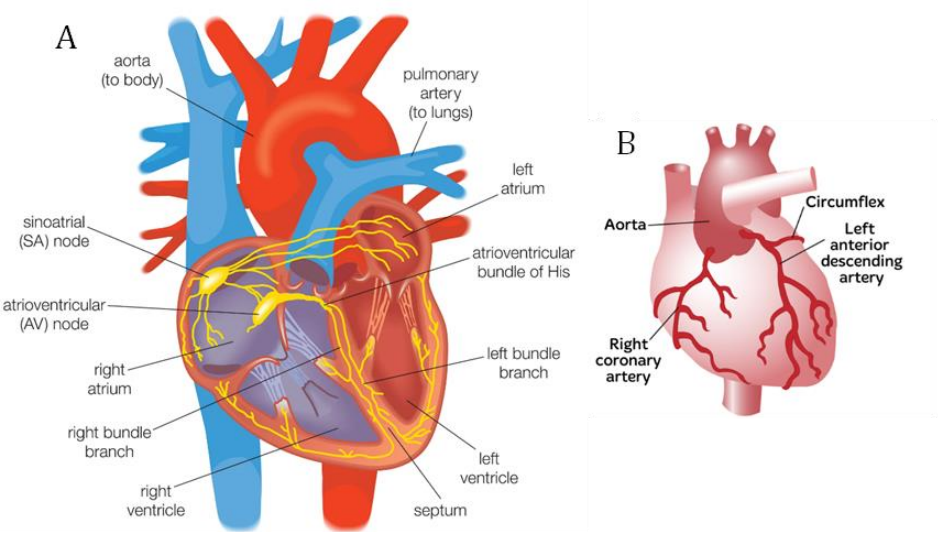

Figure 1-1 Cardiac anatomy

(A) Diagram of the chambers of the heart and electrical conduction system. (B) Coronary arteries diverge from the aortic root into left and right branches. Images from (A) Encyclopaedia Britannica and (B) Heart Foundation NZ.

1.1.2 Cardiac contraction

As mentioned above, cardiomyocytes are the contractile cells within the heart. Cardiomyocytes are striated muscles cells packed with myofibrils containing the contractile units termed sarcomeres which are comprised of actin and myosin filaments as well as the large protein titin (Henderson et al. 2017) (Figure 1-2). To facilitate succinct contraction and relaxation of the heart, neighbouring cardiomyocytes are connected by intercalated disks, containing gap junctions, desmosomes, and adherens (Estigoy et al. 2009). Gap junctions facilitate the transmission of electrical activity between cardiomyocytes through connexon channels comprised of connexin proteins. Desmosomes, and adherens, are involved in transmitting mechanical strength, with interactions to the contractile proteins (Estigoy et al. 2009; Henderson et al. 2017).

To produce contraction and relaxation actin and myosin filaments go through a cross-bridge cycle. Contraction is initiated by binding of calcium to troponin C on actin filaments exposing the site for myosin heads to bind and following a conformational change in the angle of the myosin head the actin filament is drawn into the centre of the sarcomere creating contraction. The myosin head is then released utilising energy provided by adenosine triphosphate (ATP) and the cycle restarts, binding a new actin site creating further contraction (Figure 1-2) (Levick 2010). Relaxation occurs when calcium levels return to a resting level. The contraction relaxation cycle is continuous in the heart and is regulated by calcium release in response to excitation.

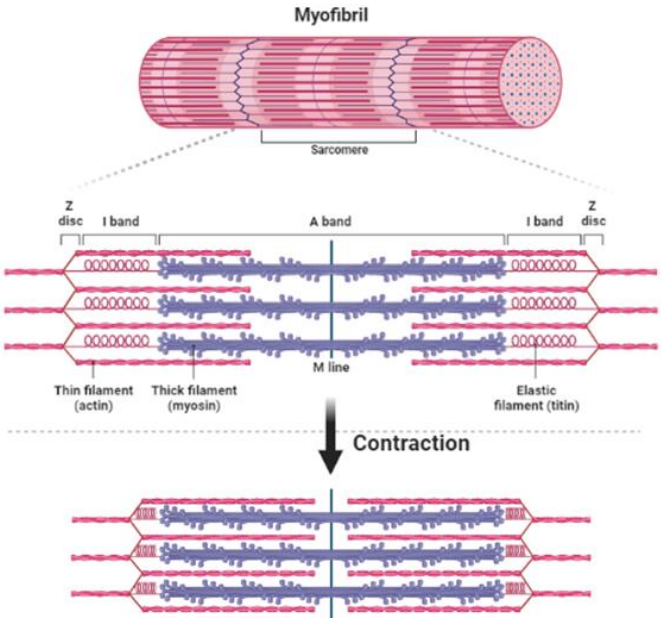

Figure 1-2 Cardiomyocyte contraction

Myofibrils are comprised of sarcomeres which contain the contractile proteins actin and myosin. During contraction myosin filaments bind actin and pull them towards the centre of the sarcomere. Image created on BioRender.

1.1.3 Cardiac excitation-contraction coupling

The regulation of calcium release in cardiomyocytes is linked to the electrical excitation of the cell by an action potential in a process called excitation-contraction coupling (ECC). Rapid depolarisation during the initial phase of a cardiac action potential activates L-type voltage-gated calcium channels (LTCC) facilitating an inward calcium current. The rise in intracellular calcium activates a further rise in calcium

through activating the opening of ryanodine receptors (RyR) releasing calcium from the sarcoplasmic reticulum (SR), termed calcium-induced calcium release. It is the large calcium release from the SR which provides the calcium needed to bind troponin C on actin filament and initiate contraction (Figure 1-3). To allow relaxation, the calcium is removed from the sarcoplasm mainly through re-uptake into the SR by the SR calcium ATPase (SERCA) but also by release from the cell through calcium ATPase or sodium calcium exchangers on the sarcolemma, in addition to uptake by the mitochondria through the mitochondrial calcium uniport (Figure 1-3) (Bers 2002; Njegic et al. 2020).

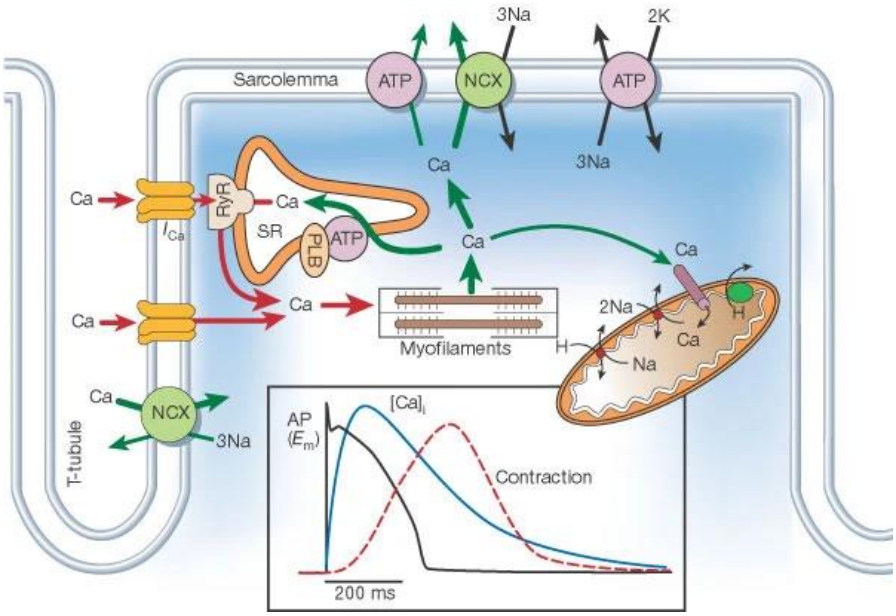

Figure 1-3 Cardiac excitation contraction coupling

Calcium influx (I_{Ca}) into the cell via the L-type calcium channels is triggered by the depolarisation phase of the cardiac action potential. The increase in calcium triggers a larger release of calcium from the sarcoplasmic reticulum (SR), calcium binds to actin filament facilitating contraction. Calcium is removed to allow relaxation through reuptake into the SR via the SR ATPase or removed from the cytosol out of the cell or into mitochondria. Image taken from (Bers 2002)

1.1.4 Cardiac innervation

The action potentials initiating cardiac contraction are fired from pacemaker cells in the sinoatrial node. Action potentials are conducted across myocytes in the atria to the atrioventricular node, where the electrical impulse is delayed allowing atrial contraction. The impulse is then conducted through the bundle of His and Purkinje fibres into the ventricular myocytes initiating ventricular contraction (Figure 1-1A).

Although pacemaker cells can spontaneously generate action potentials, they are also under extrinsic control by the autonomic nervous system allow regulation of firing frequency. Parasympathetic stimulation decreases, whereas sympathetic activity increases activity in pacemaker cells. Sympathetic nerves also innervate cardiomyocytes across the heart and can therefore regulate cardiac contractility as well as heart rate.

Sympathetic stimulation increases the levels of catecholamines, noradrenaline and adrenaline, which bind to the adrenergic receptors (ARs). There are five types of cardiac ARs present within the heart: β1, β2, β3, α1A and α1B (Myagmar et al. 2017). ARs are G-protein coupled receptors (GPCR), G-proteins are trimeric proteins comprised of α, β and γ subunits distinguished into 4 families (G_i, G_s, G_q and $G_{12/13}$) based on the α subunit. Activation of an AR triggers the dissociation of the α subunit from βγ subunits by exchange of GDP for GTP, with the α subunit then able to interact with the associated effector proteins (Kamato et al. 2015; McCudden et al. 2005).

1.1.4.1 Beta-adrenergic receptors

The β-ARs are the predominant receptors found on cardiomyocytes, with β1-ARs found to be present on all cardiomyocytes (Myagmar et al. 2017). The β2 subtype is thought to be present at low levels in cardiomyocytes, although predominantly located on other cell types within the heart as is the β3 subtype (Myagmar et al. 2017). β1- and β2-ARs are coupled to the stimulatory G-protein (G_s), activation of the receptor triggers the dissociation of the $G\alpha_s$ subunit which then activates a membrane-bound enzyme adenylyl cyclase (AC). AC catalyses the conversion of ATP into cyclic adenosine monophosphate (cAMP), which in turn activates protein kinase A (PKA). PKA phosphorylates various effector molecules, including LTCC, phospholamban, RyRs and contractile proteins, which can modulate cardiac function by altering calcium handling (de Lucia et al. 2018) (Figure 1-4A). β2-ARs are also coupled to the inhibitory G-protein (G_i), and therefore are capable of exerting opposing effects on contractile function (Mahmood et al. 2022).

1.1.4.2 Alpha-adrenergic receptors

Two subtypes of α1-ARs are reportedly present within cardiac myocyte, the α1B subtype is present in all myocytes whereas the α1A has been found to be present on 60% of myocytes (Myagmar et al. 2017). The α1-ARs are coupled to the $G_{q/11}$ family of

G-proteins, upon receptor binding the $G\alpha_{q/11}$ subunit activates phospholipase C (PLC) located at the cell membrane. PLC facilitates the cleavage of phosphatidylinositol 4,5-diphosphate (PIP2) into two second messengers, inositol triphosphate (IP_3) and diacylglycerol (DAG). IP_3 mediates an increase in intracellular calcium by opening of the IP_3 receptor located on the SR allowing greater calcium release, whilst DAG activates protein kinase C (PKC) (Kamato et al. 2015). PKC can phosphorylate calcium regulating proteins including CaMKII and LTCC, which in turn increases the intracellular calcium levels (J et al. 2008) (Figure 1-4B).

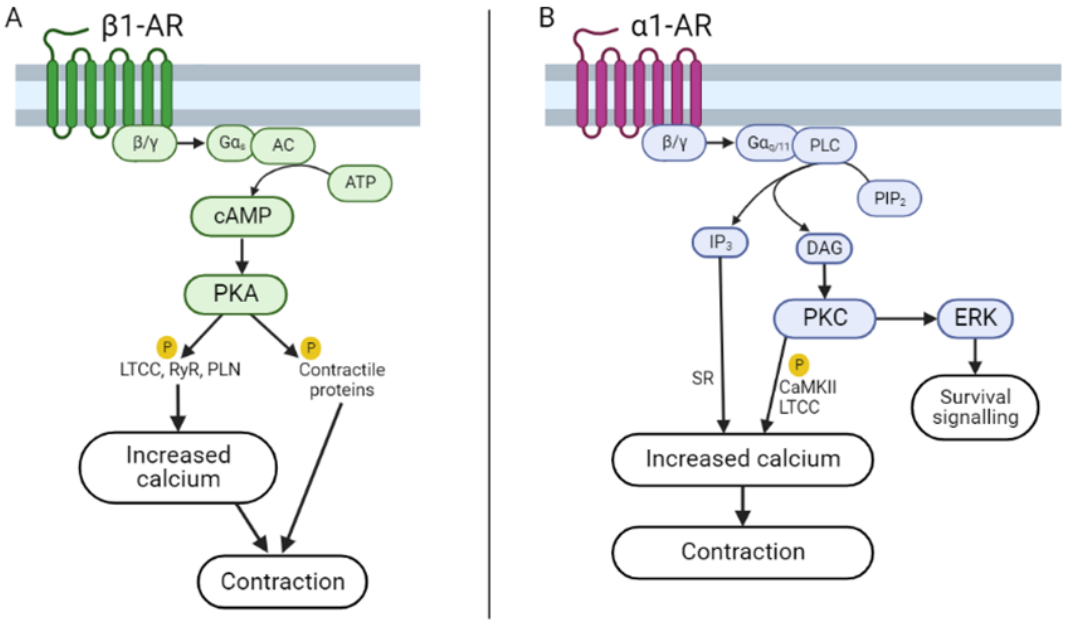

Figure 1-4 Adrenergic receptor signalling pathway in cardiomyocytes

(A) β1-adrenergic signalling – Activation of adenylyl cyclase (AC) facilitates conversion of ATP to cAMP, subsequently activating protein kinase A (PKA) which phosphorylates various effector proteins including calcium handling and contractile proteins. (B) α1-AR signalling pathway through – Phospholipase C (PLC) is activated and produces inositol triphosphate (IP_3) and diacylglycerol (DAG) from phosphatidylinositol 4,5-diphosphate (PIP_2). Intracellular calcium levels are raised facilitating an increase in contraction. Activation of α1-AR can also activate ERK signalling. Image created on BioRender.

1.1.5 Cardiac metabolism

To support continuous contraction the energy demand in the heart is high, cycling around 6kg of ATP every day (Neubauer 2007). However, the store of ATP in the heart is relatively low therefore continuous ATP generation is required and cardiomyocytes are abundant in mitochondria to facilitate this. ATP is primarily generated (>95%) through oxidative phosphorylation in the mitochondria under normal conditions. Glycolysis and the tricarboxylic acid (TCA) cycle also play a role in energy production, however in the healthy heart this contribution is relatively small. The heart can utilise various substrates for the product of energy, primarily through the β-oxidation of fatty acids, but also glucose, lactate, ketone bodies and some amino acids (Lopaschuk et al. 2010; Zuurbier et al. 2020). The final product of substrate breakdown is acetyl-CoA which goes on to enter the TCA cycle, producing the reducing equivalents nicotinamide adenine dinucleotide (NADH) and flavin adenine dinucleotide ($FADH_2$) which then go on to enter the electron transport chain (ETC) producing ATP by oxidative phosphorylation (Figure 1-5) (Zuurbier et al. 2020).

1.1.5.1 Oxidative phosphorylation and the electron transport chain

The ETC, located within the inner mitochondrial membrane (IMM), is the site of oxidative phosphorylation. The ETC is comprised of five complexes, four electron donors/acceptors (complexes I, II, III and IV) and the F1/F0 ATP synthase (complex V). The transfer of electrons between the complexes I-IV creates energy which enables the transport of protons across the IMM into the inner membrane space. The transfer of electrons between complexes is facilitated by cytochrome c and ubiquinone. The electrochemical gradient generated by proton movement is then utilised by the F1/F0 ATP synthase to generate ATP (Figure 1-5). NADH and $FADH_2$ produced via the TCA cycle donate electrons to complex I and II respectively.

1.1.5.2 Substrate utilisation

1.1.5.2.1 Fatty acids

Fatty acids are the primary substrate utilised to produce energy in the heart, accounting for round 50-70% of ATP generated. Fatty acids enter the cell by diffusion or via fatty acid transporters. Once inside the cell, fatty acyl CoA synthetase converts the fatty acids into long-chain acyl CoAs. To allow the long chain acyl CoA to pass into the mitochondrial matrix it is temporarily converted to acyl-carnitine by carnitine-

palmitoyl transferase I (CPT-I) and converted back to acyl CoA inside the mitochondrial matrix by CPT-II. Acyl-CoA then undergoes β-oxidation producing acetyl-CoA as well as NADH and $FADH_2$ (Figure 1-5) (Lopaschuk et al. 2010).

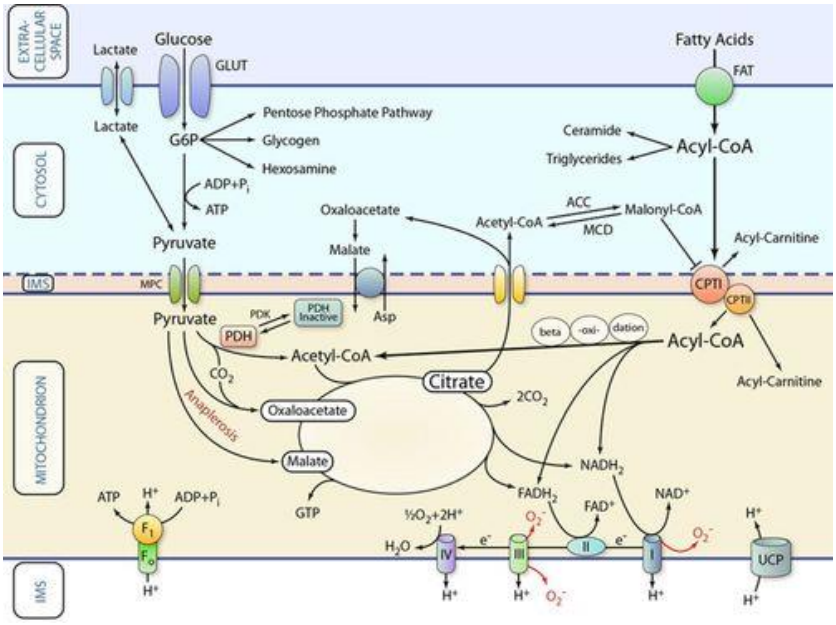

Figure 1-5 Cardiac metabolism

Production of ATP in the mitochondria through the TCA cycle and electron transport chain. Acetyl-CoA, the end-product of glycolysis or fatty acid β-oxidation, enters the TCA cycle. The reducing equivalents NADH and FADH are produced and go on to donate electrons to the complexes of the electron transport chain, providing the energy to set up a proton gradient which the F1/F0 ATP synthase utilises to produce ATP. Figure from (Doenst et al. 2013).

1.1.5.2.2 Glucose

Glucose is a secondary substrate for cardiac metabolism, either up taken into the cell by glucose transporters or derived from glycogen stores. Glucose is broken down by glycolysis, the initial step is phosphorylation by hexokinase to glucose-6-phosphate in a reaction requiring ATP. Hexokinase is inhibited by an increase in glucose-6-phosphate and therefore influences the rate of this reaction. Glucose-6-phosphate then undergoes several steps of glycolysis ultimately producing pyruvate, NADH and two ATP molecules (Figure 1-6). Pyruvate can then enter several pathways (Figure 1-5). Under aerobic conditions pyruvate is transported into the mitochondria by the mitochondrial pyruvate carrier and converted by the pyruvate dehydrogenase complex to acetyl-CoA, which can then enter the TCA cycle. In the absence of aerobic conditions anaerobic glycolysis

occurs, pyruvate is reduced to lactate, by lactate dehydrogenase producing ATP. The other fate of pyruvate is the carboxylation to oxaloacetate or malate, which contributes to replenishment of the pool of intermediates in the TCA cycle in a process called anaplerosis.

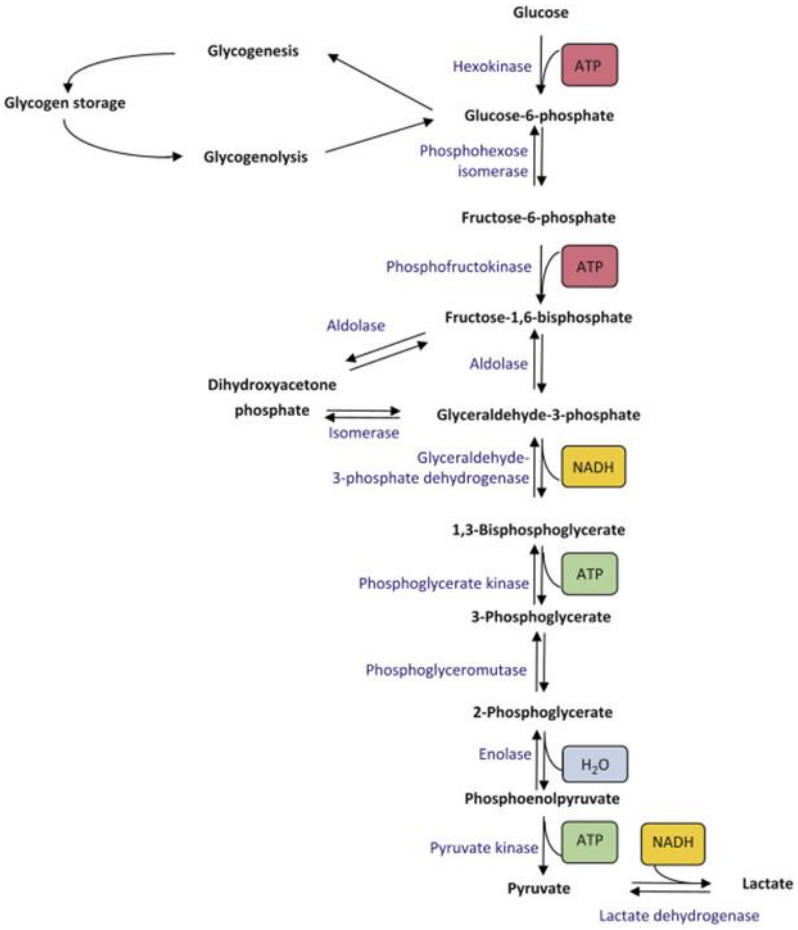

Figure 1-6 Glycolysis pathway

The steps involved in glycolysis to produce pyruvate from glucose-6-phosphate, derived from glucose or glycogen stores. Under aerobic conditions pyruvate would then enter the mitochondria, in anaerobic conditions pyruvate is converted to lactate producing ATP. Figure from (Werner et al. 2016)

1.2 Pathophysiology of ischemic injury

Disruption to normal cardiac physiological function occurs in pathological conditions. Ischemia in the heart occurs because of reduced blood supply, depriving the tissue of its supply of oxygen and nutrients. Ischemia can affect a regional area of the heart when caused by a blockage in a coronary artery, as is the case during myocardial infarction (MI) or affect the whole heart during global ischemia as is the case during

cardiopulmonary bypass surgery (CPB). Furthermore, the reperfusion of an ischemic area can exacerbate injury which will be discussed below. Ischemia, and subsequent reperfusion, disrupts the metabolic and ionic homeostasis in the cells which leads to irreversible cell damage.

1.2.1 Metabolic and ionic changes during ischemia

As oxygen delivery is ceased during ischemia, energy production in the heart switches from oxidative phosphorylation to anaerobic glycolysis, triggering metabolic changes within the heart. With no supply of glucose, glycogen is the primary substrate for anaerobic glycolysis, and as discussed above, lactate is produced as a by-product (Jennings and Reimer 1991). The production of lactate causes cellular pH levels to fall, consequently inhibiting glycolysis further reducing ATP levels. Levels of creatine phosphate fall, and intracellular phosphate (P_i) levels are increased (Suleiman et al. 2001). The lack of ATP during ischemia is a trigger for the development of ischemic contracture, a state of hyper-contraction in the heart as cross-bridge cycles formed cannot be released due to lack of ATP resulting in rigor complexes (Cross et al. 1996; M. Li et al. 2023).

Accumulated intracellular H^+, due to the drop in pH, will trigger the removal of H^+ from the cell in exchange for sodium (Na^+) via the Na^+/H^+ exchanger. $Na^=$ accumulates in the cell, triggering the sodium calcium exchanger (NCX) to reverse removing Na^+ from the cell. NCX reversal brings calcium into the cell and intracellular calcium will continue to rise during ischemia (Figure 1-7). Increased intracellular calcium levels are normally regulated by NCX and calcium ATPases on the cell membrane and SR however they are inhibited due to lack of ATP (Suleiman et al. 2001). One way for calcium to be removed from the cytosol is through the mitochondrial calcium uniporter, therefore increasing mitochondrial calcium (Figure 1-7).

Uncontrolled increases in cytosolic calcium precedes irreversible myocardial injury (Murphy and Steenbergen 2008a). During a prolonged period of ischemia, the increase in intracellular calcium will lead to cellular death (Figure 1-8). Increased calcium levels can activate degradative enzymes including phospholipases and proteases which can cause irreversible cell damage, disrupting cellular structures and triggering necrosis and apoptosis (Sanada et al. 2011; Suleiman et al. 2001).

1.3 The effect of reperfusion

The return of oxygen and nutrients, provided by restoration of blood flow, to an ischemic tissue is termed reperfusion. After a relatively short period of ischemia, reperfusion may be able to rescue ischemic tissue. However, after a prolonged period of ischemia the metabolic and ionic changes that have taken place predispose the heart to further injury upon reperfusion (Figure 1-8).

The reintroduction of blood supply facilitates the rapid removal of lactate build up from the extracellular space, re-establishing the gradient for outward movement of H^+ from the cell to restore intracellular pH. H^+ is removed via the Na^+/H^+ exchanger, the resultant Na^+ influx further increases intracellular Na^+ levels. The accumulated Na^+ is removed in exchanged for Ca^{2+} via reverse mode action of the NCX (Murphy and Steenbergen 2008b) (Figure 1-7). Therefore, intracellular calcium levels further rise upon reperfusion, as mentioned above this can lead to activation of degradative enzymes which can compromise the cells integrity.

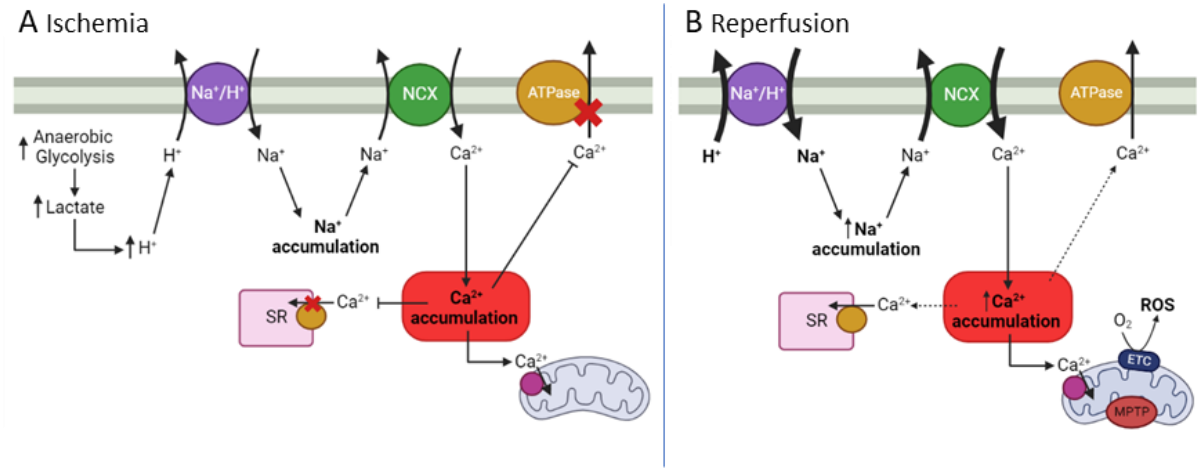

Figure 1-7 Ionic changes during ischemia and reperfusion

During ischemia (A) the increase in H^+ triggers ionic changes leading to accumulation of Na^+ and subsequently Ca^{2+}. Upon reperfusion (B) Na^+ and Ca^{2+} accumulate further and reactive oxygen species (ROS) are generated facilitating opening of the mitochondrial permeability transition pore (MPTP). NCX – Sodium-calcium exchanger, SR – Sarcoplasmic reticulum. Image created on BioRender.

In addition to the increase in calcium loading, another detrimental factor associated with reperfusion is a burst of ROS as oxygen is rapidly reintroduced to the cell (Figure 1-7). Mitochondria damaged from ischemia are unable to efficiently transfer electrons due to damage to the ETC, generating ROS at complex I and III. Together, increased calcium levels and ROS are two of the main drivers of mitochondrial transition pore (MPTP) opening upon reperfusion, a key mediator of cellular death during I/R injury (Murphy and Steenbergen 2008a).

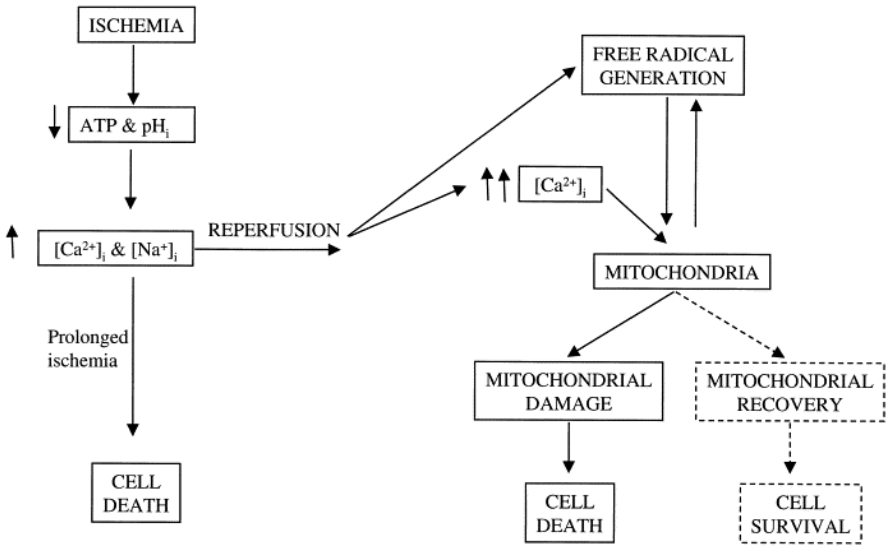

Figure 1-8 Ischemia with or without reperfusion can lead to cell death

Extended periods of ischemia can lead to cellular death due to increased intracellular calcium. Reperfusion causes a further increase in calcium and production of free radicals which can also induce cell death through mitochondrial damage. Mitochondria may be salvaged on reperfusion if the ischemic period is short. Image taken from (Suleiman et al. 2001).

1.3.1 Mitochondrial permeability transition pore

The MPTP is a non-specific pore located on the IMM which is triggered to open by high levels of calcium in the mitochondrial matrix. The sensitivity of the MPTP to calcium is enhanced by the presence of ROS, increased phosphate levels, and reduced adenine nucleotides, all conditions present during I/R (Baines 2009; Halestrap 2009). However opening of the MPTP is thought to only occur at the onset of reperfusion, not

during ischemia, as the lactic acid accumulation produces acidic conditions that prevent MPTP opening (Griffiths and Halestrap 1995).

Opening of the MPTP allows molecules under 1.5kDa to pass through, this movement of molecules creates a colloid osmotic pressure across the IMM as proteins are unable to pass through. The pressure leads to swelling of the mitochondria and eventually rupture. Rupture releases enzymes from the mitochondria, such as cytochrome c, that can then trigger cellular death by apoptosis and necrosis (Halestrap and Richardson 2015; Ong et al. 2015). If the extend of mitochondrial pore opening can be limited or reversed early in reperfusion, then the damaging effects can be stopped. The ability to inhibit the MPTP has provided key information in the involvement of MPTP in I/R injury. Cyclosporin A (CsA) can inhibit MPTP opening and has been used to show that blocking the MPTP is protective against I/R injury in rat hearts (Crompton et al. 1988; Griffiths and Halestrap 1993; Hausenloy et al. 2012).

1.4 Ischemic myocardial injury

Ischemic injury in the heart is detrimental as cardiomyocytes are terminally differentiated and unable to regenerate and repair. During a myocardial infarction (MI) an area of the heart is rendered ischemic due a blockage in a coronary artery. Incidence of MI is very prevalent across the world, with around 100,000 hospital admissions in the UK each year due to MI (BHF 2022). The survival rate following MI is increasing, around 1.4 million people alive in the UK are thought to have suffered an MI (BHF 2022). Survival rates have increased since the introduction of percutaneous coronary intervention to facilitate early reperfusion of the infarcted area (Cahill and Kharbanda 2017). However, reperfusion of an infarcted area can be associated with further injury (Figure 1-8). Nevertheless, MI is the leading cause of heart failure worldwide (Jenca et al. 2021). Following MI, as lost cardiomyocytes cannot be regenerated a complex process of cardiac remodelling occurs to maintain the integrity of the LV wall. Over time this impacts cardiac function and can lead eventually to heart failure. Heart failure reduces patients' quality of life and is a major burden on health services with no definitive cure.

1.5 Cardiac remodelling after cardiac injury

Cardiac remodelling following MI is a complex process involving cellular and molecular changes which manifest as changes in LV structure as well as function (Cohn et al. 2000; Prabhu and Frangogiannis 2016). Prolonged periods of ischemia, or ischemia followed by reperfusion, leads to intracellular changes that result in energy depletion and calcium loading which impact the mitochondria, and trigger cellular death by necrosis or apoptosis (discussed above). As the adult heart is terminally differentiated the loss of cardiomyocytes is critical and extensive remodelling follows to stabilise the myocardial wall.

Cardiac remodelling is arbitrarily divided into two stages, early and late-stage remodelling. The early stage is associated with an inflammatory response and infarct expansion, with the latter stage associated with deposition of extracellular matrix (ECM) components creating scar tissue to stabilise the LV wall (Figure 1-9) (Fraccarollo et al. 2012; Richardson et al. 2015; Sutton and Sharpe 2000).

Initially there is an inflammatory phase triggered by necrotic cardiomyocytes that have died because of injury. Inflammatory cells, including neutrophils and macrophages, infiltrate the damaged area (Burchfield et al. 2013; Fraccarollo et al. 2012). Matrix metalloproteinases are activated and degrade ECM material and recruited macrophages phagocytose the cellular debris. To maintain structural support in the myocardial wall granulation tissue is formed of ECM components such as fibrin, fibronectin and glycosaminoglycans (Richardson et al. 2015). Cytokines, growth factors and hormones upregulated by the inflammatory cells present begin to recruit and activate fibroblasts.

As the inflammatory phase becomes supressed, the reparative phase can begin where fibroblasts deposit ECM components in the damaged areas of the myocardium. Fibroblasts migrate to the injured area and proliferate, but they can also be differentiated from a diverse range of cell types including pericytes, smooth muscle cells, endothelial cells, and mesenchymal stem cells although the relative contribution of these is not clear (Alex and Frangogiannis 2018; Richardson et al. 2015). Fibroblast differentiation into myofibroblasts results in a more contractile phenotype and ability to deposit ECM proteins, including collagen. MMP activity decreases as collagen deposition increases, creating a net deposition of collagen forming the basis of scar

formation in the injured area. Collagen deposition in the infarcted area, termed reparative fibrosis, leads to scar formation and is crucial to maintaining structural integrity of the heart (Fraccarollo et al. 2012). The scar tissue undergoes maturation and collagen fibres cross-link creating tensile strength in the myocardial wall, helping to prevent rupture and further dilation (Burchfield et al. 2013).

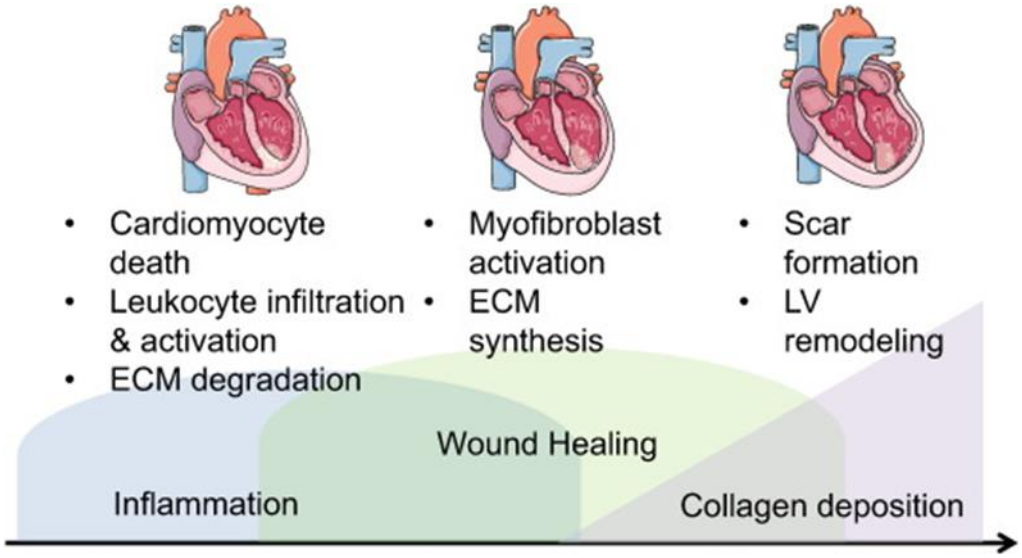

Figure 1-9 Cardiac remodelling over time

The progression of cardiac remodelling over time involves early and late-stage changes. Figure from (Nielsen et al. 2019).

1.5.1 Cardiac remodelling into heart failure

Cardiac remodelling is necessary to stabilise the myocardial wall following MI but ultimately these changes detrimentally affect cardiac function leading to heart failure and greater susceptibility to cardiac arrythmias. Deposition of scar tissue increases wall stiffness and can disrupt electrical conduction. Increased wall stress can cause myocyte hypertrophy in the border zones, alongside wall thinning and chamber dilation this can lead to increased end diastolic and end systolic volumes and reduced ejection fraction (EF) (Cohn et al. 2000). In humans, LV EF has been shown to recover in some patients at 6-8 weeks post-myocardial infarction (MI), but many patients do not have a strong recovery with EF staying below 50%. In addition, reduced EF is a key determinate of outcome following an MI (Chew et al. 2018).

1.5.2 Downregulation of cardiac β-adrenergic receptors

As cardiac function declines, firing of the sympathetic nervous system increases to stimulate an increase in cardiac contractility to improve cardiac function. Acutely this is beneficial but sustained elevation of sympathetic drive is detrimental to the heart and involved in disease progression into heart failure (Lohse et al. 2003; Mahmood et al. 2022). Sustained sympathetic drive, increasing the level of circulating catecholamines, leads to down-regulation of the β-ARs, which involves desensitisation as well as reduced receptor number (Bristow et al. 1986; Fowler et al. 1986). β-AR signalling is involved in the regulation of ECC, activating PKA which phosphorylates various calcium handling proteins. Chronic stimulation can lead to hyperphosphorylation of the RyRs and cause SR calcium leak, further leading to a decline in cardiac function and potentiating arrythmias (Andersson and Marks 2010; Dridi et al. 2020). Reduced efficiency of β-AR signalling will disrupt signalling and regulation of contractility, diminishing the inotropic reserve. Given this, β-AR are targeted by β-blockers in the treatment of heart failure (de Lucia et al. 2018).

Whilst the β-ARs become downregulated in failing hearts, the cardiac α1-ARs are not affected in the same way, there is reportedly no decline in receptor number or function (Janssen et al. 2018; Jensen et al. 2014).

1.5.3 Metabolism changes

The heart consumes large amounts of energy to maintain normal cardiac function, to do so it utilises various substrates as discussed above (1.1.5). However, during heart failure there are changes in metabolism resulting in a decline in energy production, with the failing heart being referred to as an engine out of fuel (Neubauer 2007). Various factors contribute to the decline in metabolism, including alterations in substrate utilisation with a reduced contribution of fatty acids, and reduced capability for oxidative phosphorylation partly due to mitochondrial damage (Lopaschuk et al. 2021; Neubauer 2007). Altered metabolism leads to energy deficiency which contributes to the progression of heart failure.

1.5.4 Understanding the progression of the cardiac remodelling process

Given the deleterious effects that results from ischemic injury and triggering of the cardiac remodelling process, it is critical to understand the disease progression. Despite current extensive research, there has been no break thorough treatment to

improve outcomes following MI, limiting the progression in heart failure. Therefore, it is important to fully understand the progression of cardiac remodelling and identify targets or biomarkers of cardiac impairment to help design therapeutic interventions. The use of omics studies, such as proteomics and metabolomics, allows investigation further into the molecular changes and can uncover pathways involved in disease progression. The utilisation of these, alongside structural and functional changes, will allow for an integrated look at how cardiac remodelling progresses over time.

1.6 Cardioprotection against ischemia reperfusion injury

Unlike MI, which is an unexpected ischemic event, placing a patient onto CPB during cardiac surgery is a planned procedure allowing for protective strategies to be put in place prior to and during the ischemic period, as well as upon reperfusion. Cardioplegia (discussed below) is routinely used during CPB to minimise the extent of I/R injury within the heart. Whilst current cardioplegic strategies are effective at protecting the heart, exploring strategies that can further improve outcomes is important, particularly for high-risk complex patients. Patients undergoing CPB are likely to have presence of cardiac disease pathology and co-morbidities, the presence of pathology may affect the response to I/R injury and protective mechanisms (Suleiman et al. 2011).

1.7 Cardioplegia

Cardioplegic solution is a high K^+ solution which depolarises the membrane, moving the resting membrane potential more positive to a point where sodium channels are inactivated and therefore an action potential cannot be initiated. This means the heart will rapidly arrest in diastole (Chambers and Fallouh 2010). Rapid arrest of the heart preserves energy substrates during ischemia, and the level of ATP is thought to be closely linked to recovery of the heart upon reperfusion (Hearse et al. 1974; Suleiman et al. 2011). This effect can be observed as a delay in ischemic contracture which occurs when ATP is depleted, or production of ATP has declined (Cross et al. 1996; Hearse et al. 1977; Steenbergen et al. 1990). Both of which are delayed by the preservation of substrates due to rapid cardioplegic arrest. The development of the cardioplegic solution widely used today, St Thomas' solution, involved several iterations of cardioplegic solutions being proposed before cardioplegia was widely introduced into clinical practice (reviewed by (Dobson et al. 2013)). The use

of cardioplegia does minimise injury and extend the length of the ischemic period a heart can withstand, but protection against I/R injury could still be improved further.

1.8 Pre-conditioning

Pre-conditioning is a cardioprotective strategy in which the heart receives a stimulus prior to ischemia, that confers protection to the heart during I/R, reducing injury and improving recovery. These interventions include innate cardiac ability such as ischemic preconditioning (IPC) where the heart is exposed to brief ischemic periods prior to an extended ischemic period (Murry et al. 1986). The protective effect of IPC has been shown to be mediated by PKC and involve reduced MPTP opening (Clarke et al. 2008; Javadov et al. 2003; Khaliulin et al. 2007). It has been shown that the effects of IPC can be mimicked by preconditioning with drugs that target survival signalling pathways, including β-adrenergic receptors and cAMP signalling pathways (Asimakis et al. 1994; Lochner et al. 1999).

1.8.1 β-adrenergic pre-conditioning

Stimulating β-ARs as a pre-conditioning strategy prior to ischemia is protective against I/R injury (Khaliulin et al. 2010; Nasa et al. 1997; Tong et al. 2005). Stimulation of β-ARs, as discussed above (Figure 1-4), activates cAMP and subsequently PKA, which then evokes an inotropic response in the heart. The protective mechanism behind PKA has been suggested to involve modulation of calcium activated protease activity (Inserte et al. 2004). Additionally, a decrease in glycogen content in response to the inotropic effect of β-AR stimulation has been proposed as a mechanism for protection. With less substrate availability during ischemia anaerobic glycolysis will be reduced, subsequently the ionic changes leading to calcium loading during ischemia will be reduced (Asimakis et al. 1994; Cross et al. 1996; Khaliulin et al. 2010). The consequence of calcium loading is opening of the MPTP upon reperfusion, stimulation of β-ARs by isoprenaline prior to ischemia has been shown to reduced MPTP opening (Khaliulin et al. 2010; M. J. Lewis et al. 2022). A reduction in glycogen content can be linked to the MPTP by modulation of hexokinase II binding to mitochondria, increased binding of hexokinase is correlated to reduced infarct size upon reperfusion (Halestrap et al. 2015). Furthermore, PKA may activate PKC through increased ROS production and calcium accumulation with isoprenaline treatment increasing PKC within the heart (Khaliulin et al. 2010). PKC signalling has been shown to be an important pathway in

cardioprotection, it has been implicated in the protection afforded by IPC (K. Matsumura et al. 2000) and consecutive activation of PKA and PKC provides stronger protection than PKA alone (Khaliulin et al. 2010; M. Lewis et al. 2018).

1.8.2 cAMP permeable analogues

cAMP is the main secondary messenger in the β-AR signalling pathway where it is classically thought to primarily activate PKA (Figure 1-4A). However, in addition to PKA signalling, cAMP can also activate a PKA-independent pathway involving the alternative target of Epac (exchange protein directly activated by cAMP) (Bers 2007; de Rooij et al. 1998; Lezoualc'h et al. 2016). cAMP analogues can be used to target either the cAMP/PKA pathway or cAMP/Epac pathway individually or in combination. This has allowed investigation of the contribution of each pathway to cardioprotection. Stimulation of each pathway is cardioprotective but optimal protection against I/R injury is achieved when both pathways are activated using cAMP analogue 8-Bromoadenosine- 3', 5'- cyclic monophosphate (8-Br) (Khaliulin et al. 2017; M. J. Lewis et al. 2022). The cardioprotective effect of 8-Br involves activation of PKC (Khaliulin et al. 2017), Epac can activate PLC, which through production of DAG and IP3 produces PKC (Cazorla et al. 2009; Oestreich et al. 2007).

The mechanism of protection by 8-Br involves reduced opening of the MPTP. The addition of 8-Br to the non-ischemic hearts was associated with reduced MPTP opening in response to calcium and increased hexokinase II binding to mitochondria (Khaliulin et al. 2021). The reduced opening of the MPTP has also been measured post-ischemia in hearts pre-treated with 8-Br (M. J. Lewis et al. 2022).

1.8.3 Targeting alpha-1A receptor signalling pathways

The α1A-ARs are present on 60% of cardiomyocytes and as mentioned above stimulation of the receptors induces an inotropic response, this has been shown following A61603 treatment in isolated mouse ventricular myocytes and human cardiac tissue (Janssen et al. 2018; Myagmar et al. 2017). Targeting α1-ARs, specifically the α1A subtype, has shown cardioprotective benefit in cardiac disease models including improved cardiac remodelling post-infarction with α1A-AR overexpression (Du et al. 2006; Montgomery et al. 2017; X. Zhao et al. 2015). Furthermore, the α1A-AR have been implicated in the protection by ischemic pre-conditioning (Perez 2021; Rorabaugh et al. 2005).

α1A-ARs signal through the Gq pathway, involving PKC, which mediates the contractile response and activation of the downstream targets such as extracellular signal-related kinase (ERK) signalling (Myagmar et al. 2019). Activation of ERK survival signalling pathways is a downstream target of α1A-AR stimulation and has been attributed to the cardioprotective effects observed (Huang et al. 2007). ERK signalling has been shown to protect against ischemic injury and activated as part of successful pre-conditioning (Lips et al. 2004). Additionally, PKC is known to be involved in mediating protective effects of cardioprotective strategies (discussed above).

Largely previous experiments investigating the protection afforded by α1A-AR involved transgenic models. The α1A-AR can be specifically targeted using the selective agonist A61603 (Knepper et al. 1995), which has enabled the investigation of this receptors signalling pathways/mechanism and protective effect. Selective stimulation of α1A-ARs by A61603 prior to ischemia has not been investigated previously, it may be a promising pre-conditioning strategy.

1.9 Hypothesis and Objectives

1.9.1 Original PhD hypothesis

The following is the original hypothesis that has been changed as a result of Covid-19 related interruptions:

"Cardiac remodelling following acute infarction is age dependent, and remodelled immature hearts show increased vulnerability to ischemic cardioplegic arrest and reperfusion".

1.9.2 Updated PhD hypotheses

1. Cardiac remodelling, involving structural, functional, and molecular changes, following acute infarction is time-dependent, and remodelled hearts have increased susceptibility to ischemia reperfusion injury.
2. Cardiac adrenergic stimulation and cAMP analogues confer cardioprotection against cardioplegic ischemic arrest and reperfusion

To address these hypotheses, the following objectives have been addressed:

- Objective 1 – Investigate cardiac remodelling in adult rat hearts at different time points following acute ischaemic infarction.
  Expected outcome: Cardiac remodelling following acute ischaemic infarction will differ across time. Potential therapeutic targets or biomarkers of cardiac remodelling will be identified.
- Objective 2 – Investigate whether post-injury remodelled adult rat hearts are more vulnerable to ischemic arrest and reperfusion injury.
  Expected outcome: Remodelled hearts that were previously subjected to an acute insult will sustain more injury compared to control hearts not subjected to a previous insult.
- Objective 3 – Investigate cardioprotective strategies during cardioplegic ischemic arrest and reperfusion by targeting adrenergic receptors, with the potential to test in remodelled hearts.
  Expected outcome: Efficacy of cardioprotective interventions may differ in remodelled hearts.

2 Materials and Methods

2.1 Materials

Listed below are the materials used throughout this thesis and where they were purchased:

Bayer
Baytril

Biolog Life Science Institute
8- Bromoadenosine- 3', 5'- cyclic monophosphate, acetoxymethyl ester

Bio-Rad
Quick Start™ Bradford reagent

Bio-Techne
A61603 hydrobromide

Cambridge Bioscience
Antimycin A

Ceva Animal Health Ltd
Vetergesic® - Buprenorphine

Ethicon
2-0 Mersilk suture, round body
3-0 Mersilk suture, round body
4-0 Mersilk suture, conventional cutting

Merck Life Science UK Ltd
NADH
Phosphomolybdic acid solution 10% w/v

Parker laboratories
Aquasonic ultrasound gel

Roche
cOmplete™ Mini EDTA-free Protease Inhibitor Cocktail
PhosSTOP Phosphatase Inhibitor Cocktail

Sigma-Aldrich Company Ltd
2,3,5-Triphenyltetrazolium Chloride (TTC)
Bovine Serum Albumin (BSA)
Calcium ionophore A23187
Cyclosporin A
Dimethyl sulfoxide (DMSO)
DPX mounting medium
Ethyleneglycol- bis(β-aminoethyl)-N,N,N',N'-tetraacetic Acid (EGTA)
Glutaraldehyde

Isoprenaline
Magnesium Chloride ($MgCl_2$)
MOPS
Nitrilotriacetic acid
Nonidet P-40
Phosphate buffered saline (PBS) tablets
Phosphotungstic acid solution 10% w/v
Potassium thiocyanate
Sodium deoxycholate
Sodium dodecylsulphate
Sodium phosphate dibasic (Na_2HPO_4)
Sodium phosphate monobasic dihydrate ($NaH_2PO_4.2H_2O$)
Sucrose
Triethanolamine

ThermoFisher Scientific UK Ltd
D-glucose anhydrous
Formaldehyde
Magnesium Sulfate Heptahydrate ($MgSO_4 \cdot 7H_2O$)
Pierce™ Rapid Gold BCA Protein Assay Kit
Potassium Chloride (KCl)
Potassium Dihydrogen Orthophosphate (KH_2PO_4)
Sodium Hydrogen Carbonate ($NaHCO_3$)

Tocris
Cyclosporin A
Rotenone

VWR International Ltd
Calcium Chloride solution (1M) ($CaCl_2$)
Pyruvic Acid Sodium Salt
Sodium Chloride (NaCl)

Vetoquinol Uk Ltd
Antisedan (Atipamezole)
Narketan (Ketamine)
Domitor (Medetomidine)

Wockhardt UK Ltd
Heparin Sodium

2.2 Solutions

Table 2-1 Krebs buffer

Chemical	Concentration (mM)
$CaCl_2$	1.2
Glucose	11
KCl	4.8
KH_2PO_4	1.2
$MgSO_4$	1.2
NaCl	120
$NaHCO_3$	25

Table 2-2 Cardioplegia

Chemical	Concentration (mM)
$CaCl_2$	1.2
Glucose	11
KCl	20
KH_2PO_4	1.2
$MgCl_2$	15
$MgSO_4$	1.2
NaCl	120
$NaHCO_3$	25

Table 2-3 Fixative solution

Chemical	Concentration
Phosphate buffer ($22.5mM\ NaH_2PO_4.2H_2O$, $76.76mM\ Na_2HPO_4$ - pH 7.4)	0.1M
$CaCl_2$	0.5mM
D-glucose anhydrous	1.7mM
Glutaraldehyde	1% (v/v)
Paraformaldehyde	1% (w/v)

Table 2-4 RIPA buffer

Chemical	Concentration
Prepared in PBS (1 PBS tablet/200ml)	
Nonidet P-40 detergent	1% (v/v)
Sodium deoxycholate	0.5% (w/v)
Sodium dodecylsulphate	0.1% (w/v)

Table 2-5 Mitochondrial isolation buffers

Buffer	Contents
A	Sucrose 300mM Tris-HCl 10mM (pH 7.2) EGTA 1mM (pH7.2)
A Final Wash (AFW)	Sucrose 300mM Tris-HCl 10mM (pH 7.2)
B	Buffer A + 5mg/ml BSA

Table 2-6 Mitochondrial swelling buffer

Chemical	Concentration (mM)
KSCN	150
MOPS	20
Tris	10
Nitrilotriacetic acid	2
A23187 (C7522 Sigma)	0.002
Rotenone	0.0005
Antimycin	0.0005

2.3 Animals

For all experiments, animals used were adult male Wistar rats obtained from Envigo (Cambridgeshire, UK). All animals were housed in the Animal Services Unit at the University of Bristol, maintained on a 12-hour light/dark cycle with free access to standard rat chow and water. Animals were housed in Tecniplast 1500 conventional rat cages, with groups of two to four animals per cage. The details of animal weights for each set of experiments are specified throughout the Methods section.

2.4 Model of LAD occlusion to induce myocardial infarction

2.4.1 Animals for LAD occlusion surgery

Animals used for LAD occlusion or sham surgery were housed in the Animal Services Unit for 5-7 days prior to surgery. At the time of surgery animals weighed between 220-280g. Naïve animals used as a comparison for sham animals weighed 325-355g, similar to the weight of sham animals at the 4-week termination point.

2.4.2 Surgery procedure

Animals were anaesthetised via intramuscular injection in the hind limb of ketamine (50mg/kg) and medetomidine (0.2mg/kg) in combination. Animals were intubated and ventilated with a small animal ventilator (Harvard Apparatus) at a rate of 60 breaths per minute with a volume of 0.1ml/g. Surgery was performed in the supine position on a heat mat to maintain animals body temperature throughout, monitored by rectal temperature probe.

For the LAD occlusion surgery, an incision was made in the skin on the left side of the chest. The chest muscles were carefully blunt dissected away, and a purse string suture was prepared in the chest muscles ready for closure at the end of surgery using a 2-0 mersilk suture. A retractor was then placed within the chest muscles and opened to expose the ribs. Access to the chest cavity was made by puncturing the 5th intercostal space and retracting the ribs carefully as not to damage heart or lung. At this point the heart can be seen in the chest cavity. The pericardium was then broken, and pressure applied to the chest to exteriorise the heart from the chest cavity. The LAD coronary artery could then be identified and occluded by ligation with 3-0 mersilk suture. At this point, animals assigned to the sham group had the suture placed under the LAD but no ligation was made. The heart was returned to the chest cavity and the retractor was

removed. Baytril (5mg/kg) was given directly into the chest cavity and the purse-string suture placed at the beginning of the surgery was pulled tight to close the chest. The skin opening was then closed using a 4-0 suture. Atipamezole (0.85mg/kg) was administered via intramuscular injection in the hind limb for anaesthetic reversal. Ventilation was ceased once breathing had recovered, and animals were extubated.

Animals were placed in a clean cage to recover, with a heat mat to help maintain body temperature and monitored closely. Once recovered fully from the anaesthetic, Buprenorphine (0.03mg/kg) was given as analgesic and further doses were given for 48 hours following surgery. Animals were monitored daily following surgery and weight was taken twice a week to assess recovery (Figure 2-1). Animals were housed for up to 4 weeks following surgery, some animals were terminated at the earlier time-points of 3-days and 2-weeks post-surgery.

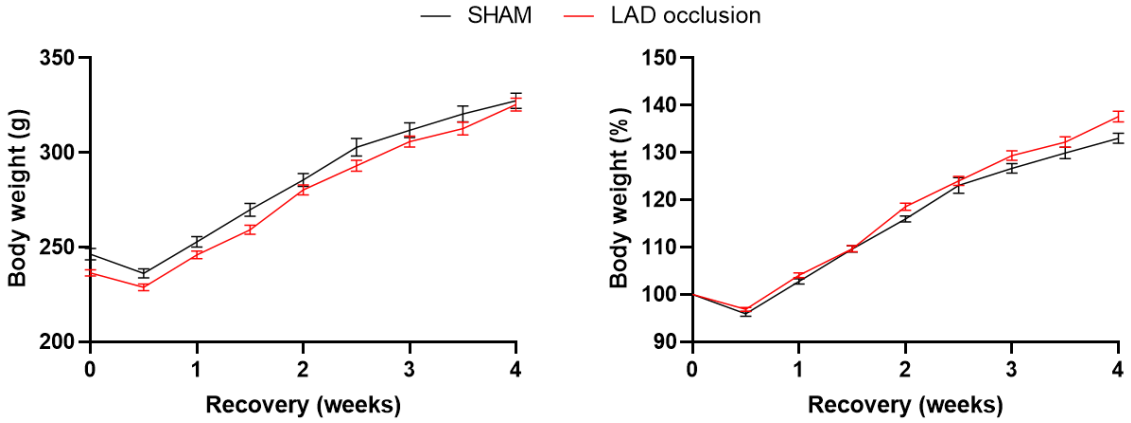

Figure 2-1 Body weight changes during recovery from surgery

Body weight taken across recovery from surgery as raw values (A) and percentage of initial value (B) for LAD occlusion and sham animals.

In total 101 successful surgeries were completed (57 LAD, 44 Sham), of these 7 died or were terminated due to ill health during the recovery period (6 LAD, 1 Sham). Giving a post-operative survival rate in the LAD occlusion group of 89% and in the sham group of 97.7% (Figure 2-2). From the 94 animals that survived to their pre-determined endpoint, 73 were utilised in the data shown throughout this thesis. The remainder were used in preliminary studies and optimisation of LAD occlusion surgery. The number of animals assigned to each protocol is detailed below in Table 2-7.

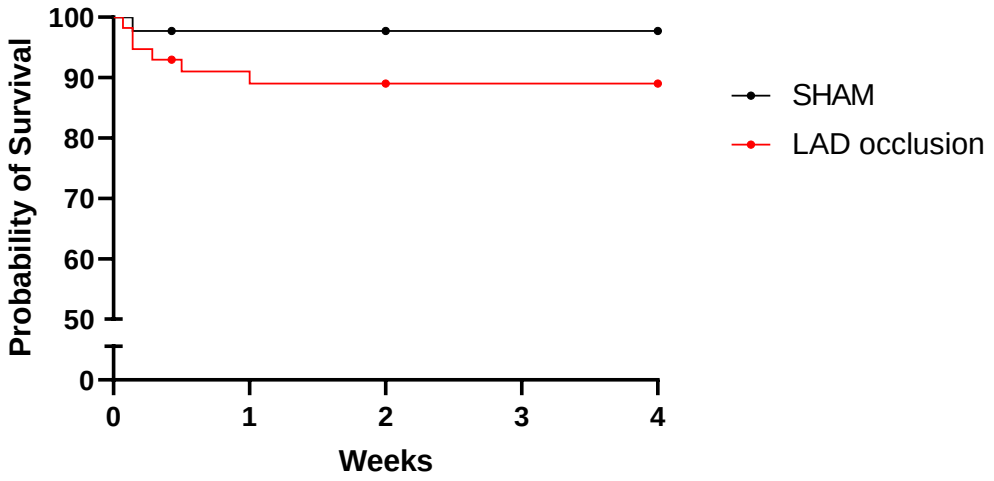

Figure 2-2 Survival curve for LAD occlusion and Sham groups

Survival of LAD occlusion (n=57) and Sham (n=44) animals. End-point terminations occurred at 3-days (LAD n=6, sham n=6), 2-weeks (LAD n=10, sham n=7) and 4 weeks (LAD n=35, sham n=30)

Table 2-7 N numbers used across different protocols

Protocol	Time post-surgery	LAD	Sham
Sample collection	3-days	6	6
	2-weeks	8	7
	4-weeks	8	6
Ischemia reperfusion	4-weeks	16	16

2.4.3 Echocardiography

Echocardiography was performed prior to termination to assess cardiac function using a Vevo 3100 machine and MX250 probe (Visualsonics, Fujifilm), set to the cardiology imaging mode. Animals were anaesthetised via inhalation of 5% isoflurane for induction, reduced to 1-2% for anaesthesia maintenance. Animals were placed in the supine position on a heated platform and limbs were attached to electrocardiography pads for heart rate monitoring. Heart rate was maintained between 350-450 bpm for all echocardiography recordings. Hair was removed on the left side of the chest and Aquasonic ultrasound gel was applied to enhance transmission. The parasternal long-axis view was identified, and recordings were taken in m-mode (Figure 2-3). Analysis was performed using Vevo Lab 3.1 software. Measurements were made using the trace

tool (Figure 2-3) using m-mode images which calculates various measures of cardiac function using the equations in Table 2-8.

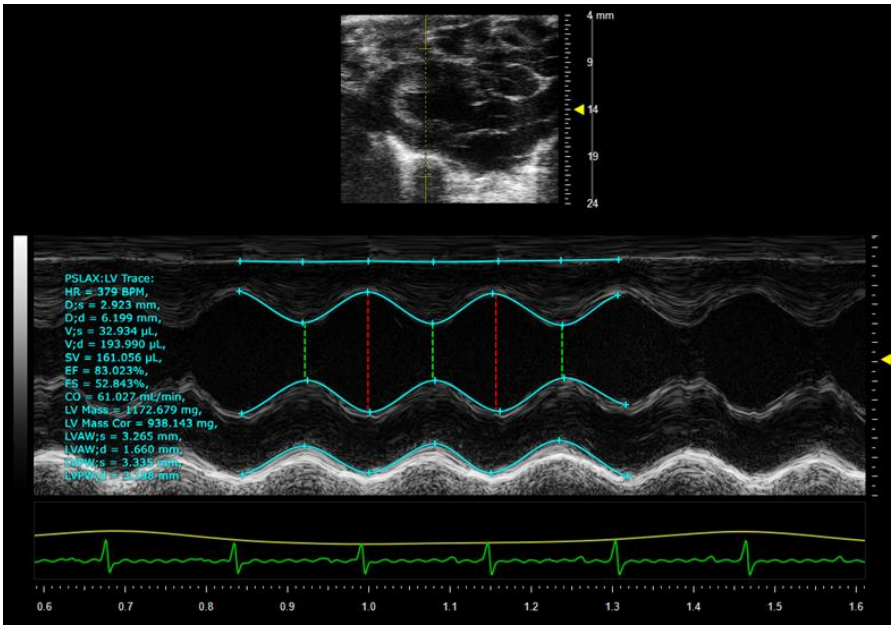

Figure 2-3 Echocardiography analysis - LV trace tool in m-mode

Echocardiography recording in m-mode, analysed using LV trace tool (Red – end diastole, green – end systole)

Table 2-8 Echocardiography analysis calculations using LV trace tool in Vevo Lab 3.1

D;s – Systolic diameter, D;d – Diastolic diameter

Measurement	Units	Equation
Systolic volume (V;s)	µL	$\frac{7}{(2.4 + Average\ D;s)\ x\ Average\ D;s^3}$
Diastolic volume (V;d)	µL	$\frac{7}{(2.4 + Average\ D;d)\ x\ Average\ D;d^3}$
Stroke volume (SV)	µL	$Diastolic\ volume - Systolic\ volume$
Ejection Fraction (EF)	%	$100\ x\ \left(\frac{Stroke\ Volume}{Diastolic\ volume}\right)$
LV Fractional Shortening (FS)	%	$100\ x\ \left(\frac{Average\ D;d - Average\ D;s}{Average\ D;d}\right)$

2.4.4 Termination of surgery animals

Animals were terminated by intraperitoneal (IP) injection of pentobarbital (100mg/kg) in combination with heparin (100IU/kg), followed by cervical dislocation. Following termination, the chest was opened and blood samples taken via cardiac puncture. The heart was then excised and placed into 4^{o}C Krebs buffer (Table 2-1). Kidneys were also removed and stored for future analysis.

2.4.5 Blood collection

Blood samples were collected by cardiac puncture from the LV before the heart was excised and centrifuged in EDTA coated tubes for 5mins, 2000g at 4^{o}C. The plasma supernatant was aliquoted and stored at -80 ^{o}C.

2.5 Langendorff setup

Langendorff is an ex vivo isolated heart perfusion technique (Bell et al. 2011) . Freshly excised hearts were cannulated onto a Langendorff perfusion setup (Figure 2-4). Hearts were cannulated via the aorta, above the aortic valve, allowing for retrograde perfusion of the heart via the coronary arteries. The time taken for cannulation of hearts was under 2-minutes between excision and perfusion on the setup. Hearts were perfused with Krebs buffer (Table 2-1), heated to 37^{o}C and oxygenated in the reservoir chambers. The Langendorff setup used was constant flow setup, the flow rate of perfusion was controlled by a peristaltic pump and set depending on animal weight.

2.5.1 Ex-vivo functional measurement

Function of the heart was assessed on the Langendorff setup using a balloon inserted in the LV (Figure 2-4B) attached to a pressure transducer. Balloons were made from clingfilm and filled with water. When deflated balloons were inserted into the LV via the left atrium and then inflated to a volume that produced an end diastolic pressure (EDP) of 5-10 mmHg. The pressure data was recorded on LabChart software (Figure 2-5), from the pressure trace several functional parameters could be measured. Left ventricular developed pressure (LVDP) was calculated as the difference between LV end diastolic and systolic pressure. Heart rate (HR) was measured, and rate pressure product (RPP) could be calculated as the product of LVDP and HR. Contractility measurements including Max dP/dt and contractility index were also taken to assess contractile function.

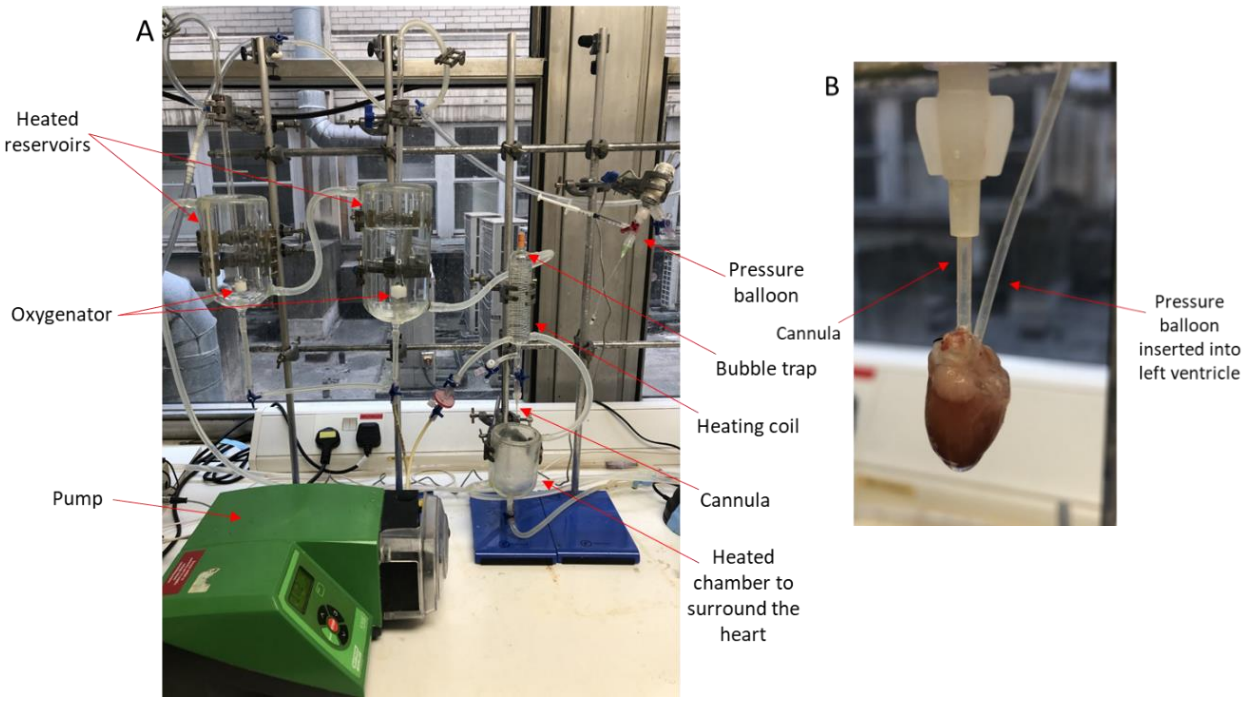

Figure 2-4 Langendorff setup

(A) Langendorff setup, (B) Cannulated heart with pressure balloon inserted into the left ventricle.

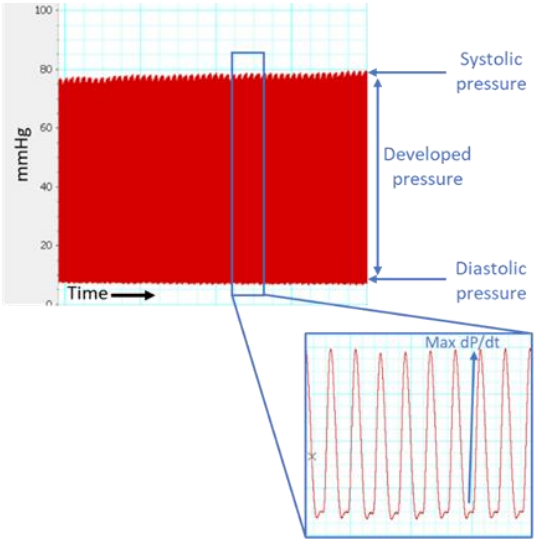

Figure 2-5 Representative pressure trace from Langendorff left ventricle balloon

Pressure trace measured on Langendorff from balloon in the left ventricle, annotated to show measurements recorded from the trace.

2.6 Sample collection to study remodelling

To explore the cardiac remodelling process over time animals were terminated at three time-points (3-days, 2-weeks, and 4-weeks) following LAD occlusion to assess functional, structural, and molecular changes. The sample collection process used allowed samples for each type of analysis to be collected from each heart (Figure 2-6)

Hearts were canulated on the Langendorff setup and initially perfused with Krebs buffer (Table 2-1). Cardioplegic solution (Table 2-2) was then perfused at 1ml/min for 5 minutes to arrest the heart in diastole. Arresting the heart with cardioplegia relaxes the myocardium which facilitates higher quality electron microscopy images (discussed below). The apex was then removed and frozen immediately in liquid nitrogen, to be used for proteomic analysis (Figure 2-6). Perfusion was then switched to fixative solution (Table 2-3) for 5 minutes. The heart was removed from the Langendorff setup, a 1-2mm slice was taken from the apex end for electron microscopy (EM) and the upper section of the heart was placed in 4% PFA for histology (Figure 2-6).

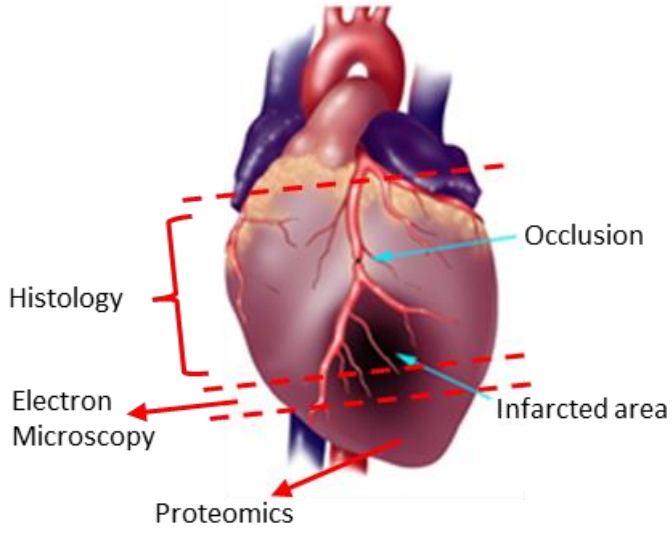

Figure 2-6 Overview of sample collection

Representation of where tissue samples were taken from for histology, electron microscopy and proteomics. Image modified from (Wu et al. 2011)

2.7 Histology/Light microscopy

The tissue section collected for histological evaluation was perfusion fixed in fixative solution (Table 2-3), once removed from the Langendorff setup the tissue

section was placed into 4% formaldehyde for 24 hours, after which it was moved into phosphate buffered saline (PBS). The samples were trimmed and placed into cassettes for tissue processing, where water in the samples is gradually replaced with ethanol to facilitate wax infiltration (ThermoFisher Scientific Excelsior AS Tissue Processor). Once processed, tissues were embedded in paraffin wax (Thermo Scientific HistoStar Embedding Workstation) in an orientation to allow cross-sectional sections of the heart to be made. 5µm tissue sections were cut by microtome and mounted onto Superfrost Plus™ Gold Adhesion microscope slides ready for staining. Slides were stained for Haematoxylin and Eosin (H&E), Elastic Verhoeff-Van Gieson (EVG) and Masson's Trichrome.

2.7.1 H&E and EVG

H&E and EVG staining was completed using an Automatic Slide Stainer (Thermo Scientific Varistain 24-4) at the University of Bristol by the Level 7 histology technicians. After staining, slides were mounted in DPX mounting medium.

H&E staining combines two dyes haematoxylin and eosin to differentially stain the acidic and basic structures of a cell. Haematoxylin is a basic dye which stains acidic structures, such as the nuclei, purple/blue. Whereas eosin is an acidic dye staining the basic structures pink, this includes the cytoplasm proteins. H&E staining facilitates the visualisation of the tissue structure and cellular organisation (Figure 2-7A). EVG staining visualises elastic fibres present in tissue; iron haematoxylin stains the elastic fibres dark blue/black (Figure 2-7B).

2.7.2 Masson's Trichrome

Masson's trichrome staining visualises collagen fibres by staining them in blue whilst tissue fibres are stained red (Figure 2-7C). Slides were stained in Mayer's hematoxylin for 1 minute, then placed under running warm tap water for 10 minutes and rinsed in distilled water. Slides were then stained in Biebrich scarlet-acid fuchsin solution for 15 minutes and rinsed in distilled water. Slides were then placed in 5% phosphomolybdic-5% phosphotungstic acid solution to differentiate for 15 minutes. Slides were rinsed in distilled water and placed into aniline blue solution for 2 minutes, then transferred to 1% acetic acid solution for 5 minutes to differentiate. Slides were rinsed in distilled water before rapid dehydration and cleared in xylene before mounting with DPX mounting medium.

2.7.3 Image acquisition

Histology images were acquired using the PreciPoint microscope and scanner, which captures complete scans of each section. Using the Micropoint software higher magnification images can be taken from specific areas of interest, as seen in Figure 2-7A.

2.7.4 Image analysis

Image analysis was done using Fiji-Image J software, the scale was set for each image prior to analysis. From cross-sectional H+E images measurements were taken of wall thickness in the infarct area, remote LV, septal wall, and RV, as well as LV lumen area (Figure 2-8A). Wall thickness measurements were an average of three measurements taken along each wall. Infarct area was determined as the percentage of the midline affect by the LAD occlusion (Figure 2-8B), as previously described (Takagawa et al. 2007). Quantification of elastin fibres and collagen was completed using colour thresholding and expressed as a percentage of the total tissue area.

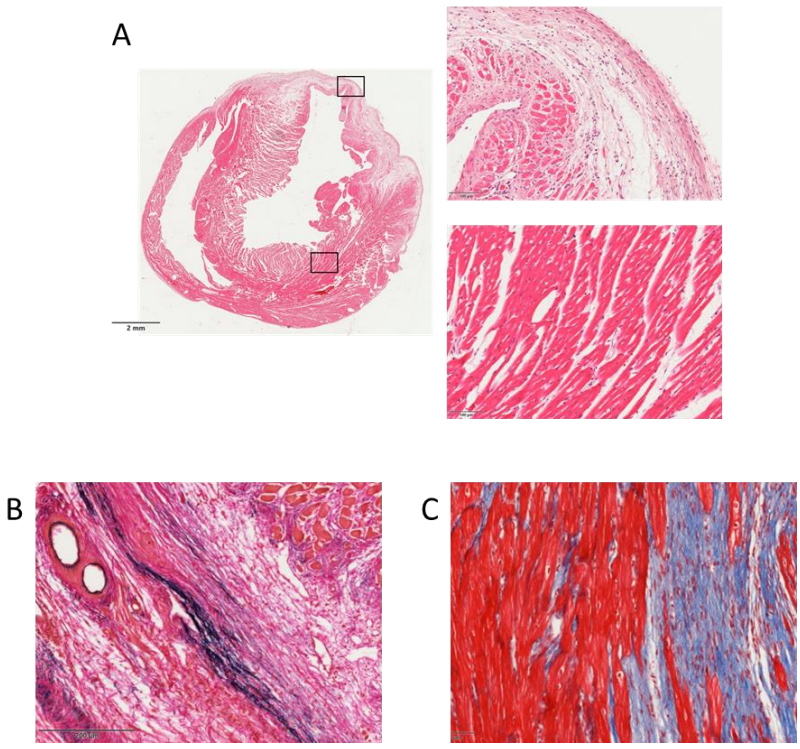

Figure 2-7 Histology examples

Representative images of histology staining. (A) Cross-sectional image of H+E staining, tissue fibres stained pink and nuclei blue, with higher magnification images from infarct and remote areas of the LV. (B) EVG staining with elastic fibres stained dark blue/black. (C) Masson's Trichrome staining, collagen fibres in blue and tissue fibres in red

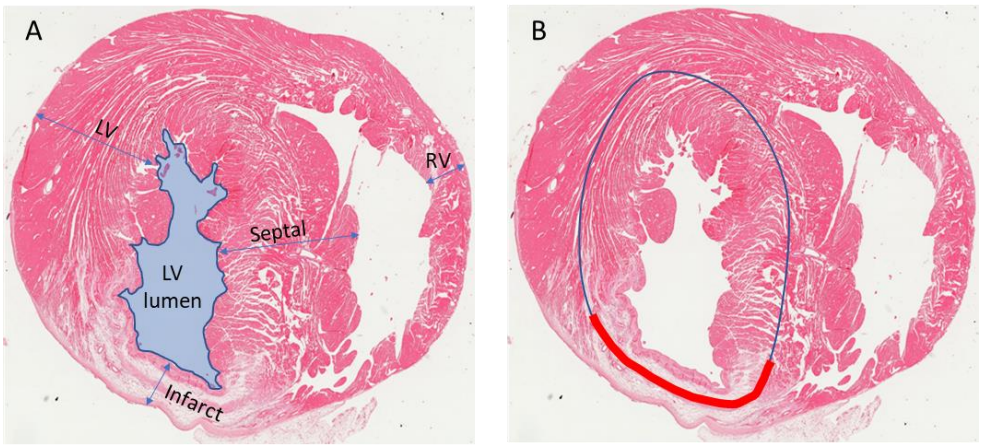

Figure 2-8 Location of measurements taken from H+E images

Representative images to show (A) the locations of wall thickness measurements and (B) quantification of infarct size (red) as a percentage of the LV midline (blue).

2.8 Electron microscopy

Tissue samples were collected for electron microscopy to investigate changes in the ultrastructure of the heart following MI. Cross-sectional tissue samples were taken from each heart following perfusion with cardioplegic solution to relax the tissue and subsequent perfusion with fixative solution (section 2.6). Relaxed myocardium is important for EM images as contraction of the tissue can distort internal components of the cell such as mitochondria. The tissue section taken was a 1-2mm slice from above the apex, these sections included the infarcted area (Figure 2-6). The tissue sections were stored in fixative solution for 24 hours before being transferred into phosphate buffer (Table 2-3). From each cross-sectional tissue sample smaller sections were cut for EM analysis, collected from the infarct area, border zone and remote region of the LV.

The tissue samples were processed by the Wolfson Bioimaging facility at the University of Bristol. The samples were dehydrated, embedded, and stained using uranyl acetate (3% w/v) and lead citrate (94mM lead nitrate, 140mM sodium citrate and 0.19mM NaOH). The blocks were sectioned in an orientation to give longitudinal sections of cardiac tissue.

2.8.1 Image acquisition and analysis

Images were acquired using the FEI Tecnai 12 120 kV BioTwin Spirit transmission electron microscope with FEI Ceta 4k x 4k CCD camera. Images were acquired at various magnification, higher magnification to visualise the overall morphology and lower magnification to study structures such as mitochondria. Images were taken in areas of relaxed myocardium, indicated by visualisation of the I band in the sarcomere. An example EM image of healthy myocardium with some characteristic features annotated is shown in Figure 2-9.

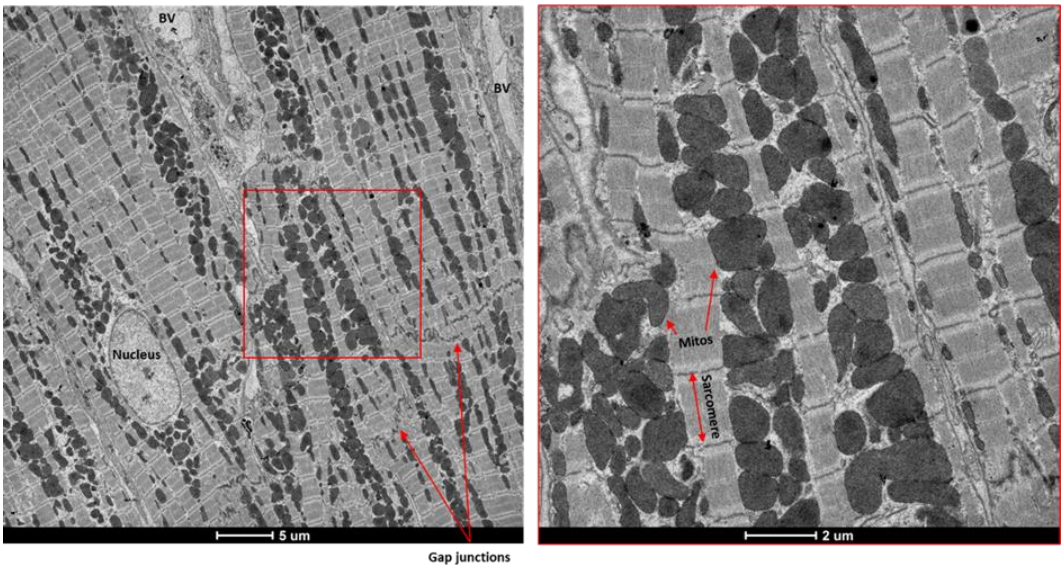

Figure 2-9 Electron microscopy image

Representative electron microscopy image of healthy rat myocardium. Righthand image is a higher magnification of the indicated area (red box). Sarcomeres display clear I band indicating relaxed tissue. Mitos – mitochondria.

2.9 Metabolomics

Metabolomics is the study of metabolites within tissue or blood samples. In this study metabolomic analysis was completed using ^{1}H-Nuclear Magnetic Resonance (NMR). Metabolomic analysis was performed on the plasma samples obtained from blood collected at termination by cardiac puncture (section 2.4.5). Metabolomic analysis was performed on samples from all time-points, 3-days (LAD n=5, Sham n=6), 2-weeks (LAD n=6, Sham n=5) and 4-weeks (LAD and Sham n=8) plus samples from naïve animals (n=4).

2.9.1 Sample preparation and Nuclear Magnetic Resonance (NMR)

Sample preparation and running of NMR was performed by Matt Goodwin at the Metabolomics Facility, University of Bristol. Plasma samples were mixed in equal volumes (80µl) with sodium phosphate buffer (75 mM Na_2HPO_4, 0.08% sodium 3-(trimethylsilyl) propionate-2,2,3,3-d4, 0.04% sodium azide in 80%/20% H_20/D_2O, pH 7.4). Samples were then transferred into 3 mm NMR tubes. A pooled sample was prepared by mixing 5µl from each individual plasma sample together. Synthetic controls were prepared with 0.8 mM alanine, 5 mM glucose and 6.2 mM (0.04%) sodium azide.

NMR spectra were acquired using a Bruker Avance III HD 500 MHz spectrometer equipped with a nitrogen-cooled triple resonance probe (CryoProbe Prodigy TCI) equipped with SampleJet auto-sampler with cooled (6°C) sample storage running Bruker Topspin 3.6.2. 1D NOESY (noesygppr1d pulse sequence, 256 scans, 3.9 s acquisition time) and CPMG spectra (cpmgpr1d pulse sequence, 256 scans, 3.3 s acquisition time) were acquired on each sample.

2.9.2 Metabolomic analysis

For each sample, from the CPMG traces the area of each peak was measured using MestReNova x64 software. Where multiple peaks are related to the same metabolite, the sum of the peak areas was used. Any differences in peaks between sample groups were analysed, and the identification of these peaks was done by evaluation on Chenomx Software (Figure 2-10), comparison to available databases and previous literature. Peaks of interest will need to undergo spiking experiments to confirm metabolite identity.

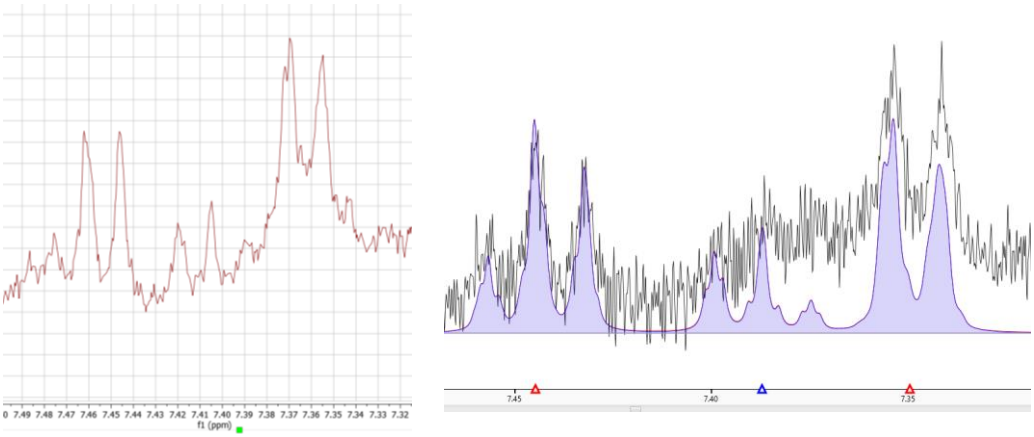

Figure 2-10 Example of Chenomx evaluation

2.10 Proteomics

Proteomic and phospho-proteomic analysis was performed on apical tissue collected from hearts across all time-points post-surgery; 3-days (LAD n=5, Sham n=5), 2-weeks (LAD n=5), 4-weeks (LAD n=5, Sham n=5). Samples from naïve hearts were included for comparison to sham (n=4).

2.10.1 Protein extraction

Apex tissue, collected at termination, was removed from -80 storage and a section cut for protein extraction. For LAD hearts where infarcted tissue was present in the apex, the tissue used for extraction was taken from the surrounding tissue. Tissue samples were weighed and added to homogenisation tubes. RIPA buffer, pH 7.4 (Table 2-4), with the addition of phosphatase inhibitor and protease inhibitors, was added to each sample (10µl per mg). Homogenisation beads were added to each tube. Tubes were homogenised in the cold room at 4^{o}C using a tissue homogeniser, set to maximum speed for 25 seconds, this was repeated 4-5 times to ensure complete homogenisation. Samples were placed back on ice between each repetition to ensure tissue samples remained cool. Tissue samples were then left on ice to shake for 30 minutes. The tubes were then centrifuged at 13000g for 10 minutes at 4^{o}C. The supernatant was removed, aliquoted into eppendorffs and stored at -80^{o}C. One aliquot would be used for protein quantification of each sample, the rest were stored for proteomics and future use.

2.10.2 Protein quantification

To quantify the protein concentration in each sample a BCA protein assay was performed, using the Pierce™ Rapid Gold BCA kit. Briefly this involved creating a range of BSA standards with an increasing level of protein concentration to create a standard curve. Protein samples were diluted 1:10 in RIPA buffer (Table 2-4, pH7.4) to ensure they would be in the range of the standard curve. Samples and standards were added in duplicate to a 96-well plate. The Rapid Gold BCA reagent mixture, containing a copper chelator, was then added to each well. The plate was shaken for 30 seconds and then left for 5 minutes at room temperature. Absorbance of each sample was then determined at a wavelength of 490nm on a plate reader. From the absorbance a standard curve was created using the known standards, and this was used to determine the unknown concentrations of the samples. Once protein concentration for each sample had been

determined, samples were diluted in RIPA buffer to a concentration of 2mg/ml for proteomic analysis.

2.10.3 Tandem Mass Tagging sample preparation and nano-LC mass spectrometry

Proteomic and phospho-proteomic analysis was completed by the Dr. Kate Heesom at the Proteomic Facility, University of Bristol. Protein identification and quantification was performed using the Tandem Mass Tagging (TMT) approach. Samples were TMT labelled within the facility, samples were fractioned and analysed on a Orbitrap Fusion Lumos mass spectrometer by nano-LCMSMS (Figure 2-11B). The TMTpro reagents label every peptide in a sample and contain an amine reactive group, a mass normalisation group, and a mass reporter region (Figure 2-11A). TMT reagents are isobaric tags, meaning they all have the same overall mass, with different reporter region mass allowing for quantification of each sample.

Proteomics and phospho-proteomics were completed as previously described (Abdul-Ghani et al. 2022; Skeffington et al. 2020). Briefly, protein samples were digested overnight in trypsin, then labelled with TMT reagents (Figure 2-11A) according to the manufacturer's protocol (ThermoFisher Scientific) and pooled together. The pooled sample was prepared and fractionated by high pH reversed-phase chromatography using an Ultimate 3000 liquid chromatography system (ThermoFisher Scientific). For phospho-proteome analysis the TMT-labelled pooled sample was prepared and subjected to TiO2-based phosphopeptide enrichment according to the manufacturer's instructions (Pierce). High pH RP fractions (Total proteome analysis) or the phospho-enriched fractions (Phospho-proteome analysis) were further fractionated using an Ultimate 3000 nano-LC system in line with an Orbitrap Fusion Lumos mass spectrometer (Thermo Scientific). All spectra were acquired using an Orbitrap Fusion Lumos mass spectrometer controlled by Xcalibur 3.0 software (Thermo Scientific) and operated in data-dependent acquisition mode using an SPS-MS3 workflow.

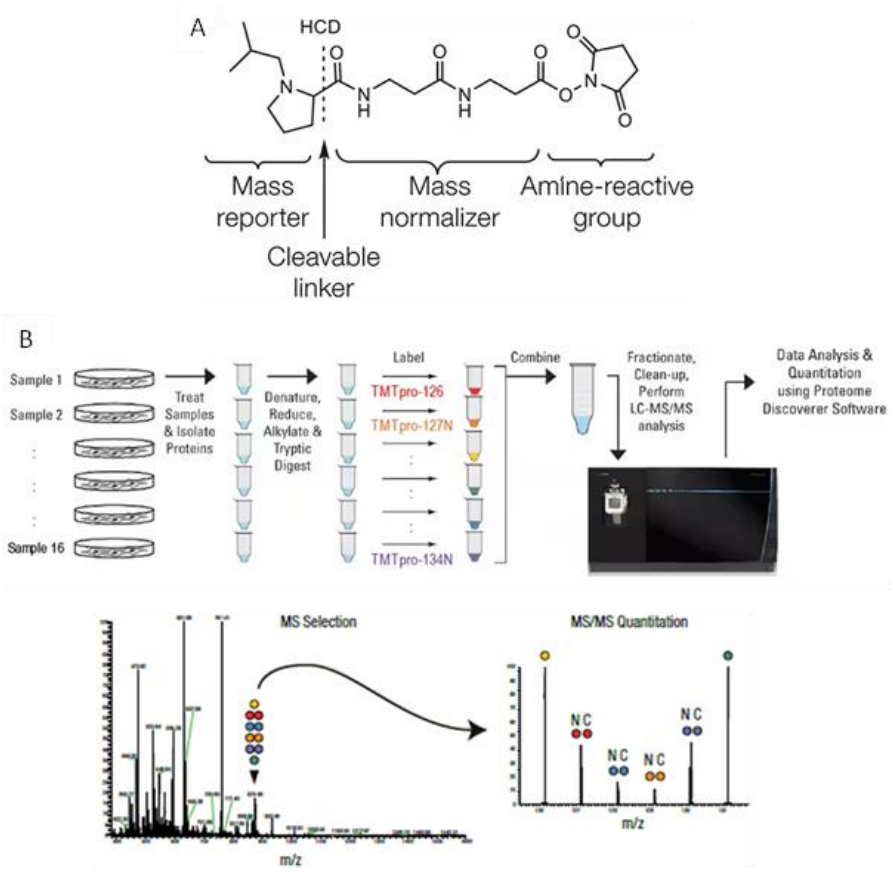

Figure 2-11 TMT reagent structure

(A) Structure of the TMTpro reagent's functional regions. (B) Summary of tandem mass spectrometry procedure. Images from ThermoFisher Scientific.

2.10.4 Proteomic and phospho-proteomic data analysis

Analysis of the raw data was performed by Dr Philip Lewis (University of Bristol proteomic facility) using Proteome Discoverer software (Thermo Scientific, version 2.4), a Sequest search was run against the Uniprot Rat database. Analysis of phospho-protein data was set up the same as total protein but with phosphorylation at serine, threonine, and tyrosine included as possible peptide modifications. For total protein data analysis normalisation to total peptide amount was included for each sample, this was not included for phosphoprotein analysis as phospho-enrichment may alter the amount of peptide. The false discovery rate cut-off for all data was 5%. Protein levels were normalised to an internal standard which was a pool of all samples.

For the proteomic analysis a range of comparisons were made to compare different sample groups, the comparisons included: 3-day LAD/3-day Sham, 4-week LAD/4-week Sham, 3-day LAD/2-week LAD, 4-week LAD/2-week LAD, 3-day LAD/4-

week LAD, 3-day Sham/Naïve, 4-week Sham/Naïve. In each comparison only proteins or phosphoproteins that were detected in all samples were included in the analysis. For each comparison fold changes (FC) were calculated and differences between groups analysed by Student's T.Test. A significantly differentially expressed protein (DEP) is defined as a protein with a ± 1.3-FC and a p-value <0.05. A 1.3 FC cut off was used in accordance with previous studies (Abdul-Ghani et al. 2022; Bond et al. 2019). Volcano plots were plotted with the $\log_2$(FC) against -$\log_{10}$(p-value), dotted lines are included to show FC and p-value cut offs with significant DEPs highlighted in red.

2.10.4.1 Pathway analysis

Ingenuity Pathway Analysis (IPA) software was used to identify enriched canonical pathways, for both proteins and phospho-proteins. IPA was carried out on three of the comparisons: 3-day LAD/3-day Sham, 4-week LAD/4-week Sham and 3-day LAD/4-week LAD. For each comparison IPA was performed using all proteins or phosphoproteins with a significant difference in expression, including proteins or phospho-proteins not present in every sample. For each canonical pathway a p-value of the overlap is given with a significance level set at p<0.05, and a Z-score is generated which is an estimation as to the activation or inhibition of a pathway with a score of greater than 2 or -2 classified as a prediction rather than a trend. For each identified canonical pathway, the list of proteins linked to the pathway is given. IPA was performed Dr Philip Lewis (University of Bristol proteomic facility).

2.11 Ischemia reperfusion experiments

Studies to investigate I/R injury and cardioprotective strategies were completed using the Langendorff setup (section 2.5).

2.11.1 Animals for ischemia reperfusion studies

Experiments to investigate cardioprotection against I/R injury were completed in control healthy hearts or failing hearts. Control animals used to study I/R were 275-300g at the point of termination. Animals were sacrificed by intraperitoneal injection of pentobarbital (100mg/kg), followed by cervical dislocation. Animals used to study I/R in failing hearts were 4-weeks post LAD occlusion, weighing 300-350g at the point of termination, these animals were terminated as detailed above (2.4.4) in combination

with heparin. Following termination, the chest was opened, the heart was excised and placed into 4°C Krebs buffer (Table 2-1). Hearts were immediately cannulated onto the Langendorff setup (Figure 2-4) via the aorta.

2.11.2 Protocol

Once cannulated on the Langendorff setup, following a stabilisation period, hearts were subjected to a period of normothermic ischemia followed by reperfusion. To initiate ischemia the flow of Krebs buffer through the Langendorff system was stopped, ceasing perfusion of the heart. During ischemia hearts were submerged in warmed Krebs buffer to maintain the temperature at 37°c. In cardioplegia experiments, warm cardioplegic solution (Table 2-2) was perfused at 5ml/min for 2 minutes to arrest the heart at the start of ischemia and the heart was subsequently immersed in 37°C cardioplegia for the duration of ischemia. The duration of ischemia and reperfusion was dependent on the experiment and presence of cardioplegic arrest, the different protocols used are detailed at the beginning of Chapter 6 and 7. In the experiments investigating cardioprotective potential of adrenergic stimulation, drugs were given prior to ischemia or cardioplegic arrest (see section 2.11.3).

In all I/R experiments, regardless of duration or presence of cardioprotective strategies, three outcomes were measured to assess I/R injury. Functional recovery across reperfusion (section 2.12), release of cardiac injury marker lactate dehydrogenase (LDH) (section 2.13) and extent of injury in the myocardial tissue measured by Triphenyltetrazolium chloride (TTC) staining (section 2.14).

2.11.3 Drugs targeting the adrenergic receptor pathways

In this thesis three drugs targeting the adrenergic receptor pathways are tested: A61603, Isoprenaline and 8- Bromoadenosine- 3', 5'- cyclic monophosphate (8-Br) (Table 2-9). A61603 pre-conditioning had not been previously investigated in this setup and therefore was tested in ischemia alone before testing in combination with cardioplegic arrest. A61603 was tested at 50nM and 10nM to determine any differences in inotropic response or protection at the two concentrations. The EC50 of A61603 is reported as 6.9nM (Luo et al. 2007). Isoprenaline and 8-Br have previously been shown to protect the heart against ischemia within our research group and by others, in this study these drugs were tested in addition to cardioplegic arrest only. The concentration of isoprenaline was selected as it evoked a significant inotropic response in the heart.

Concentrations used for 8-Br (5 and 10μM) were based on previous research (Khaliulin et al. 2017; M. J. Lewis et al. 2022).

Table 2-9 Adrenergic drugs used

Chemical	Concentrations used	Administration time (minutes)	Adrenergic receptor pathway
A61603	10nM, 50nM	3	Selective α1A agonist
Isoprenaline	100nM	3	Non-selective β agonist
8-Br-cAMP-AM	5uM, 10uM	5	Cell permeable cAMP analogue

2.11.3.1 Administration of drugs

Drugs were delivered to the heart in Krebs buffer, the delivery method varied (see below), but all were warmed to 37°C and oxygenated.

2.11.3.1.1 A61603

A61603 was administered via perfusion from the second heated reservoir on the Langendorff setup. At the point of drug addition the three way tap was adjusted to facilitate flow of the drug solution to the heart, this could be easily reversed at the end of the 3-minute treatment period.

2.11.3.1.2 Isoprenaline

Isoprenaline was also given via perfusion from the second heated reservoir on the Langendorff setup, as discussed above for A61603. Isoprenaline is a light-sensitive drug, so the chamber was encased in foil to reduce light exposure.

2.11.3.1.3 8-Br-cAMP-AM

Administration of 8-Br was done via infusion from a syringe pump, attached just above the cannula. Whilst the infusion was running, the flow from the Langendorff setup was continued diluting the 8-Br infusion in the warm and oxygenated Krebs buffer.

2.12 Functional analysis during Langendorff ischemia reperfusion studies

Pressure balloons inserted in the LV (2.5.1) allowed measurement of LV function prior to and during ischemia and across reperfusion (Figure 2-12). As mentioned above,

EDP was set to 5-10mmHg for all hearts, and the pressure trace recorded allows for measurements of LVDP, HR, RPP and contractility parameters.

Measurement of LV function during the stabilisation period prior to ischemia gave the initial baseline values used for assessing the percentage recovery of functional parameters during reperfusion. In experiments where drug pre-conditioning was involved the response of LV function to drug stimulation could be evaluated, functional measurements were taken across drug perfusion and the subsequent washout period. During ischemia the LV pressure balloon recorded the ischemic contracture of the heart, an increase in pressure is placed on the balloon as contracture occurs. Measurements were taken across ischemia to analyse the profile of contracture, the time to onset of contracture and the peak pressure reached during contracture. During reperfusion, functional measurements were taken every 5 minutes. Data to assess functional recovery was expressed as either the raw values or as a percentage of the pre-ischemic baseline value to account for variations in initial values.

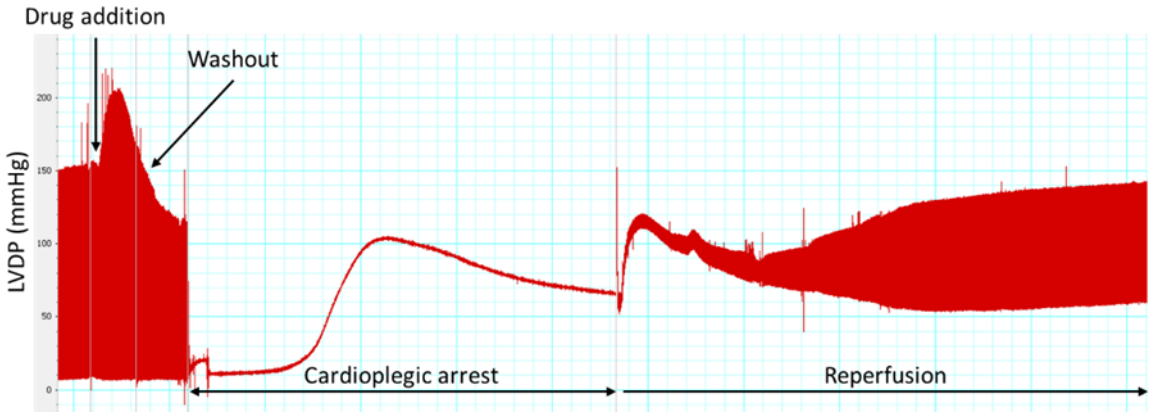

Figure 2-12 LV pressure trace

Example LabChart trace showing LV pressure changes across drug addition, washout, cardioplegic ischemia arrest and reperfusion

2.13 Lactate dehydrogenase measurement

Lactate dehydrogenase (LDH) is a marker of cardiac injury. Effluents for LDH measurement were collected prior to ischemia and during reperfusion at various time-points. Collected effluents were stored at 4^{o}C, and measurement of LDH activity was always performed on the same day as collection. In 1.5ml cuvettes 80µl of sample was

added to 910µl of LDH buffer (100mM Triethanolamine and 100µM NADH, pH 7.4) heated to 37°C. The change in absorbance was then recorded at 340nm following the addition of 10µl 0.1M sodium pyruvate for 5 minutes at 37 °C. The rate of change in optical density was calculated and LDH activity was calculated:

Enzyme Activity (mU/ml) = Rate of change in OD x 1000000/6.22/80

Enzyme activity was plotted across time to create a curve, from which the area under the curve (AUC) could be calculated and analysed.

2.14 TTC staining

TTC staining was used to quantify the extent of injury in the heart at the end of reperfusion. 1% TTC solution was made in PBS and warmed to 37°C, at the end of reperfusion it was perfused through the heart at a rate of 10ml/min for 2 minutes. The heart was removed from the Langendorff setup and briefly emersed in 4% PFA. The heart was then frozen for ~1 hour before slicing cross-sectional and storing in 4% PFA for 24 hours. Slices were imaged on a scanner and analysed using FIJI Image J software. TTC stains injured tissue in white/yellow and healthy tissue in red (Figure 2-13). Injured tissue was quantified and expressed as a percentage of the at-risk area. When assessing extent of injured tissue in failing hearts, the original infarct from LAD occlusion was removed from the image before analysing for percentage injury from the secondary IR insult, giving a percentage injury of the remaining healthy at-risk tissue (Figure 2-13B).

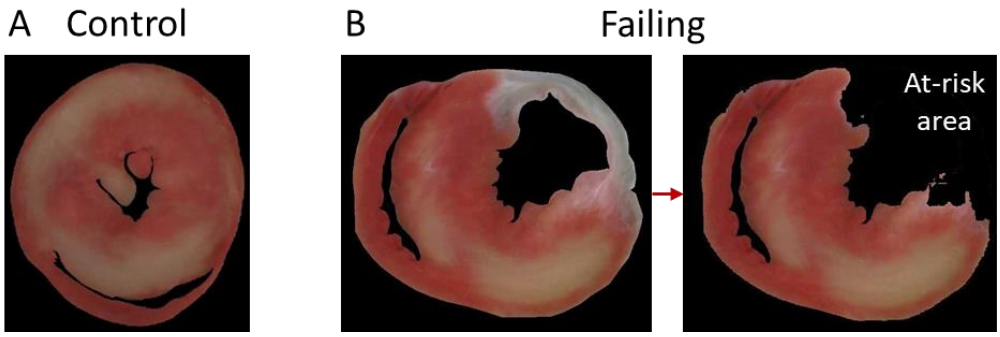

Figure 2-13 TTC staining and at-risk area

Representative images of TTC staining with injured tissue stained yellow/white. For healthy hearts (A) the at-risk area is the entirety of the heart slice. For failing hearts (B) the LAD occlusion induced infarcted area is removed prior to TTC analysis, giving an at-risk area not including the infarct area.

2.15 Mitochondrial swelling experiments

To assess the involvement of the MPTP in the protection by cardioplegia and 8-Br, mitochondrial swelling was measured. Mitochondria are isolated from the ventricles at 10 minutes of reperfusion, and the extent of swelling is measured following calcium addition measured via change in absorbance using a spectrophotometer.

2.15.1 Mitochondrial isolation

At 10 minutes of reperfusion the ventricles were cut away from the heart and placed into 5ml Buffer B (Table 2-5). The ventricles were roughly chopped, and the tissue transferred into a homogeniser tube containing 3ml buffer A (Table 2-5). The tissue was homogenised using a Polytron homogeniser (Kinematica) at 10000 rpm for 3 x 10 second bursts. The homogenised tissue solution was made up to 30ml using buffer B and centrifuged at 2000 x g for 90 seconds to remove cellular debris. The supernatant was retained and ultracentrifuged at 11300 rpm for 5 minutes (Beckman Optima L-90K ultracentrifuge). The supernatant was discarded, and the pellet was resuspended in 1ml of buffer AFW (Table 2-5) before being made up to 30ml and ultracentrifuged again at 11300 rpm for 5 minutes. The supernatant was discarded, and the pellet was resuspended in 200µl of Buffer AFW to give the final yield of isolated mitochondria. Throughout the mitochondrial isolation the tissue was maintained on ice, and homogenisation was completed in the cold room, the isolated mitochondria were stored on ice until the swelling assay was completed.

2.15.2 Mitochondrial protein quantification

Quantification of the protein level in the isolated mitochondria was determined using a Bradford assay. For the assay the mitochondrial sample was diluted 10-fold in buffer AFW (Table 2-5). Four BSA standards of varying concentrations were made up in buffer AFW (5 mg/ml, 2.5 mg/ml, 1mg/ml and 0.5mg/ml) and a blank of AFW only was used. 10µl of each standard and sample was added to cuvettes containing 3ml Bradford reagent and mixed well. After fifteen minutes at room temperature the cuvettes were read on a spectrophotometer at a wavelength of 595nm. A standard curve was generated from the standards, from which the protein level in the sample was determined.

2.15.3 Measurement of mitochondrial swelling

For the swelling assay, 1.4mg of mitochondria were added to 7ml of swelling buffer (pH 7.2, Table 2-6) to give a final concentration of 0.2mg/ml. After shaking carefully this was divided equally into two cuvettes and read on a spectrophotometer at 520nm. Absorbance was measured for 60 seconds before the addition of $CaCl_2$ to give a concentration of 100µM Ca^{2+} in the sample, the measurement was then continued until 300 seconds to observe the effect of the calcium addition. This was then repeated in the presence of a known MPTP inhibitor, cyclosporin A (CsA). 2µM CsA was added to the isolated mitochondria two minutes prior to calcium addition.

2.15.4 Analysis of mitochondrial swelling data

From the traces obtained from the spectrophotometer recordings two measurements were taken: the maximal rate of mitochondrial swelling and the maximum change in optical density to represent maximal swelling (Figure 2-14).

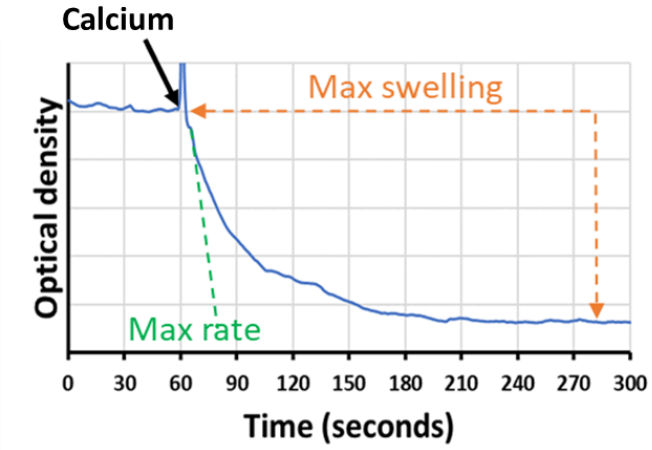

Figure 2-14 Analysis of mitochondrial swelling trace

Representative trace showing mitochondrial swelling following the addition of calcium, represented by a change in optical density. Parameters measured are shown, maximal rate (green) and maximal swelling (orange).

2.16 Data presentation and statistical analysis

All graphs were created using GraphPad Prism software (version 9), all data is displayed as mean ± standard error of the mean. Statistical analysis was carried out using IBM SPSS Statistics software. For all statistical analysis the significance level was set at $p<0.05$.

Student's T.Test was used when comparing two-groups. For comparison of three or more groups one-way ANOVA was used, with Tukey's post-hoc analysis for significant ANOVA results. The Welch's ANOVA with Games Howell post-hoc analysis was used when assumptions were not met.

When two independent variables were present a two-way ANOVA was performed. If a significant interaction between the two independent factors was found, then post-hoc analysis was completed within each individual independent factor. When there is no significant interaction, the main effects are reported. In the case of one independent variable being a repeated measure, a two-way repeated measures ANOVA is performed with the same reporting of findings.

Naïve data is displayed in graphs alongside LAD and Sham data in some instances, this data was separately analysed by one-way ANOVA compared to sham groups. This analysis was to compare the effect of the surgery procedure, a comparison to the LAD group was not needed.

3 Temporal changes in LV function and cardiac structure following myocardial infarction

3.1 Introduction

Ischemic injury in the heart leads to cardiomyocyte death and triggers a repair process termed cardiac remodelling. Animal models provide a vital tool to investigate disease progression and study the remodelling process. MI and ensuing remodelling into heart failure can be replicated in animal models by occlusion of a coronary artery, commonly the LAD, inducing ischemia (Lindsey et al. 2018).

Injury induced by MI leads to an impairment in cardiac function, this can be assessed using echocardiography, a non-invasive technique that is widely used in rodent studies (Zacchigna et al. 2021). Significant impairment in cardiac function has been shown to occur early following MI in previous rodent studies, as shown by a reduction in EF (Darbandi Azar et al. 2014; F. Yang et al. 2002). Suggesting functional impairment may occur ahead of large changes in structure and cellular composition of the infarcted area.

Structural changes occur following MI as dead cardiomyocytes are removed and replaced over time by collagenous scar tissue (Prabhu and Frangogiannis 2016). The initial phase involving cellular infiltration as immune cells infiltrate the area in response to injury, the later phase characterised by the presence of fibroblast and collagen deposition. Assessment of the ultrastructure will facilitate investigation of other cell types that have a potential role in cardiac remodelling including telocytes and pericytes. There has been no comprehensive assessment of the temporal changes in cardiac structure, including ultrastructure, in rat hearts post-MI.

3.2 Aims

The aim of this chapter is to explore the temporal changes in cardiac function and structure over 4-weeks following MI. LV function will be measured by echocardiography and structural changes assessed by histology and electron microscopy.

3.3 Methods

Myocardial infarction was induced by LAD occlusion in adult male Wistar rats, animals were terminated at 3 time-points (3-days, 2-weeks, and 4-weeks) following surgery. Echocardiography recordings were taken prior to termination. Following termination hearts were cannulated on the Langendorff setup for sample collection and perfusion fixation.

3.3.1 Echocardiography

Echocardiography was performed on all animals prior to termination to obtain in vivo measurements of cardiac function using a Vevo 3100 machine (Visualsonics, Fujifilm). Briefly, animals were anaesthetised with isoflurane and placed supine on a heated platform. Electrocardiography recording was taken throughout, and echocardiography recordings were taken in m-mode in the parasternal long-axis view. Analysis was performed using Vevo Lab 3.1 software.

3.3.2 Histology

Cross-sectional tissue sections were cut for histological analysis to assess structural changes following LAD occlusion. H+E, EVG and Masson's Trichrome staining was completed, details in the methods section. After staining slides were scanned using a PreciPoint microscope and visualised on the Micropoint software. Image analysis was completed on Fiji-Image J software.

3.3.3 Electron Microscopy

A cross-section of fixed tissue was cut for electron microscopy analysis, from which smaller samples were taken from the infarct area, remote LV, and RV. Tissue samples were processed, sectioned, and stained by the Wolfson Bioimaging facility at the University of Bristol. Images were acquired using the FEI Tecnai 12 120 kV BioTwin Spirit transmission electron microscope with FEI Ceta 4k x 4k CCD camera.

3.4 Results

3.4.1 The effect of LAD occlusion on LV function

Induction of MI by LAD occlusion led to an impairment in cardiac function across 4-weeks post-MI. Ejection fraction and fractional shortening were significantly reduced following LAD occlusion, and by 4-weeks post-MI systolic and diastolic volumes were significantly increased compared to sham.

At all time-points ejection fraction was reduced following LAD occlusion in comparison to Sham (Figure 3-1A). Ejection fraction was unchanged between the sham groups, with values of 78.03 ± 2.7% at 3-days, 79.34 ± 1.6% at 2-weeks and 81.49 ± 1.9% at 4-weeks. LAD occlusion reduced the ejection fraction to 54.67 ± 6.2% at 3-days, 42.95 ± 3.9% at 2-weeks and 47.92 ± 2.5% at 4-weeks. These ejection fraction values are not significantly different between time-points in the LAD occlusion groups.

Fractional shortening showed the same pattern as ejection fraction, with a reduction at all time-points following LAD occlusion (Figure 3-1B). In the LAD groups fractional shortening was 29.71 ± 4.7% at 3-days, 22.24 ± 2.3% at 2-weeks and 25.9 ± 1.6% at 4-weeks compared to 47.82 ± 2.7%, 49.07 ± 1.6% and 53.18 ± 1.7% in sham groups respectively. There were no significant differences in fractional shortening between time-points in either the LAD occlusion or sham groups.

Systolic and diastolic volumes did change across time following LAD occlusion (Figure 3-1C-D). Systolic volume was increased at all time-points in the LAD group compared to sham, this effect was greater at 2- and 4-week time points, and not a significant change at 3-days. Systolic volume was increased in the 2-week LAD group compared to 3-day LAD group (211 ± 21.9 vs 94.6 ± 20.2µl), with no change from the 2-week to 4-week LAD group. Systolic volume did not significantly change across time in the sham groups. Diastolic volume was comparable between LAD and sham groups at the 3-day time-point but was significantly higher ($p<0.0001$) in LAD groups at 2-weeks and 4-weeks compared to sham. Between the LAD groups, diastolic volume increased at 2-weeks compared to 3-days (369.5 ± 22.6 vs 198.8 ± 24.2µl) but was unchanged between 2-weeks and 4-weeks. End systolic and end diastolic volume at 4-weeks post-MI have a strong relationship with infarct size. The same relationship is not seen with ejection fraction or fractional shortening (data in appendix, Figure 10-1).

Echocardiography of naïve animals showed no effect of sham surgery on cardiac function, across all four parameters there were no significant differences between any of the sham groups compared to naïve (Figure 3-1).

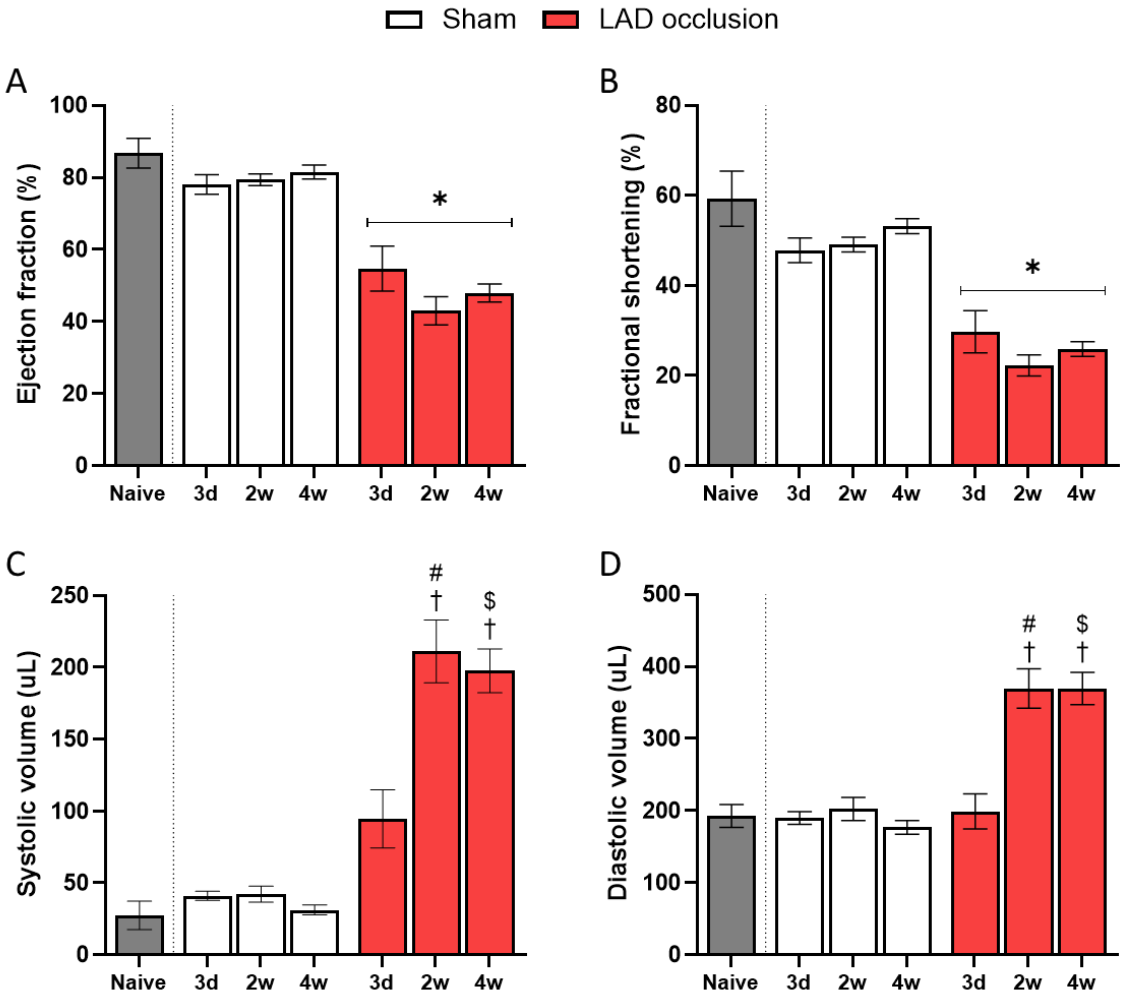

Figure 3-1 Changes in cardiac function over time following LAD occlusion

*Echocardiography measurements from Sham and LAD occlusion animals at 3-days (n=4, n=5), 2-weeks (n=6, n=5), and 4-weeks (n=23, n=22) post-surgery, and naïve animals (n=4). (A) Ejection fraction and (B) Fractional shortening, no interaction of group/time analysed by two-way ANOVA, main effect of group displayed *p<0.05. (C) Systolic volume and (D) Diastolic volume, significant interaction of group/time analysed using two-way ANOVA, post hoc analysis displayed († p<0.05 vs 3d LAD, # p<0.05 vs 2w Sham, $ p<0.05 vs 4w Sham). (A-D) Naïve compared to Sham in separate analysis by one-way ANOVA, p>0.05.*

3.4.2 The effect of LAD occlusion on cardiac structure

The figure below shows H+E staining of hearts subjected to LAD occlusion to induce MI (Figure 3-2). At the 2-week and 4-week time-points post-MI characteristic wall thinning can be observed in the LV. At the 3-day time-point there is more variation in the progression of the injury, wall thinning is not present in all hearts at this stage (Figure 3-2).

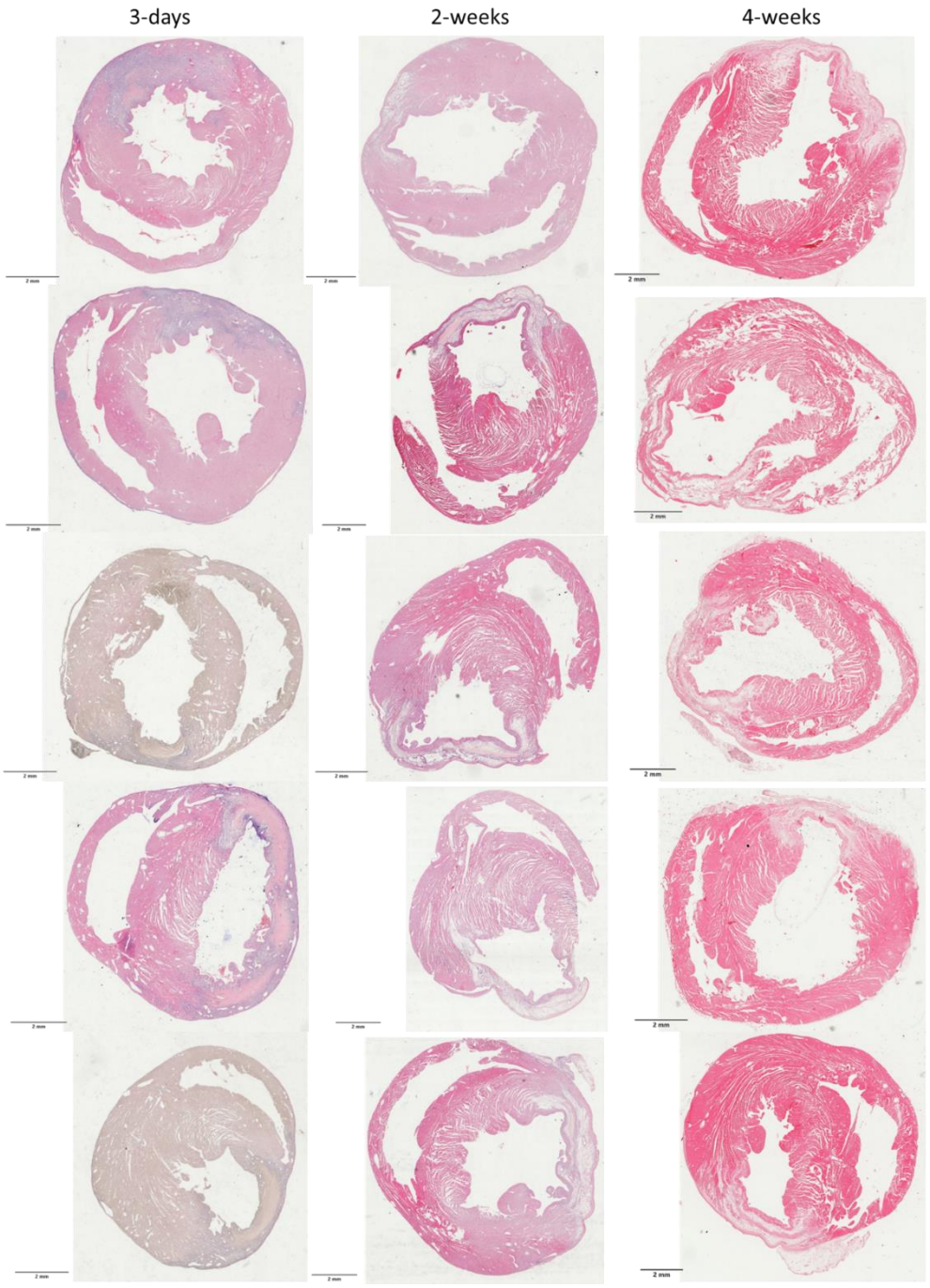

Figure 3-2 Cross-sectional H+E images of hearts 3-days, 2-weeks, and 4-weeks post-MI induced by LAD occlusion

3.4.2.1 Infarct size

Infarct size was measured as a percentage of the LV midline, there was no significant difference between infarct size at each time-point (Figure 3-3). There is a large amount of variation at the 3-day time-point as discussed above.

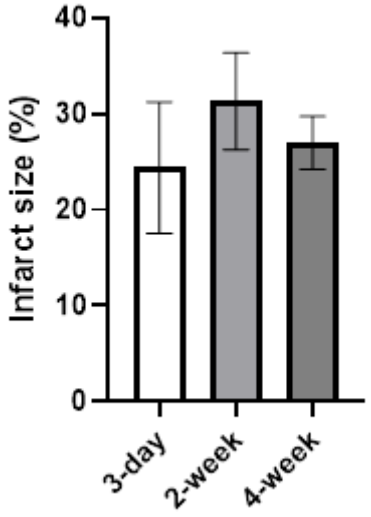

Figure 3-3 Infarct size

Infarct size, measured as a percentage of the LV midline, at 3-days, 2-weeks and 4-weeks post-MI induced by LAD occlusion. Analysed by one-way ANOVA, p>0.05.

3.4.2.2 Changes in composition of the infarct area

The composition of the infarct area changes over time, at the 3-day time-point cardiomyocytes are still present. Cellular infiltration can be observed indicated by the increase in nuclei density in the infarct and border areas. Some infarct areas show cardiomyocytes that appear devoid of nuclei, with cellular infiltration at the outer edges of the LV wall. This is not seen in remote areas of the LV in LAD hearts (Figure 3-4).

Over-time following LAD occlusion in the infarcted area the presence of cardiomyocytes is reduced and can be visualised by H+E staining (Figure 3-5A, D). By 2- and 4-weeks post-MI cardiomyocyte presence in the infarct area is reduced as cells are lost due to apoptosis and necrosis. Cellular infiltration can be observed in the infarct border zones at both 2- and 4-weeks post-MI (Figure 3-5B, E). The remote regions of the LV showed no changes compared to sham.

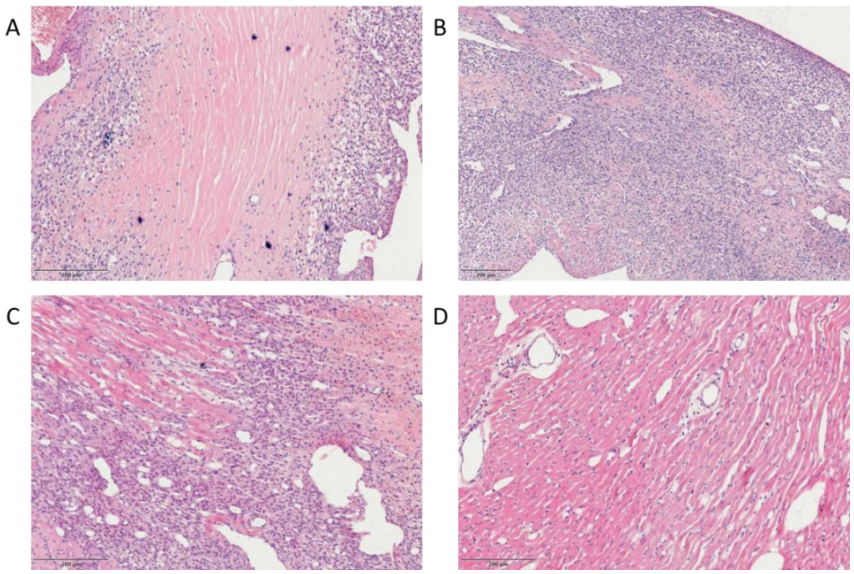

Figure 3-4 H+E images from hearts 3-days post-MI induced by LAD occlusion

Representative images from the infarct area (A-B), border zone (C) and remote area (D) from hearts 3-day post LAD occlusion.

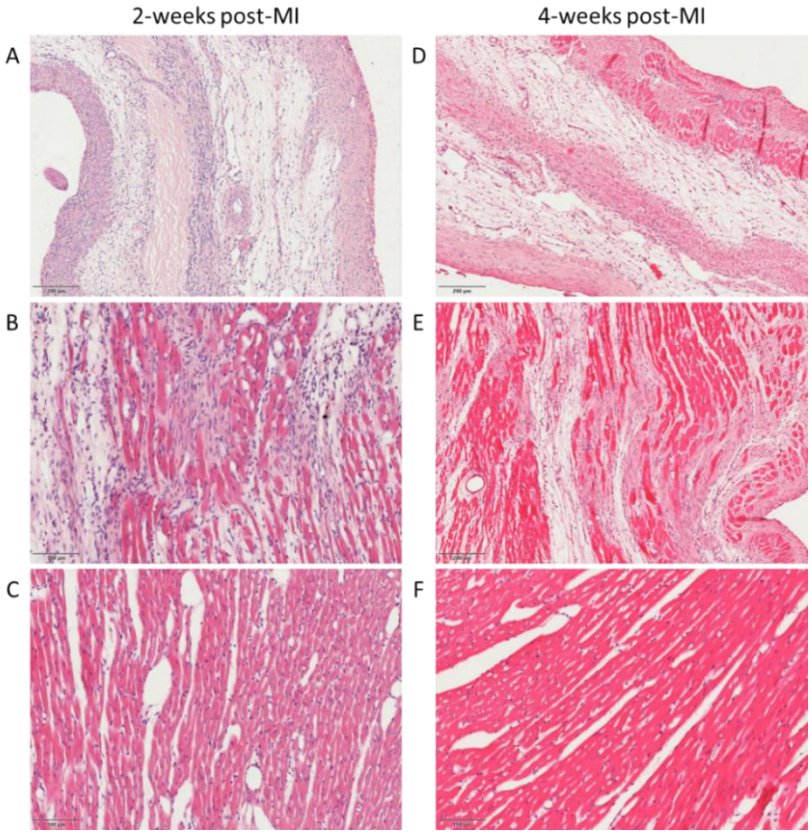

Figure 3-5 H+E images 2-week and 4-week post-MI

Infarct area (A, D), border zone (B, E) and remote areas (C, F) of the LV of rat hearts 2- and 4-weeks post-MI induced by LAD occlusion.

3.4.2.3 Structural changes in sham hearts

Largely sham hearts showed no structural changes, no wall thinning was observed at any time point (Figure 3-6). In a few sham hearts, cellular infiltration could be seen in the LV at the location where the LAD occlusion would be and may have been a response to the suture needle being inserted under the LAD vessel (Figure 3-7A). In one heart, 3-days post sham surgery, there appeared to be cardiomyocyte loss, but this was not seen in any other sham heart (Figure 3-7B).

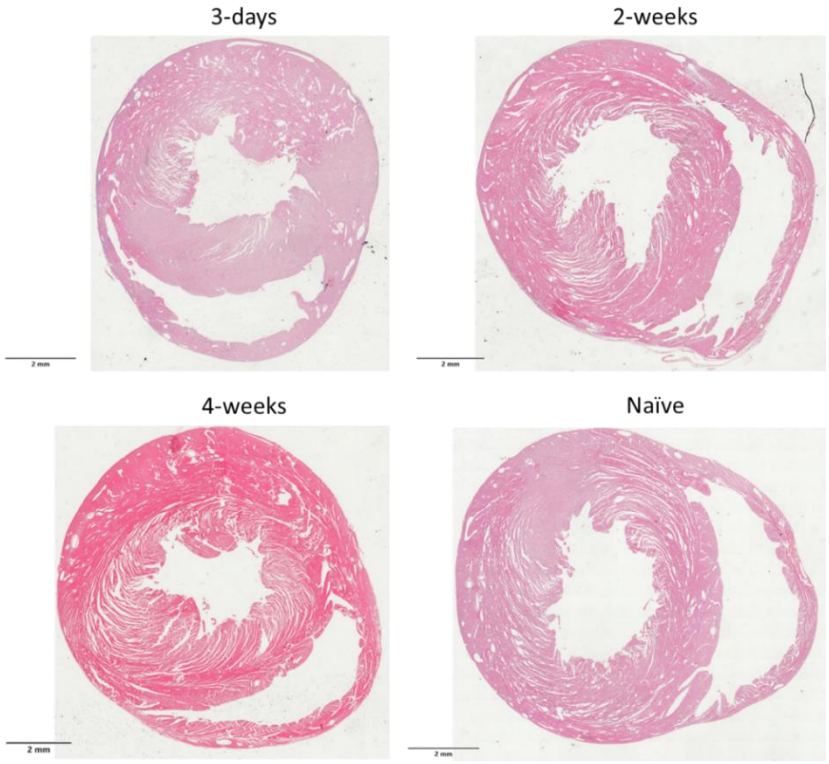

Figure 3-6 Representative H+E images from Sham animals at 3-days, 2-weeks, and 4-weeks post-surgery

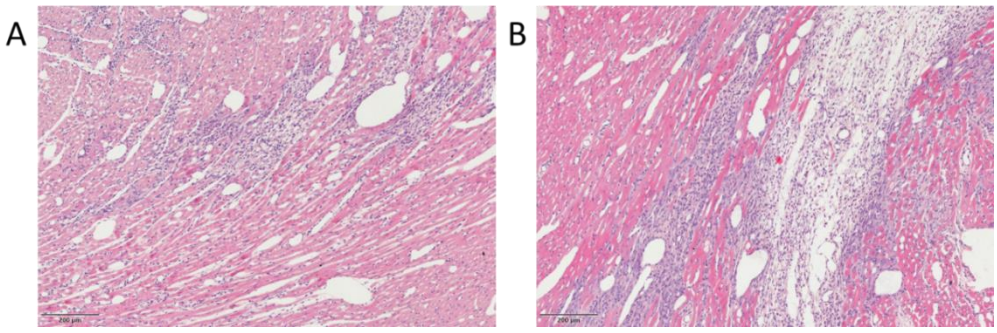

Figure 3-7 LV Sham hearts

3.4.2.4 Effect of LAD occlusion on LV lumen size

Measurements of the LV lumen area show increased LV lumen size at all time points following LAD occlusion (Figure 3-8). LV lumen area is expressed as a percentage of the total cross-sectional area of the heart to account for the increase in heart size over time.

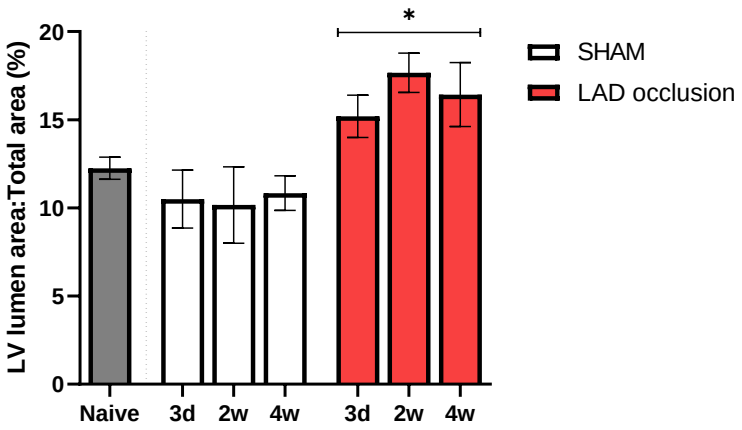

Figure 3-8 LV lumen

*LV lumen measurements from Sham and LAD occlusion animals at 3-days, 2-weeks, and 4-weeks post-surgery, and naïve animals. No interaction of group/time analysed by two-way ANOVA, main effect of group displayed *p<0.05. Naïve compared to Sham in separate analysis by one-way ANOVA, p>0.05.*

3.4.2.5 Effect of LAD occlusion on ventricle wall thickness

Measurements of wall thickness were made of the infarct area, remote LV wall, intraventricular septal wall, and the RV wall (Figure 3-9).

The infarct area of the LV had significantly reduced wall thickness in comparison to the LV of sham hearts at all time-points (Figure 3-9A). The thickness of remote regions of the LV was not significantly different. The septal wall had increased thickness in the LAD group compared to sham, with a greater increase at 2-weeks and 4-weeks. The thickness of the RV wall was significantly different between LAD occlusion and sham groups, with an increase in thickness over time.

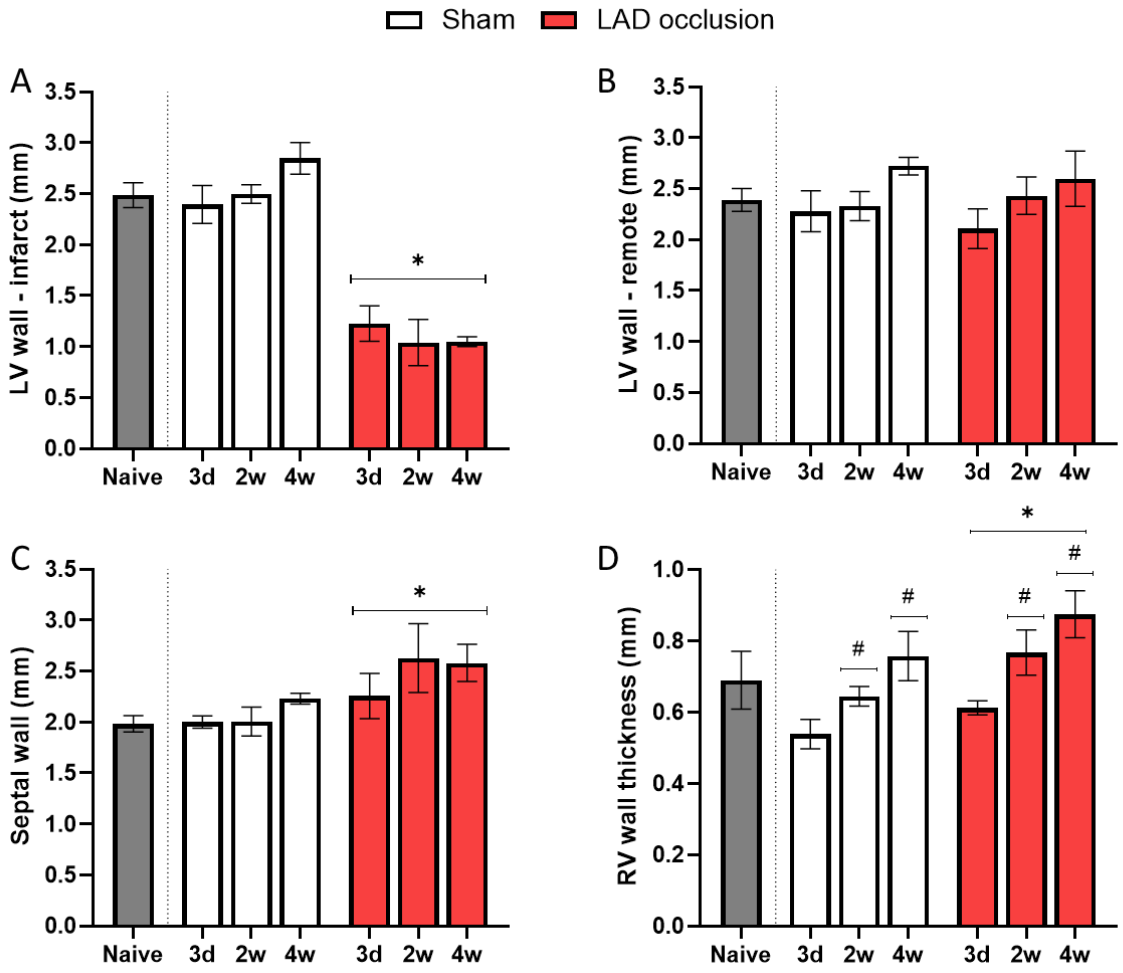

Figure 3-9 Wall thickness measurements

*Wall thickness measurements from Sham and LAD occlusion animals at 3-days, 2-weeks, and 4-weeks post-surgery, and naïve animals. (A) Infarct area of the LV, (B) remote area of the LV, (C) Septal wall, (D) RV wall. All analysed by two-way ANOVA for interaction of group/time ($p>0.05$), main effect of group *$p<0.05$ vs sham and time #$p<0.05$ vs 3d displayed. (A-D) Naïve compared to Sham in separate analysis by one-way ANOVA, $p>0.05$.*

3.4.2.6 ECM deposition in the infarct area

Collagen deposition occurs over time following LAD occlusion in the infarct area, as cardiomyocytes are lost from the area collagen levels increase. A small amount of collagen is beginning to be deposited by 3 days post-MI, the level of collagen measured in the LV of naïve hearts has been displayed for comparison (Figure 3-10). The percentage collagen in the infarct area at 3-days post-MI was 28.71 ± 3.6% and significantly increased at 2 weeks and 4 weeks post-MI to 66.83 ± 2.7% and 68.61 ± 2.1% respectively.

.

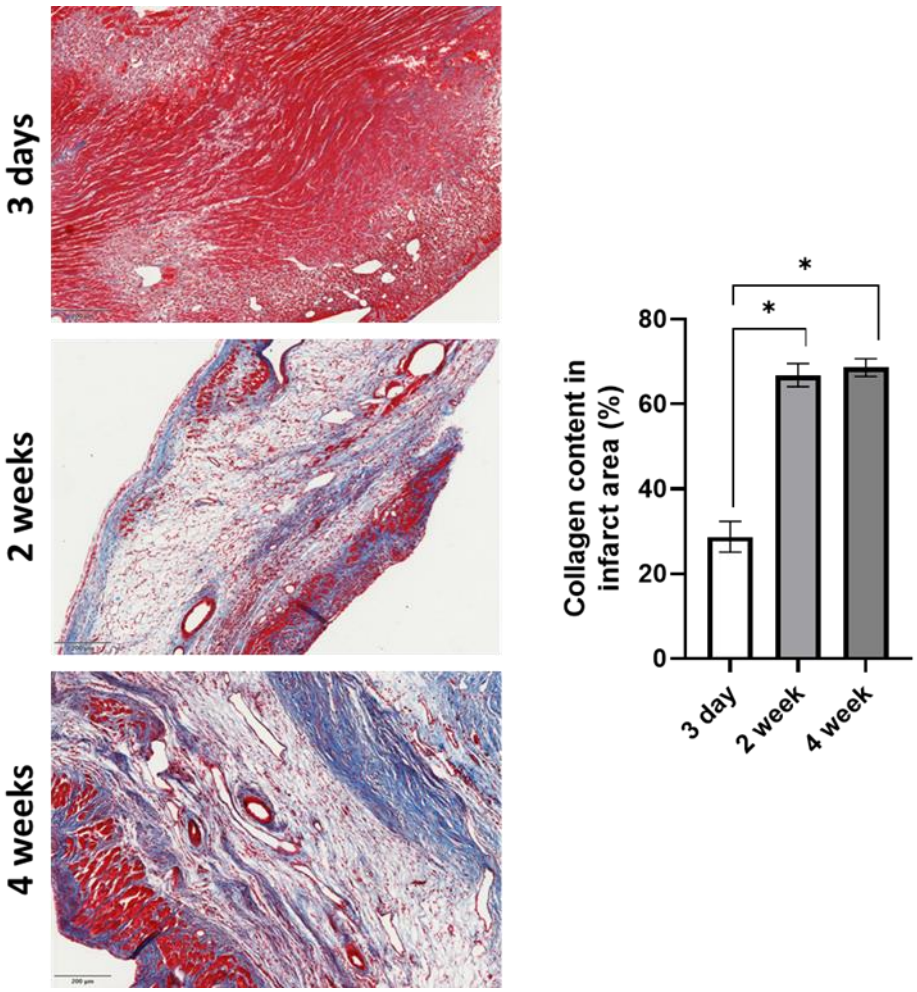

Figure 3-10 Collagen deposition in the infarct area

*Representative images of Masson's Trichrome staining showing collagen fibres in blue and quantification of collagen content in the infarct area of hearts 3-days, 2-weeks and 4-weeks post-MI induced by LAD occlusion. Analysed by one-way ANOVA with Tukey's post-hoc, *p<0.05*

In addition to increased collagen deposition, elastin fibres increase in the infarct area over-time which can be visualised by EVG staining. These fibres are not seen in naïve or sham hearts at any time-point (Figure 3-11).

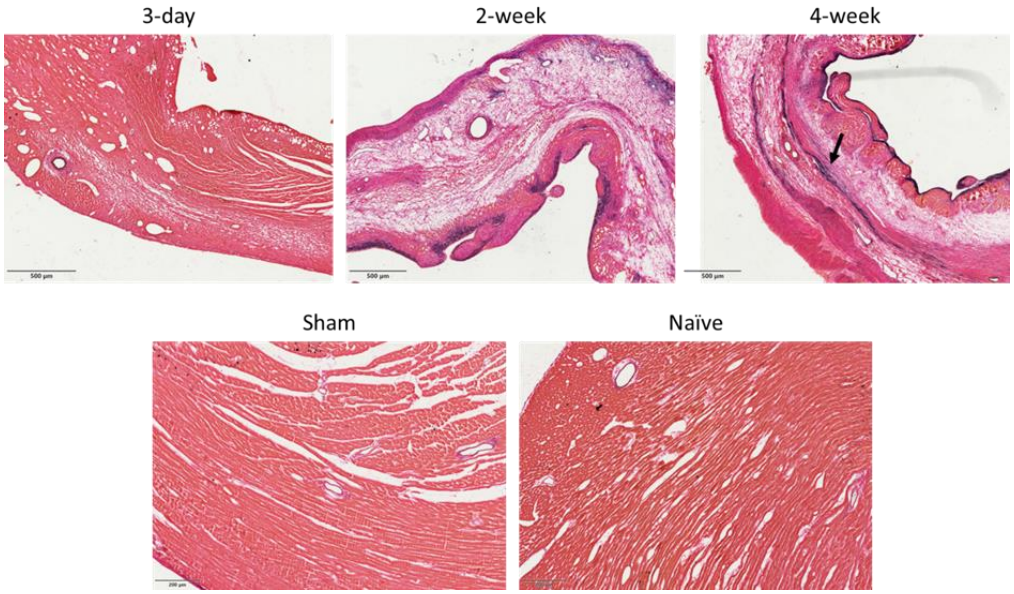

Figure 3-11 Elastin fibres in the infarct area

Representative images of EVG staining showing elastin fibres (dark purple, highlighted by arrow) in the infarct area of hearts 3-days, 2-weeks, and 4-weeks post-MI, as well as sham (4-week) and naive.

3.4.2.7 Collagen in remote areas of the LV

Diffuse collagen content in the remote region of the LV and septal wall in LAD occlusion hearts was also measured and compared to LV collagen content in sham hearts. As collagen is located around blood vessels, large blood vessels were avoided in the images analysed. Collagen content was slightly higher in the remote region of the LV wall in LAD occlusion groups at 2-weeks and 4-weeks post-MI in comparison to the corresponding sham group, but no significant differences were found (Figure 3-12B). In the septal wall collagen content was significantly increased in the LAD group at all time points, with a greater increase seen at 2-weeks and 4-weeks in comparison to the respective sham groups (Figure 3-12C). Comparison of the sham groups to naïve hearts showed no significant differences in the collagen content of the LV or septal wall (Figure 3-12).

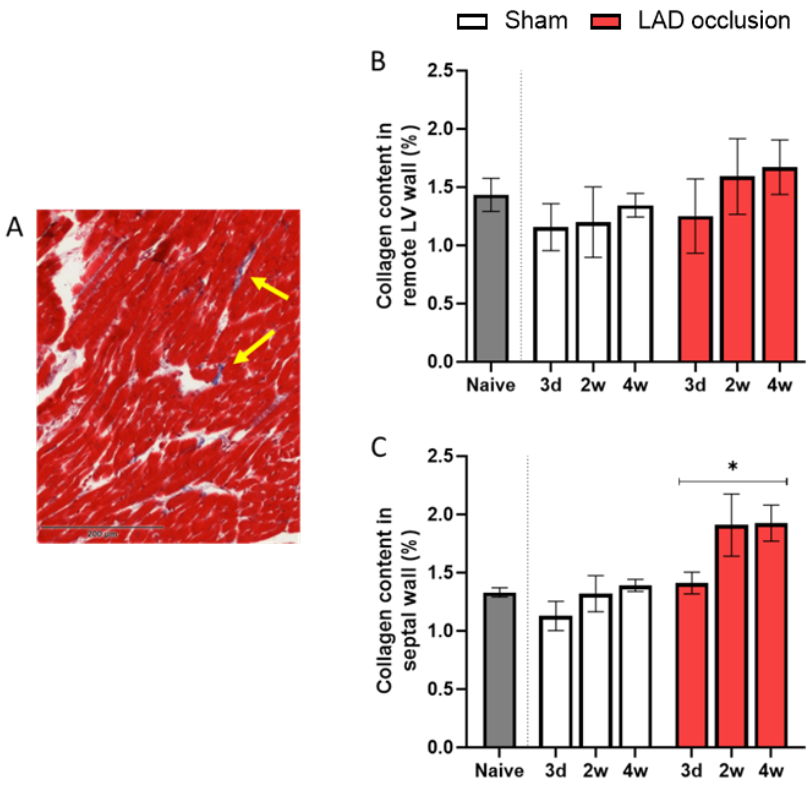

Figure 3-12 Collagen content in the remote regions of the LV

Image showing diffuse collagen in the remote LV (A). Collagen content from remote LV wall (B) and septal wall (C) of Sham and LAD occlusion animals at 3-days, 2-weeks, and 4-weeks post-surgery, and naïve animals. Analysed by two-way ANOVA for interaction of group/time ($p>0.05$), main effect of group displayed $*p<0.05$. Naïve compared to Sham in separate analysis by one-way ANOVA, $p>0.05$.

3.4.3 The effect of LAD occlusion on the ultrastructure of the heart

The ultrastructure of the heart can be examined using electron microscopy. Different areas of the heart were examined for changes in ultrastructure.

3.4.3.1 Infarct zone

The infarct area shows progressive remodelling across time following LAD occlusion, with a loss of cardiomyocytes replaced with ECM components. At 3-days post-MI cardiomyocytes are still present in the infarct area, some are intact but largely myocytes are disrupted with evidence of damaged mitochondria. There is evidence of immune cells within the blood vessels and in the extracellular space. In the extracellular space there is evidence of fibroblasts and other infiltrating cells, as well as extensive

cellular debris (Figure 3-13). At 2-weeks, there is still evidence of some cardiomyocytes although largely the infarct area is comprised of fibroblasts and deposited collagen fibres (Figure 3-14). By 4-weeks the infarct area is primarily composed of deposited collagen fibres, the presence of fibroblasts is reduced compared to 2-weeks (Figure 3-15). There is evidence of telocytes, cellular structure with elongated telepodes, in the infarct area at both the 2- and 4-week time points (Figure 3-14 and Figure 3-15).

3.4.3.2 Infarct border zone

The border zone was assessed at the 4-week time-point. The border zone represents the area where infarcted tissue is connected to the non-infarcted areas. There is evidence of cardiomyocytes interspersed with collagen fibres and fibroblasts, as well as telocytes (Figure 3-16). There is some disruption of mitochondria in the cardiomyocytes in this area.

3.4.3.3 LV of sham hearts

Images from the LV of sham hearts show no evidence of disruption in the cardiomyocytes and no signs of cellular infiltration (Figure 3-17). There is some evidence of fibroblast presence and collagen deposition, but it is located around vasculature indicative of perivascular fibrosis (Figure 3-17D). There was no evidence of immune cells in the sham hearts 3-days post-MI.

3.4.3.4 Remote areas of the LV in LAD hearts

Remote areas of the LV appear unaffected following MI, with ultrastructure similar to that seen in sham hearts. Cardiomyocytes are intact, densely packed with mitochondria and there is no signs of cellular infiltration or fibrosis.

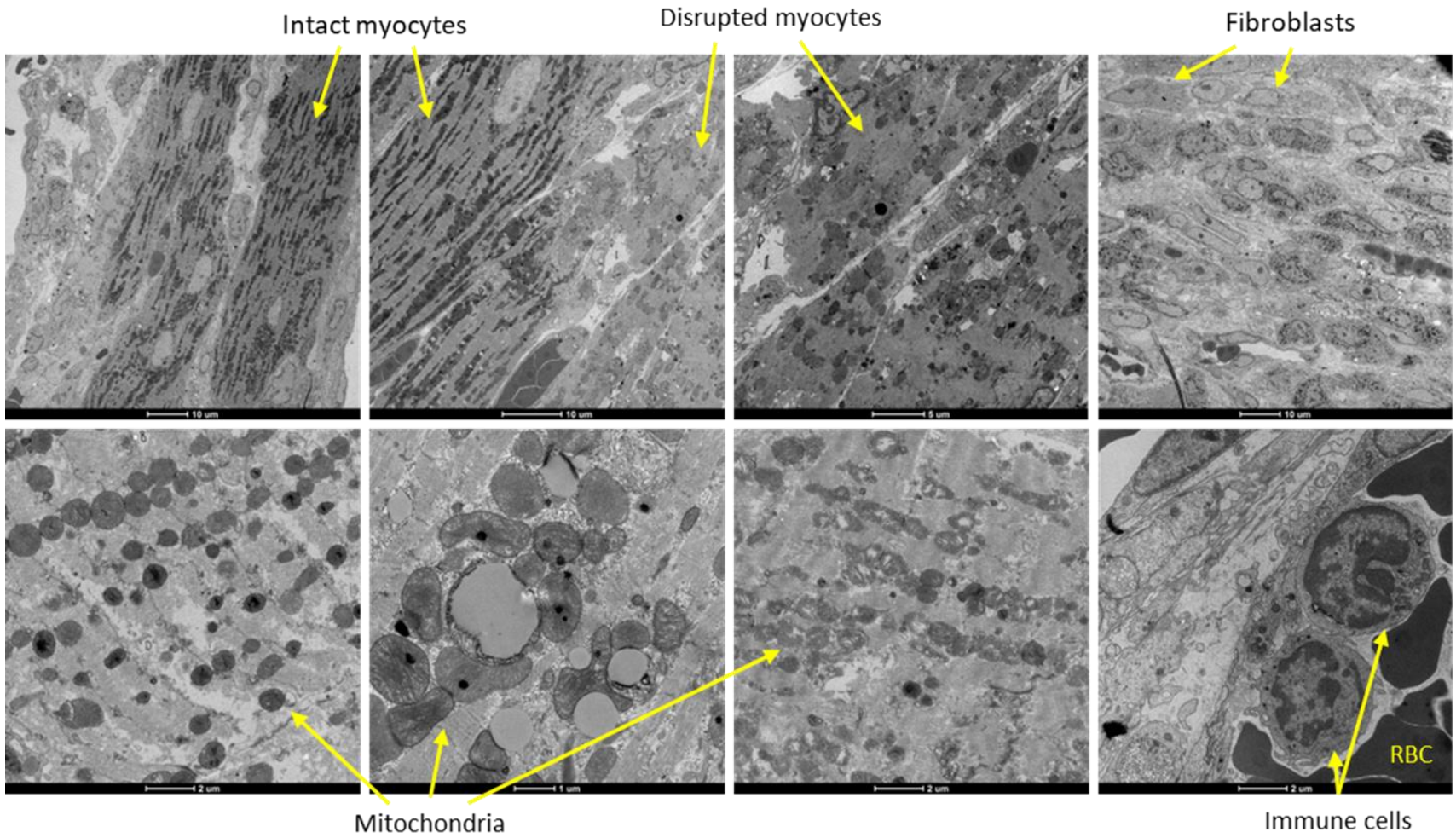

Figure 3-13 Infarct area of LV 3-days post-MI

Representative images from infarct area 3-days post-MI induced by LAD occlusion. Annotations show intact and disrupted myocytes, fibroblasts, mitochondria and immune cells.

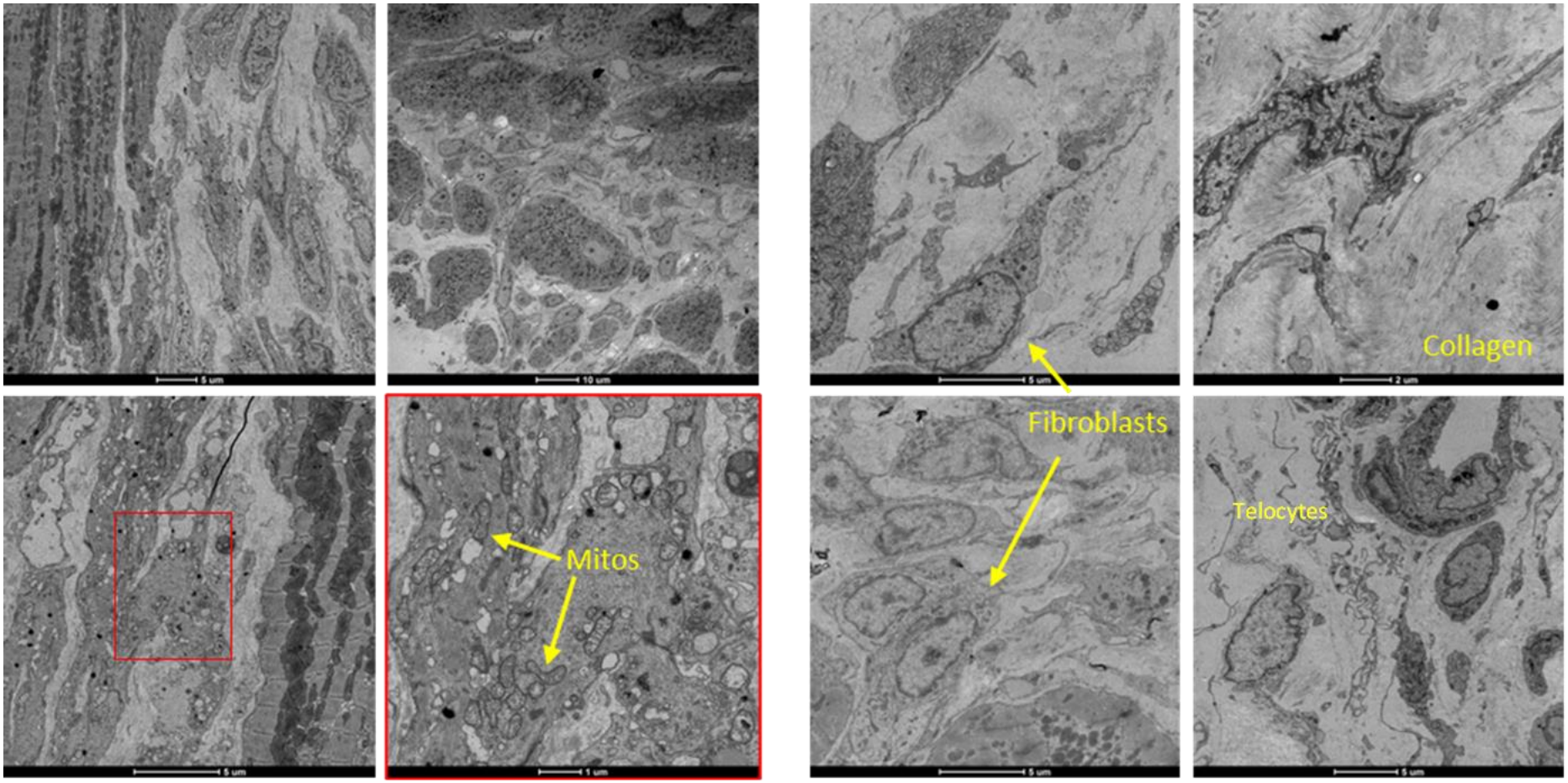

Figure 3-14 Infarct area of LV 2-weeks post-MI

Representative images from infarct area 2-weeks post-MI induced by LAD occlusion. Annotations show fibroblasts, mitochondria and collagen deposition.

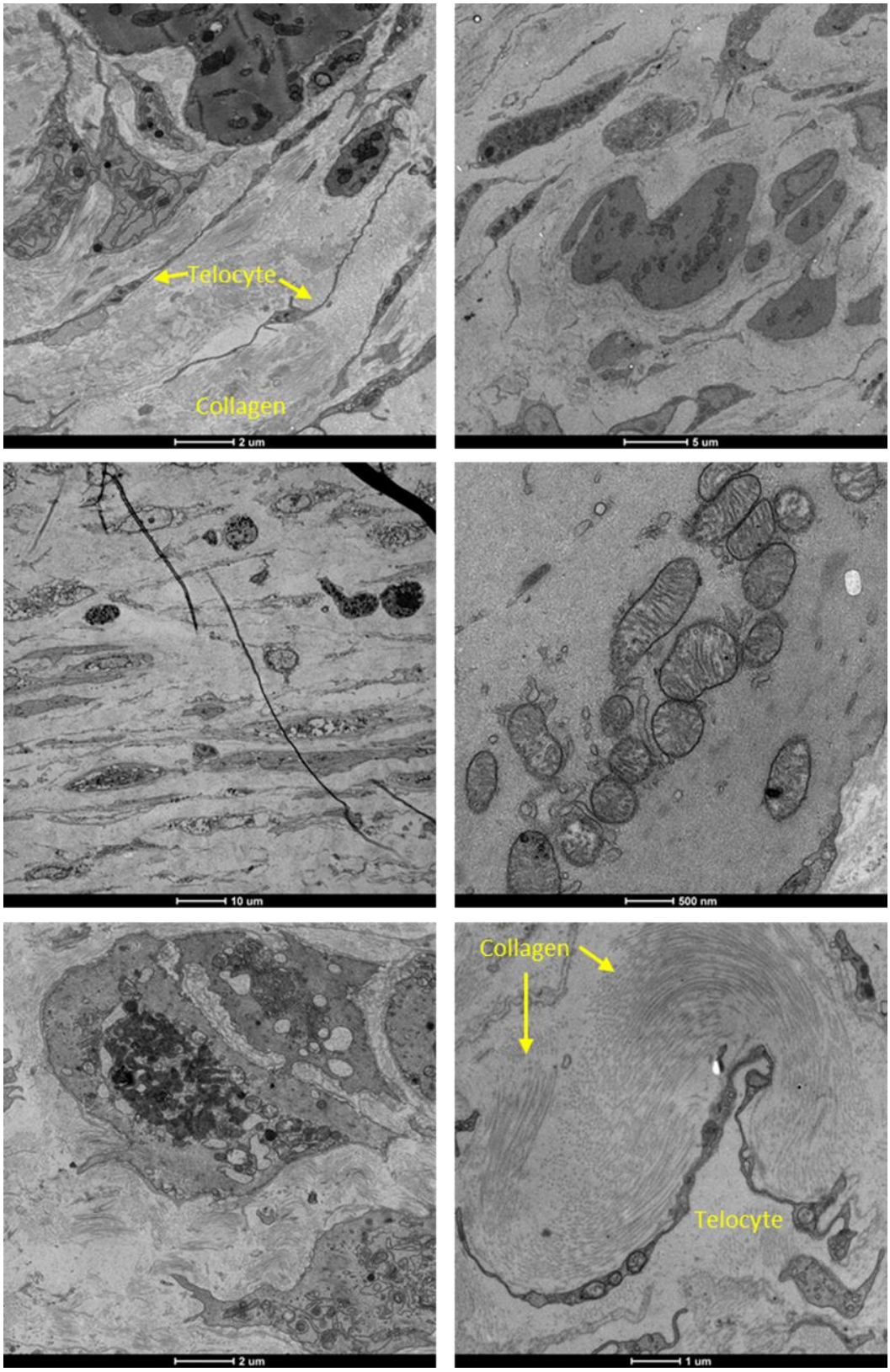

Figure 3-15 Infarct area of LV 4-weeks post-MI

Representative images from infarct area 4-weeks post-MI induced by LAD occlusion. Annotations show telocytes and collagen deposition.

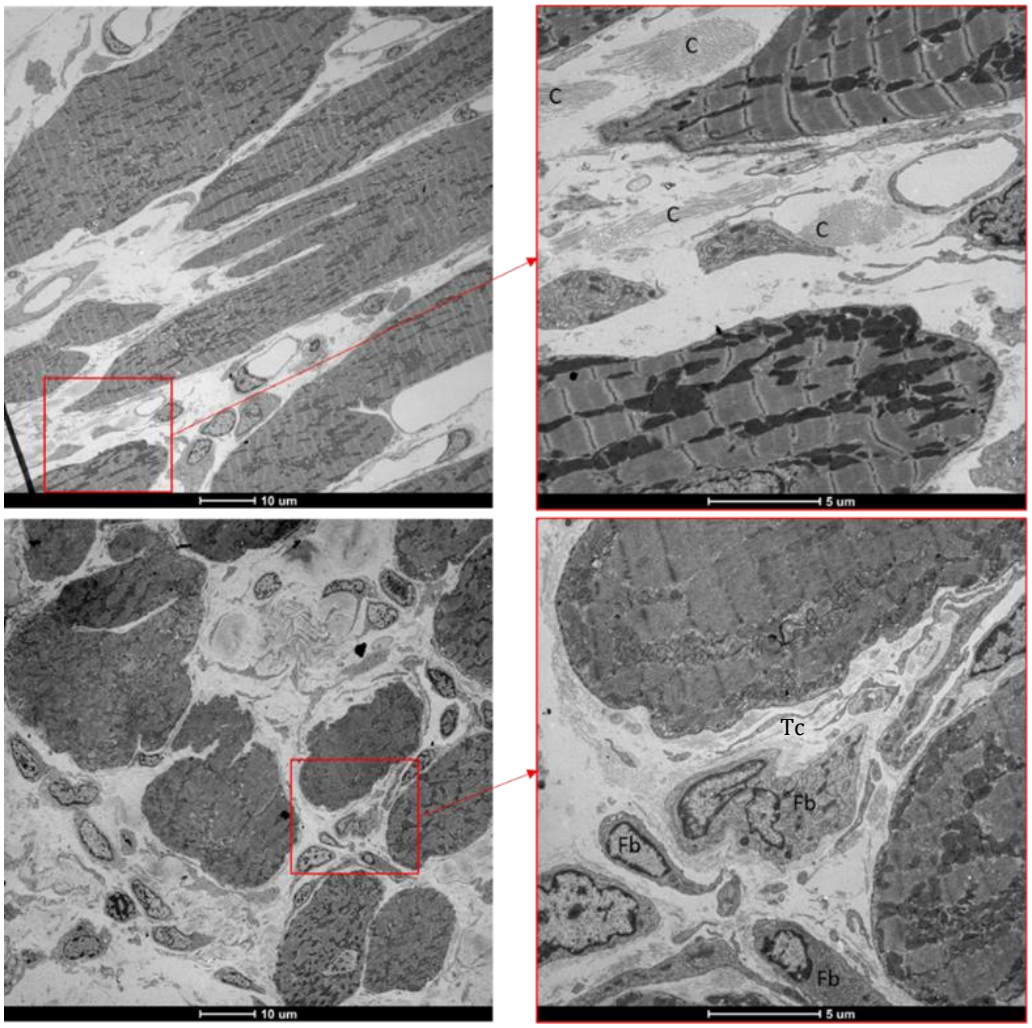

Figure 3-16 Infarct border zone 4-weeks post-MI

Images from the LV border zone 4-weeks post-MI, cardiomyocytes can be seen interspersed with collagen (C) depositions, fibroblasts (Fb) and telocytes (Tc).

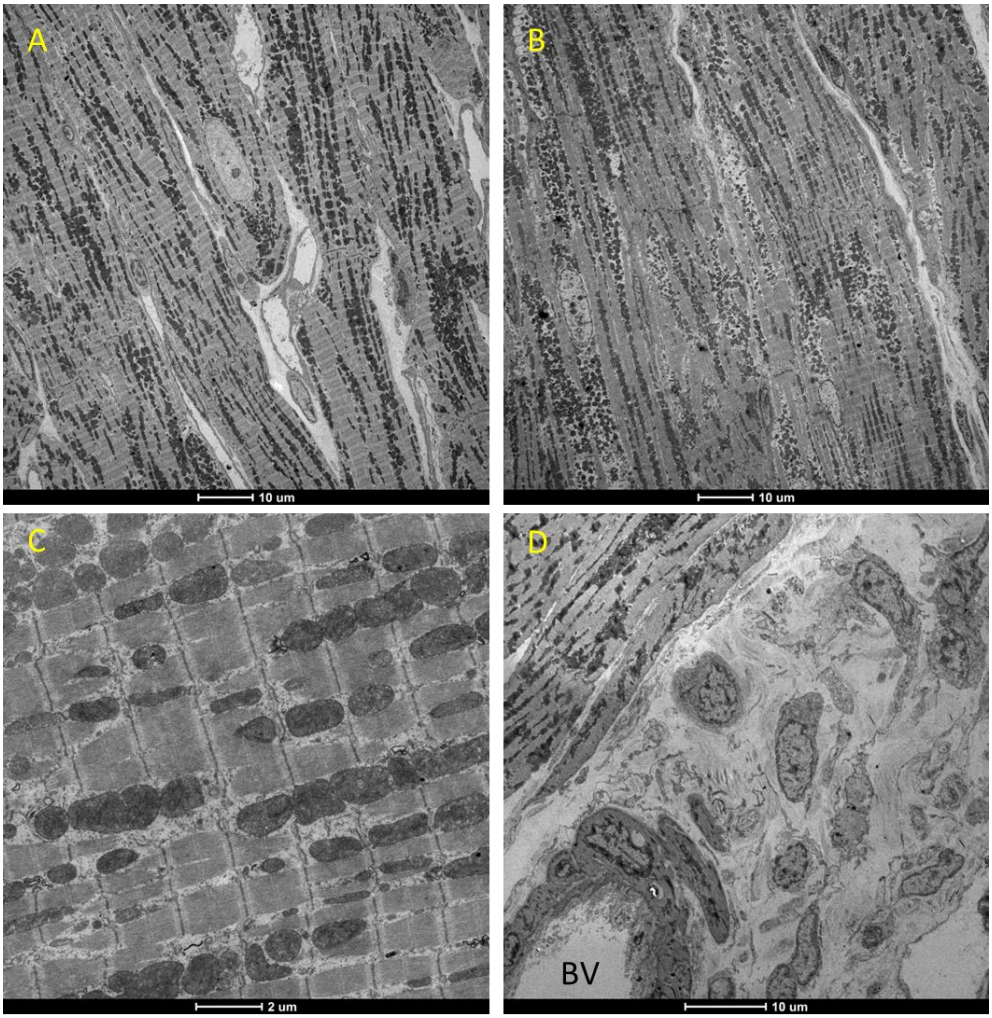

Figure 3-17 Sham LV

Representative images from the LV of sham hearts 3-days (A), 2-weeks (B) and 4-weeks (C) after surgery. (D) Evidence of fibroblasts and collagen deposition around a BV.

3.4.4 The effect of LAD occlusion on mitochondrial morphology

At 3-days post-MI mitochondria in the cardiomyocytes in the infarct area show signs of distress and disruption, with a rounded morphology and cristae disruption. Mitochondria in the remote area of the LV in LAD hearts and in sham hearts show no signs of disruption (Figure 3-18). At 2- and 4-weeks post-MI cardiomyocytes are less present as shown above, in the few disrupted cardiomyocytes still present mitochondria show reduced cristae density (Figure 3-15). Mitochondria within cardiomyocytes in the border zone 4-weeks post-MI were healthy with little sign of cristae disruption (Figure 3-16). Mitochondria in sham and naïve hearts, as well as remote LV areas of LAD hearts, at the later time-points show no evidence of damage.

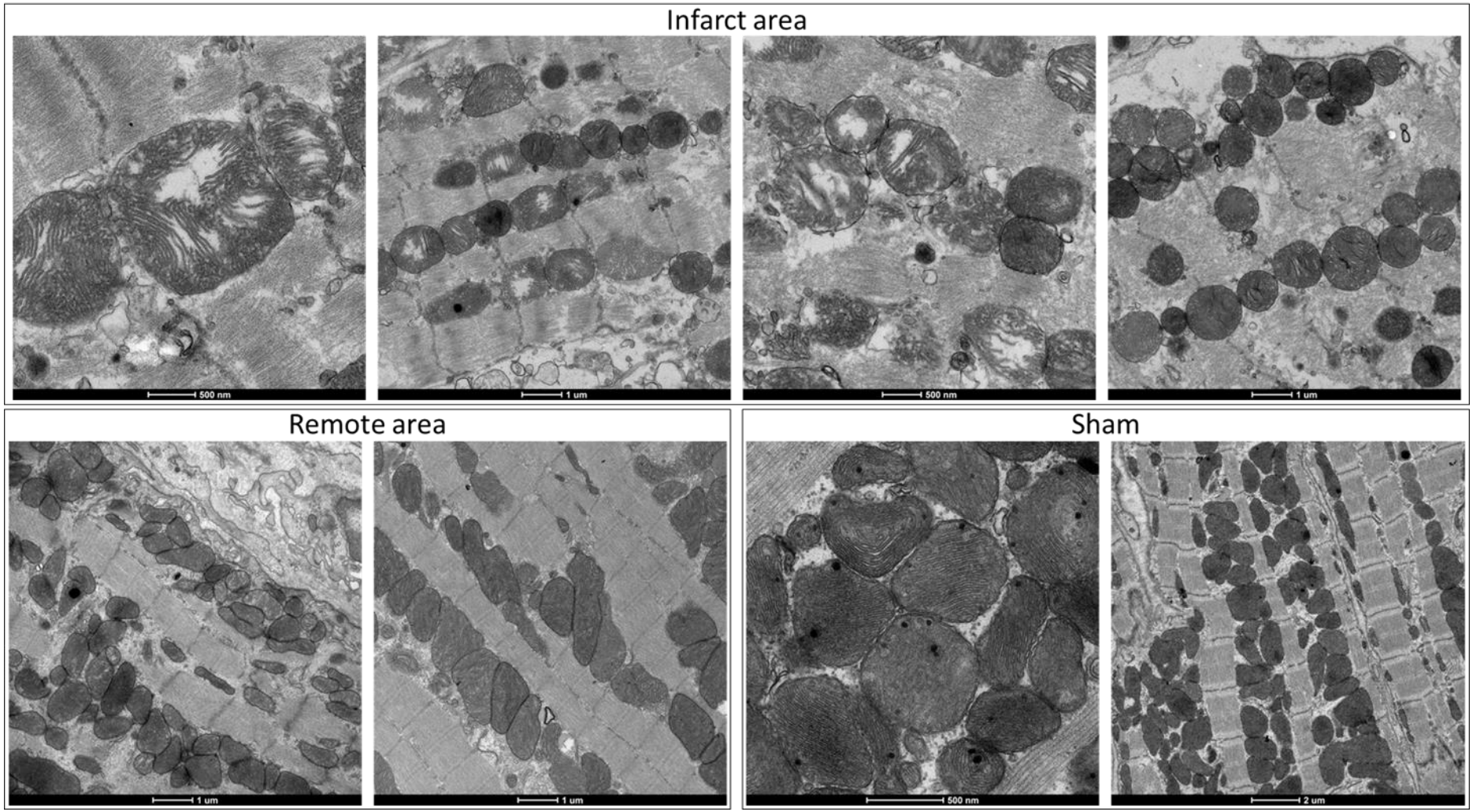

Figure 3-18 Mitochondria in hearts 3-days after LAD occlusion or sham surgery

Images of mitochondria from the infarct area and remote area of the LV following LAD occlusion, and from the LV of sham hearts

3.5 Discussion

3.5.1 Key findings

- Functional changes in the LV occur early after MI, ejection fraction and fractional shortening are significantly reduced 3-days post-MI. Systolic and diastolic volumes increase between 3-days and 2-weeks post-MI, with no further change at 4-weeks.
- Structural changes are present early after MI, with wall thinning and increased LV lumen size present by the 3-day time-point.
- Extensive collagen deposition in the infarct area occurs by 2-weeks post-MI, and reactive fibrosis in remote areas of the LV can be observed at 4-weeks.
- Telocytes appear in the infarcted area at 2-weeks post-MI.
- Sham hearts show little functional or structural changes at any time point in comparison to naïve hearts.

3.5.2 Functional impairment evident 3 days after MI

The induction of MI, and the progression towards heart failure, following LAD occlusion was confirmed in this study by echocardiography. Animals in the LAD occlusion group had significant changes in all measures of cardiac function by 4-weeks post-MI. The fall in ejection fraction and fractional shortening was present early after MI at 3-days with little change at subsequent time-points. This supports previous findings in rats reporting no change in fractional shortening from 7-days to 2-months following the initial decline (Cieniewski-Bernard et al. 2008). Decline in cardiac function occurs quickly after MI due to the detrimental effects on cardiomyocytes impairing contractility. Previous studies have shown this early drop in ejection fraction and fractional shortening, occurring within the first 24 hours post-MI in rat hearts (Bai et al. 2020; Yokota et al. 2020). Furthermore, reduction in ejection fraction is associated with clinical outcome in patients (Chew et al. 2018).

Increased end systolic and diastolic volumes also change over time following MI, systolic volume increased slightly by the 3-day time-point with the diastolic volume increase later. Previous study using magnetic resonance imaging saw the same pattern in functional impairment following MI in rats, with EF dropping at the 3-day time-point with little further change to 33 days, whereas diastolic volume increased between 3-days and 33-days (Tougaard et al. 2022). Increased end systolic volume is expected

with a decline in ejection fraction, a greater blood volume resides in the ventricles following contraction. Along with increased end diastolic volume it also reflects LV dilation. The increase in pre-load will exert a greater pressure on the LV wall, triggering stronger cardiac contraction, as described by Frank-Starling law. To facilitate increased contraction the remaining healthy cardiomyocytes may become hypertrophied to compensate (White et al. 1987). End systolic volume may provide a better predictor of survival over ejection fraction (White et al. 1987). There was a stronger relationship between end systolic volume or end diastolic volume against infarct size than the other echo parameters in this study.

3.5.2.1 Cardiac function in sham compared to naïve hearts

Echocardiography recordings for sham and naïve animals were comparable to previous recordings in Wistar rats (Darbandi Azar et al. 2014; Esmaeili et al. 2017). Importantly the naïve animals included in this work had comparable LV function to Sham animals indicating no adverse effects of sham surgery on functional parameters, this agrees with previous work in mice (Iyer et al. 2016).

3.5.3 Structural changes after MI

Following ischemia cardiomyocytes die as a consequence of the metabolic and ionic changes that occur. This triggers an influx of immune cells to clear the cellular debris, as well as fibroblasts and other cell types involved in the cardiac remodelling process. Substantial cellular infiltration was observed early after MI, as visualised by H+E staining. Looking at the ultrastructure helps to visualise the cells present in this area, immune cells could be observed along with fibroblasts. 3-days post-MI in rat heart may therefore be the point at which the immune cell response is becoming suppressed and synthesis of ECM by fibroblasts is occurring. Some collagen deposition can be observed early after MI but does increase following the 3-day time-point. At later time-points the infarct area is primarily comprised of ECM and cellular debris with presence of cell types involved in the remodelling process, fibroblasts and telocytes which are discussed below.

As cardiomyocytes are lost following ischemia the integrity of the LV wall is comprised, and wall thinning occurs in the affected area. This can be observed from the 3-day time-point, however the extent of thinning at the 3-day time-point is variable. This could be because infarct expansion is still occurring at this stage, these hearts still

have extensive cellular infiltration suggesting the immune response and phagocytosis of damaged myocytes is ongoing. Progression of wall thinning has previously been measured in rat hearts following MI, finding a progression of wall thinning over time (Fishbein et al. 1978). As infarct expansion and wall thinning occurs, the LV becomes dilated. This can be reflected by the progressive increased in LV diastolic volumes on echocardiography but is also seen as an increase in LV lumen size. LV lumen size was increased across all time-points, this measurement was normalised to the total area of the heart which increased over time in both LAD and sham groups (data not shown).

3.5.4 Structural changes in remote regions of the heart after MI

Remote areas of the LV containing healthy myocardium are affected in response to ischemic injury as changes occur to compensate for the decline in cardiac function. The finding of increased collagen presence in the septal wall alongside an increase in septal wall thickness at the later stages of remodelling indicates some changes to MI in the remote areas structurally. Increased interstitial fibrosis and myocyte size has been observed previously 8-weeks post-MI in rats supporting this finding (Lal et al. 2005). Hypertrophy of remote regions of the heart occurs to increase contractile function to compensate for the decline in cardiac function and try to maintain cardiac output.

3.5.5 Structural changes in sham and naïve hearts

Sham surgery does not involve occlusion of the LAD, but the suture needle is still passed under the LAD which may induce some damage. Overall sham hearts showed little evidence of damage or structural changes, there was no wall thinning or development of scar tissue. Cellular infiltration occurs in the early time-point after LAD occlusion, partly reflective of an immune response to injury. There was a couple of sham hearts in which a small amount of cellular infiltration and damage in the LV was observed, which is potentially the site of entry of the suture needle. There was no evidence of immune cell presence in the EM images, and no increase in fibroblast presence, collagen deposition, or observed changes in mitochondria.

3.5.6 Extracellular matrix deposition and fibroblast presence

Collagen and the ECM deposition is crucial for the formation of scar tissue in the infarct area. As has been shown previously, as well as in this work, increased collagen deposition in the infarct scar is seen over time (Cleutjens et al. 1995; Lindsey and Zamilpa 2012). Collagen is deposited by fibroblast and their activated form

myofibroblasts, providing tensile strength to the infracted area to prevent excessive dilation or rupture. Collagen content in the infarct area is unchanged between 2-weeks and 4-weeks, suggesting a plateau of collagen deposition. As the remodelling process progresses collagen fibres become cross-linked as part of scar maturation. Therefore, there may be differences in cross-linkage of collagens at these later time-points. Furthermore, several collagen subtypes exist, the main fibrillar types present in the heart are collagen type I and III. But there is evidence to suggest non-fibrillar collagen subtypes contribute to the remodelling process (Shamhart and Meszaros 2010). Further assessment with specific staining could highlight the collagen types present in the infarct area at each time-point.

Aside from collagen, elastin is a major component of the ECM cross-linking with fibrillin to form elastic fibres. Elastin fibres facilitate elasticity and recoil and are highly expressed around blood vessels and other elastic tissue (Kielty et al. 2002). Presence of elastin fibres increases over time following MI, and in the infarcted area elastin fibres provide elasticity that is absent following the loss of cardiomyocytes and helps to prevent against excessive LV dilation and rupture. Increasing the elastin content of infarcted tissue is reported to be beneficial against infarct expansion (Mizuno et al. 2005).

An increase in collagen content was measured in the septal wall of LAD hearts 4-weeks post-MI. This agrees with previous findings of increased collagen in non-infarcted regions following MI (Cleutjens et al. 1995; Kim et al. 2010; Wei et al. 1999). Collagen subtypes, and other components of the ECM present in the apex of the heart will be explored later in the proteomic studies completed.

3.5.6.1 Temporal change in fibroblasts in the ECM

Cardiac fibroblasts are responsible for the deposition of ECM, during the remodelling process this is crucial for the formation of scar tissue in the infarct region. Cardiac fibroblasts are highly expressed in the heart and regulate ECM turnover under normal conditions, however during the remodelling they response to the increase in pro-inflammatory cytokines. Fibroblasts become activated to myofibroblasts which possess a contractile phenotype, with greater ability to migrate and proliferate, and secrete ECM components (Porter and Turner 2009). Therefore expectedly, cardiac fibroblast presence is increased in the infarcted area, seen across all time-points in this

study. Fibroblasts can be identified early after infarction, present in the infarct area by the 3-day time-point. Large numbers of fibroblasts can be seen by 2-weeks post-MI, and they are still present in the infarct area to a lesser extent 4-weeks post-MI, as well as in the border zone. This pattern of fibroblast presence is in agreement with previous findings, where fibroblast presence post-MI persisted to 8 weeks (Sun and Weber 1996).

3.5.7 Mitochondria disruption is evident early after MI

Severe disruption of mitochondria is observed in the infarct area early after MI at 3-days. Mitochondria are central to ischemic injury and the mediation of cell death. At later time-points cardiomyocyte presence is limited in the infarcted area therefore mitochondria are less present. There is some evidence of disrupted mitochondria in the remaining cardiomyocytes in the border zone at 4-weeks post-MI, however this is not seen in every heart. Investigation of mitochondria in heart failure following MI in rats has previously been reported, one study observed disruption to cristae density up to 6 months after MI in the border zone in rat hearts (Stepanov et al. 2017), with others reporting increased mitochondrial number and reduced size at later stages of remodelling (L. Chen et al. 2009; Liu et al. 2014). However, in these previous studies the representative images do not show relaxed myocardium and the presence of contraction can alter the mitochondrial morphology. Mitochondria are the powerhouses of the cardiomyocytes producing energy for the cellular function, therefore disruptions in mitochondria will have significant impact on the cell. Furthermore, disrupted swollen mitochondria may be prone to rupture which can release pro-apoptotic factors initiating cell death.

Contrary to previous reports, in this study there did not appear to be any changes in mitochondrial morphology in the LV non-infarcted tissue (Stepanov et al. 2017). Mitochondria in cardiomyocytes can be characterised into three populations: subsarcolemmal, interfibrillar and perinuclear. Each providing energy for different cellular processes and possessing slightly different structural characteristics (Hollander et al. 2014). Further analysis into the mitochondria size and number in the remote areas of the LV may reveal any subtle changes within each distinct mitochondrial population not evident from visual assessment of the images.

3.5.8 Telocytes are present in the infarcted area by 2-weeks post-MI

Telocytes are a relatively newly identified cell type, the term telocytes being coined in 2010, they are characterised by thin prolongations called telepodes extending from the main cell body (Faussone Pellegrini and Popescu 2011; Kostin 2016; Popescu and Faussone-Pellegrini 2010). In this study telocyte structures were identified in the infarct area at 2-weeks and 4-weeks post-MI. The role of these cells is still under debate, and the involvement of telocytes in MI is inconclusive (reviewed by (Hostiuc et al. 2018)). There is evidence to suggest telocytes may be involved in neo-angiogenesis in the infarcted heart (Manole et al. 2011). Previous work in rat hearts post-MI has shown a decrease in expression of telocytes following MI up until the 4-week time-point (B. Zhao et al. 2013). Decreased presence of telocytes is also reported in human failing hearts (Richter and Kostin 2015). My work shows presence in the infarcted area however further investigation into control hearts is needed to determine if this is an increase in number post-MI. Reintroduction of telocytes into the heart at the time of MI induction was successful in minimising infarcted area and restore LV function (B. Zhao et al. 2013), highlighting an importance of this cell type in the remodelling process. The telocytes identified in this study were often colocalised with deposition of collagen given their presence in the infarct area, this may suggest an involvement in cardiac fibrosis. Cardiac telocytes share similar characteristics with pericytes in the heart, another cell type not well characterised but suggested to be involved in cardiac repair processes. Pericytes have a physiological role in vascular homeostasis, however they may also contribute to inflammation, fibrosis and tissue repair following MI (Alex and Frangogiannis 2019). Pericytes implicated in myofibroblast activation and collagen deposition in other organs, but this has not conclusively been shown in cardiac fibrosis.

3.6 Summary

Ischemic infarction in the heart results in a decline in cardiac function as well as dramatic structural changes. The progression of cardiac remodelling is a dynamic process, involving cellular death followed by deposition of ECM to support the infarcted area preventing cardiac rupture. This work shows a decline in cardiac function early following MI, with a progressive increase in cardiac volumes. Additionally, it provides information on the structural changes that occur across the remodelling process in rat hearts post-MI. This work provides evidence of cardiac telocytes being present in the

infarcted area, which may have a role in the cardiac remodelling process. Whether these functional and structural changes are also seen at the molecular level will be addressed in the next chapter.

4 Proteomic changes in the heart over time following myocardial infarction

4.1 Introduction

The process of cardiac remodelling following MI is associated with functional and structural changes as discussed in the chapter above. It is important to understand the changes driving this cardiac remodelling at the molecular level. Quantitative proteomic analysis facilitates the understanding of changes in protein expression, enabling investigation of the changes occurring as a result of MI. In addition, post-transcriptional modifications in the form of phosphorylation can be assessed by the use of phospho-proteomic analysis (Gomez-Mendoza et al. 2021; O'Reilly et al. 2018). Post MI cardiac remodelling involves dramatic structural & functional changes in the infarct region (see Chapter 3), with a change in composition to scar tissue. However, away from the infarcted area in remote regions of the LV changes can still be observed at the molecular level. Crosstalk between regions of the heart has been shown previously in response to cardiac injury across different pathologies (Abdul-Ghani et al. 2022; Littlejohns et al. 2014). Previous studies have identified changes in protein expression in infarct tissue as well as border zone and remote regions following MI or I/R in animal models (reviewed in (Gomez-Mendoza et al. 2021)).

By taking an unbiased approach to proteomic analysis, proteins relating to different aspects of the remodelling process can be assessed. Furthermore, there are no comprehensive studies assessing changes in the cardiac phospho-proteome over time following MI. Identification of novel proteins involved in the remodelling process may provide new therapeutic targets.

4.2 Aims

The aim of this chapter is to evaluate the impact of MI on protein and phosphoprotein expression in cardiac tissue, and to assess this at different time points to study the progression of cardiac remodelling. Differences in protein and phosphoprotein expression between Sham and naïve animals will also be completed to investigate any effect of sham surgery.

4.3 Methods

Proteomic and phospho-proteomic analysis was performed on apical tissue collected from hearts across all time-points post-surgery; 3-days (LAD n=5, Sham n=5), 2-weeks (LAD n=5), 4-weeks (LAD n=5, Sham n=5). Samples from naïve hearts were included for comparison to sham (n=4).

4.3.1 Sample collection and protein extraction

Samples for proteomic analysis were taken from the apex and stored at -80^{o}C. Sections were taken from the apex tissue for protein extraction, in hearts from the LAD groups infarct tissue was avoided. Briefly protein extraction involved homogenisation of tissue in RIPA buffer with phosphatase and protease inhibitors before centrifugation to obtain the supernatant. A small amount of the supernatant was used for protein quantification using the Pierce™ Rapid Gold BCA kit. Once protein concentration was determined, samples were adjusted to 2mg/ml for proteomic analysis.

4.3.2 Proteomic and phospho-proteomic analysis

Proteomic and phospho-proteomic analysis was completed at the proteomic facility at the University of Bristol. Protein identification was performed using TMT and reverse phase nano-liquid chromatography (RP nano-LC MS/MS) using a LTQ-Orbitrap Fusion Lumos mass spectrometer.

Analysis of the raw data was performed by Dr Philip Lewis (University of Bristol proteomic facility) using Proteome Discoverer software (Thermo Scientific, version 2.4). False discovery rate cut-off for all data was 5%. FC ratios between groups were calculated and a cut off value of ± 1.3-fold was considered differentially expressed based on similar studies (Abdul-Ghani et al. 2022; Bond et al. 2019). Unpaired students t.test was used to identify significant changes with a significance level set at $p<0.05$. Volcano plots display Log_2(FC) on the horizontal axis with -log10 of p-value displayed on the vertical axis, dashed lines on volcano plots indicate 1.3-fold cut-off and p=0.05.

Enriched canonical pathways were identified by IPA software, for both proteins and phosphoproteins. For each canonical pathway a p-value of the overlap is given with a significance level set at $p<0.05$, and a Z-score is generated which is an estimation as to the activation or inhibition of a pathway with a score of greater than 2 or -2 classified as a prediction rather than a trend.

4.4 Results

The overall changes in protein and phosphoprotein expression are displayed below, as well as some selected sub-groups of proteins involved in the remodelling process.

4.4.1 Changes in cardiac proteome at different time-points following LAD occlusion

For proteomic analysis only proteins detected in all samples were included, for all comparisons this was 5034-5037 proteins.

Comparison of LAD to sham hearts at the 3-day and 4-week time-point shows a greater number of proteins were differentially expressed at 3-days than 4-weeks when compared to their respective sham controls. There were 2630 proteins significantly differentially expressed following LAD occlusion compared to sham at 3-days post-MI, 1597 proteins with increased expression and 1033 with decreased expression in LAD compared to sham (Figure 4-1). At the 4-week time-point only 220 proteins were significant differently expressed in the LAD group compared to sham, 182 proteins with increased expression and 38 with decreased expression (Figure 4-1).

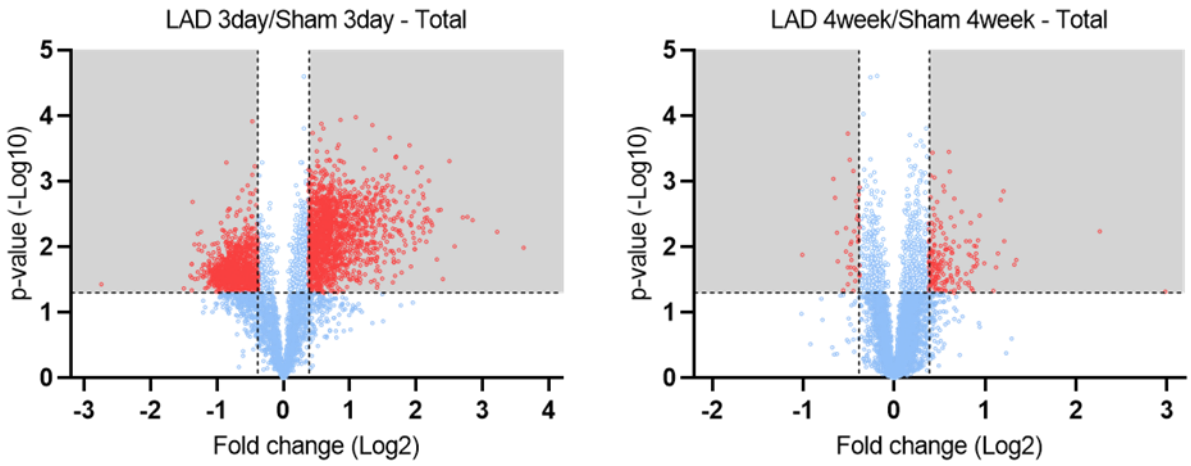

Figure 4-1 Proteomic changes in hearts subjected to LAD occlusion in comparison to sham at 3-days and 4-weeks post-surgery

Volcano plots highlighting significantly differentially expressed proteins (red) in following LAD occlusion compared to sham at 3-days and 4-weeks post-surgery.

Protein expression following LAD occlusion changes across time (Figure 4-2). In all time-point comparisons of LAD groups, the greatest difference was between the 3-day and 4-week time points with 2838 proteins significantly differently expressed (1148 increased and 1690 decreased in 4-week vs 3-day). A greater number of proteins were differentially expressed between 3-days to 2-weeks (2164 proteins, 1103 increased and 1061 decreased at 3-days vs 2-weeks) in comparison to 2-weeks to 4-weeks (306 proteins, 19 increased and 287 decreased at 4-weeks vs 2-weeks).

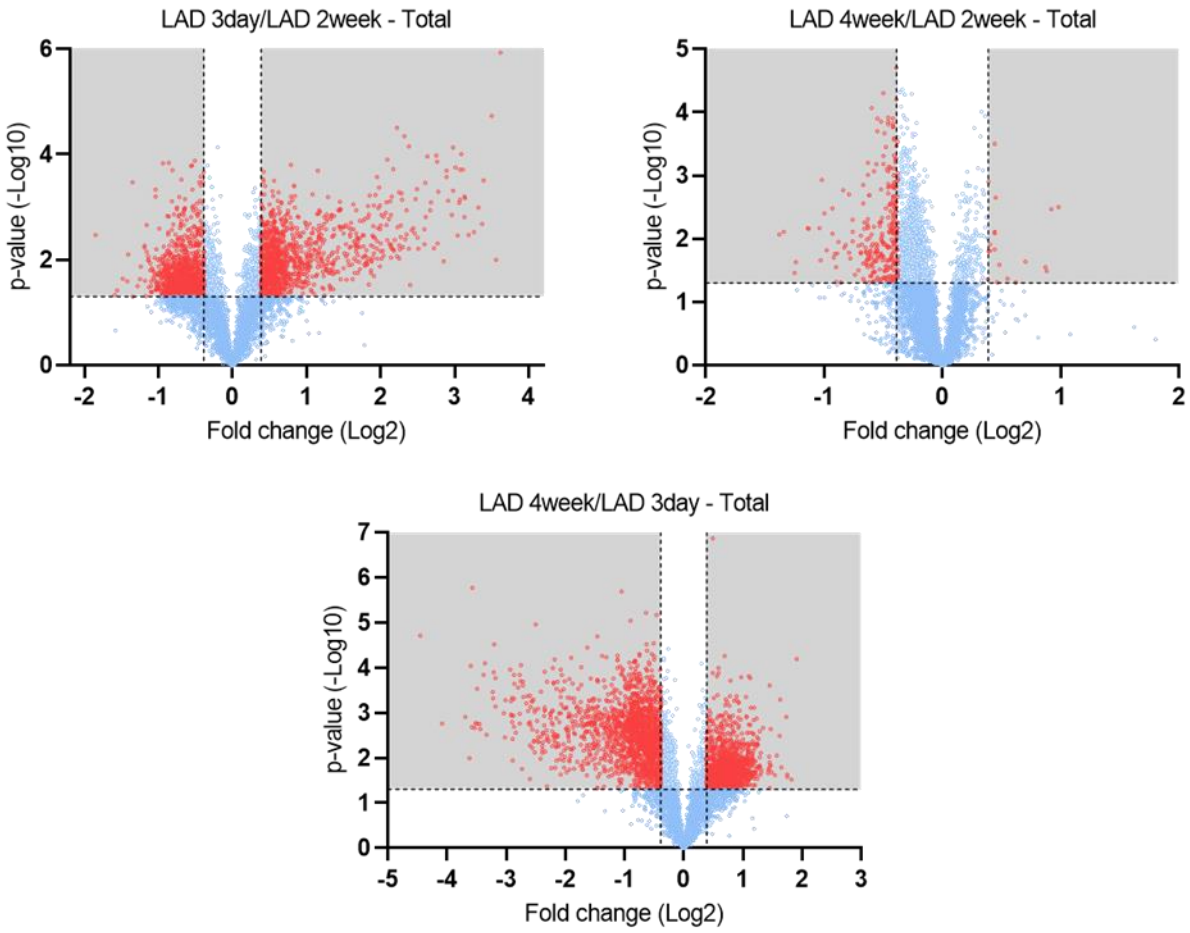

Figure 4-2 Changes in protein expression following LAD occlusion over time

Volcano plots highlighting significantly differentially expressed proteins (red) at different time-points following MI induced by LAD occlusion.

4.4.2 Antioxidant proteins

Antioxidant enzymes work to counteract increases in oxidative stress due to high levels of ROS, a situation known to arise following MI. This study found several antioxidant proteins were significantly upregulated following LAD occlusion compared to sham 3-days post-surgery, including glutathione peroxidase and myeloperoxidase. Other antioxidants including catalase and superoxide dismutase (SOD) were downregulated. By 4-weeks post-surgery, only glutathione peroxidase 7 was significantly differentially expressed with increased expression (Figure 4-3).

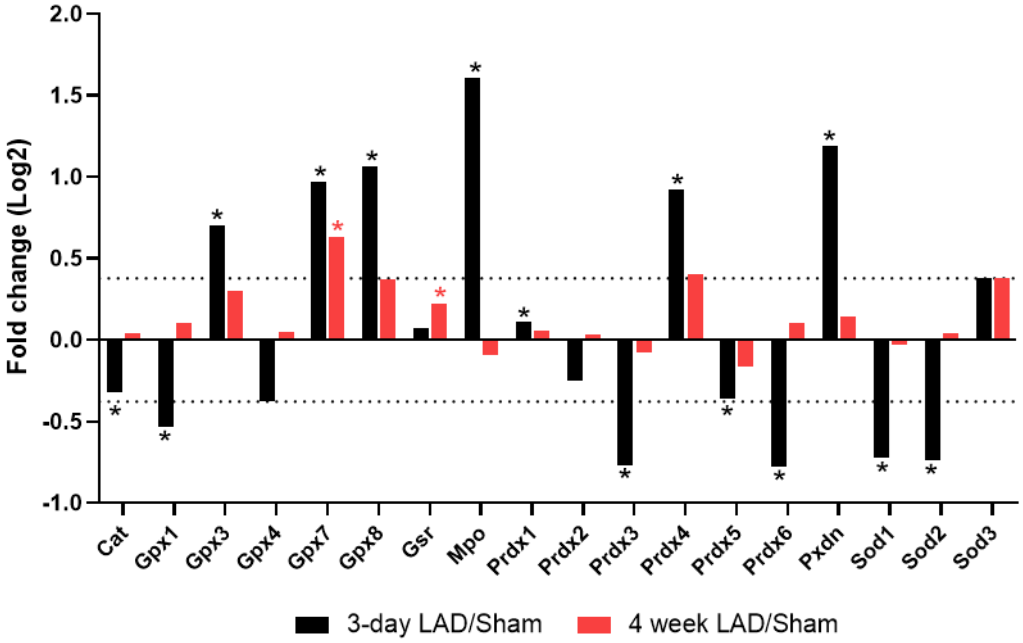

Figure 4-3 Antioxidant proteins

*Change in antioxidant proteins following LAD occlusion at the 3-day and 4-week time-point compared to respective time-point matched sham groups. Cat – Catalase, Gpx – Glutathione peroxidase, Gsr -Glutathione reductase, Mpo – Myeloperoxidase, Prdx – Peroxiredoxin, Pxdn – Peroxidasin, Sod – Superoxide dismutase. Dashed line indicates 1.3 FC, *p<0.05 LAD vs Sham analysed by students T.Test*

4.4.3 Cell death/inflammatory related proteins

The initial stage following MI involves cardiomyocyte death. Several proteins involved in cellular death by apoptosis are upregulated following MI at the 3-day time-point in the LAD group compared to Sham, including caspases, apoptosis regulator BAX, and C-reactive protein (Figure 4-4A). The abundance of apoptosis-related proteins reduced over time following MI, as shown by reduced abundance in each subsequent time-point in LAD groups (Figure 4-4B).

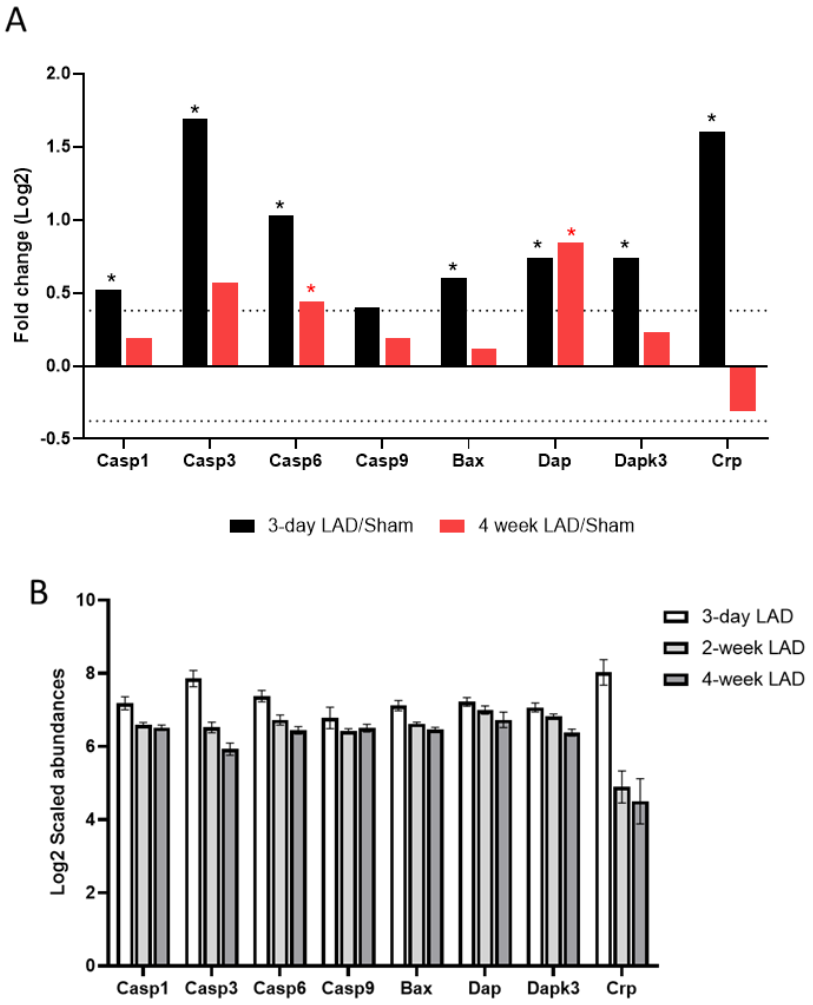

Figure 4-4 Apoptosis related proteins

*(A) Changes in proteins involved in apoptosis following LAD occlusion at the 3-day and 4-week time-point compared to respective time-point matched sham groups. Casp – Caspase, Bax – Apoptosis regulator BAX, Dap – Death-associated protein 1, Dapk3 – Death-associated protein kinase 3, Crp – C-reactive protein. Dashed line indicates 1.3 FC, *p<0.05 LAD vs Sham analysed by students T.Test. (B) Changes in abundance of apoptosis-related proteins in LAD hearts at different time-points following MI.*

4.4.4 Matrix metalloproteinases

Matrix metalloproteinases (MMPs) are enzymes that breakdown ECM components. Two MMPs were identified in the proteomic analysis, MMP2 and MMP14, both were significantly upregulated 3-days post-MI in the LAD group compared to sham (Figure 4-5A). The abundance of each MMP reduced over time following MI in the LAD groups (Figure 4-5B).

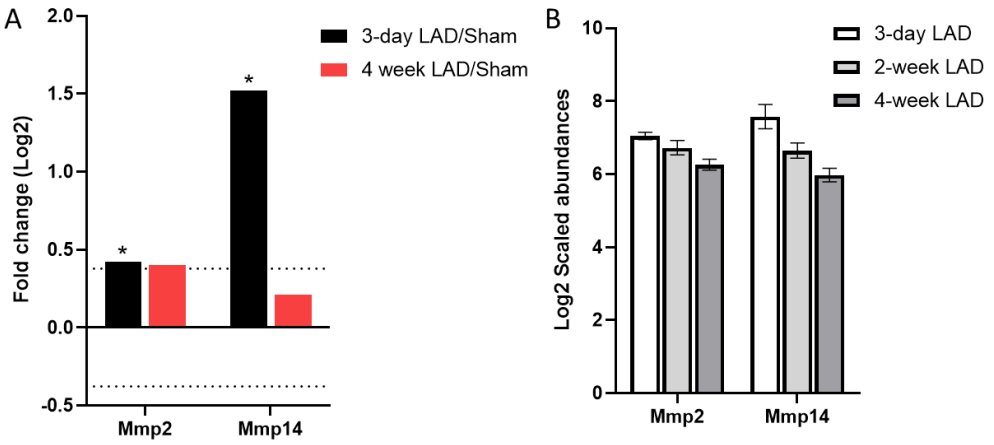

Figure 4-5 Changes in MMP proteins following MI

*(A) Changes in MMP-2 and MMP-14 following LAD occlusion at the 3-day and 4-week time-point compared to respective time-point matched sham groups. Dashed line indicates 1.3 FC, *p<0.05 LAD vs Sham analysed by students T.Test. (B) Changes in abundance of MMP proteins in LAD hearts at different time-points following MI.*

4.4.5 Extracellular matrix proteins

Collagen is a major component of the ECM and there are several types, of which 17 were identified in all samples in this study. Collagen is significantly upregulated following LAD occlusion. 8 types of collagens were increased at 3-days, where at the 4-week time-point only 1 type of collagen (Col18a1) was significantly increased compared to the respective sham group (Figure 4-6A). The change in abundance of each collagen type in LAD groups across time can be seen in Figure 4-6B.

Other ECM components, such as proteoglycans, were also significantly upregulated following MI at 3-days in line with the increase in collagen. Several of these proteins remained upregulated in the LAD group 4-weeks post-MI (Figure 4-7).

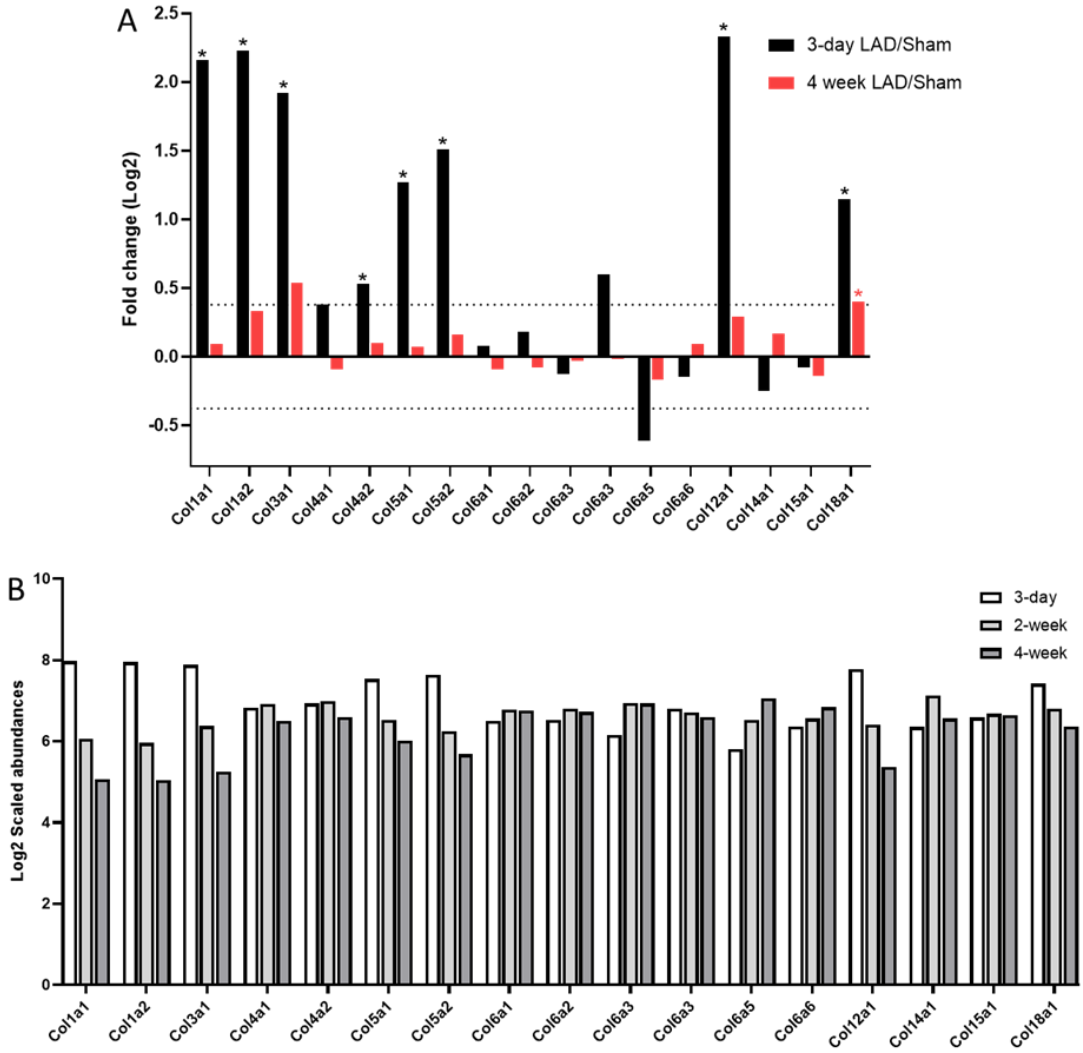

Figure 4-6 Collagen proteins

*(A) Change in collagen proteins following LAD occlusion at the 3-day and 4-week time-point compared to respective time-point matched sham groups. Dashed line indicates 1.3 FC, *p<0.05 LAD vs Sham analysed by students T.Test. (B) Change in abundance of collagen proteins across time following MI in LAD groups.*

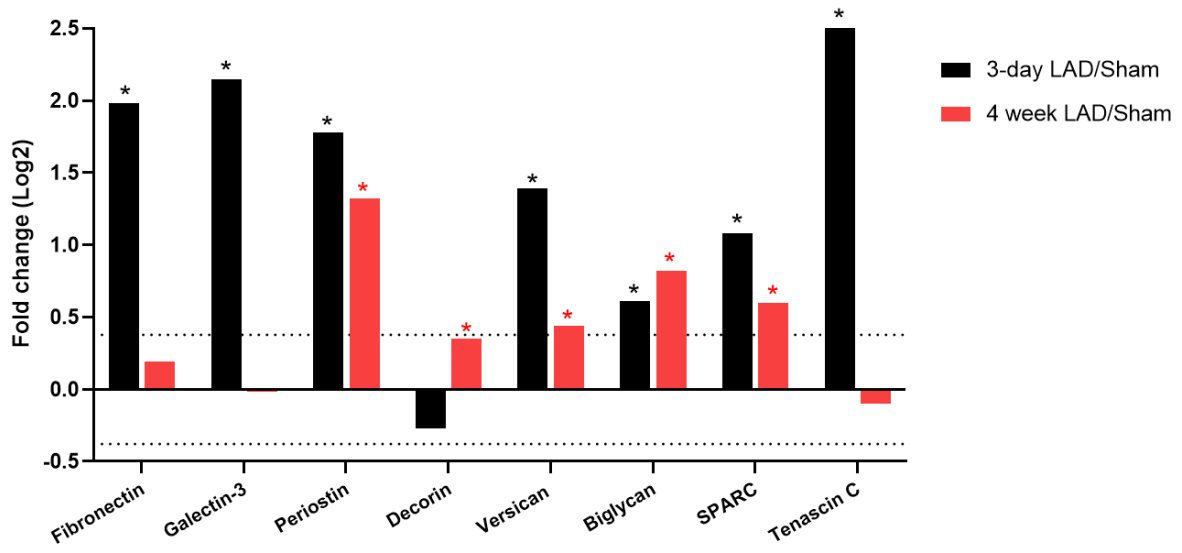

Figure 4-7 Extracellular matrix proteins

*Change in ECM proteins following LAD occlusion at the 3-day and 4-week time-point compared to respective time-point matched sham groups. Dashed line indicates 1.3 FC, *p<0.05 LAD vs Sham analysed by students T.Test.*

4.4.6 Calcium handling proteins

Calcium handling is central to excitation-contraction coupling. Proteins involved in calcium handling, including phospholamban, RyR, LTCC and SERCA, are all significantly downregulated 3-days post LAD occlusion in comparison to sham. These proteins also show decreased expression in the LAD group at 4-weeks, but the change is less than 1.3-fold (Figure 4-8).

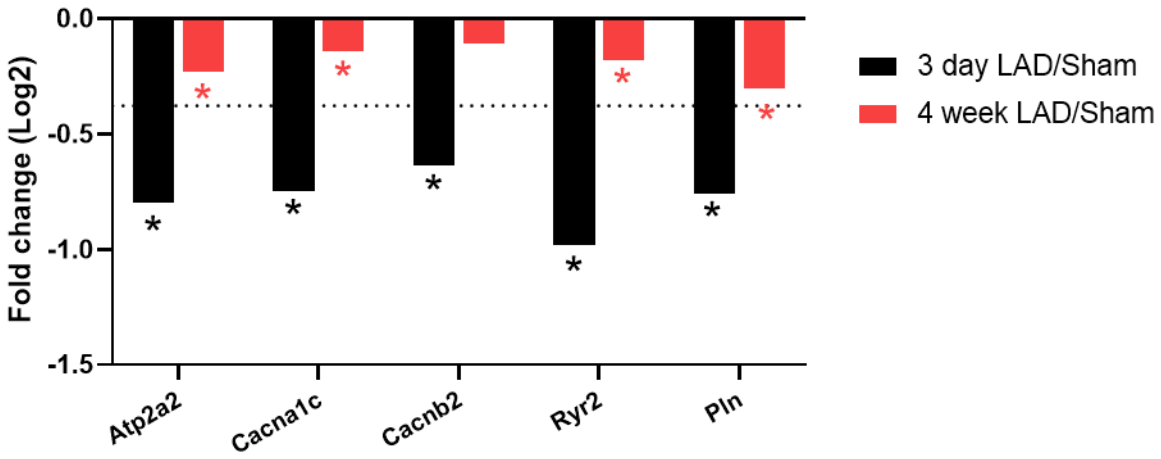

Figure 4-8 Calcium handling proteins

*Change in calcium handling proteins following LAD occlusion at the 3-day and 4-week time-point compared to respective time-point matched sham groups. Atp2a2 – SERCA, Cacna1c – Voltage-dependent L-type calcium channel subunit alpha, Cacnb2 – Voltage-dependent L-type calcium channel subunit beta-2, Ryr2 – Ryanodine receptor 2, Pln – Phospholamban. Dashed line indicates 1.3 FC, *p<0.05 LAD vs Sham analysed by students T.Test*

4.4.7 Ion channels/transporters

Subunits of both the sodium/potassium-transporting ATPase and the voltage-gated sodium channel were identified as differentially expressed proteins, as well as the ATP-sensitive inward rectifier potassium channel (Figure 4-9). Several changes were still present at the 4-week time-point, with the sodium/potassium-transporting ATPase subunit alpha-3 significantly upregulated only at 4-weeks post-MI.

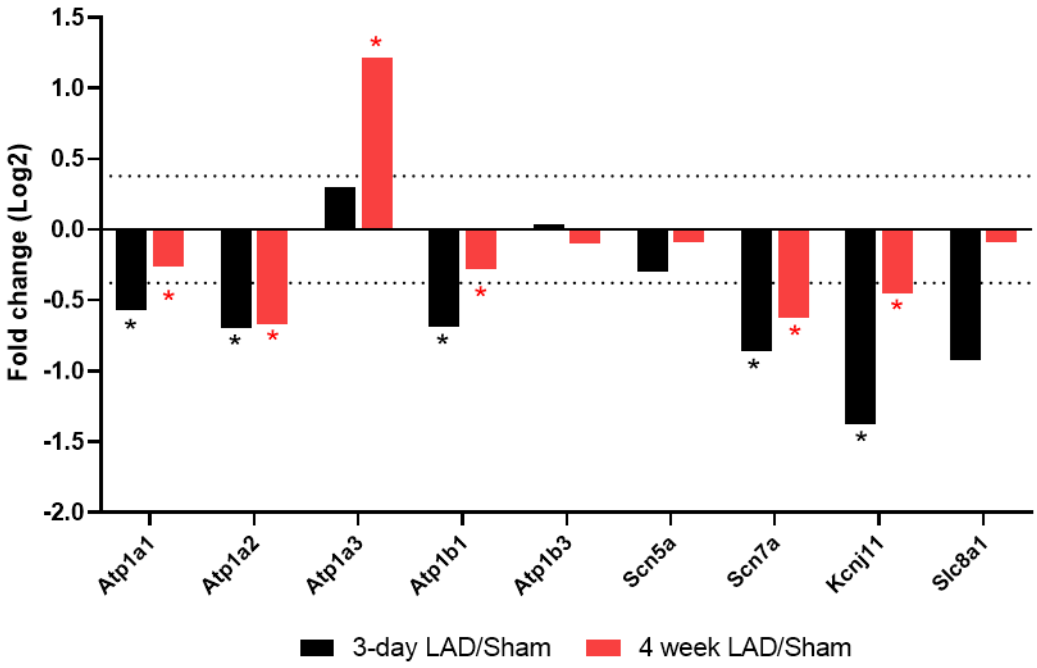

Figure 4-9 Channel/transport proteins

*Changes in proteins associated with cell-cell junctions in the heart following LAD occlusion at the 3-day and 4-week time-point compared to respective time-point matched sham groups. Atp1a1 – Sodium/potassium-transporting ATPase subunit alpha-1, Atp1a2 – Sodium/potassium-transporting ATPase subunit alpha-2, Atp1a3 – Sodium/potassium-transporting ATPase subunit alpha-3, Atp1b1 – Sodium/potassium-transporting ATPase subunit beta-1, Atp1b2 – Sodium/potassium-transporting ATPase subunit beta-2, Scn5a – Sodium channel protein type 5 subunit alpha, Scn7a – Sodium channel protein, Kcnj11 – ATP-sensitive inward rectifier potassium channel 11, Slc8a1 – Sodium/calcium exchanger 1. Dashed line indicates 1.3 FC, *p<0.05 LAD vs Sham analysed by students T.Test.*

4.4.8 Cell-cell junction proteins

Proteins relating to cell-cell junctions were also identified among the differentially expressed proteins following MI, with most downregulated (Figure 4-10).

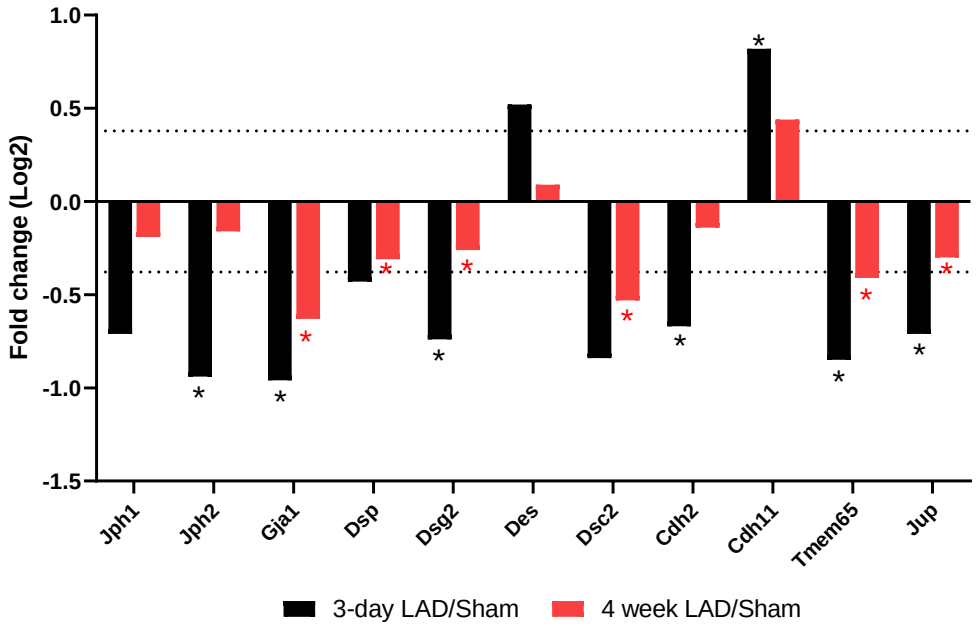

Figure 4-10 Cell junction proteins

*Changes in proteins associated with cell-cell junctions in the heart following LAD occlusion at the 3-day and 4-week time-point compared to respective time-point matched sham groups. Jph – Junctophilin, Gja1 – Gap junction alpha-1 protein (Connexin-43), Dsp – Desmoplakin, Dsg - Desmoglein, Des – Desmin, Dsc – Desmocolin, Cdh – Cadherin, Tmem – Transmembrane, Jup - Plakoglobin. Dashed line indicates 1.3 FC, *p<0.05 LAD vs Sham analysed by students T.Test.*

4.4.9 Mitochondrial proteins and cardiac metabolism pathways

Proteins relating to mitochondria were differently expressed at all time-points in the LAD groups compared to sham. A higher number were identified as differentially expressed at 3-days post-MI, with the majority downregulated, in comparison to at 4-weeks (Figure 4-11).

Proteins associated with mitochondrial fission and fusion were among the significant DEPs. Mitochondrial fusion proteins, mitofusin 1 and Opa1 were downregulated 3-day post-MI. Mitochondrial fission regulator (Mtfr2) was upregulated

3-days post-MI in LAD hearts. Prohibitin, a protein involved in mitochondrial fission, was downregulated 3-days post-MI in LAD hearts.

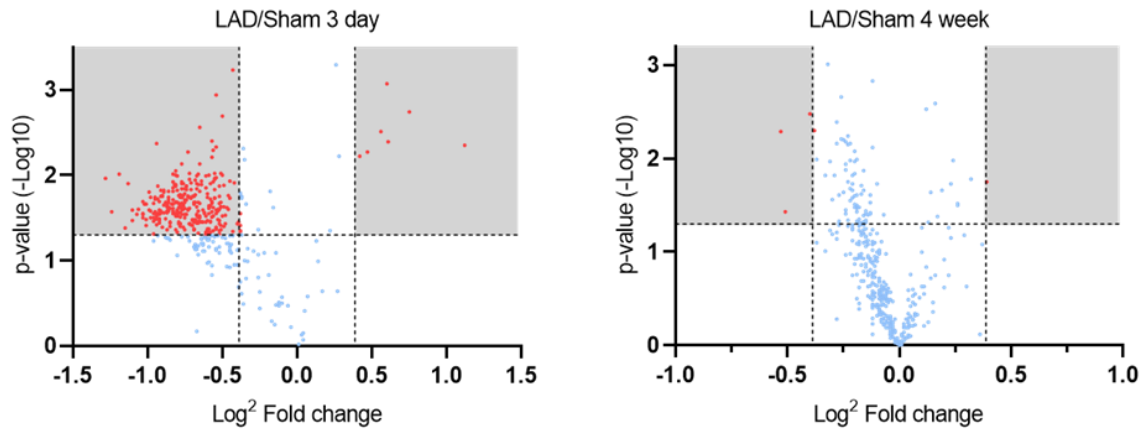

Figure 4-11 Mitochondrial proteins

Volcano plots highlighting significantly differentially expressed mitochondrial proteins (red) in LAD groups at different time points following MI

Mitochondria are central to the production of energy in the heart as the location of the TCA cycle and the ETC. Proteins comprising each of the complexes of the ETC were among the proteins with reduced expression at 3-days post-MI. At 4-weeks post-MI the same proteins were not significantly changed in comparison to the sham group. Looking at the 2-week time-point reveals these mitochondrial complex proteins are only downregulated at the initial 3-day time-point; expression is reduced at 3-days compared to 2-weeks but there is no change from 2-weeks to 4-weeks in the LAD groups. Enzymes associated with the TCA cycle including isocitrate dehydrogenase, succinyl CoA synthase and fumarase were also downregulated at the 3-day time-point in comparison to naïve

Fatty acids and glucose are the primary substrates for cardiac metabolism, broken down by β-oxidation and glycolysis respectively to produce acetyl-CoA which enters the TCA cycle. Proteins associated with fatty acid metabolism were downregulated following MI, at both 3-days and 4-weeks compared to sham hearts, including Acyl-CoA dehydrogenase and subunits of the mitochondrial trifunctional protein (Figure 4-12). Carnitine-palmitoyl transferases I and II were also

downregulated 3-days post-MI. Proteins involved in glycolysis were downregulated 3-days post-MI, whereas expression was upregulated 4-weeks post-MI. The mitochondrial pyruvate carrier was significantly upregulated 4-weeks post-MI, as was glutamine-fructose-6-phosphate aminotransferase 2.

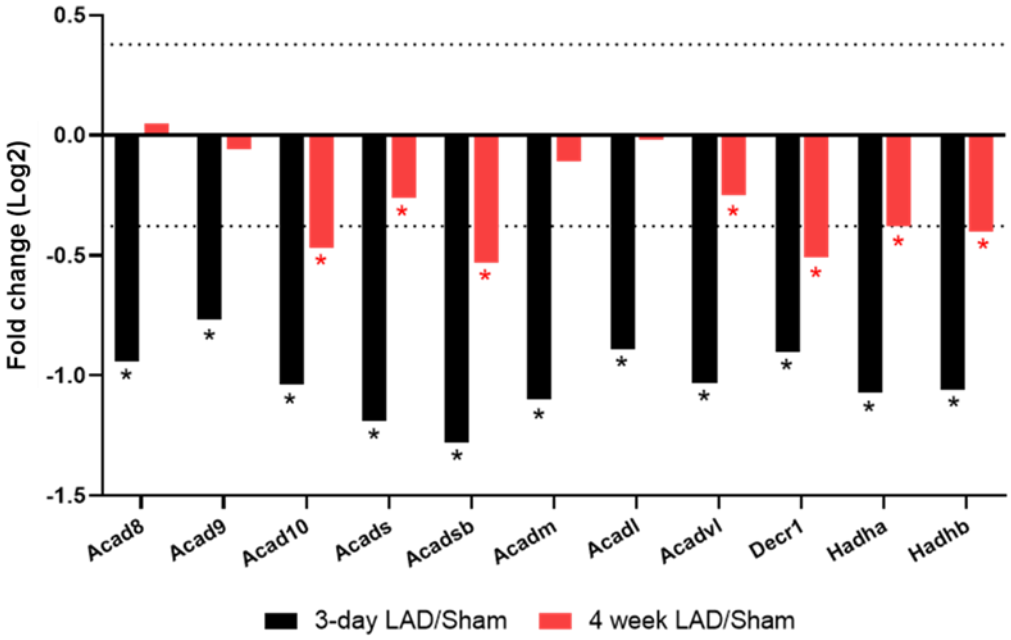

Figure 4-12 Fatty acid metabolism

*Changes in proteins associated with fatty acid β-oxidation in the heart following LAD occlusion at the 3-day and 4-week time-point compared to respective time-point matched sham groups. Acad8 – Acyl-CoA dehydrogenase family member 8, Acad9 – Acyl-CoA dehydrogenase family member 9, Acad10 – Acyl-CoA dehydrogenase family member 10, Acads – Short-chain-specific acyl-CoA dehydrogenase, Acadsb – Short/branched chain specific acyl-CoA dehydrogenase, Acadm – Medium-chain specific acyl-CoA dehydrogenase, Acadl – Long-chain specific acyl-CoA dehydrogenase, Acadvl – very long chain specific acyl-CoA dehydrogenase, Decr1 – 2,4-dienoyl-CoA reductase, Hadha – Trifunctional enzyme subunit alpha, Hadhb – Trifunctional enzyme subunit beta. Dashed line indicates 1.3 FC, *p<0.05 LAD vs Sham analysed by students T.Test.*

4.4.10 Cardiac proteome enriched canonical pathways following LAD occlusion

IPA was performed on proteins identified for both 3-day and 4-week LAD/Sham comparisons, selected enriched pathway are shown in (Figure 4-13 and Figure 4-14).

At 3-days post-MI the most significantly enriched pathway is mitochondrial dysfunction. Identified enriched pathways with a zScore indicative of downregulation are related to cardiac metabolism, including oxidative phosphorylation, the TCA cycle, fatty acid β-oxidation and glycolysis. The top significant pathways with upregulation include EIF2 signalling, Granzyme A signalling and Sirtuin signalling. The Sirtuin proteins identified as part of this pathway were Sirt 3 and Sirt 5.

At 4-weeks post-MI several of the top enriched canonical pathways involved Rho signalling, including Rac and Cdc42, regulation of the actin cytoskeleton and integrin signalling. Other enriched pathways included fatty acid B-oxidation and oxidative phosphorylation which were downregulated. Mitochondrial dysfunction was also a significantly enriched pathway.

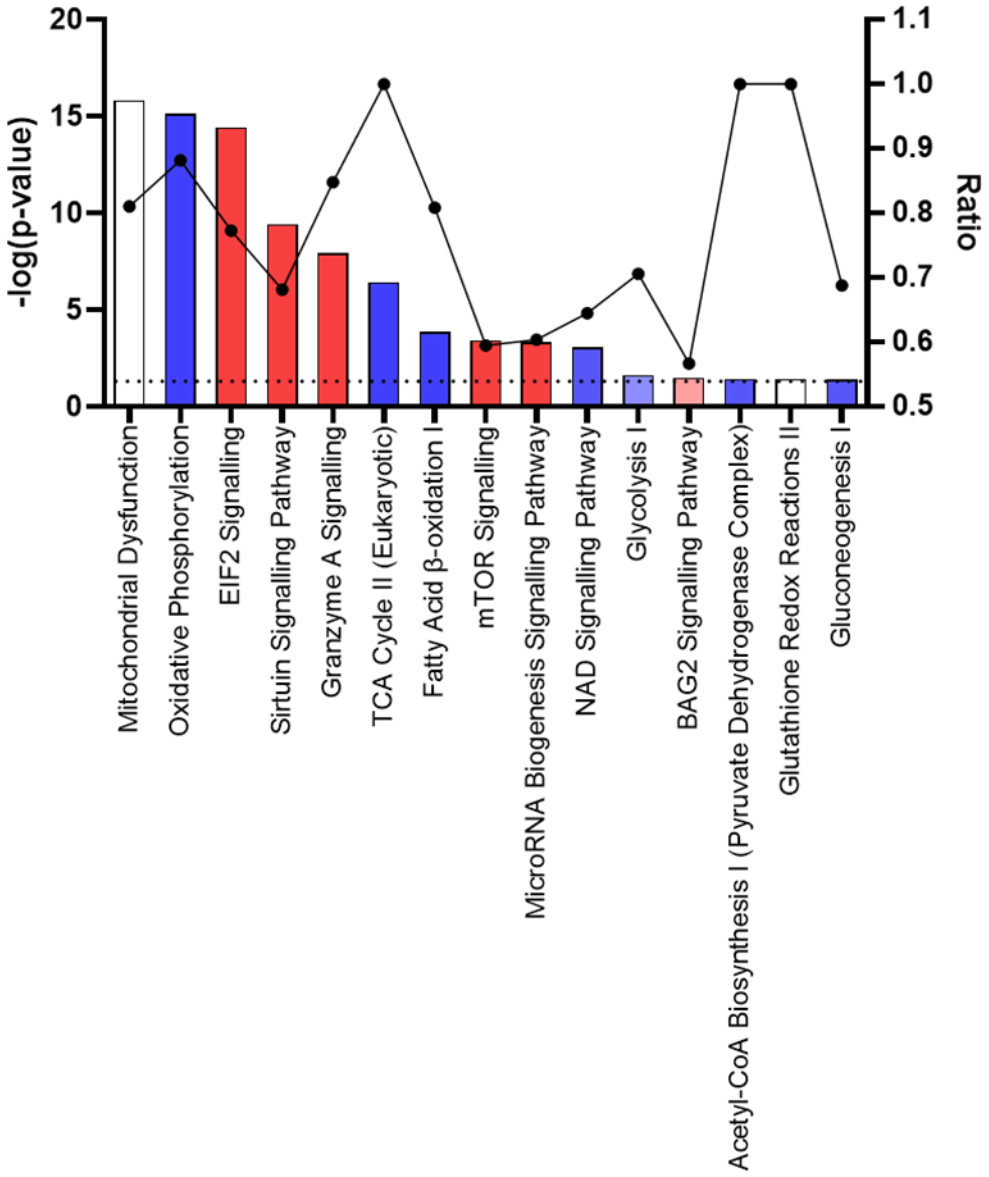

Figure 4-13 Enriched canonical pathways for proteins at 3-day LAD compared to sham

Identified pathways are displayed with -log(p-value) on the left y-axis (bar chart), dashed line represents p=0.05. The ratio (line chart) is displayed on the right y-axis. The bar colours indicate the z-score (where given) by IPA, blue indicating down-regulation and red up-regulation with darker shade associated with greater values.

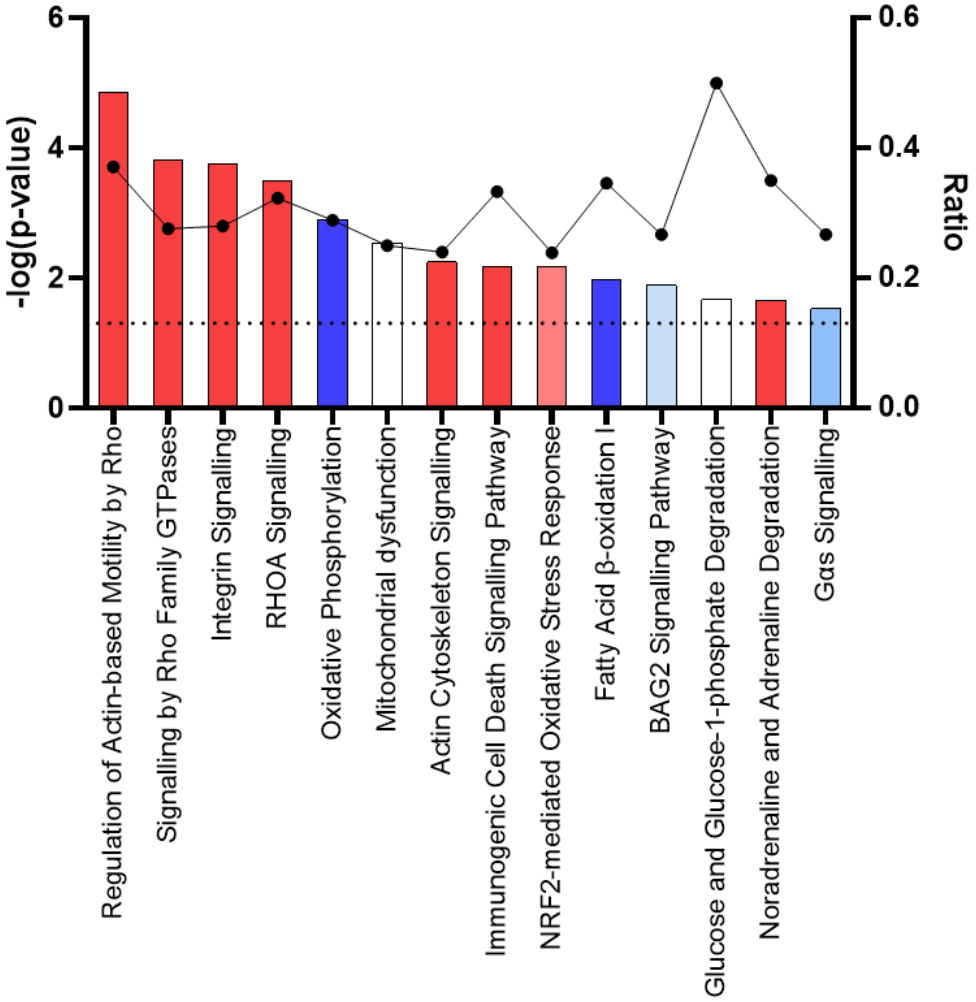

Figure 4-14 Enriched canonical pathways for proteins at 4-weeks LAD compared to sham

Identified pathways are displayed with -log(p-value) on the left y-axis (bar chart), dashed line represents p=0.05. The ratio (line chart) is displayed on the right y-axis. The bar colours indicate the z-score (where given) by IPA, blue indicating down-regulation and red up-regulation with darker shade associated with greater values.

4.4.11 Changes in cardiac phospho-proteome at 3-days and 4-weeks post LAD occlusion compared to sham

For phospho-proteomic analysis only phospho-proteins detected in all samples were included, for all comparisons this was 3025-3035 phosphoproteins.

As with total protein, comparison of LAD to sham hearts at the 3-day and 4-week time-point shows a greater number of phospho-proteins were differentially expressed at 3-days compared to 4-weeks. 643 phospho-proteins were significantly differentially expressed following LAD occlusion compared to sham at 3-days post-MI, 510 with increased expression and 133 with decreased expression in LAD compared to sham (Figure 4-15). At the 4-week time-point 86 phospho-proteins were significant differently expressed in the LAD group compared to sham, 29 with increased expression and 38 with decreased expression (Figure 4-15).

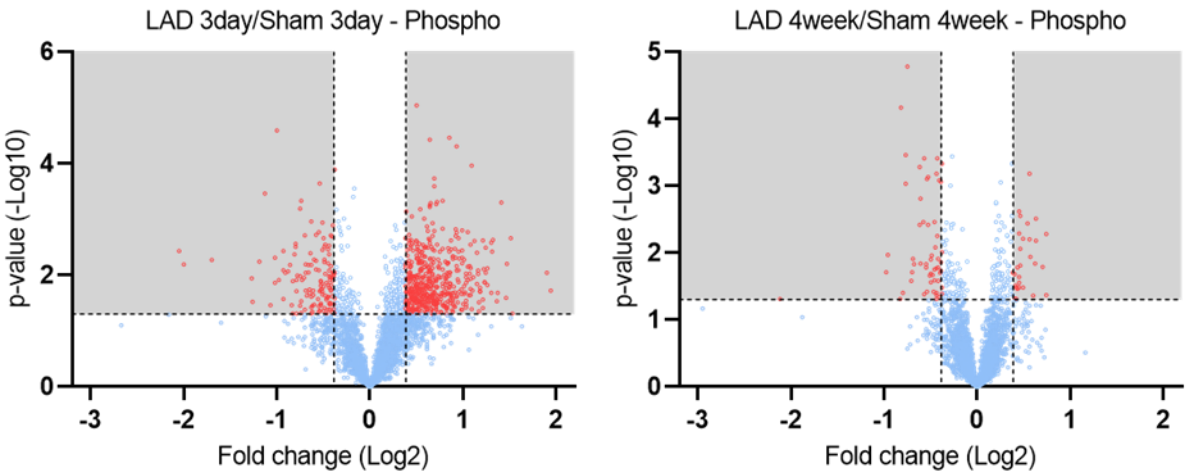

Figure 4-15 Phospho-protein expression in LAD compared to sham hearts at 3-days and 4-weeks

Volcano plots highlighting significantly differentially expressed phosphoproteins (red) in LAD groups compared to sham at 3-days and 4-weeks post-surgery

Selected phospho-proteins with differential expression are displayed in (Table 4-1). The phospho-proteins differentially expressed included calcium handling proteins phospholamban, RyR, SERCA and L-type calcium channels, with increased phosphorylation at the 3-day time-point. Phosphorylation of mitochondrial fission regulator 2 is changed following MI. Various structural proteins exhibit changes in phosphorylation post-MI, as well as gap junction protein connexin43.

Table 4-1 Significantly differentially expressed phospho-proteins in LAD hearts compared to sham 3-days and 4-weeks post-MI

					3-day LAD/Sham		**4-week LAD/Sham**	
Protein	Gene	Accession	Peptide	Phosphosites	Fold change	p-value	Fold change	p-value
Calcium handling proteins								
Phospholamban	Pln	P61016	T3	T17	**1.49**	**0.01**	0.97	0.09
			S3; T4	S16; T17	**1.65**	**0.02**	1.13	0.95
Ryanodine receptor 2	Ryr2	F1LRZ1	S2; S3	S2692; S2693	**1.31**	**0.01**	1.20	0.01
			S8	S2813	**1.64**	**0.00**	0.97	0.81
			T4	T1857	**1.62**	**0.03**	1.04	0.52
			S3	S2807	**2.18**	**0.00**	1.08	0.71
SERCA	Atp2a2	P11507	S3	S38	**1.50**	**0.02**	1.09	0.28
Voltage-dependent L-type calcium channel subunit alpha	Cacna1c		S3	S1689	**1.34**	**0.04**	1.01	0.96
Calcium/calmodulin-dependent protein kinase type II subunit delta	Camk2d	P15791	T3	T287	**1.78**	**0.01**	1.18	0.09
			T9	T371	**1.60**	**0.02**	1.55	0.00
Mitochondrial								
Mitochondrial fission regulator 2	Mtfr2	A0A8I5Y6Z0	S13	S261	**0.56**	**0.01**	1.05	0.59
			S7; Y1	S283; Y277	**0.77**	**0.03**	1.08	0.26
			S10	S755	**1.37**	**0.02**	1.07	0.16
			S4	S391	0.85	0.29	**1.63**	**0.02**

Junctional								
Gap junction alpha-1 protein	Gja1	P08050	S18; S19	S364; S365	**2.01**	**0.02**	**1.55**	**0.01**
			S12; S19	S255; S262	**1.77**	**0.02**	1.23	0.08
			S6; S9; T7	S325; S328; T326	1.21	0.13	**1.34**	**0.03**
Junctional cadherin 5-associated	Jcad	F1M6T3	S7	S930	0.94	0.79	**1.30**	**0.02**
Structural								
Titin	Ttn	A0A8I5ZUN3	S5; S7	S34218; S34220	**0.58**	**0.05**	1.16	0.02
			S4; S6	S2077; S2079	**1.82**	**0.02**	**1.54**	**0.01**
Myomesin 1	Myom1	A0A8I6GFM8	S8	S1088	2.16	0.01	**1.36**	**0.03**
Myomesin 2	Myom2	A0A8I6AC90	S3; S5	S136; S138	**1.55**	**0.01**	0.97	0.58
			S2	S153	**1.76**	**0.01**	1.10	0.42
			S3; S5	S153; S155	**1.89**	**0.00**	1.12	0.19
			S4	S153	**1.51**	**0.02**	0.98	0.74
Caveolae-associated protein 2	Cavin2	Q66H98	S27	S217	**1.55**	**0.01**	1.28	0.14
			S4; S8	S358; S362	**1.60**	**0.02**	0.89	0.28
			S12; S13; S27	S202; S203; S217	**1.31**	**0.03**	0.96	0.54
Microtubule-associated protein 1A	Map1a	G3V7U2	S7	S1134	**1.80**	**0.00**	1.08	0.50
			S8	S598	**1.50**	**0.01**	0.89	0.18
			S15	S1897	**1.61**	**0.01**	0.94	0.50
			S7	S1574	0.79	0.09	**0.74**	**0.02**
			S1; S11; S7	S1757; S1767; S1763	1.07	0.65	**0.67**	**0.00**
			S10	S1643	**1.39**	**0.03**	**0.69**	**0.04**
			S9	S1784	1.08	0.31	**0.77**	**0.00**

Microtubule-associated protein 1B	Map1b	P15205	S3; S7	S1786; S1790	0.91	0.53	**0.57**	**0.00**
			S15; S4	S1382; S1371	0.77	0.08	**0.69**	**0.00**
			S14	S1148	0.79	0.12	**0.71**	**0.02**
			S11	S1812	**0.63**	**0.01**	**0.67**	**0.00**
			S3; S7	S1389; S1393	1.37	0.11	**0.62**	**0.01**
			S6	S1009	**0.60**	**0.03**	**0.65**	**0.00**
			S5	S884	**0.62**	**0.01**	**0.59**	**0.00**
			T2	T1923	0.91	0.35	**0.58**	**0.00**
			S4	S1420	**0.65**	**0.04**	**0.69**	**0.00**
			S4	S1908	1.08	0.27	**0.59**	**0.00**
			S4; S5	S824; S825	**0.70**	**0.02**	**0.74**	**0.00**
Filamin A	Flna	A0A8I5ZV49	S3	S2152	**0.73**	**0.00**	0.90	0.06
			S15	S2180	**0.74**	**0.00**	0.98	0.80
Vimentin	Vim	P31000	S4	S325	**0.49**	**0.00**	0.97	0.68
			S10	S420	**0.42**	**0.01**	**0.56**	**0.05**
			S6	S56	**1.91**	**0.00**	**0.65**	**0.01**
			S9	S459	0.93	0.69	**0.61**	**0.02**
Tensin	Tns1	A0A8I5Y194	S10; S13	S1093; S1096	**1.80**	**0.02**	0.91	0.50
			S21	S1393	**1.59**	**0.01**	1.12	0.39
			S11; S3	S1040; S1032	**1.76**	**0.02**	1.15	0.20
			S11	S1040	**1.87**	**0.04**	1.21	0.02
			S16; S19	S1045; S1048	**1.91**	**0.01**	0.89	0.52
			T9	T1452	**1.57**	**0.03**	1.09	0.27
			S1	S1104	**1.55**	**0.02**	0.94	0.45
			S13	S1335	**1.80**	**0.01**	1.17	0.05

			S11	S1333	**1.59**	**0.01**	1.11	0.23
			S12; S5	S1438; S1431	**1.65**	**0.03**	1.01	0.96
Metabolism								
Pyruvate dehydrogenase E1 component subunit alpha	Pdha1	A0A8I6GKV6	S5	S293	1.6	0.13	**0.7**	**0.02**
			S6	S232	1.37	0.29	**0.51**	**0.02**
			T5	T231	1.83	0.16	**0.58**	**0.04**
Creatine kinase	Ckm	A0A0G2JSP8	T3	T35	**1.52**	**0.02**	1.15	0.00
			T3	T322	**1.77**	**0.05**	1.18	0.01
			S3	S372	**1.31**	**0.03**	1.19	0.05
			S5	S16	**1.46**	**0.01**	1.11	0.26
Glycogen synthase	Gys1	A2RRU1	S10; S6	S645; S641	**1.61**	**0.02**	0.91	0.59
			S3	S698	**2.31**	**0.04**	1.16	0.52
			S3; S7	S653; S657	**1.49**	**0.04**	1.00	0.93

4.4.12 Cardiac phospho-proteome enriched canonical pathways following LAD occlusion

IPA was performed on phospho-proteins for both 3-day and 4-week LAD/Sham comparisons, selected enriched pathway are shown in (Figure 4-16 and Figure 4-17) Pathways enriched at both time-points included β-adrenergic signalling, and the associated PKA signalling and cAMP-mediated signalling pathways. Dilated cardiomyopathy signalling is also identified at both time-points. Gluconeogenesis is an enriched pathway at both time points, with glycolysis enriched by 4-weeks, both with z-scores indicating pathway inhibition. Enriched pathways in the 3-day LAD group included response to oxidative stress and ERK/MAPK signalling. Creatine-phosphate biosynthesis and calcium signalling were identified at 4-weeks in the LAD group.

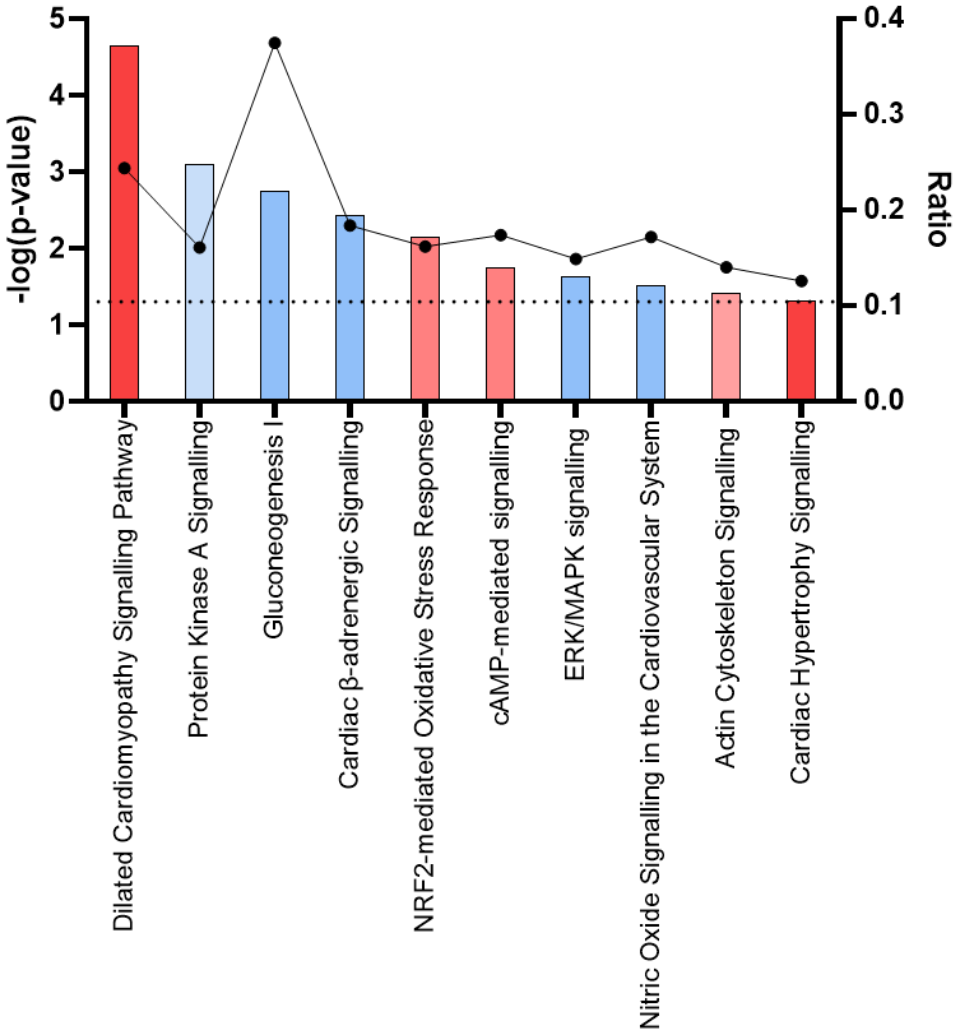

Figure 4-16 Enriched canonical pathways for phosphoproteins at 3-day LAD compared to sham

Identified pathways are displayed with -log(p-value) on the left y-axis (bar chart), dashed line represents p=0.05. The ratio (line chart) is displayed on the right y-axis. The bar colours indicate the z-score (where given) IPA analysis, blue indicating down-regulation and red up-regulation with darker shade associated with greater values.

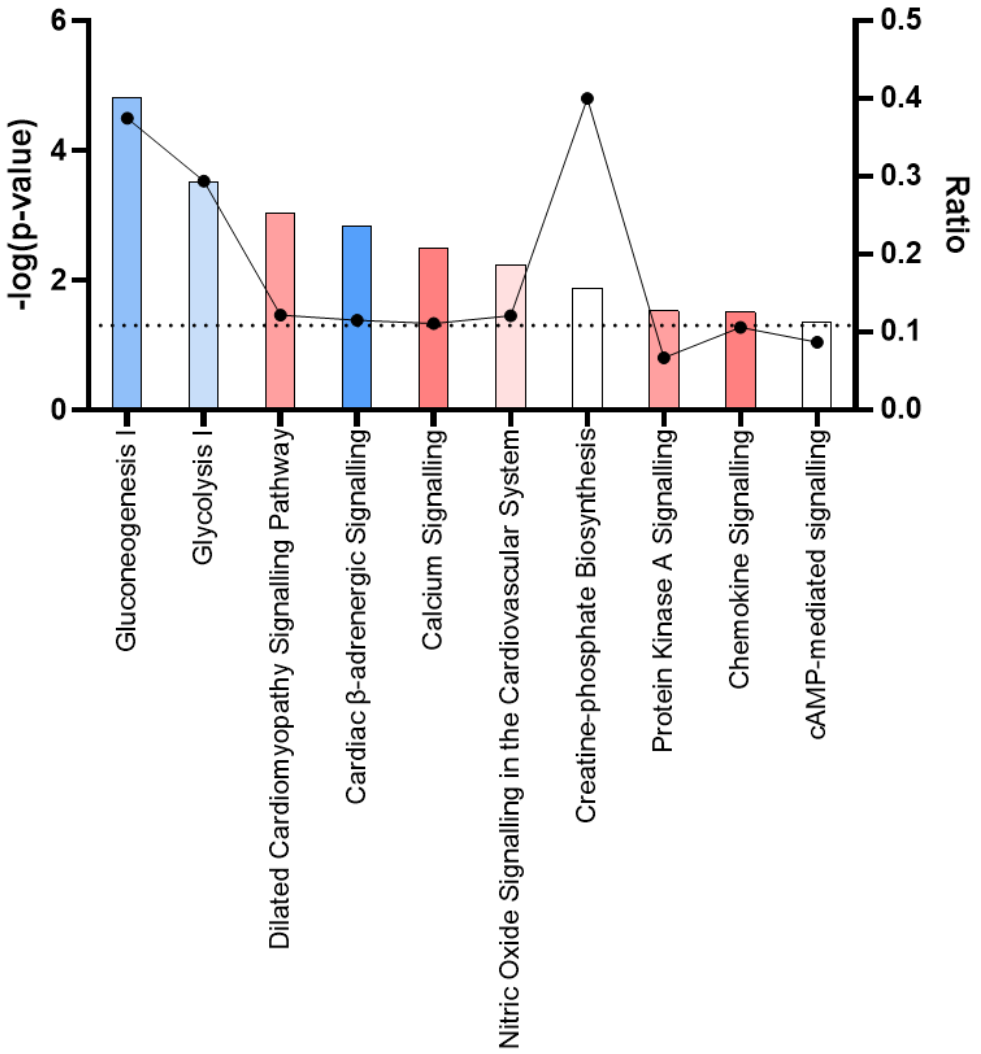

Figure 4-17 Enriched canonical pathways for phosphoproteins at 4-weeks LAD compared to sham

Identified pathways are displayed with -log(p-value) on the left y-axis (bar chart), dashed line represents p=0.05. The ratio (line chart) is displayed on the right y-axis. The bar colours indicate the z-score (where given) by IPA, blue indicating down-regulation and red up-regulation with darker shade associated with greater values.

4.4.13 Effect of sham surgery on cardiac proteome

Protein expression in sham hearts at two time-points, 3-days and 4-weeks post-surgery, was compared to protein expression in naïve hearts to determine any effect of the surgical procedure. As can be seen in the volcano plots in Figure 4-18 at 3 days post-MI the sham hearts had more significantly DEPs compared to naïve, than the sham group at 4 weeks post-MI. In 3-day sham hearts there were 410 significantly DEPs compared to naïve hearts, with 364 up-regulated and 46 downregulated. By 4-weeks post sham surgery only 16 proteins were significantly differentially expressed, 10 upregulated and 6 downregulated.

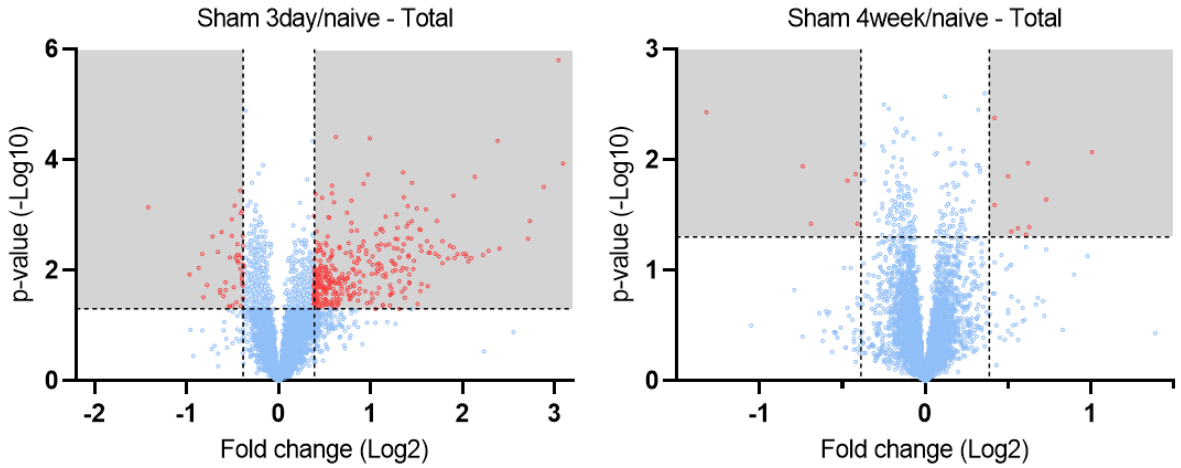

Figure 4-18 Protein expression in sham hearts at 3-days or 4-weeks compared to naïve
Volcano plots highlighting significantly differentially expressed proteins (red) in sham hearts at (A) 3-days or (B) 4-weeks post-surgery compared to naive hearts.

In sham hearts at 3-days post-surgery there was an upregulation of proteins related to apoptosis/cell death and antioxidant proteins including superoxide dismutase 3, catalase and glutathione peroxidase. Several collagen proteins were also upregulated as well as MMP 2 and 14 (Figure 4-19).

Significantly differently expressed proteins at 4-week sham compared to naïve include collage type 6 alpha 3 chain, sarcosine dehydrogenase and prohibitin.

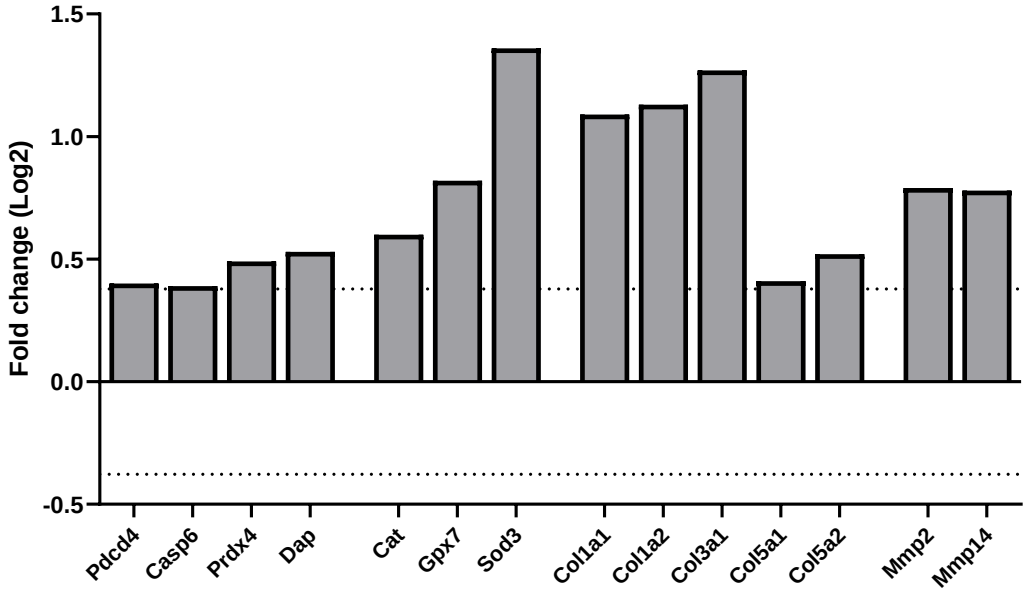

Figure 4-19 Significantly differentially expressed proteins 3-day Sham/naïve

Changes in proteins in the heart following sham surgery at the 3-day time-point compared to naïve. Pdcd4 – Programmed cell death 4, Casp6 – Caspase 6, Prdx4 – Peroxiredoxin 4, Dap – death associated protein, Cat – Catalase, Gpx7 – Glutathione peroxidase 7, Sod3 – Superoxide dismutase 3, Col1a1 – Collagen type 1 alpha 1, Col1a2, Collagen type 1 alpha 2, Col3a1 – Collagen type 3 alpha 1, Col5a1 – Collagen type 5 alpha 1, Col5a2 – Collagen type 5 alpha 2, Mmp2 – Matrix metalloproteinase 2, Mmp14 – Matrix metalloproteinase 14. Dashed line indicates 1.3 FC, all proteins displayed were significantly different (p<0.05) Sham 3-day vs naïve analysed by students T.Test.

4.4.14 Effect of sham surgery on the cardiac phospho-proteome

Differences in phospho-proteins between sham and naïve hearts was also determined. As with total protein, the number of differentially expressed phospho-proteins is higher in the 3-day sham group compared to naïve than in 4-week sham group (

Figure ***4-20***). At 3 days post sham surgery 209 phospho-proteins were significantly differentially expressed, 141 with increased expression and 68 with decreased expression compared to naïve. At 4 weeks post sham surgery 39 phospho-proteins were significantly differentially expressed, 35 with increased expression and 4 with decreased expression compared to naïve.

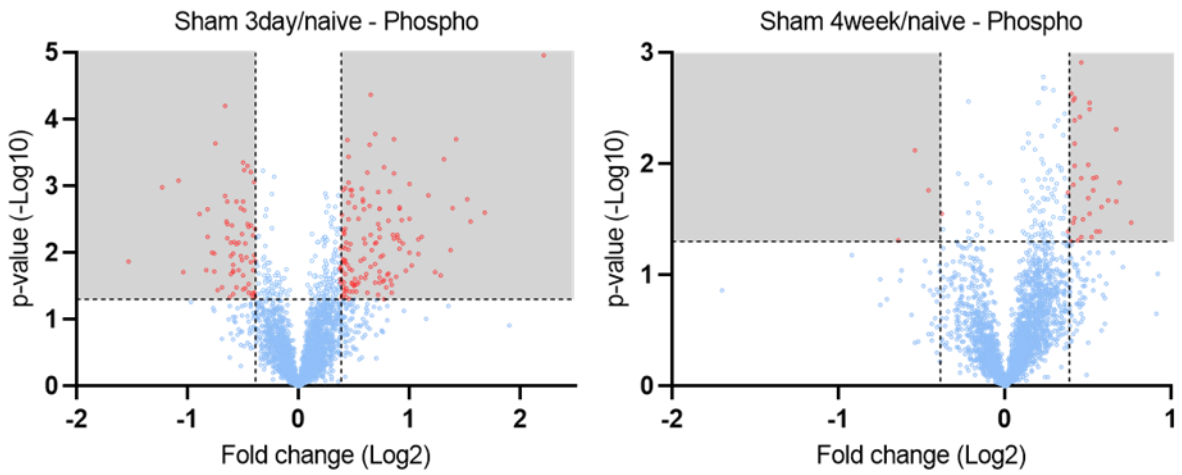

Figure 4-20 Phospho-protein expression in sham hearts at 3-days or 4-weeks compared to naïve

Volcano plots highlighting significantly differentially expressed phosphoproteins (red) in sham hearts at (A) 3-days or (B) 4-weeks post-surgery compared to naive hearts.

4.4.14.1 Differentially expressed phosphoproteins

Selected differentially expressed phospho-proteins of interest in 3-day sham/naïve are displayed in Table 4-2. Among the phospho-proteins increased in the sham group at 3-days was PLN, RyR and contractile proteins. Mitochondrial fission regulators were also identified with changes in phosphorylation.

Table 4-2 Significantly differentially expressed phosphoproteins - 3-day sham/naïve

Protein	Gene	Accession	Peptide	Phosphosites	Fold change	p-value
Bcl2-like 13	Bcl2l13	D3ZT71	S3	S387	1.88	0.01
			S1	S387	1.87	0.01
Glycogen synthase	Gys1	A2RRU1	S20, T14	S728, T722	0.65	0.02
			S20	S728	0.66	0.00
MAP2K4delta	Map2k4	S4VP54	S11, T8	S403, T400	0.35	0.01
Microtubule-associated protein 1A	Map1a	G3V7U2	S10	S1643	0.66	0.01
			S2	S2602	0.73	0.04
			S3	S319	1.31	0.00
Microtubule-associated protein 1B	Map1b	P15205	S15, S4	S1382, S1371	0.71	0.02
			S14	S1148	0.72	0.03
			S3, S7	S1389, S1393	0.56	0.02
			T2	T1923	0.64	0.00
Mitochondrial fission regulator 1-like	Mtfr1l	Q5XII9	S3	S235	1.65	0.02
Mitochondrial fission regulator 2	Mtfr2	A0A8I5Y6Z0	S4	S391	0.66	0.02
Mitogen-activated protein kinase 14	Mapk14	G3V617	T7, Y9	T180, Y182	1.74	0.02
Myosin light chain kinase 3	Mylk3	E9PT87	S3	S444	1.61	0.01
			S3	S155	2.68	0.00
			S3	S155	3.21	0.00
Myosin-binding protein C	Mybpc3	P56741	T2	T287	1.65	0.00
			S3	S312	4.64	0.00
			T11	T296	1.91	0.00
Phospholamban	Pln	P61016	S2	S16	1.79	0.04
			S3	S16	2.11	0.01
			T3	T17	1.34	0.04
			S3, T4	S16, T17	2.62	0.00
			S2, T3	S16, T17	1.85	0.01
			T4	T17	2	0.01
Ryanodine receptor 2	Ryr2	F1LRZ1	S3, S9	S2807, S2813	1.39	0.00
Titin	Ttn	A0A8I5ZUN3	S1, S6	S33986, S33991	1.37	0.01
			S3, S5	S281, S283	1.32	0.03
		A0A8I6A794	S6	S5014	1.37	0.00
			S3	S5014	1.39	0.00
			S6	S4094	0.69	0.01
Troponin	Tnni3	P23693	S2, S3	S23, S24	2.16	0.01
			S3, S4	S23, S24	2.12	0.01
			S1	S23	2.93	0.00

4.5 Discussion

4.5.1 Key findings

- Several differentially expressed proteins and phospho-proteins were identified in apex tissue at different time points following MI induced by LAD occlusion
- Changes in cardiac proteome and phospho-proteome are high 3-days post-MI, the early phase associated with apoptosis, stress response and mitochondrial dysfunction.
- The sham group at 3-days post-surgery show significant alterations in the cardiac proteome and phospho-proteome suggesting adverse effects of the surgical procedure.

4.5.2 Changes in the cardiac proteome and phospho-proteome in response to MI

Cardiac remodelling is a dynamic process triggered following cardiac injury, leading to scar formation and transition into heart failure. However, the molecular mechanisms behind these processes are still not fully understood. By utilising quantitative proteomics this work investigated the molecular changes occurring over-time during the remodelling process in adult rat heart. The data presented in this work show time dependent molecular changes following MI. The initial 3-day time-point post-MI is associated with the greatest number of protein and phospho-protein expression changes, highlighting it as a crucial point of the remodelling process. This is concurrent with previous findings in mice where the number of differentially expressed proteins increased across the first 72 hrs in the infarct zone, with many of the proteins identified at 24 hrs still identified 72 hrs post-MI (Y. F. Li et al. 2019b). The remodelling process is ongoing and evolving, with protein expression changes from 3-days to 2-weeks, and to a lesser extent from 2-weeks to 4-weeks post-MI. This supports previous findings of greater gene expression changes at the earlier stage post-MI in mice (Yokota et al. 2020). The changes in cardiac proteome were present in the apex of the heart, in this model the apex tissue taken for proteomic analysis was bordering the LV infarct area. The apex consists of the LV apex which may be susceptible to damage from LAD occlusion. Changes in protein expression may reflect either changes in protein synthesis or protein degradation. By studying phosphorylation, we can also gain an insight into the post-translational modifications of proteins which provide information on activation or inhibition in addition to total protein expression. Changes in cardiac

phospho-proteome in the rat heart following MI has not been extensively studied or reported.

4.5.3 Changes in proteins associated with apoptosis evident at the early stage of remodelling

The early stage of cardiac remodelling is associated with cellular death by apoptosis and necrosis, initiated due to ischemia creating disruption to ionic and metabolic homeostasis. Subsequently this triggers an inflammatory response in the heart (Prabhu and Frangogiannis 2016). This is reflected by the increased expression of known apoptosis and inflammation markers, as well as enriched pathways related to the stress-response, identified at the 3-day time-point in LAD animals.

Caspases 1, 3 and 6 are upregulated, caspase 1 is characterised as an inflammatory caspase, with 3 and 6 as executioner caspases (McIlwain et al. 2013). The EIF2 signalling pathway, upregulated 3-days post-MI, is activated in response to stress as part of the integrated stress response system (Santos-Ribeiro et al. 2018). These findings in the apex of the heart may suggest that the stress response and initiation of apoptosis occurs in border zones around the infarcted area. Given the up-regulation of these factors at 3-days in this remote region, it may reflect expansion of the infarct area occurs into this region. The infarct area is unlikely to be at its final size at 3-days, given the findings with differential extent of infarction in the histological assessment at 3-days in the above chapter. Inhibition of caspases has been shown to attenuate cardiac injury following MI with/without reperfusion (Chandrashekhar et al. 2004; Mocanu et al. 2000; Yarbrough et al. 2010), highlighting their importance in the remodelling process. With apoptosis markers present in the apex, an area which borders the infarct area and is considered susceptible following LAD occlusion, targeting them may protect against excessive cellular death facilitating infarct expansion.

4.5.4 Oxidative stress

Oxidative stress arises when the production of ROS overwhelms the innate protective antioxidant mechanisms leading to uncontrolled levels. Oxidative stress is a key driver in the damage induced by MI, activating cell death pathways. Mitochondria are a primary source of ROS, particularly when the ETC is disrupted and significant disruption to mitochondria is seen early post-MI (Y. R. Chen and Zweier 2014). The level

of oxidative stress is controlled by antioxidant enzymes, several of which were differentially expressed following MI.

Glutathione peroxidase and peroxiredoxin 4 were increased early post-MI, whereas other sub-types of peroxiredoxin and glutathione 1 were downregulated at 3-days. Levels of catalase and SOD were decreased following MI, this has been observed in patients following MI (Aladag et al. 2021). All markers of oxidative stress declined from 3-days post-MI to 4-weeks, only glutathione peroxidase 7 remained significantly differentially expressed 4-weeks post-MI. Some antioxidants were still at increased level by 2-weeks with the decline coming to 4-weeks (data not shown), suggesting oxidative stress is elevated across the first weeks post-MI. Increased hydrogen peroxide has been observed at 7-days post-MI in a mice, with a suggestion sustained increase in oxidative stress may influence remodelling (Pendergrass et al. 2011). Given the detrimental effects known to be caused by increased oxidative stress, modulation of this response could have therapeutic potential. Overexpression of catalase following MI has shown benefit in mice with improved cardiac function (Pendergrass et al. 2011).

Peroxidasin and Myeloperoxidase (MPO) were both increased early post-MI, reported to be part of the same family of peroxidase-cyclooxygenase superfamily. Peroxidasin is linked to formation of ECM components, with involvement in collagen IV cross-linking (Kovacs et al. 2021). Involvement of peroxidasin with the cardiac remodelling process following MI has not been reported. Myeloperoxidase is known to be associated with detrimental effects in a range of cardiovascular diseases. MPO is released by circulating leukocytes including neutrophils during the inflammatory response following injury and is associated with increased oxidative stress (Ramachandra et al. 2020). It was significantly upregulated at the 3-day time-point in this study, reflecting an ongoing immune response and increase oxidative stress at this time. The increase in MPO was diminished by 4-weeks post-MI with a decline from 3-days to 2-weeks followed by no further change with time (data not shown). Further confirming the role of MPO in injury, it has also been identified as a diagnostic marker for MI and predictor of mortality (Kolodziej et al. 2019; Omran et al. 2018). The finding of upregulation in this study confirms the potential of MPO as a critical target for protection against detrimental effects of cardiac injury (reviewed in (Ramachandra et al. 2020).

4.5.5 Matrix metalloproteinases (MMPs)

MMPs are proteolytic enzymes that respond to inflammation and facilitate ECM degradation early after infarction, with elevated MMP levels correlated to LV dysfunction (DeLeon-Pennell et al. 2017). MMP-2 and MMP-14 were identified in this proteomic analysis, with increased expression at 3-days post-MI. Both MMPs have been previously found to be upregulated post-MI, MMP-2 peaking in the earlier stages of repair with MMP-14 also present at the later stages of remodelling (Lindsey and Zamilpa 2012; Peterson et al. 2000). Inhibition of MMP-2 has been shown to improve the outcome after MI in mice (S. Matsumura et al. 2005), highlighting their crucial role in the remodelling process. The action of MMPs needs to subside to facilitate an increase in collagen synthesis over degradation, MMP level is controlled by the presence of TIMPs (tissue inhibitors of metalloproteinases). Unfortunately, TIMPs were not identified in this proteomic analysis.

4.5.6 Changes in extracellular matrix components

Cardiac fibrosis and the deposition of ECM in the infarcted area to form scar tissue is central to the remodelling process. Collagen is produced and deposited by fibroblasts in the infarcted area, and during maturation of the scar tissue become cross-linked to form a rigid structure, maintaining tensile strength in the LV wall. Collagen is the primary component of the ECM in the heart, but it is also comprised of fibronectin, glycosaminoglycans and proteoglycans. The ECM proteins not only contribute to cardiac structure but are also involved in signalling (Frangogiannis 2017). Therefore, the ECM proteins are heavily involved in the remodelling process.

4.5.6.1 Collagen proteins

As seen in the histology images shown in the previous chapter, as well as previous work (Lindsey and Zamilpa 2012), collagen is much more prevalent in the infarcted area at the later stages of remodelling. This proteomic analysis reveals an increase in collagen, as well as other ECM proteins, in the non-infarcted apex. The increased expression was seen early after MI at the 3-day time-point, with few collagens significantly differentially expressed in comparison to sham at 4-weeks. Previous animal model studies have reported an increased in collagen content, peaking within the first week post-MI before plateauing.

Collagens can be characterised as fibrillar (1, 3 and 5) and non-fibrillar (4 and 6) (Shamhart and Meszaros 2010). Collagen types 1 and 3 are the primary collagen subtypes present in the cardiac ECM, both decrease in abundance over-time in the apex tissue following MI. Collagen type 5 was increased at the early 3-day time-point, this collagen type is thought to be associated with collagen 1 and reported to increase in cardiac disease pathology (Shamhart and Meszaros 2010). The upregulated found in this study suggests it likely has an involvement in the early remodelling process, supporting previous work showing collagen type 5 depletion was detrimental, leading to increased scar size (Yokota et al. 2020).

The non-fibrillar forms of collagen, type 4 and 6, which are involved in organisation of the ECM and have also previously implicated in cardiac remodelling (Shamhart and Meszaros 2010). Collagen type 4, both α1 and α2 chains, were upregulated early after MI in this study. This supports previous findings of these collagen subunits increased in the peripheral zone early after MI (Yamanishi et al. 1998). Collagen 6 wasn't found to be significantly differentially expressed in this study but has been previously reported to be involved in the remodelling process with Col6a1 null mutant mice having greater recovery following MI (Luther et al. 2012; Shamhart and Meszaros 2010). Collagen 18a1 was the only collagen subtype identified as upregulated at the 4-week time-point compared to sham. Targeting Col18a1 has been previously tested as a protective strategy following MI, due to the potential anti-angiogenic effects of endostatin which is produced by cleavage of Col18. These studies reported worse outcomes, confirming an important role of collagen 18 in cardiac remodelling (Isobe et al. 2010; Sugiyama et al. 2018).

Modulation of cardiac fibrosis needs careful consideration in the context of MI as some level of fibrosis is crucial to the tensile strength in the infarct area, preventing excessive dilation or cardiac rupture.

4.5.6.2 Other extracellular matrix proteins

Collagen deposition, particularly in the infarcted area is crucial for tensile strength. However, the ECM is comprised of other proteins that are integral to maintaining elasticity in the heart, cell-matrix interactions as well as signalling. These proteins are involved in the reparative process following MI (Dobaczewski et al. 2010).

Fibronectin, galectin-3 and tenascin-C were upregulated at the 3-day time-point post-MI with little change in expression between LAD and Sham groups at 4-weeks. These proteins have been highlighted previously as increased early post-MI, involved in inflammation, the immune response and fibrosis. Galectin-3 being identified as a biomarker for cardiac disease, and elevated levels have been shown within 24 hours post-MI in rodents supporting the finding of increased expression at 3-days in this study (Hara et al. 2020; Hashmi and Al-Salam 2015). Tenascin C and fibronectin have also been reported previously to be increased post-MI (Knowlton et al. 1992; Willems et al. 1996). Tenascin C is thought to contribute adversely to the remodelling process, whilst fibronectin is thought to be beneficial in the remodelling process through modulation of cardiac progenitor cell expansion (Kimura et al. 2019; Konstandin et al. 2013). These previous studies identified these changes in the infarcted LV, this work suggests these changes also can be identified in non-infarcted tissue.

Several ECM proteins, periostin, versican, biglycan and SPARC, remained upregulated at 4-weeks in the LAD group, albeit to a lesser extent. Biglycan is a proteoglycan associated with cardiac remodelling and fibrosis, it can elevate TGF-β which is a known mediator of the remodelling process (Bereczki et al. 2007; Bereczki and Santha 2008). Biglycan mRNA levels have been reported to peak 7-days post-MI in rats, with an increase still observed at 42 days compared to sham (Ahmed et al. 2003). Integrin signalling was also identified as an enriched pathway 4-weeks post-MI, integrins link the cytoskeleton to the extracellular matrix and are known to be involved in cardiac fibrosis and hypertrophy (C. Chen et al. 2016; Meagher et al. 2021).

4.5.7 Structural proteins

Following MI several proteins relating to structural components of the heart were found to be different in comparison to sham, with increased phosphorylation at both early and late stages of remodelling. Proteins relating to cell-cell connections were downregulated at both early and late stages of remodelling, including gap junction, desmosomal and cadherin junction proteins, supporting previous findings in rat hearts (Matsushita et al. 1999). Changes in Connexin43 have previously been identified in tissue from patients with ischemic cardiomyopathy (Kostin et al. 2003). Additionally in this study we identified increased phosphorylation of Connexin43 at both 3-days and 4-weeks post-MI. Disruption to junctions between adjacent cardiomyocytes may interfere

with electrical conduction and mechanical function of the heart, facilitating the development of arrythmias further disrupting cardiac function.

4.5.8 Mitochondria and cardiac metabolism

Several mitochondrial related proteins were downregulated early after MI at 3-days, with mitochondrial dysfunction identified as an enriched canonical pathway at both 3-days and 4-weeks post-MI. Mitochondria are central to the production of energy in the heart, generating ATP via the TCA cycle and oxidative phosphorylation. Given the decreased expression of proteins comprising the complexes of the ETC reported in this study and by others previously (L. Yang et al. 2017), oxidative phosphorylation is going to be significantly impaired following MI, as identified by pathway analysis.

A decline in energy is observed in the failing heart and alterations in substrate utilisation occur. Various substrates can be utilised in cardiac metabolism, the contribution of these is known to change during the progression to heart failure. The main substrate utilised under physiological conditions are fatty acids, converted to acetyl-CoA via β-oxidation. Downregulated proteins at 3-days post-MI were associated with fatty acid metabolism, this was also supported by IPA analysis revealing inhibition of fatty acid β-oxidation at both 3-days and 4-weeks post-MI. This supports previous findings in LV tissue from rats 1-day and 14-days post-MI (Guo et al. 2017). Decreased expression of proteins involved in fatty acid metabolism has been previously reported in rat hearts 1-day post-MI, in agreement with our findings at 3-days (Remondino et al. 2000).

Heart failure has been associated with a reduced utilisation of fatty acid β-oxidation at the late stages, with an increase in utilisation of glycolysis (Neubauer 2007). However, this work also reported the glycolysis pathway to be enriched identified as downregulated. Reduced phosphorylation of pyruvate dehydrogenase E1 alpha subunit 4-weeks post-MI may support an increase in glucose utilisation, phosphorylation is inhibitory to the conversion of pyruvate, the end-product of glycolysis, into acetyl-CoA (Patel and Korotchkina 2001). Furthermore, previous research reports changes in protein expression in remote areas of the myocardium associated with increase glucose metabolism 8-weeks post-MI in rats (Remondino et al. 2000).

Increased use of glucose may occur at the early stages post-MI to provide the energy to enhance function in response to cardiac injury. Increased phosphorylation of glycogen synthase was identified 3-days post-MI, phosphorylation of this protein is inhibitory thereby reducing glycogen synthesis, potentially increasing the availability of glucose for substrate utilisation (Palm et al. 2013). Although the IPA analysis does not support an increase of glycolysis or gluconeogenesis at 3-days post-MI.

Given the known changes in cardiac metabolism that are clearly involved in the cardiac remodelling process, metabolism may offer a target for intervention.

4.5.9 Changes in calcium handling following MI

Calcium handling proteins are central to the initiation of cardiac contraction, through the transduction of excitation-contraction coupling. There is a reduction in calcium handling proteins (L-type channels, PLN, RyR, SERCA) at both time-points in comparison to sham, to a greater extent 3-days post-MI. Increased phosphorylation of these proteins modulates their activity, this may be to enhance calcium signalling to improve cardiac contraction. Phospholamban is a regulator of SERCA pump activity, phosphorylation removes the inhibitory effect on SERCA allowing greater uptake of calcium into the SR. The phosphorylation sites identified S16 and T17 are phosphorylated by cAMP and CaMKII respectively (Rodriguez et al. 2004). SERCA is also phosphorylated at site S38, a site linked to CaMKII, which is also thought to increase pump activity. SERCA is the main calcium transporter into the SR, increased pump activity mediates a quicker relaxation of the contractile proteins. The L-type calcium channels and ryanodine receptors are involved in the calcium release from the SR that initiates contraction, both were found to be phosphorylated. Phosphorylation of these calcium handling proteins mediates a positive inotropic and lusitropic effect, mediating an increase in contractile function. This is not unexpected as the cardiac function is impaired and sympathetic drive may increase early after MI to compensate. The increase in phosphorylation identified at the early time-point of 3-days post-MI only, not seen at 4-weeks, may reflect the loss of ability of the β-ARs to respond to sympathetic stimulation due to receptor downregulation, as discussed below.

4.5.10 Downregulation of β-adrenergic signalling

Downregulation of β-ARs has long been known to occur during heart failure, as shown in human heart tissue (Bristow et al. 1986; Fowler et al. 1986). Receptor

downregulation occurs in response to a chronic increase in sympathetic stimulation initiated to stimulate an increase in cardiac function (Mahmood et al. 2022). Inhibition of cardiac β-adrenergic signalling was identified in the pathway analysis in this study, at both the 3-day and 4-week time-points. Early downregulation of β-ARs has been measured in humans' post-MI and associated with progression into heart failure (Gaemperli et al. 2010). Reflective of the increased sympathetic drive, adrenaline and noradrenaline degradation was identified as an enriched canonical pathway 4-weeks post-MI, suggesting an excess of catecholamines. Degradation of catecholamines is regulated by catechol-O-methyltransferases and monoamine oxidases, which are both upregulated at the 4-week time-point (data not shown). The β-AR signalling pathway involves the stimulatory G protein alpha unit ($G\alpha_s$), activation of PKA and subsequently cAMP (Figure 1-4A). $G\alpha_s$ signalling is identified as inhibited in the IPA analysis for total protein at 4-weeks post-MI, reflecting the downregulation of β-AR signalling.

4.5.11 Sham surgery is associated with changes in the cardiac proteome and phospho-proteome

Sham surgery groups are utilised within animal studies to differentiate any responses because of the surgical procedure alone, not the intervention. With a need to strive towards reduction in animal numbers and reduce suffering, understandably there is a draw to reducing the use of sham animals. However, to do this but still produce robust data it is necessary to understand any changes the sham surgery may induce. Therefore, it was important to determine the protein expression changes in response to sham surgery, with naïve animals used as a comparison group. It is important to understand these changes to correctly interpret the effects that are a direct result of an LAD occlusion intervention. This study shows significant changes in the cardiac proteome and phospho-proteome at the early time-point of 3-days post-surgery. In comparison there are relatively few changes at the 4-week sham time-point compared to naïve.

4.5.11.1 Changes in protein expression in the sham heart 3-days post-surgery

At 3-days post-surgery the sham group was associated with several protein changes suggesting the surgical insult generates a response in the heart. Proteins involved in the inflammatory response, MMPs, apoptosis related proteins and antioxidants were upregulated in the sham heart at 3-days. The sham surgery is still a

severe procedure, animals undergo thoracotomy, heart exteriorisation and passing of a suture needle under the LAD. All factors which could produce local injury to the heart and therefore trigger a stress response in the heart. Although previous work investigating the sham environment in MI studies revealed no difference in inflammatory markers during the first week of recovery (Iyer et al. 2016). This previous work did not complete a full proteomic analysis but did analyse differences in collagen proteins and concluded there was no change in collagen protein expression in sham hearts (Iyer et al. 2016). This is contradictory to the findings in this study with an increase in collagen type 1, 3 and 5 in sham hearts. Analysis of the phosphorylation of proteins in the sham group at the 3-day time-point in comparison to the naïve hearts revealed several changes in phosphoproteins related to both calcium handling and contractile proteins.

4.6 Summary

The cardiac proteome and phospho-proteome are significantly altered following LAD occlusion, these changes were identified in cardiac tissue taken from an area bordering the infarcted zone. Following MI several protein changes occur in the heart, giving insight into the repair process the heart is undergoing. This work has supported prior findings regarding proteomic changes post-MI, with the additional insight into changes in the cardiac phospho-proteome. Understanding the cardiac remodelling process further will help to provide the information to uncover new therapeutic targets. Given the large numbers of differentially expressed proteins, analysis is ongoing to uncover novel proteins that may be important in the remodelling. This work has also identified changes in protein expression in the sham heart following surgery, highlighting the need for correct control groups for animal studies.

5 Changes in blood metabolites post-MI

5.1 Introduction

So far, this thesis has directly assessed functional, structural, and molecular changes that occur in the myocardium over time in response to MI. The presence of ischemia acutely triggers metabolic and ionic changes as discussed in the introduction, but also the subsequent cardiac remodelling process is associated with metabolic alterations. Given this, assessment of metabolites which is facilitated by the development of omics technologies can be utilised to assess the progression of remodelling and potentially uncover novel biomarkers.

A small number of studies in recent years, both clinical and animal studies, have investigated the changes in blood metabolome in cardiovascular diseases including hypertrophy, coronary disease, diabetic cardiomyopathy, and heart failure (Muller et al. 2019; Pouralijan Amiri et al. 2019; Sowton et al. 2019; Stenemo et al. 2019; Zhou et al. 2019; Zhu et al. 2019). Metabolome changes have also been reported in ST-segment elevated myocardial infarction, with increased circulating succinate levels correlating to extent of injury (Kohlhauer et al. 2018). Animal studies have explored metabolites following MI, though largely they focus on one time-point at either early or late stages. Metabolites relating to energy metabolism were changed in a rat MI model within 2 hours of coronary occlusion in cardiac tissue, with several confirmed in serum with potential as biomarkers (X. Wang et al. 2017). Metabolites in serum have been studied in a rabbit MI model but only at a single time-point of 12-weeks (McKirnan et al. 2019). Previous work in our research group (Alsadder, unpublished) revealed changes in circulating metabolites in both rodent and porcine models of MI at the 4-week time-point. This study aims to take this further and asses the temporal changes in circulating metabolites following MI in rats.

5.2 Aims

The aim of this chapter is to evaluate temporal changes in circulating metabolites following MI which could help uncover potential biomarker(s) that can be linked to functional, structural, and molecular cardiac remodelling. Additionally, a comparison of sham to naïve hearts will be made to determine any response to sham surgery.

5.3 Methods

Metabolomic analysis was performed on plasma samples obtained from blood collected at termination by cardiac puncture. Analysis was performed on samples from all time-points, 3-days (LAD n=5, Sham n=6), 2-weeks (LAD n=6, Sham n=5) and 4-weeks (LAD and Sham n=8) plus samples from naïve animals (n=4).

5.3.1 Sample collection

Blood samples were collected from hearts immediately after termination via cardiac puncture of the LV. The blood samples were centrifuged to obtain the plasma supernatant which was stored at -80^{o}C until metabolomic analysis was performed by NMR.

5.3.2 Metabolomics

Sample preparation and running of NMR was performed by Matt Goodwin at the Metabolomics Facility, University of Bristol. Samples were prepared and a pooled sample was created. Samples were run to acquire NMR spectra on a Bruker Avance III HD 500 MHz spectrometer. Full details are in the Methods section.

CPMG traces were used for analysis, measurements of peak area were made using MestReNova x64 software. Any differences in peaks between sample groups were analysed, and the identification of these peaks was done by evaluation on Chenomx Software (Figure 2-10) as well as comparison to available databases (HMBD) and previous literature (Psychogios et al. 2011; Soininen et al. 2009).

5.4 Results

Identified peaks are displayed on a representative NMR CPMG spectrum in Figure 5-1. The area of each peak was measured and is displayed in

Figure **5-2** expressed as the fold change between LAD occlusion and Sham groups at each time-point. The peak area of the identified metabolites at different time points in both sham and LAD hearts is displayed in Figure 5-3. By looking at both the difference between the LAD and sham groups as well as the profile over time, metabolites of interest were identified and analysed further.

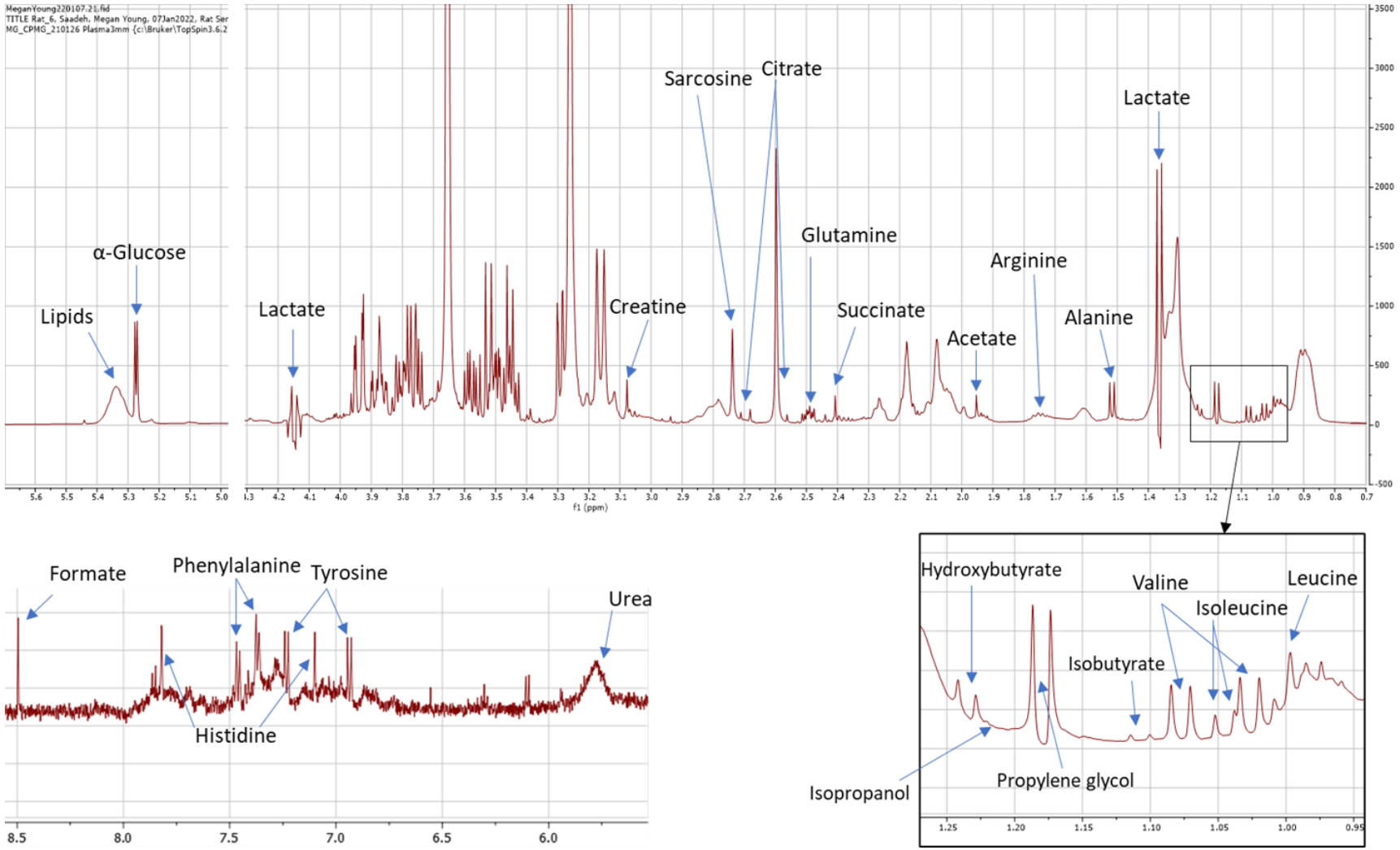

Figure 5-1 Annotated CPMG NMR spectra

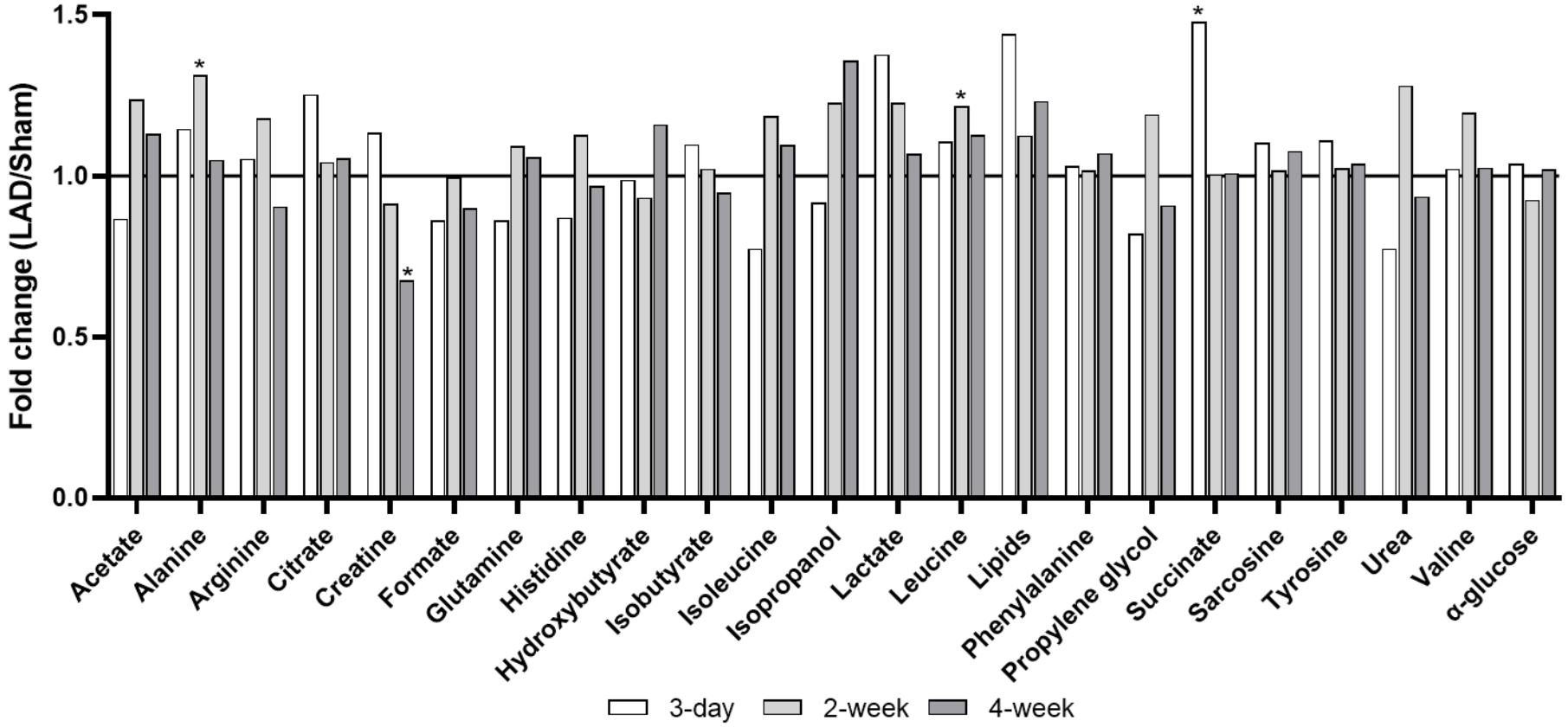

Figure 5-2 Identified metabolites

*Peak area of identified metabolites, expressed as fold change of LAD/Sham. Dotted lines represent 1.3-fold change. Difference between LAD and Sham peak areas for each time point analysed by T.Test, *p<0.05.*

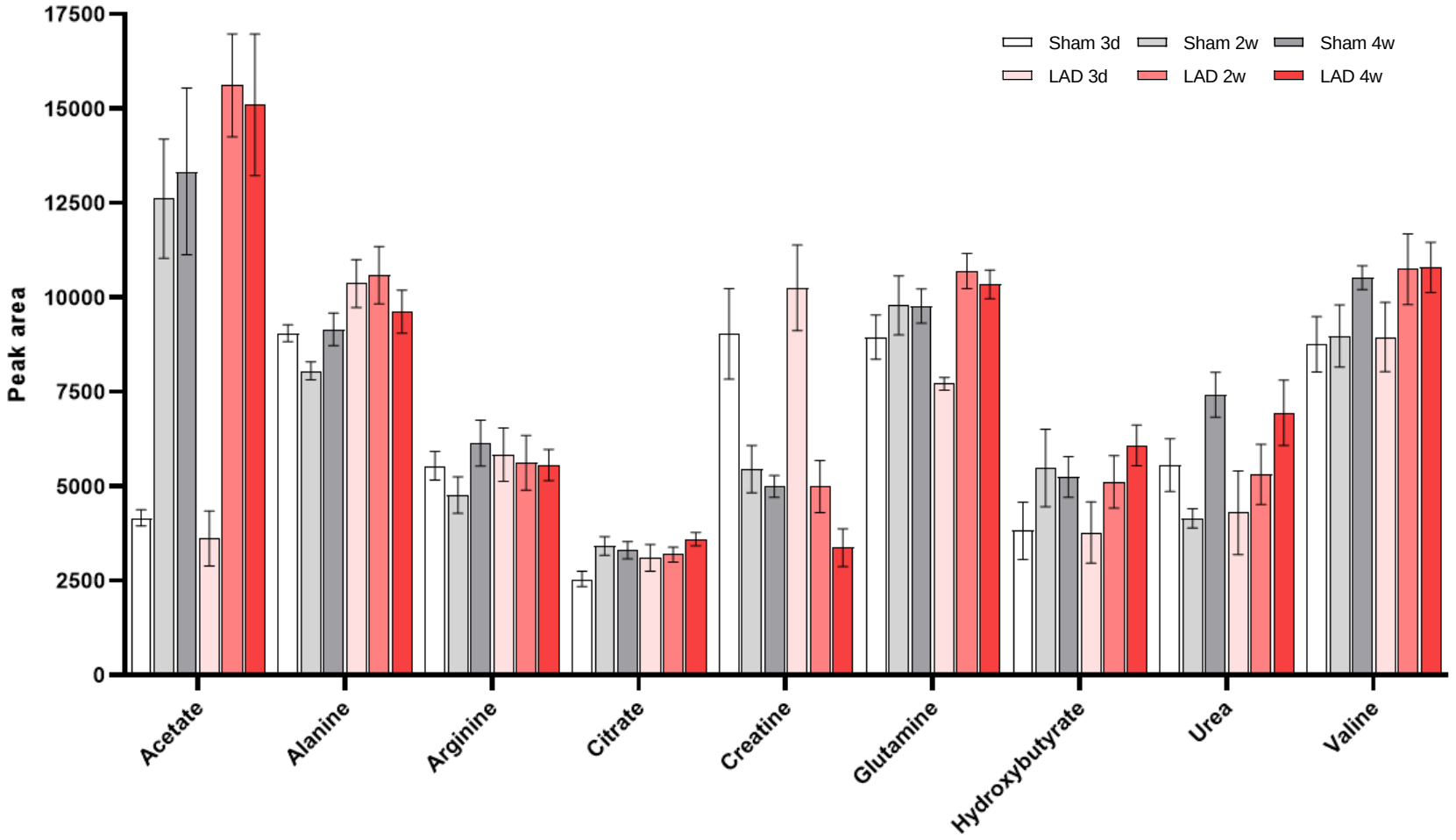
Sham 3d
Sham 2w
Sham 4w
LAD 3d
LAD 2w
LAD 4w
Peak area
17500
15000
12500
10000
7500
5000
2500
0
Acetate
Alanine
Arginine
Citrate
Creatine
Glutamine
Hydroxybutyrate
Urea
Valine

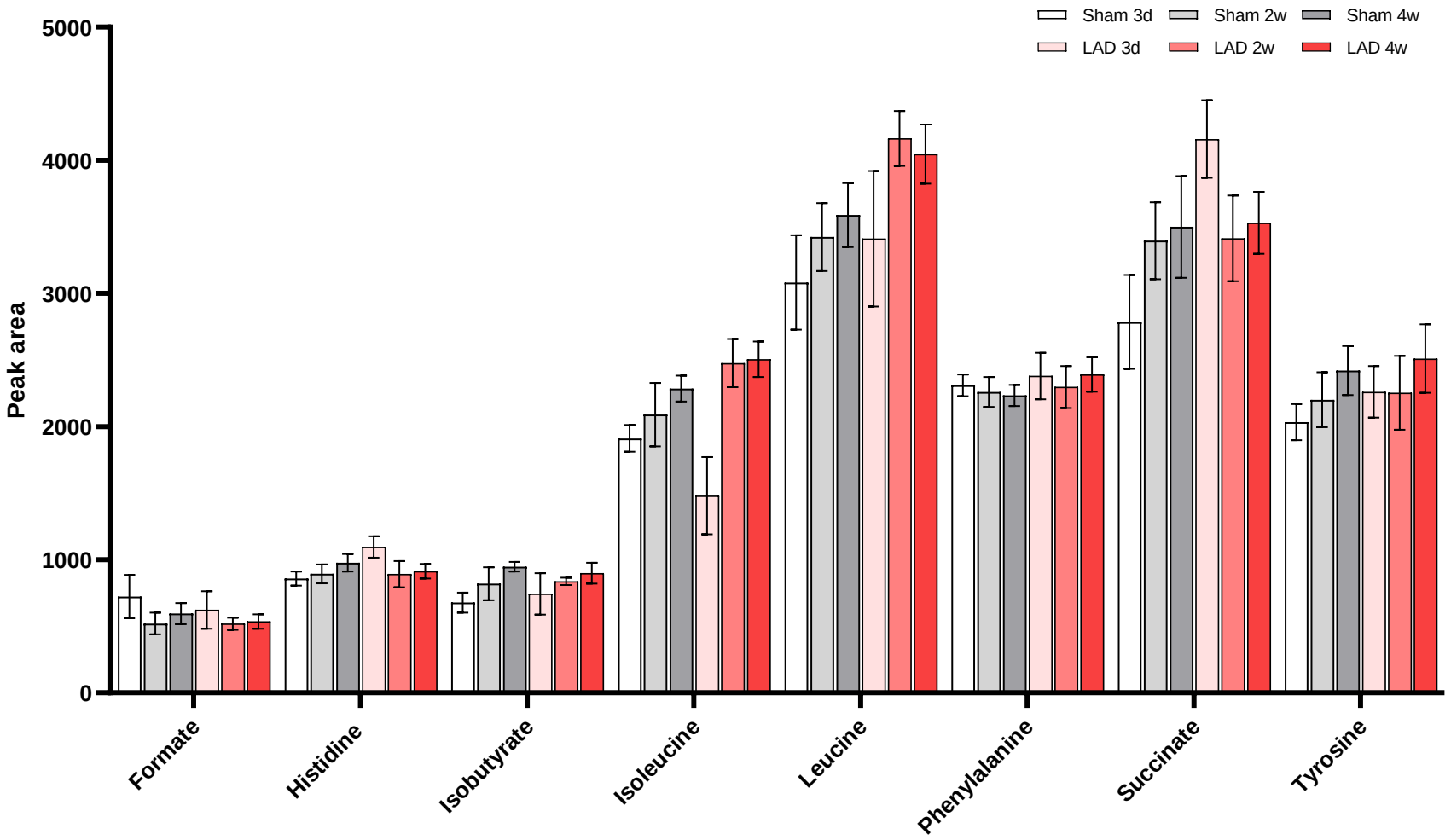
Sham 3d
Sham 2w
Sham 4w
LAD 3d
LAD 2w
LAD 4w
Peak area
5000
4000
3000
2000
1000
0
Formate
Histidine
Isobutyrate
Isoleucine
Leucine
Phenylalanine
Succinate
Tyrosine

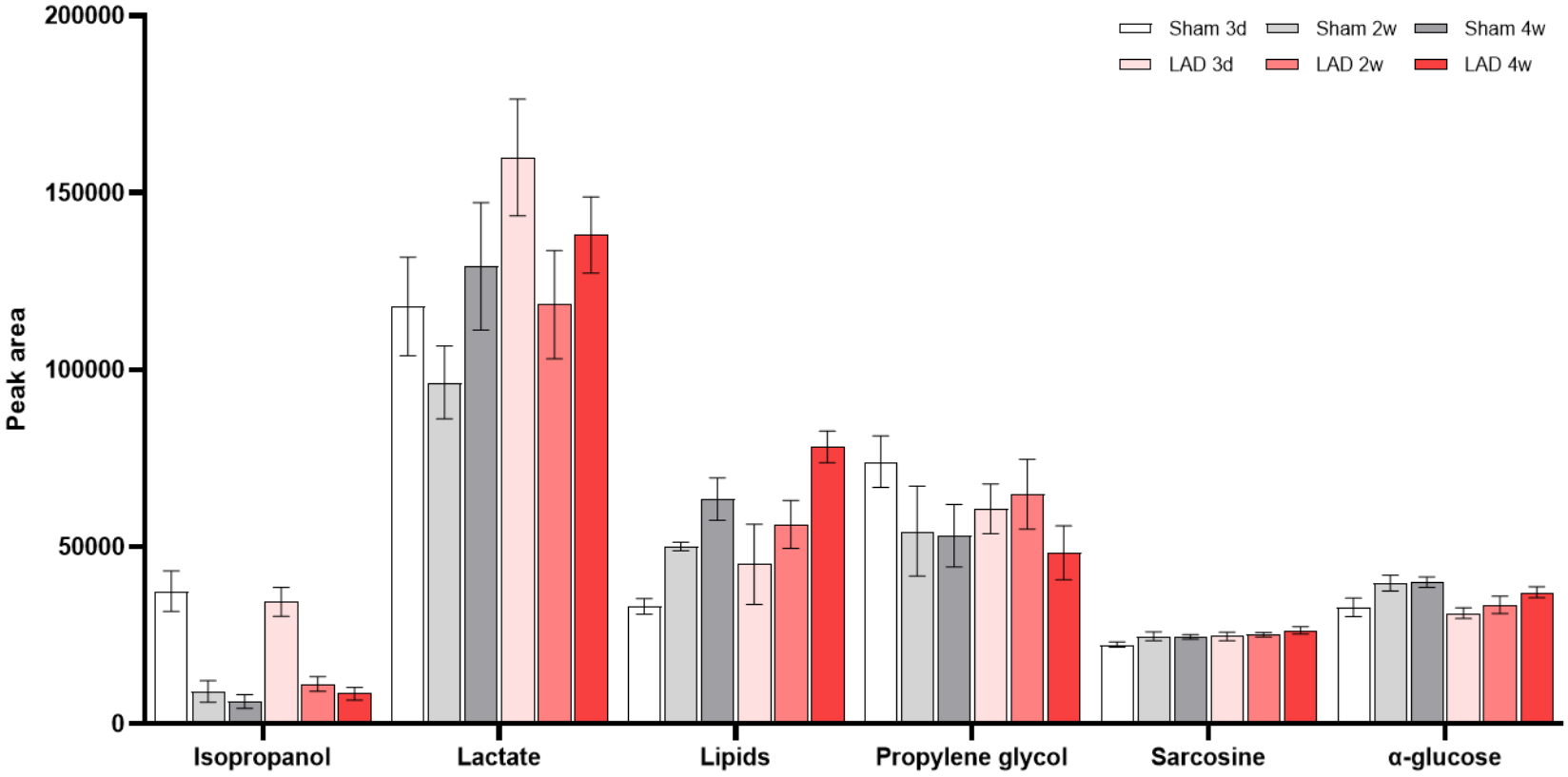

Figure 5-3 Time course of identified metabolites in both Sham and LAD occlusion groups

Peak area of identified metabolites at different time points (3-day, 2-week, and 4-week) post-surgery in sham and LAD hearts.

5.4.1 Changes in amino acids after MI

The amino acids Alanine and Leucine were found to have an increased level in the circulation in LAD groups compared to sham (Figure 5-4).

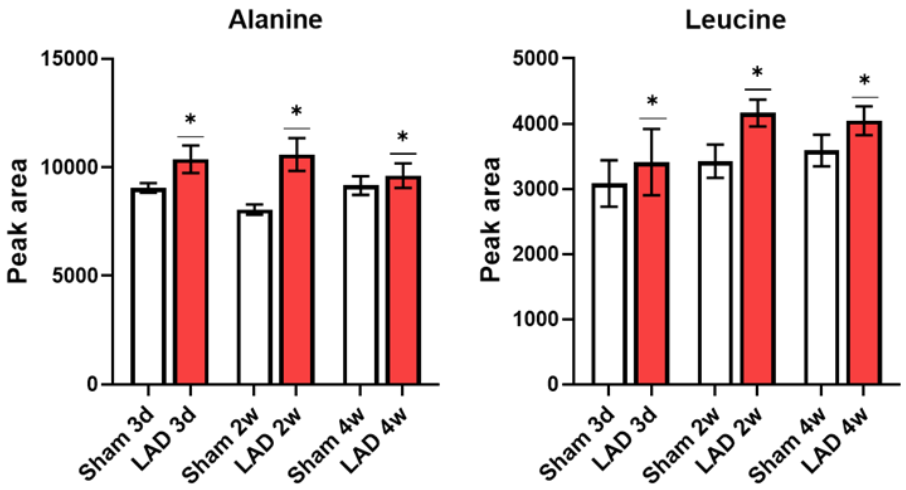

Figure 5-4 Amino acids with significant changes between LAD and sham groups

*Measurements of alanine and leucine in plasma of LAD and Sham groups at different time-points following surgery. Analysed by two-way ANOVA, main effect of group displayed *p<0.05 vs sham.*

5.4.2 Changes in lactate and succinate after MI

Lactate and succinate showed significant increases in the LAD group compared to sham at the 3-day time-point (Figure 5-5).

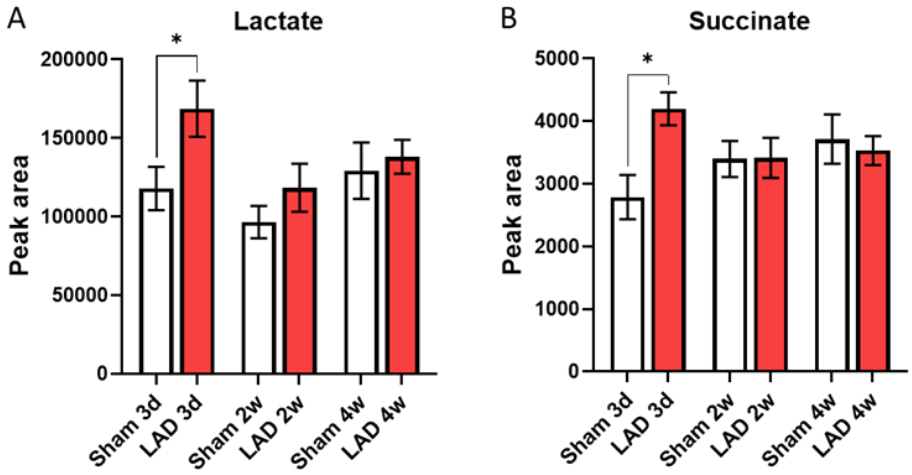

Figure 5-5 Circulating metabolites increased early following MI

*Measurement of (A) lactate and (B) succinate in plasma of LAD and Sham groups at different time-points following surgery. Analysed by two-way ANOVA, significant interaction of group/time, post-hoc analysis displayed (*p<0.05).*

5.4.3 Changes in circulating lipids following MI

Levels of circulating lipids were increased in the LAD group compared to sham. In addition, the level of lipids increased over time in both sham and LAD groups (Figure 5-6).

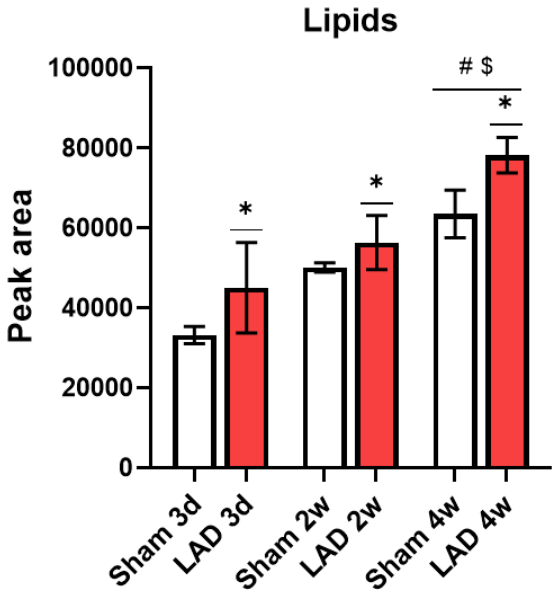

Figure 5-6 Circulating lipids increased following MI

*Measurement of lipids in plasma of LAD and Sham groups at different time-points following surgery. Analysed by two-way ANOVA, main effect of group (*p<0.05 vs sham) and time (#p<0.05 vs 3d, $p<0.05 vs 2w) displayed.*

5.4.4 Changes in metabolites early post-MI

Acetate and creatine were significantly different at the 3-day sham time-point in comparison to later sham time-points and the naïve group (Figure 5-7). Levels of acetate or creatinine were not significantly different between LAD and sham groups at the 3-day time-point, indicating the changes in these metabolites were a response to the surgery procedure itself.

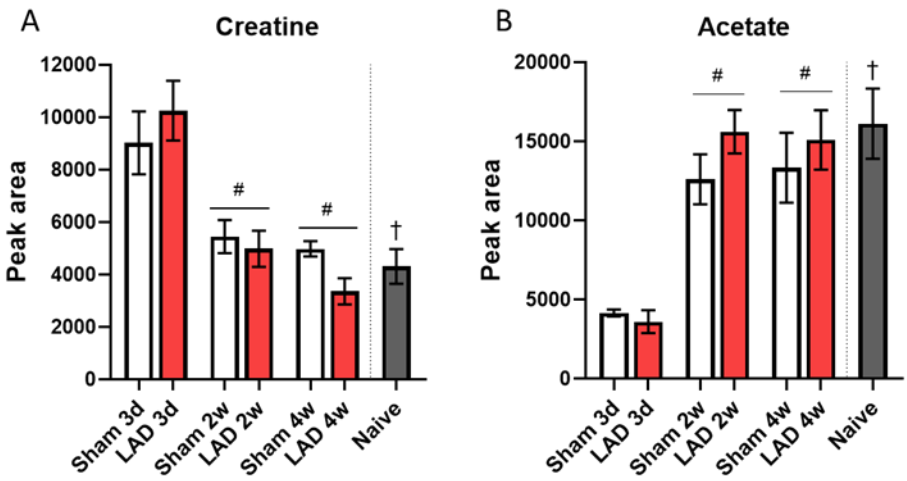

Figure 5-7 Circulating metabolites changed at 3-day time-point in LAD and sham groups

Measurement of (A) creatine and (B) acetate in plasma of LAD and Sham groups at different time-points following surgery, as well as naïve animals. Analysed by two-way ANOVA, main effect of time (#p<0.05 vs 3d) displayed. Separate analysis to compare naïve to sham groups by one-way ANOVA, †p<0.05 vs sham 3d.

5.5 Discussion

5.5.1 Key findings

- Induction of MI in adult male rats resulted in changes in circulating metabolites, including lactate, amino acids, and intermediates of the TCA cycle.
- Metabolite differences were identified between sham and naïve hearts at the early 3-day time-point.

5.5.2 Circulating metabolites change in response to MI

Studying metabolite changes in the circulation reflects systemic changes in the body in response to MI, it may not directly reflect changes in metabolites in the heart itself. Changes that can be observed in the circulation at different time-points may provide biomarkers for injury and the subsequent progression into heart failure (J. Wang et al. 2013).

5.5.2.1 Amino acids

In this study, alanine and the branched chain amino acid (BCAA) leucine were found to be increased in the LAD group. Amino acids are a substrate that can be utilised by the heart for energy production, under physiological conditions the contribution to ATP generation is low. However, in pathological conditions in the heart the substrate utilisation and metabolism pathways are known to alter, including amino acids. Changes in branched chain amino acids, including leucine, has been previously shown post-MI in rats, both in cardiac tissue and serum (R. Li et al. 2019a). They reported an initial decrease in leucine in serum followed by a persistent increase suggestive of a decline in BCAA metabolism (R. Li et al. 2019a). Our findings support this, with a bigger difference in leucine levels in plasma at 2-weeks post-MI, little change is observed at 3-days. In contrast, BCAA biosynthesis pathways have been identified as changing early post reperfusion in STEMI patients undergoing percutaneous coronary intervention (Surendran et al. 2019). Both alanine and leucine have been previously identified as elevated in cardiac tissue from patients with ischemic disease (Suleiman et al. 1998). More recently, alanine has been reported to be reduced 12-weeks post-MI in rabbits (McKirnan et al. 2019), suggesting the increase observed in this study early post-MI may not persist at later stages of remodelling. Alanine is a substrate for gluconeogenesis in the liver, increase circulating levels of alanine may reflect an increase in utilisation of glucose for energy production in the early stages post-MI.

5.5.2.2 Lactate

Increased levels of circulating lactate in LAD animals, over 1.3-fold compared to sham, was found 3-days post-MI although the increase was not quite significant. The lack of significance might be a result of small n numbers in the early time-point groups. Lactate is a by-product of anaerobic glycolysis (Figure 1-6), therefore an increase in circulating levels early after MI may be reflective of an initial switch to utilising anaerobic glycolysis to produce sufficient energy to maintain cardiac function in response to an ischemic insult. Lactate can also be utilised as a substrate for energy production therefore levels may be increased to promote energy production. In the clinical situation elevated lactate levels are associated with worse outcomes from cardiac incidents (Lazzeri et al. 2015; Park et al. 2021). Previous animal studies have shown lactate is increased in serum in rats subjected to coronary artery ligation within 2 hours post-MI (X. Wang et al. 2017), our work suggests this increase continues up until the 3-day time point.

5.5.2.3 Succinate

At the early time-point following MI levels of succinate were increased in the LAD group. Succinate is an intermediate of the TCA cycle, crucial to the production of ATP via oxidative phosphorylation. Succinate is known to accumulate during cardiac ischemia (Chouchani et al. 2014), and clinical trials have shown elevated circulating succinate levels have potential to predict outcome from MI in STEMI patients (Kohlhauer et al. 2018). This current work highlights further the response in succinate to MI, with elevated levels present in the blood 3-days post-MI.

5.5.2.4 Lipids

The levels of circulating lipids were higher in the LAD group across all time points, with a greater increased compared to sham at later stages. Fatty acids are the primary substrate utilised for energy generation; in the failing heart the substrate utilisation is thought to alter with reduced reliance on fatty acid metabolism (Neubauer 2007). The increase in circulating lipids in the LAD group at the later time-point may reflect this change in substrate utilisation.

5.5.3 Changes in circulating metabolites in response to sham surgery

Given the surgical procedure that is used to induce MI involves damage to other tissues as the muscles are dissected to allow access to the heart, the comparison to

naïve hearts is important to determine changes that are reflective of the surgical procedure.

Throughout this thesis comparisons have been made between sham and naïve hearts to understand the sham environment further. This work has identified that changes can also be measured in the circulation in response to sham surgery at the early 3-day time-point. Metabolites were identified that were significantly different in the 3-day sham group compared to naïve but with no change to the respective LAD group, indicating a response to the surgery procedure. Therefore, if a comparison was made between LAD and naïve, without a sham group included in the study, the wrong conclusion may be drawn. This is an important consideration for animal studies, highlighting the need for the inclusion of sham groups to differentiate the effects of the intervention and the surgical procedure

5.6 Summary

This study identified several metabolites that were significantly changed in response to MI at different time-points. These findings support previous research into metabolite changes during cardiac disease and heart failure, not all of which had been previously shown in a rat model of MI. Investigating circulating metabolites can provide further insight into the response to MI and the cardiac remodelling process, as well as help to uncover potential biomarkers. Changes in metabolism related pathways may not only offer potential biomarkers for diagnosis but may further highlight the crucial involvement of metabolism in progression to heart failure, and the need to investigate this as a potential area for therapeutics. Additionally, this work showed changes in response to sham surgery which show consideration needs to be taken when using control naïve groups instead of sham.

6 Cardioprotective potential of α1A-adrenergic receptor stimulation against IR injury in healthy and failing hearts

6.1 Introduction

During CPB surgery the heart is stopped to facilitate surgical intervention, rendering the heart ischemic. Ischemia, and the subsequent reperfusion (I/R), triggers calcium overload and excess ROS production (detailed in Chapter 1) which initiates cell death via necrosis or apoptosis, partly mediated by opening of the MPTP (Suleiman et al. 2001). The resultant injury in the heart can lead to cardiac remodelling into failure and facilitate arrythmias. Cardioprotective strategies have been sought to protect against this injury, predominantly the use of cardioplegia to arrest the heart during CPB surgery. However, the level of protection could be improved and therefore it is necessary to investigate additional cardioprotective strategies that may help to protect the heart against injury induced by I/R.

Targeting β-ARs in the heart prior to ischemia as a pre-conditioning strategy is beneficial against I/R in healthy hearts (Nasa et al. 1997; Tong et al. 2005). Although the β-ARs are the primary adrenergic receptors on cardiomyocytes, α1A-ARs are also present and have been shown to elicit an inotropic response in some myocytes when stimulated (Myagmar et al. 2017). In addition to positive inotropy, stimulation of α1A-ARs activates myocyte survival signalling via activation of the ERK signalling pathway which has been previously targeted to protect against ischemic injury (Huang et al. 2007; Lips et al. 2004). Overexpression of α1A-ARs has been shown to protect against cardiac remodelling following infarction and selective activation by the agonist A61603 showed protection against doxorubicin cardiomyopathy (Du et al. 2006; Montgomery et al. 2017; X. Zhao et al. 2015). Furthermore, α1A-ARs have also been shown to protect against ischemic injury (Perez 2021; Rorabaugh et al. 2005; Zhang et al. 2021). However, thus far there are no studies using the selective agonist A61603 to stimulate the α1A-ARs prior to ischemia as a preconditioning stimulus to test its efficacy for protection against I/R.

The susceptibility of the heart to I/R, and the response to cardioprotective strategies, may change in the presence of pathophysiology, for example heart failure (Ferdinandy et al. 2007). Therefore, cardioprotective strategies should be investigated in both normal and diseased hearts. If pre-conditioning of the heart by targeting α1A-ARs is protective, it may provide an alternative to β-AR pre-conditioning in pathophysiological states, such as heart failure, when β-ARs are desensitised (Lohse et

al. 2003). It has been previously reported the α1A-AR inotropic response is not lost in failing human hearts (Janssen et al. 2018).

6.2 Aims

The aim of this chapter was to investigate the cardioprotective efficacy of an α1A-AR agonist A61603 against I/R injury in healthy and failing rat hearts.

6.3 Methods

6.3.1 Animals

Adult male Wistar rats were used for all experiments. Naïve animals for obtaining healthy hearts weighed 275-300g, culled via IP injection of pentobarbital followed by cervical dislocation. Animals for obtaining failing hearts were 4-week post LAD occlusion to induce MI (sham animals 4-weeks post-surgery were used as controls) and weighed 300-350g, culled via IP injection of pentobarbital in combination with heparin followed by cervical dislocation.

By utilising the in vivo model to induce MI and recover the animals for 4-weeks it gives a disease model with a degree of heart failure, subsequently cannulating these hearts ex vivo and subjecting them to I/R injury allows testing of pre-conditioning strategies in a diseased heart.

6.3.2 Ischemia reperfusion protocols

Freshly excised hearts were cannulated on the Langendorff setup and perfused with oxygenated Krebs buffer at 37^{o}C. The flow rate of perfusion is set according to animal weight. The initial experiments completed on healthy hearts, perfusion was set at a flow rate of 10ml/min. The animals used for the failing heart experiments had a higher body weight and therefore perfused at 12 ml/min. Pressure balloons were inserted into the LV following cannulation to assess function, with EDP set at 5-10mmHg. Following a stabilisation period of Krebs buffer perfusion, hearts were subjected to 30 minutes ischemia followed by 60 minutes reperfusion. During ischemia perfusion was stopped and hearts were submerged in warm Krebs buffer to maintain temperature at 37^{o}C.

In the A61603 treatment group, prior to ischemia 3 minutes of drug treatment was given followed by 5 minutes washout (Figure 6-1). A61603 was made up in solution with Krebs buffer to the desired concentration, both 10 and 50nM were tested in this study. The A61603 solution was added to the second reservoir chamber on the Langendorff setup prior to perfusion to allow heating to 37°C and oxygenation. At the point of drug addition, the perfusion was switched to the A61603 and then returned to Krebs buffer for the washout period.

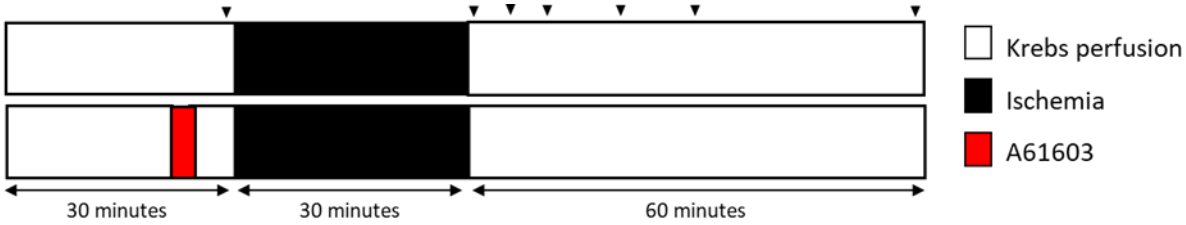

Figure 6-1. Ischemia reperfusion Langendorff protocol to study cardioprotection by A61603

Perfusion protocol: White - Krebs perfusion, Red - A61603 drug perfusion, Black - global ischemia. ▽ represents effluent collection time points for LDH measurement.

Ischemia reperfusion injury was assessed using three outcomes: functional recovery measured using LV pressure balloon, LDH release measured from effluent collection throughout reperfusion (Figure 6-1) and TTC staining for injured tissue area at the end of reperfusion. These methods are described in detail in the Methods chapter. The n-numbers for each group are displayed in Table 6-1.

Table 6-1 N numbers

	Control IR	IR+A61603 (10nM)	IR+A61603 (50nM)
Healthy	8	6	6
LAD occlusion	7	8	-
Sham	7	8	-

6.4 Results

6.4.1 A61603 pre-conditioning against I/R injury in healthy hearts

6.4.1.1 Baseline functional measurements

Baseline function measured via LV pressure balloon showed the initial values for LVDP, RPP and HR measured during the stabilisation period were not significantly different between treatment groups (Figure 6-2).

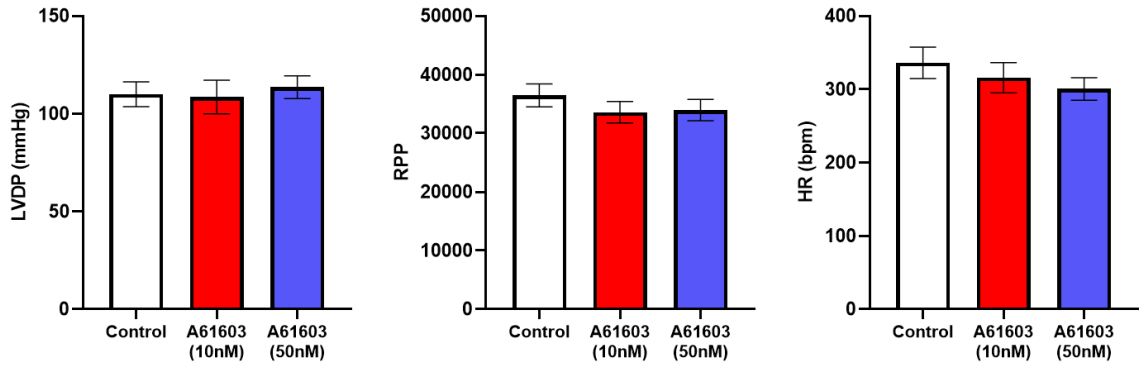

Figure 6-2 Initial values for LV function in control and A61603 treatment groups

Initial baseline measurements of left ventricle developed pressure (LVDP), rate pressure product (RPP) and heart rate (HR) for control (n=8), 10nM A61603 (n=6) and 50nM A61603 (n=6) treatment groups. Analysed by one-way ANOVA, p>0.05.

6.4.1.2 The effect of A61603 on cardiac function

Targeting α1A-ARs in healthy hearts using the drug A61603 produced a positive inotropic response at both 10 and 50nM (Figure 6-3). The response to A61603 at both concentrations initially triggered a transient rapid increase in LVDP concurrent with an increase in HR. This initial increase is followed by a fall in LVDP followed by a sustained increase reaching 130.5 ± 10.1 mmHg or 122.7 ± 3.7% of baseline for 10nM and 147.3 ± 7.8mmHg or 129.3 ± 5.9% of baseline for 50nM. RPP, which takes into account HR, follows a similar trend (Figure 6-3A.) Comparison of the response to A61603 at 10nM to 50nM showed there was no significant difference in the LVDP response between the two concentrations (Figure 6-3B).

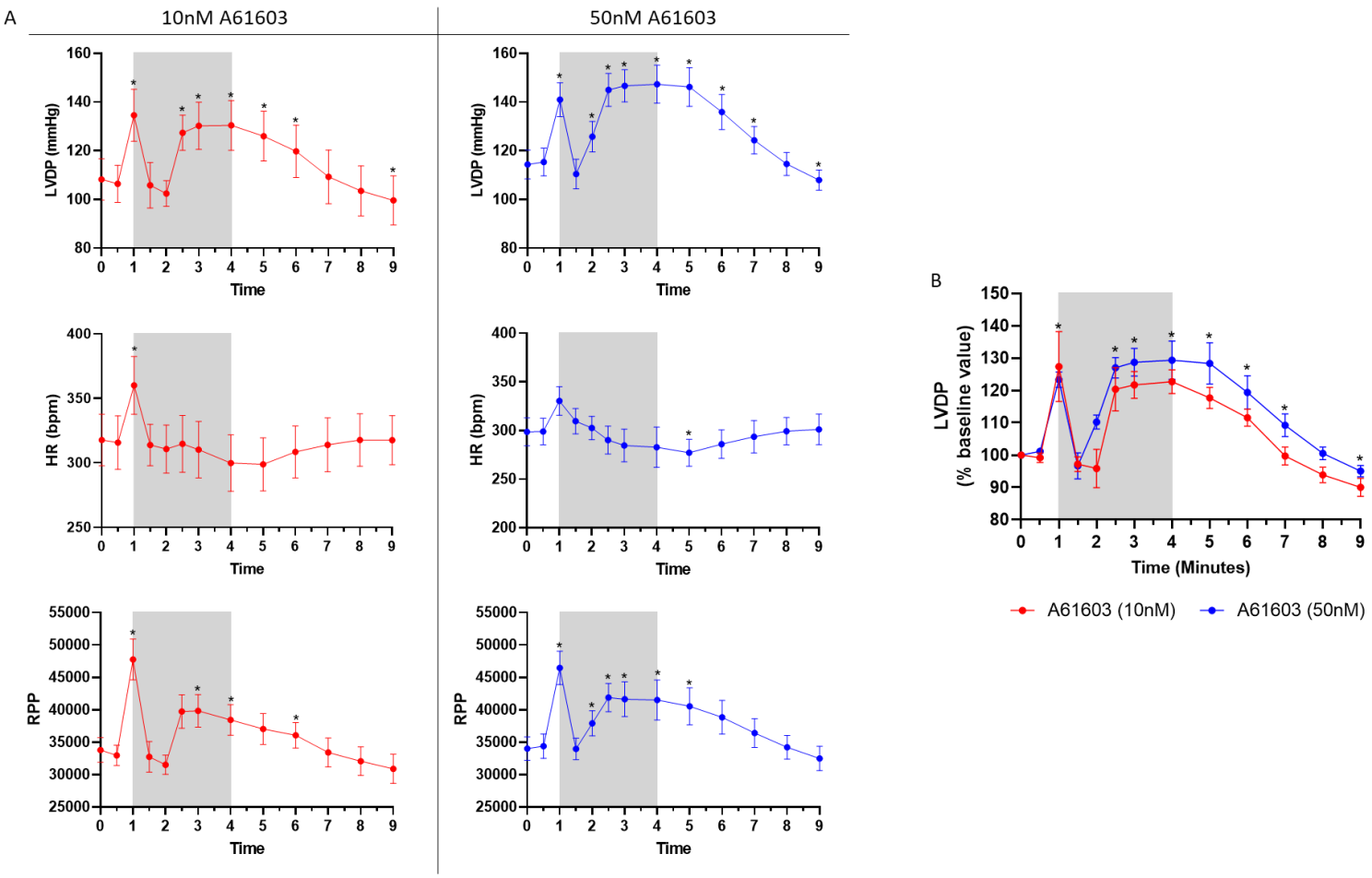

Figure 6-3 Response to A61603 drug treatment in healthy hearts

*(A) Changes in LVDP, HR and RPP during treatment with 10nM (red) or 50nM (blue) A61603 (grey box indicates drug perfusion period). Analysed by repeated-measures ANOVA, *p<0.05 vs time 0. (B) Comparison of increase in LVDP with 10nM vs 50nM A61603, displayed as % of baseline. Analysed by two-way repeated measure ANOVA, no significant interaction of time/group, significant main effect of time displayed, *p<0.05 vs time 0.*

6.4.1.3 The effect of A61603 pre-conditioning on ischemic contracture

Contracture of the heart occurs during a period of global ischemia and can be measured via the LV pressure balloon. Pre-conditioning with 50nM A61603 had a greater effect on the profile of ischemic contracture than 10nM A6163 in comparison to the control group (Figure 6-4A). Pre-treatment with 50nM A61603 resulted in an earlier onset of ischemic contracture than that seen with 10nM A61603 and control hearts (Figure 6-4B). The peak contracture reached in hearts pre-treated with 50nM A61603 was significantly higher than 10nM A61603 treated (Figure 6-4C). Despite an earlier onset of contracture in the 50nM A61603 group compared to control, the time of peak contracture was not significantly different to control. In addition, the 10nM A61603 group began contracture at the same point as the control group however the time to peak contracture was increased compared to control, indicating a slower rate of contracture in the A61603 groups compared to control.

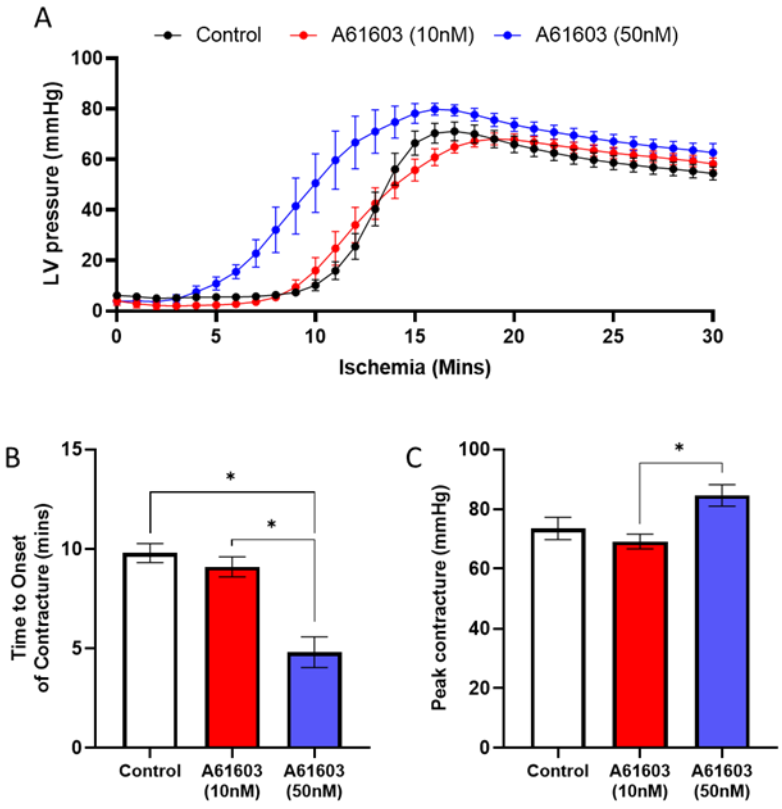

Figure 6-4 Ischemic contracture with A61603

*(A) Profile of ischemic contracture with or without A61603 pre-conditioning. (B) Time to contracture and (C) Peak contracture, analysed by one-way ANOVA with Tukey's post-hoc, *p<0.05.*

6.4.1.4 The effect of A61603 pre-conditioning on functional recovery after I/R

The recovery of LV function was recorded across 1 hour of reperfusion. Pre-conditioning with A61603 at both 10 and 50nM significantly improved recovery of LVDP and RPP (Figure 6-5A-B). There was no significant difference between the 10nM and 50nM treatment groups at 60 minutes reperfusion. At 60 minutes of reperfusion LVDP was 17.9 ± 2.8% of baseline for control hearts, increased to 36.3 ± 3.1% and 32 ± 3.8% with 10nM and 50nM A61603 pre-conditioning respectively. Max dP/dt, a marker of contractility, was increased in the 10nM A61603 group compared to control (Figure 6-5C). In the A61603 treatment groups during reperfusion EDP was reduced. EDP reduced to 81.49mmHg and 76.04mmHg in the 50nM and 10nM A61603 respectively compared to 99.13mmHg in the control group at 60 minutes reperfusion, despite a similar initial increase in EDP at the beginning of reperfusion (Figure 6-5D).

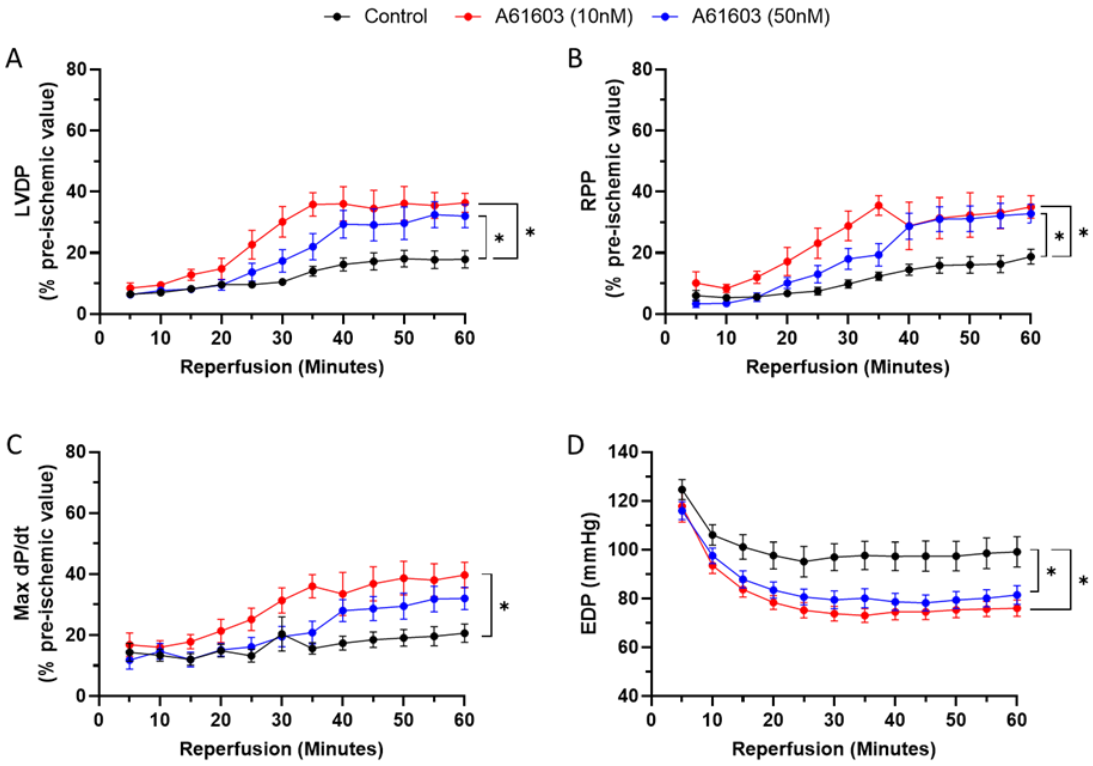

Figure 6-5 Functional recovery across reperfusion in healthy hearts with A61603 pre-conditioning

*Recovery of LVDP (A), RPP (B), Max dP/dt (C) and EDP (D) across reperfusion following 30 minutes ischemia with or without A61603 pre-conditioning. Analysed by two-way repeated measures ANOVA, significant interaction of group*time, post-hoc analysis comparing treatment groups at 60 minutes reperfusion displayed, *p<0.05*

6.4.1.5 The effect of A61603 pre-conditioning on LDH release

Release of LDH across reperfusion, a marker of cardiac injury, was not significantly different between A61603 treatment groups and control. LDH release over time was lower in the A61603 group compared to control but analysis of the AUC revealed no significant changes (Figure 6-6), control AUC 1132 ± 123 compared to 10nM A61603 888 ± 106 and 50nM A61603 857 ± 71.

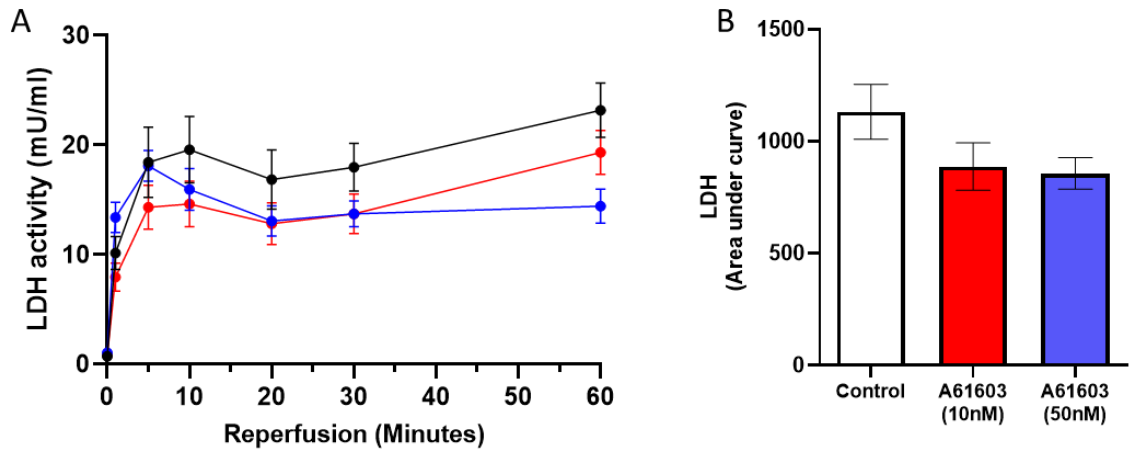

Figure 6-6 LDH release during reperfusion in healthy hearts with A61603 pre-conditioning
(A) LDH activity across 60 minutes reperfusion, following 30 minutes ischemia, with or without A61603 pre-conditioning. (B) AUC analysis for LDH release, analysed by one-way ANOVA (p>0.05)

6.4.1.6 The effect of A61603 pre-conditioning on extent of injury sustained in the myocardium

At the end of reperfusion, hearts were stained with TTC to identify the injured tissue area. In control hearts, not pre-conditioned with A61603, 43.4 ± 6.2% of the myocardium was stained white indicating injury. The extent of injury was reduced to 13 ± 2.3% and 22 ± 4.4% in hearts pre-conditioned with 10nM and 50nM A61603 respectively (Figure 6-7A). The reduction of injury with A61603 treatment can be visually observed in the representative images (Figure 6-7B).

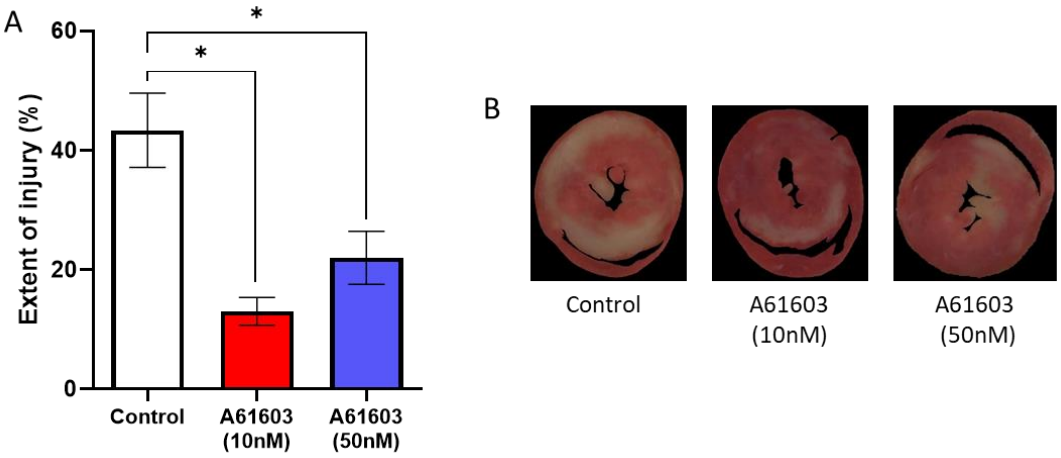

Figure 6-7 Extent of injury at the end of reperfusion following A61603 pre-conditioning in healthy hearts

*(A) Sustained injury at the end of reperfusion expressed as a percentage of the myocardium, analysed by one-way ANOVA, *p<0.05. (B) Representative images of TTC staining in hearts from each treatment group.*

6.4.2 I/R injury in failing hearts

6.4.2.1 Pre-ischemic LV function

Animals used to investigate I/R injury in failing hearts (LAD group) underwent echocardiography prior to termination to confirm reduced cardiac function. Ejection fraction was significantly reduced in the LAD occlusion group compared to Sham, 43.6 vs 80.3% (Figure 6-8A).

The initial baseline values of LVDP, HR and RPP in both groups once cannulated on the Langendorff setup, measured via the LV pressure balloon, were not significantly different (Figure 6-8B).

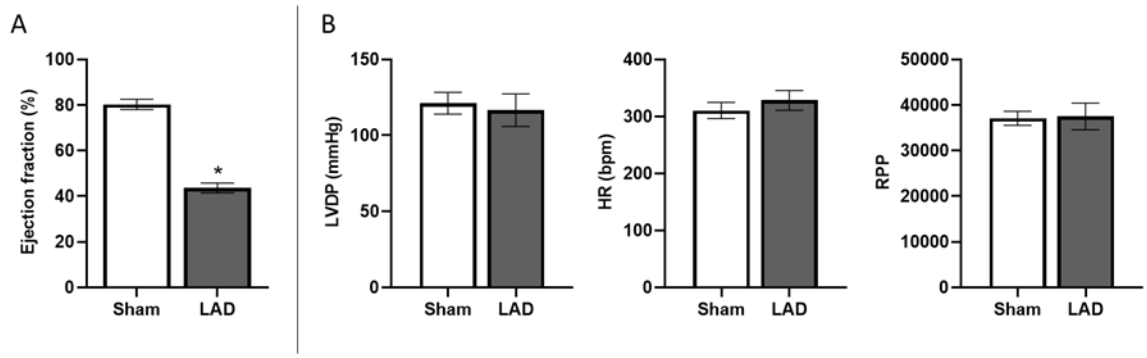

Figure 6-8 Pre-ischemic LV function in failing hearts

*(A) Ejection fraction in sham and LAD hearts 4-week post-surgery. (B) Ex vivo functional measurements in sham and LAD hearts 4-weeks post-surgery cannulated on the Langendorff setup, initial baseline values for LVDP, HR and RPP. Analysed by student's t.test, *p<0.05 vs Sham*

6.4.2.2 Changes in ischemic contracture

Development of ischemic contracture, measured by the LV pressure balloon, differs between Sham and LAD hearts subjected to ischemia (Figure 6-9A-B). The time to onset of contracture was significantly increased in the LAD group compared to Sham, 13.8 ± 0.8 vs. 9.9 ± 0.8 (Figure 6-9C), whilst peak contracture was significantly decreased in LAD hearts compared to Sham, 56 ± 5.9 vs. 87.4 ± 4.4 mmHg (Figure 6-9D).

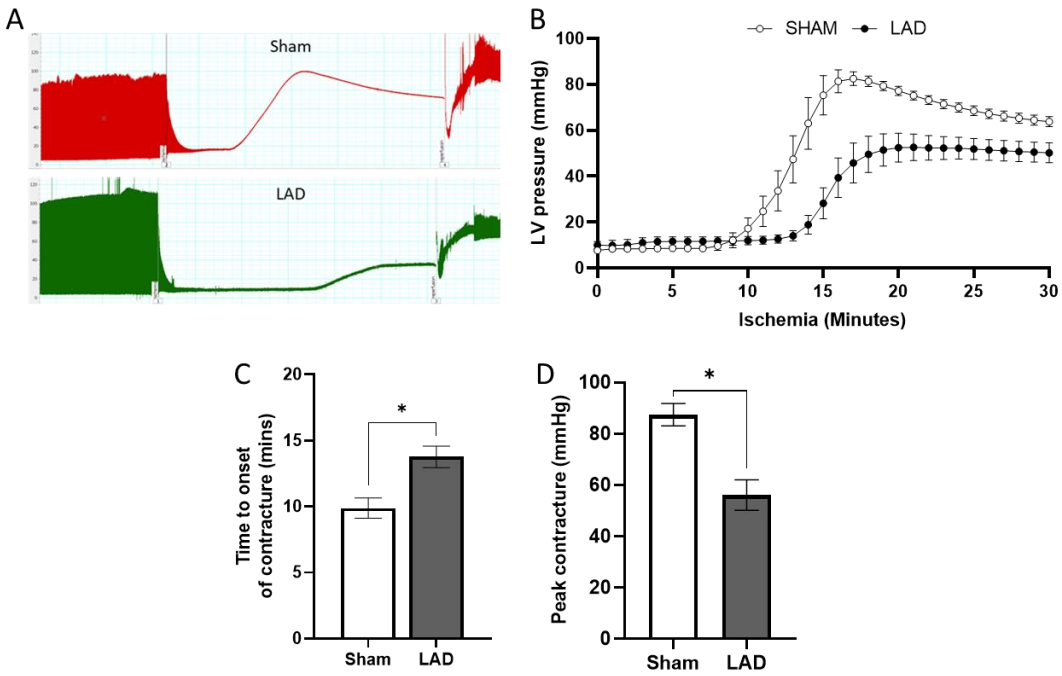

Figure 6-9. Ischemic contracture in failing hearts

*Ischemic contracture in failing (LAD occlusion) and Sham hearts across 30 minutes ischemia (A-B). Time to start of contracture (C) and Peak contracture (D), analysed by independent samples T.Test, *p<0.05.*

6.4.2.3 Functional recovery in failing hearts

Recovery of LVDP and RPP across reperfusion following ischemia was not significantly different between LAD occlusion and sham hearts, although there is a slight trend for poorer recovery in the LAD occlusion group (Figure 6-10).

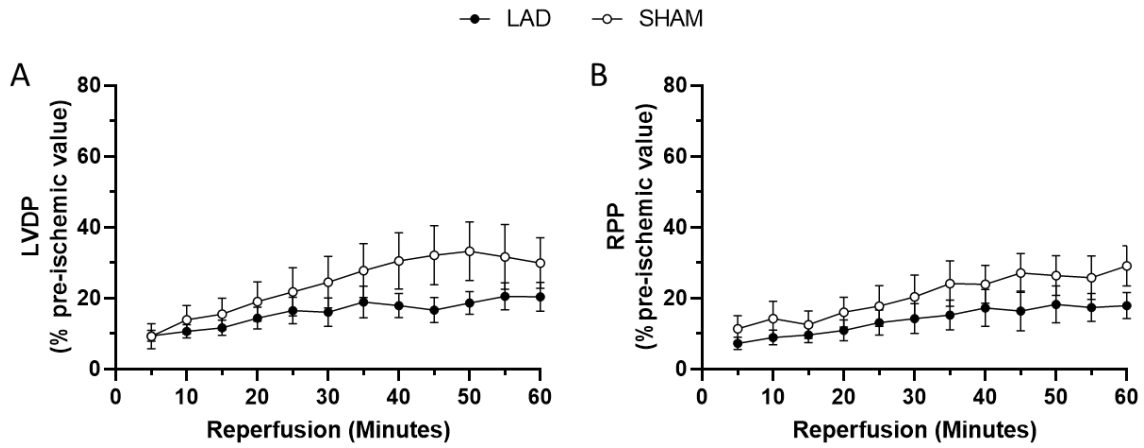

Figure 6-10. Changes in LV function during reperfusion in failing hearts

*Recovery of (A) LVDP and (B) RPP across reperfusion in failing (LAD occlusion) and Sham hearts, analysed by two-way repeated measures ANOVA, no significant interaction of surgery group*time or main effects.*

6.4.2.4 LDH release in failing hearts

Release of LDH across reperfusion was not significantly different between Sham and LAD hearts (Figure 6-11). Area under the curve (AUC) was calculated for Sham and LAD hearts, 1240 ± 203 and 1592 ± 261.

6.4.2.5 Extent of injury in failing hearts

TTC staining at the end of 60 minutes reperfusion shows injured tissue in white, with healthy tissue showing red. The infarcted area of tissue in the LV resultant from the prior LAD occlusion was identified and removed prior to analysis in the LAD group. The amount of injury sustained by LAD hearts because of IR was higher than in sham hearts (42.1 ± 6% vs. 19.9 ± 6.7%) but the difference was not significant, p=0.1091 (Figure 6-12).

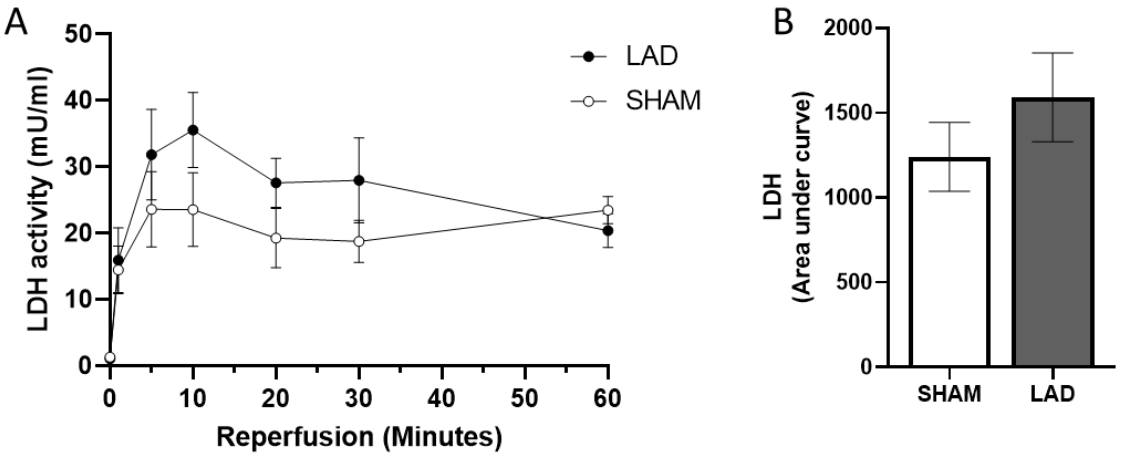

Figure 6-11. LDH release across reperfusion

(A) LDH activity across reperfusion in Sham and LAD hearts. (B) Area under curve, analysed by independent samples T.Test (P>0.05).

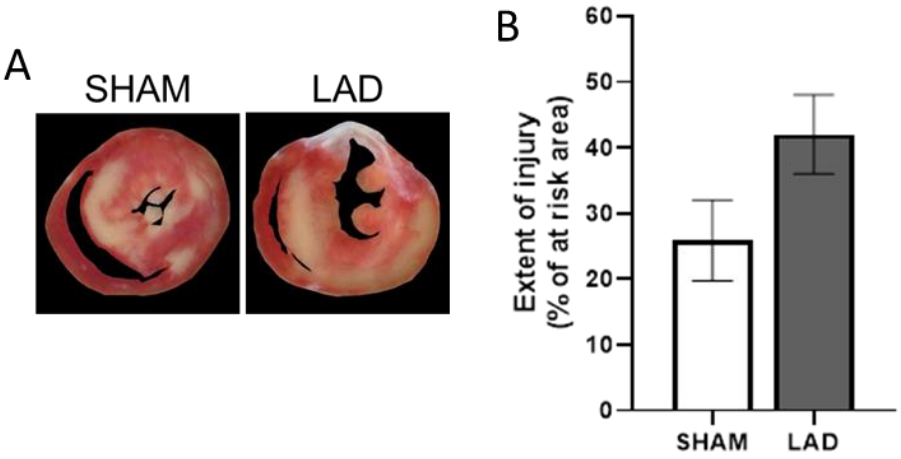

Figure 6-12. Injury sustained from ischemia reperfusion

(A) Representative images of Sham and LAD hearts stained with TTC at the end of reperfusion, injured tissue = white/yellow and healthy tissue = red. (B) Extent of injury sustained from IR calculated in sham and LAD hearts, analysed using T.Test, P>0.05.

6.4.3 A61603 pre-conditioning against I/R injury in failing hearts

Due to the similarities in protection by the 10nM and 50nM doses of A61603, the lower concentration of 10nM was utilised in experiments going forward.

6.4.3.1 The effect of A61603 on cardiac contractility

An inotropic response was observed following perfusion with A61603 in both LAD and Sham hearts (Figure 6-13). This effect was reversed following the drug washout period. A61603 drug treatment initiates an initial spike in LVDP, followed by a more sustained increase in contraction. At the end of the washout period, LVDP returns to baseline level in both groups.

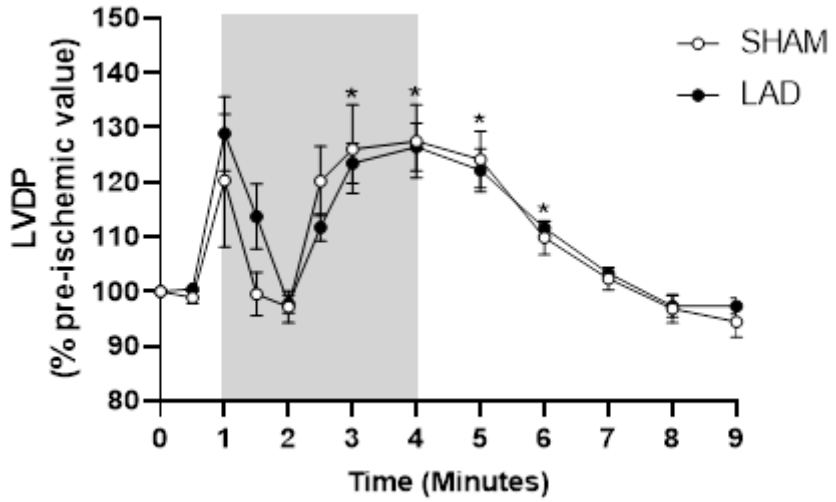

Figure 6-13. Response to A61603 drug treatment

Change in LVDP, expressed as a % of initial value, across administration of 10nM A61603 (grey) and subsequent washout, in Sham and LAD hearts. Analysed by two-way repeated measures ANOVA; no significant interaction, main effect of time ($p<0.05$ vs time 0) displayed.*

6.4.3.2 The effect of A61603 pre-conditioning on ischemic contracture

Pre-treatment with A61603 had no effect on ischemic contracture in LAD or Sham hearts (Figure 6-14A). Time to start of contracture and peak contracture overall were significantly different between Sham and LAD groups, with no main effect of A61603 treatment (Figure 6-14B, C).

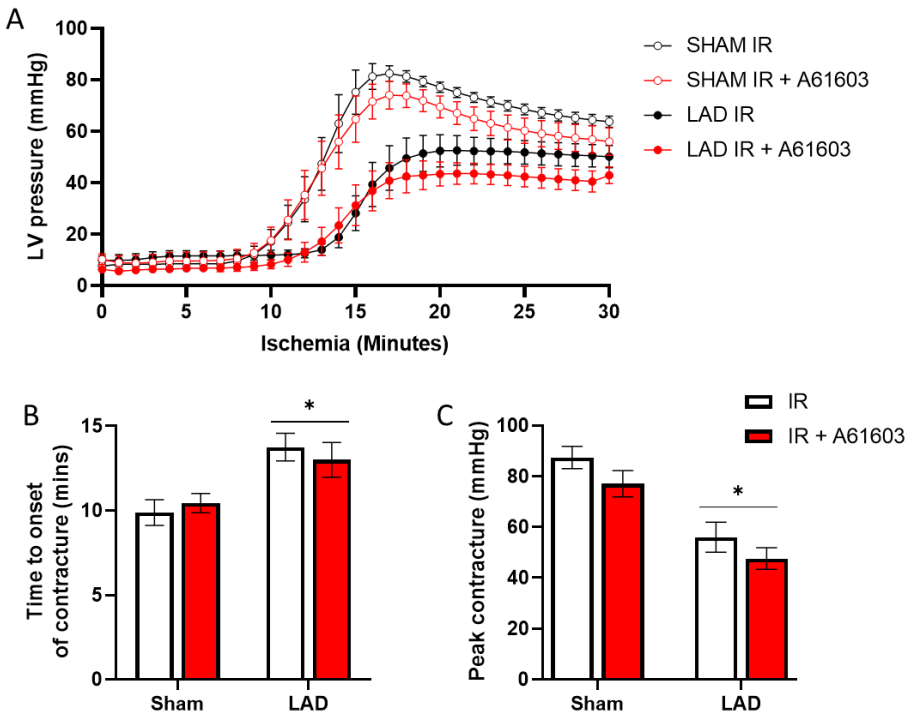

Figure 6-14. Ischemic contracture in failing hearts following A61603 pre-conditioning

(A) Ischemic contracture in LAD and Sham hearts with or without A61603 pre-conditioning. (B) Time to start of contracture and (C) Peak contracture. analysed by two-way ANOVA for effect of surgery group and A61603 treatment: no significant interaction, main effect of surgery group (p<0.05) displayed.*

6.4.3.3 The effect of A61603 pre-conditioning on functional recovery

Pre-conditioning with 10nM A61603, in LAD or Sham hearts, did not affect the recovery of LVDP across reperfusion (Figure 6-15). A small improvement in function is observed around 40 minutes in the LAD treatment group, however this difference was not significant.

6.4.3.4 The effect of A61603 pre-conditioning on LDH release

Release of the cardiac enzyme LDH did not significantly differ across reperfusion following pre-treatment with A61603 in LAD or sham hearts (Figure 6-16A). Analysis of AUC showed no difference in LDH release in LAD or sham hearts with A61603 pre-conditioning (Figure 6-16B).

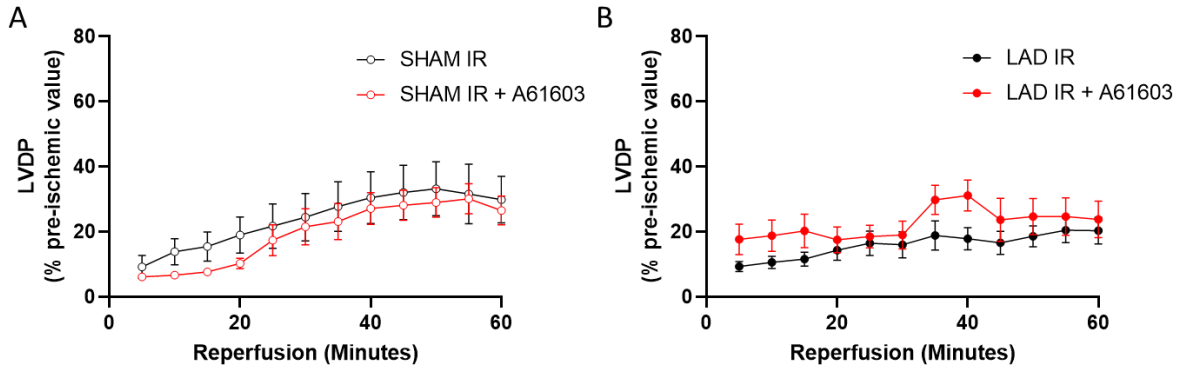

Figure 6-15. Functional recovery across reperfusion in failing hearts with A61603 pre-conditioning

LVDP measured across reperfusion in LAD and Sham animals with and without A61603 pre-conditioning. Analysed by two-way repeated measures ANOVA (p>0.05).

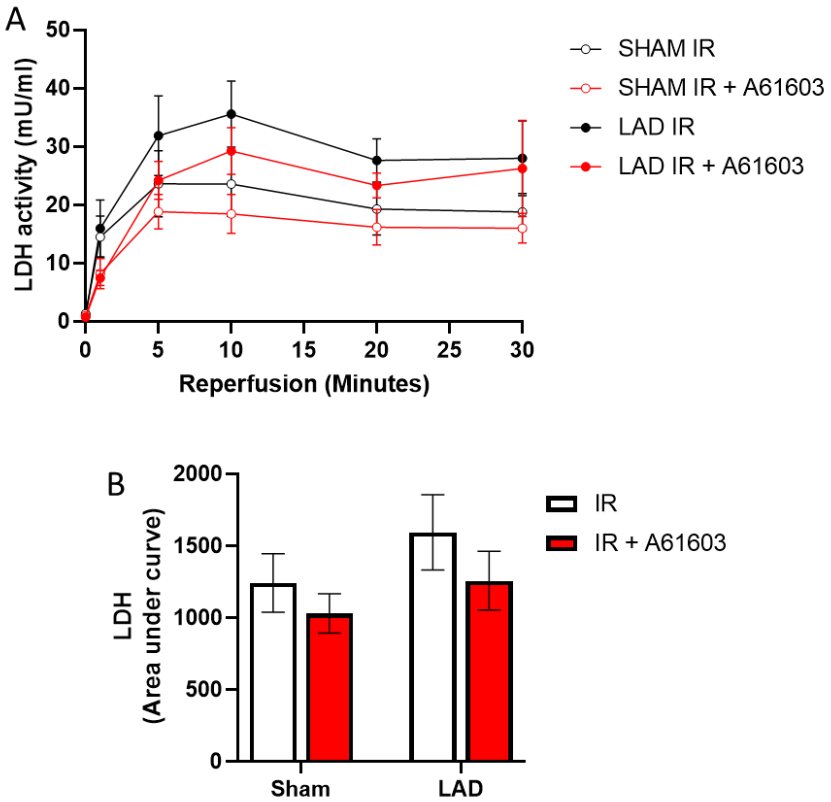

Figure 6-16. LDH release across reperfusion in failing hearts with A61603 pre-conditioning

(A) LDH activity across reperfusion in LAD and sham hearts with and without treatment with A61603 prior to ischemia. (B) Area under curve analysed by two-way ANOVA; interaction and main effects (P>0.05).

6.4.3.5 The effect of A61603 pre-conditioning on extent of injury sustained in the myocardium

TTC analysis to assess injured tissue showed that the level of injury was higher in the LAD groups compared to sham, regardless of A61603 treatment. Pre-conditioning with A61603 had a significant effect on reducing injury level in both surgery groups (Sham 19.9 ± 6.7% vs. 13.5 ± 3.4%, LAD 42.1 ±6%, vs 28 ± 2.9%) (Figure 6-17).

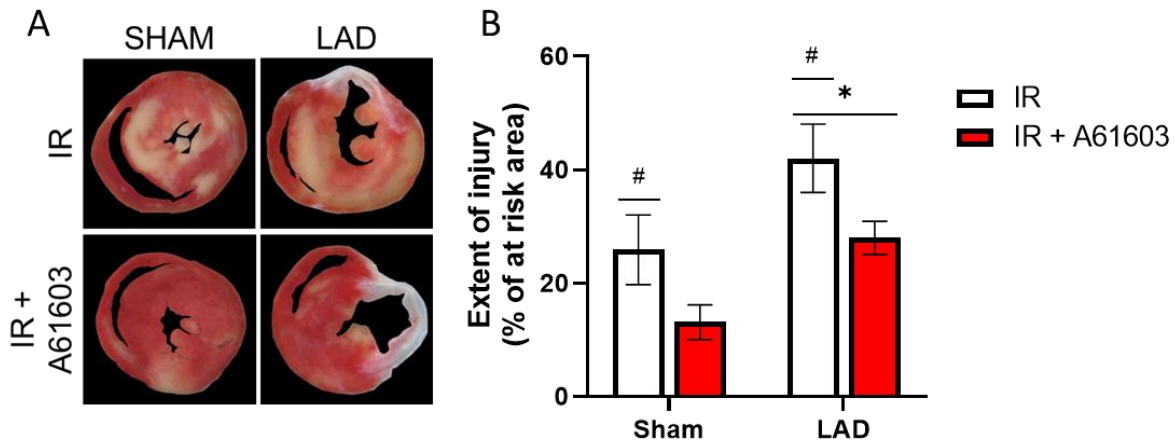

Figure 6-17. Injury sustained from ischemia reperfusion in failing hearts with A61603 pre-conditioning

Extent of injury in the myocardium of healthy (Sham) and failing (LAD) hearts sustained from IR with/without A61603 pre-conditioning. (A) Representative images of TTC staining, (B) Percentage injury in hearts at the end of 60 minutes reperfusion. Analysed by two-way ANOVA for effect of surgery group and A61603 treatment: no significant interaction, main effect of surgery group (p<0.05) and A61603 treatment (# p<0.05) displayed.*

6.5 Discussion

6.5.1 Key findings

- Stimulating the α1A-ARs using selective agonist A61603 evoked an inotropic response in rat hearts, at both 10 and 50nM.
- Only the higher dose of 50nM A61603 affected the profile of ischemic contracture, indicative of altered myocardial ATP levels during ischemia
- Pre-conditioning healthy rat hearts with 10 or 50nM was protective against I/R injury, with a similar level of protection by both doses.
- Failing hearts showed a trend towards worse outcomes following I/R injury compared to sham hearts.
- A61603 at 10nM dose evoked an inotropic response in failing hearts and protected the failing heart against I/R injury with reduced injury in the myocardium at the end of reperfusion

6.5.2 Cardioprotective efficacy of A61603 against I/R injury in healthy and failing hearts

Targeting α1A-ARs has been shown to be protective against ischemic injury in work utilising isolated myocytes and transgenic animal models (Perez 2021). The findings in this chapter have added to this prior knowledge, utilising the selective agonist A61603 as a pre-conditioning stimulus prior to I/R in an ex vivo isolated rat heart perfusion setup, investigating the cardioprotective potential in both healthy and failing hearts. Pre-conditioning the heart with A61603 was cardioprotective against global I/R injury in healthy hearts; functional recovery was improved, and injury sustained in the myocardium at the end of reperfusion was reduced. The cardioprotective response to A61603 pre-conditioning was less evident in failing hearts; functional recovery and LDH release were unchanged, however there was a reduction in the extent of injury sustained in the heart at the end of reperfusion measured by TTC staining.

6.5.3 A61603 induces positive inotropy in healthy and failing hearts

With receptors present on 60% of cardiomyocytes targeting of α1A-ARs induces positive inotropy in the heart (Myagmar et al. 2017). Activation of α1A-ARs stimulates L-type calcium channels through activation of a PLC-DAG-PKC-CaMKII pathway, potentiating inward calcium current (J et al. 2008) (Figure 1-4B). In agreement with

previous studies using human cardiac tissue, this work confirmed the positive inotropic effect with A61603 in ex vivo isolated rat hearts, and this response was not lost in the failing heart (Janssen et al. 2018). During the initial period of A61603 treatment there was a transient increase in contraction followed by a fall and subsequent sustained inotropic response. This was investigated to ensure it was not an artifact produced by the setup or method of drug addition (data not shown), it has been previously reported with non-selective α-AR stimulation by phenylephrine (Asimakis et al. 1994).

Pre-conditioning strategies, such as β-AR stimulation, that induce positive inotropy prior to ischemia are known to be protective against I/R injury. It is suggested the inotropic response depletes glycogen stores and therefore the capacity to produce ATP anaerobically during ischemia is reduced which will protect the heart (Khaliulin et al. 2010). Limiting anaerobic glycolysis during ischemia will consequently reduce the extent of acidosis due to lactate formation, leading to reduced sodium influx, ultimately reducing calcium loading (Cross et al. 1996). Additionally glycogen content can be linked to the MPTP, influencing hexokinase II binding which can alter opening of the MPTP, a key factor in I/R injury (Halestrap et al. 2015). Reduction in glycogen content was not measured in this study but may be thought to occur given the sustained positive inotropic effect observed with A61603 treatment. However, this may not be the case as previous research has shown non-selective α-AR stimulation was inotropic but did not reduce glycogen content (Asimakis et al. 1994). However, modulation of glycogen content is only one factor associated with cardioprotection with signalling pathways activated during the pre-conditioning stimulus of importance (Khaliulin et al. 2010).

6.5.4 Ischemic contracture is affected by high concentration of A61603 only

Ischemic contracture occurs when ATP levels fall during ischemia, the lack of ATP prevents relaxation of the myocardium and hypercontracture occurs (Cross et al. 1996). Earlier onset of ischemic contracture has been associated with cardioprotection by pre-conditioning strategies including IP (Kolocassides et al. 1996b). In this study the onset of ischemic contracture was altered following A61603 treatment at the higher dose of 50nM only, the lower dose of 10nM did not affect ischemic contracture. This differential effect on ischemic contracture was observed despite similar inotropy induced by the two drug concentrations, as well as similar levels of cardioprotection conferred. Positive inotropy prior to ischemia may deplete glycogen and therefore limit

ATP availability during ischemia, as discussed above. However, the inotropy induced prior to ischemia in this instance was comparable between the two concentrations and therefore does not explain the differential effects on ischemic contracture. Given this, the inotropic response and potential glycogen depletion is likely not to be the main driver of cardioprotection by A61603.

6.5.3 Potential mechanisms of A61603 protection

Pre-conditioning strategies activate signalling pathways which contributes to the protection afforded upon reperfusion. It is thought the washout period following a pre-conditioning stimulus is crucial for this to occur (Salie et al. 2017). One of the main mechanisms associated with α1A-ARs mediated protection of cardiomyocytes is through activation of ERK signalling. The activation of ERK survival signalling pathways has been shown to be necessary for the protection afforded by targeting the α1A-ARs, mediated through a Gq signalling pathway (Dahl et al. 2019; Huang et al. 2007; Myagmar et al. 2019). Activation of ERK1/2 through transgenic MEK1 mice protected against ischemic injury in vivo (Lips et al. 2004). ERK1/2 is known to be involved in the cardioprotection afforded by IPC against I/R injury (Hausenloy et al. 2005), therefore the activation of these survival signalling kinases is likely to contribute to the protection seen in this study with A61603 pre-conditioning.

Stimulation of α1A-ARs also activates another known factor in cardioprotective strategies PKC. Activation of Gq signalling pathways through α1A-ARs agonism leads to the formation of DAG from PLC and subsequent activation of PKC. PKC is a known mediator of cardioprotective strategies such as ischemic and temperature pre-conditioning (Khaliulin et al. 2007; Ytrehus et al. 1994). Furthermore, activation of PKC by adenosine is protective against I/R injury, the action of PKC is thought to involve reduction of ROS production and MPTP opening (Khaliulin et al. 2010). Therefore, there is potential of PKC involvement in A61603 pre-conditioning.

6.5.4 I/R injury in failing hearts

The presence of pathophysiology is known to alter the susceptibility of the heart to I/R injury and the cardioprotective strategies utilised to protect these hearts. Previous research investigating cardioprotection of failing hearts completed at 16 weeks post-MI reported increased susceptibility to I/R injury, as indicated by a reduction in LDH release (Khaliulin et al. 2014). Whilst this current work did not find a

difference in LDH release, the LAD failing heart group did show a trend towards decreased functional recovery and increased injury in the myocardium compared to sham, albeit not to a significant level. The failing hearts used in this study were only 4-weeks post-MI but echocardiography confirmed a significant impairment in function shown by a reduction in ejection fraction to 44%. One difference observed in the failing hearts was during ischemia, the onset of ischemic contracture was delayed in the failing hearts. Delayed onset of contracture has been previously associated with preserved ATP and reduced injury sustained from I/R, as is the case with cardioplegia (Kolocassides et al. 1996a). However, in the case of failing hearts, the delay in onset of contracture observed was not associated with protection against I/R. It may reflect alterations in ATP and calcium handling in failing hearts, or it may be the result of the reduced area of functioning healthy myocardium present to initiate sustained contraction.

6.6 Summary

Preconditioning with A61603, a selective agonist of α1A-ARs, is protective against the detrimental effects of I/R injury in both healthy and failing hearts. The mechanism of action behind the protection still requires investigation. The next step towards a clinically translational intervention is to test the cardioprotective efficacy of A61603 in combination with cardioplegia.

7 Cardioprotective efficacy of drugs targeting adrenergic pathways in cardioplegic arrest

7.1 Introduction

As discussed above, during CPB surgery the heart is subjected to global ischemia and reperfusion resulting in cardiac injury. The heart is terminally differentiated, and any level of injury sustained can be detrimental to cardiac function. Cardioplegia is routinely used to protect the heart, rapid arrest preserves energy substrates during ischemia and improves recovery during reperfusion (Hearse et al. 1974). Although cardioplegia confers some protection to the heart, there is room for other interventions to reduce the injury further. Therefore, cardioprotective strategies are sought to improve outcomes following I/R, and it is important to test these strategies in addition to the use of cardioplegic arrest as cardioplegia is routinely used in the clinical situation.

Cardioprotective strategies to protect the heart can be given prior to ischemia, termed pre-conditioning. This can be achieved with drugs targeting the adrenergic receptor pathways, as has been highlighted previously. Targeting the β-AR pathway by the non-selective agonist isoprenaline or bypassing the receptors using cAMP analogues including 8-Br has been previously shown to protect against I/R injury. The mechanism behind this protection has been shown to involve reduced opening of the MPTP, a key mediator of I/R injury (Khaliulin et al. 2010; M. J. Lewis et al. 2022). Targeting the α1-ARs is also cardioprotective, the work in the previous chapter shows pre-conditioning the heart with the selective agonist for α1A-ARs, A61603, can confer protection against I/R injury. Previously these pre-conditioning strategies have been tested under ischemic conditions without cardioplegic arrest. The cardioprotective efficacy has not be tested in combination with cardioplegia, additionally the influence of cardioplegia on MPTP opening is unknown.

7.2 Aims

The aim of this chapter is to investigate cardioprotective strategies using drugs targeting the adrenergic receptor pathways, that have previously shown promise in I/R injury, in a more clinically relevant model of cardioplegic ischemic arrest. With the future aim to evaluate any promising strategies in a disease model.

7.3 Methods

7.3.1 Animals

Adult male Wistar rats used for the experiments in this chapter weighed 275-300g. Animals were sacrificed by IP injection of pentobarbital, followed by cervical dislocation. The chest was opened, and the hearts immediately excised.

7.3.2 Ischemia reperfusion protocols

Freshly excised hearts were cannulated on the Langendorff setup and perfused with 37^{o}C oxygenated Krebs buffer (Table 2-1) at a flow rate of 10ml/min. A pressure balloon was inserted into the LV to measure function. Following a 30-minute stabilisation period, hearts were subjected to I/R according to the protocols below.

The use of cardioplegia provides protection against I/R in the heart, therefore an increased length of ischemia is required to produce a comparable level of injury to 30 minutes control ischemia. The first set of experiments was used to determine the optimal length of ischemia and reperfusion, 45 minutes of cardioplegic ischemic arrest was tested followed by one or two hours of reperfusion (Figure 7-1).

Cardioplegic arrest was initiated by perfusion of cardioplegic solution (Table 2-2) for 2 minutes at the start of ischemia at a flow rate of 5ml/min, for the remainder of the ischemic period hearts were submerged in cardioplegia.

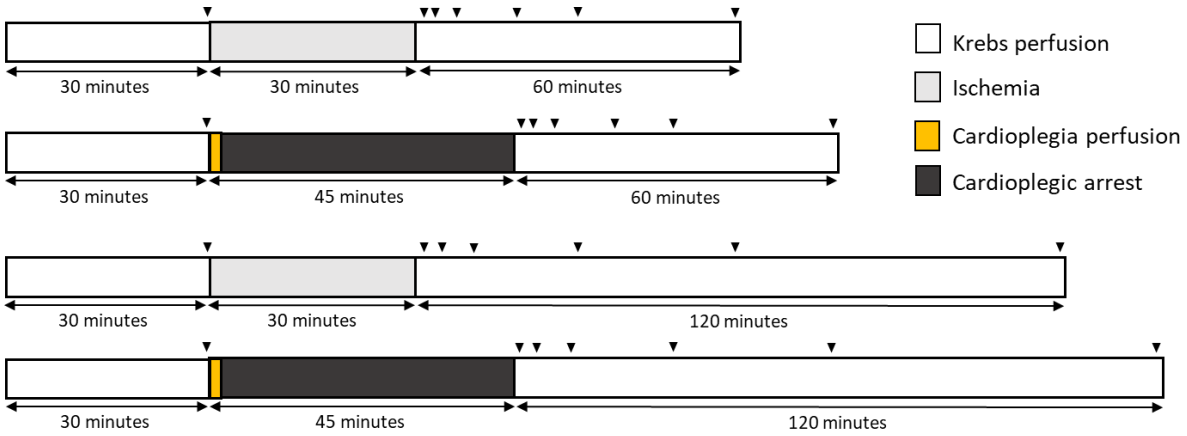

Figure 7-1 Protocols to investigate ischemic arrest time with cardioplegia

Perfusion protocols: White – Krebs perfusion, Grey – Ischemia, Yellow – perfusion of cardioplegia, Black – cardioplegic arrest. ⍰ represents effluent collection time points for LDH measurement.

Once the cardioplegic model was optimised, pre-conditioning using drugs targeting the adrenergic receptor pathways were investigated in combination with cardioplegic arrest: A61603 (10nM) (n=4), Isoprenaline (100nM) (n=6) and 8-Br-cAMP-AM (5µM and 10µM) (n=3, n=6) were tested. Drug treatment was given prior to ischemia, with a 5-minute washout period. Hearts were then subjected to 45 minutes cardioplegic ischemic arrest and 2 hours reperfusion (Figure 7-2).

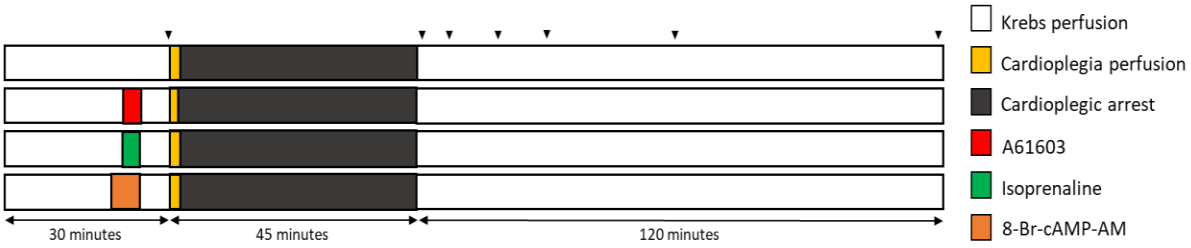

Figure 7-2. Cardioplegic ischemic arrest and reperfusion Langendorff protocols.
Perfusion protocols: White – Krebs perfusion, Yellow – perfusion of cardioplegia, Black – cardioplegic arrest, Drug treatments: Red – A61603, Green – Isoprenaline, Orange – 8-Br. ▯ represents effluent collection time points for LDH measurement.

As discussed in detail in the Methods chapter, I/R injury was assessed using three outcomes: functional recovery, LDH release and TTC staining for injured tissue area.

7.3.3 Mitochondrial swelling experiments

Mitochondrial swelling was assessed in control, cardioplegia and cardioplegia + 8-Br hearts. For the mitochondrial swelling experiments hearts were subjected to the same perfusion protocols as above (control hearts as in Figure 7-1, cardioplegia hearts with/without 8-Br as in Figure 7-2), with the exception that reperfusion in all cases was only 10 minutes.

At 10 minutes reperfusion, the ventricles were removed and homogenised before a series of centrifugation to obtain isolated mitochondria. Following quantification of the mitochondrial protein content, 0.2mg/ml of mitochondria was placed into swelling buffer (Table 2-6) and placed in a spectrophotometer. Calcium was then added to the mitochondrial mixture, initiating mitochondrial swelling that can be read as a change in absorbance. Full details can be found in the methods section.

7.4 Results

7.4.1 Cardioplegic ischemic arrest and reperfusion

7.4.1.1 Effect of cardioplegia on ischemic arrest

Onset of ischemia causes a decline in cardiac function leading to cardiac arrest. Perfusion with cardioplegia increases the rate of cardiac arrest in the heart. This can be visualised in the representative traces of LV function following initiation of ischemia alone (control) and ischemic cardioplegic arrest (Figure 7-3A-B). The time to stop contraction with cardioplegia was significantly lower than control, 10.8 ± 1.4 vs 93.5 ± 3.9 seconds (Figure 7-3C).

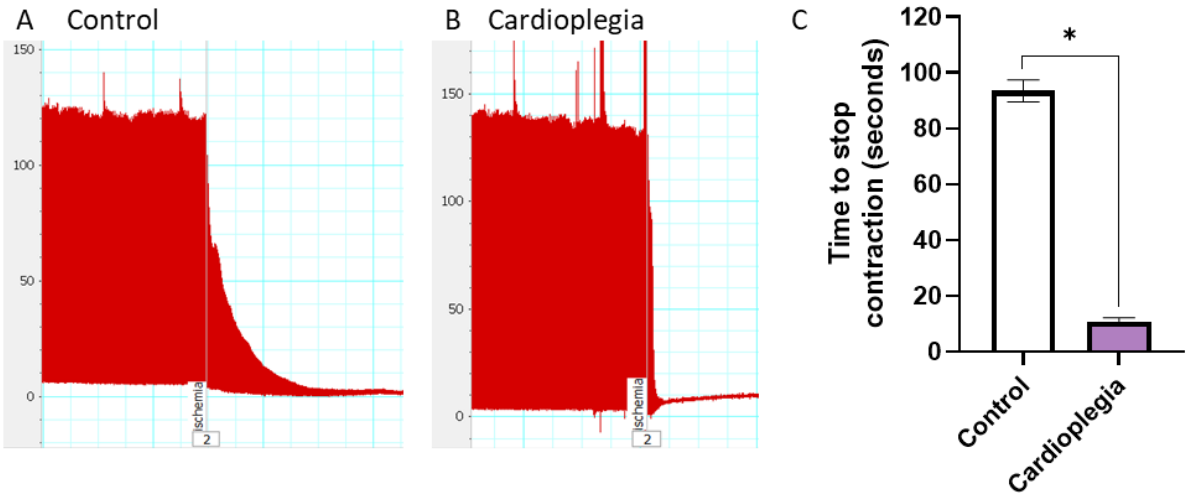

Figure 7-3. Time to arrest the heart with cardioplegia

*Time to stop contraction at the start of ischemia with and without the use of cardioplegia. *P<0.05, analysed by students T.Test.*

7.4.1.2 Effect of cardioplegia on ischemic contracture

During ischemia the heart undergoes contracture which can be measured by an increase of pressure exerted on the balloon inserted in the LV. The profile of ischemic contracture is altered during cardioplegic arrest (Figure 7-4A). With cardioplegic arrest, onset of contracture in the heart during ischemia is significantly delayed in comparison to control hearts, 20.2 ± 0.49 vs 9.6 ± 0.6 minutes (Figure 7-4B). Peak contracture in the cardioplegia group was reduced in comparison to the control group (Figure 7-4C).

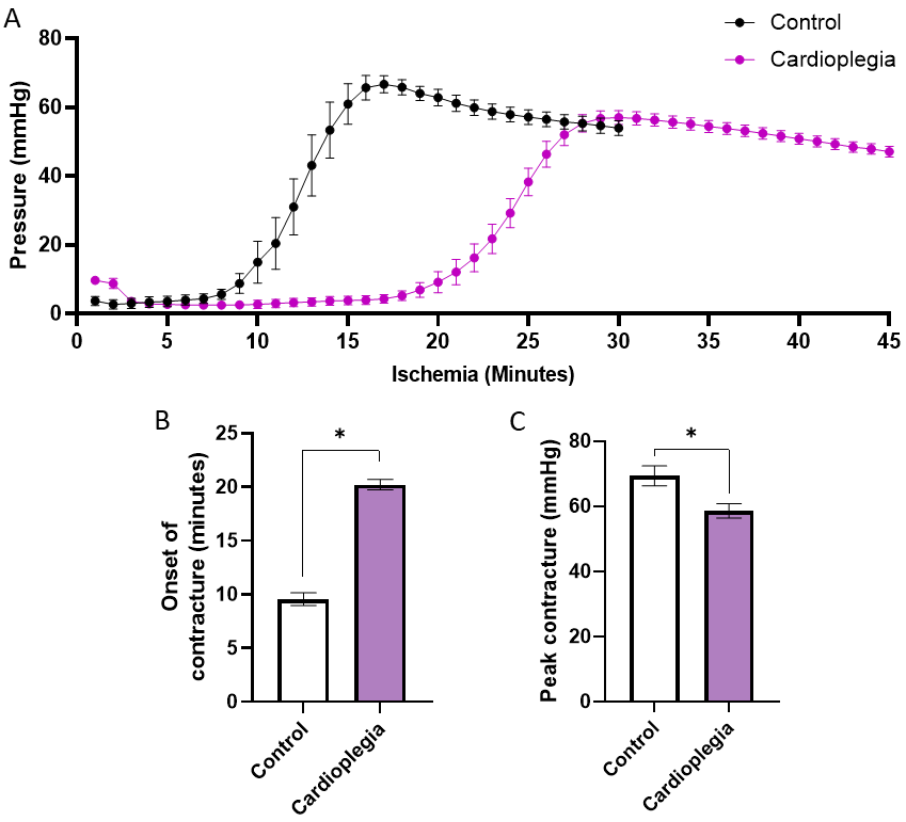

Figure 7-4. Ischemic contracture with cardioplegia

*(A) Contracture in the heart during ischemia with and without cardioplegic arrest. Onset of contracture (B) and peak contracture (C) compared between groups, *P<0.05, analysed by students T.Test*

7.4.1.3 Effect of cardioplegia on the length of ischemia

Ischemic cardioplegic arrest for 45 minutes resulted in a similar level of injury to that seen with 30 minutes control ischemia. This was shown with both 1 hour and 2 hours of reperfusion. After 1 hour of reperfusion, recovery of LVDP, LDH release and percentage injury was similar in both cardioplegia and control hearts (Figure 7-5). The same was observed with 2 hours reperfusion (Figure 7-6).

Reperfusion length of 2 hours compared to 1 hour resulted in a slightly higher percentage injury measured through TTC staining for both control (23.33 to 34.6%) and cardioplegia hearts (23.83 to 28.1%). In addition, with 1 hour of reperfusion recovery of LVDP was still increasing, extending reperfusion to 2-hours allowed for a plateau of LVDP recovery to be established. Therefore, moving forward to studies looking at pre-conditioning with cardioplegic ischemic arrest, a 2-hour reperfusion period was used.

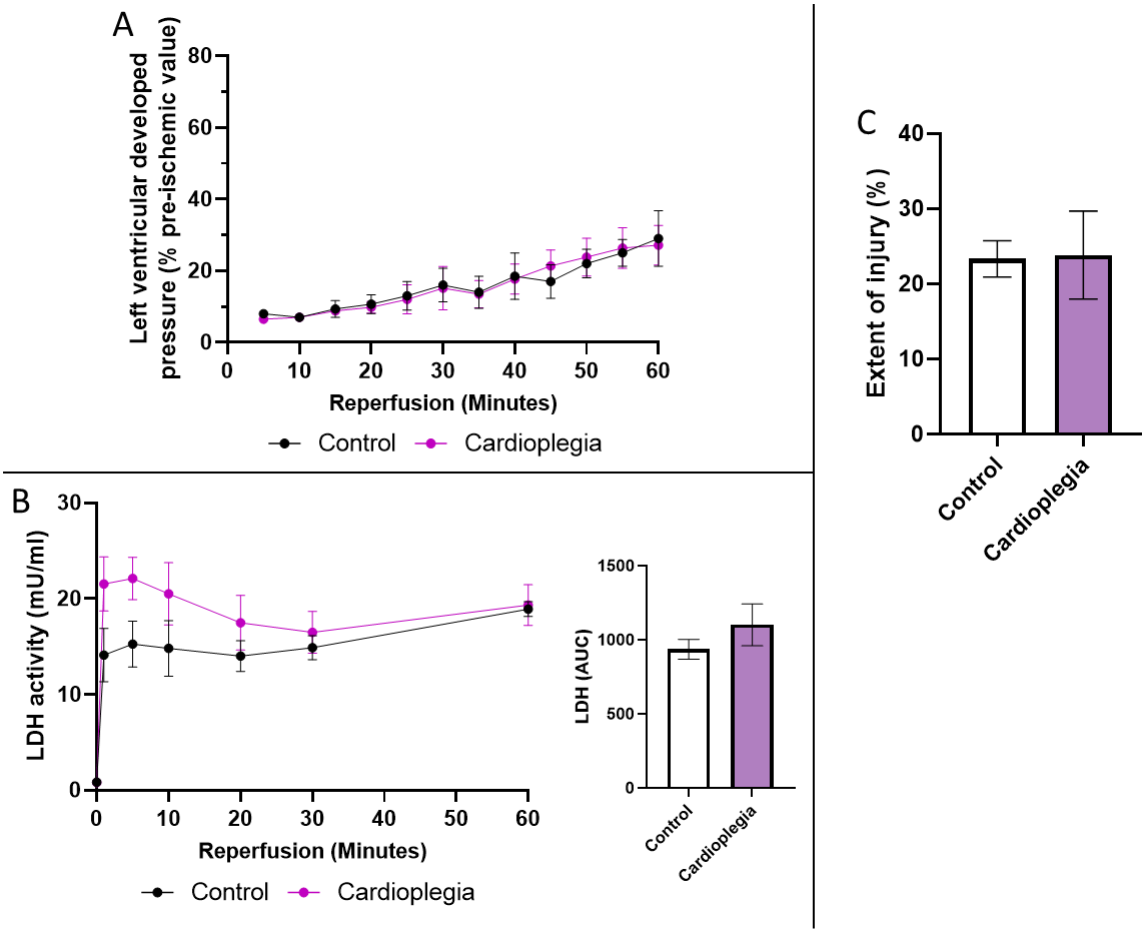

Figure 7-5 Control ischemia vs. cardioplegic ischemic arrest with 1-hour reperfusion

Recovery across 1 hour reperfusion following 30 minutes ischemia for control group (n=3) *and 45 minutes ischemia for cardioplegia group* (n=6)*. (A) Recovery of left ventricle developed pressure, analysed by two-way repeated measures ANOVA, no significant interaction, no main effect of group. (B) LDH release and area under the curve (AUC) analysis, analysed by students T.Test (P>0.05). (C) Extent of injury expressed as a percentage of at risk area, analysed by students T.Test (P>0.05).*

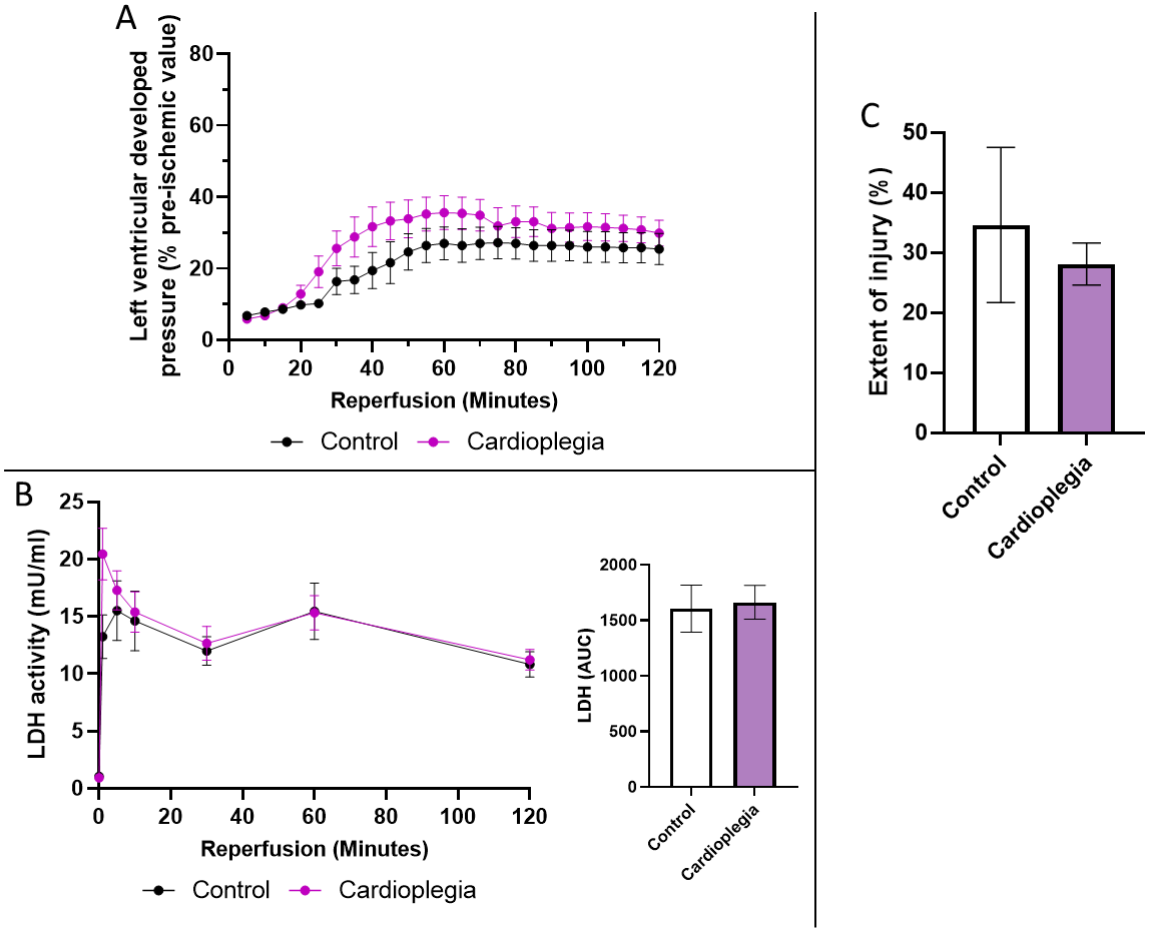

Figure 7-6 Control ischemia vs. cardioplegic ischemic arrest with 2-hour reperfusion

Recovery across 2 hours reperfusion following 30 minutes ischemia for control group (n=5) and 45 minutes ischemia for cardioplegia group (n=10). (A) Recovery of left ventricle developed pressure, analysed by two-way repeated measures ANOVA, no significant interaction, no main effect of group. (B) LDH release and area under the curve (AUC) analysis, analysed by students T.Test (P>0.05). (C) Extent of injury expressed as a percentage of at risk area, analysed by students T.Test (P>0.05).

7.4.2 Adrenergic stimulation pre-conditioning and cardioplegic ischemic arrest

7.4.2.1 Initial baseline values

Across all groups investigated, cardioplegia alone, A61603, isoprenaline, 5μM 8-Br and 10μM 8-Br, the baseline values of LV function following the stabilisation period on the Langendorff setup recorded by pressure balloon were comparable (Table 7-1). There were no significant differences between groups for any of the hemodynamic parameters measured.

Table 7-1 Baseline values for LV function

LVDP – Left ventricular developed pressure; HR – heart rate; RPP – rate pressure product; EDP – end diastolic pressure

	Cardioplegia (n=10)	A61603 (n=4)	Isoprenaline (n=6)	8-Br (5μM) (n=3)	8-Br (10μM) (n=6)
LVDP (mmHg)	121.4 ± 4.5	111.5 ± 4.9	117.2 ± 4.3	129.3 ± 11.2	126.5 ± 7
HR (bpm)	306.8 ± 13.4	313.9 ± 17.9	308.2 ± 11.6	287.3 ± 14.5	306.9 ± 15
RPP	37122 ± 1895	35082 ± 2854	36001 ± 1351	37178 ± 4089	38522 ± 1773
EDP (mmHg)	7.54 ± 0.5	7.62 ± 1.2	8.29 ± 0.8	9.14 ± 0.5	8.39 ± 1

7.4.2.2 Inotropic effect of adrenergic stimulation

Drugs targeting the adrenergic pathways can stimulate an increase in cardiac function, which can be measured via the LV pressure balloon. Representative traces showing the effect on LV function of drug treatment and the washout period for each drug given prior to cardioplegic arrest can be seen in Figure 7-7. Treatment with A61603, isoprenaline and 10μM 8-Br induced a positive inotropic response in the heart, this effect was not observed with 5μM 8-Br. The response to drug treatment was reversed during the washout period.

A61603 treatment led to an increase in both LVDP and RPP, the profile of this response was an initial sharp peak followed by a second sustained increase. Heart rate was not changed across A61603 drug treatment. The increase in LVDP and RPP was reduced across the washout period, at the end of washout LVDP was significantly lower than baseline at 89 ± 1% (Figure 7-8).

Treatment with isoprenaline initiated a positive inotropic response in the heart, at the maximal response LVDP was 143 ± 5.1% of the initial baseline value. This was accompanied by a positive chronotropic effect, with an increase in heart rate measured across drug addition and into the washout period. RPP was therefore also increased across drug addition of isoprenaline, with the maximal response 162.8 ± 4.3% of baseline. Washout of isoprenaline reversed the effects on LVDP and RPP with both falling lower than the initial baseline at the end of the washout period, 62.7 ± 5.1% and 75.6 ± 3% respectively (Figure 7-8).

Addition of 8-Br, at the higher concentration of 10μM, also increased LVDP and RPP. At the peak of drug response, LVDP was 135.7 ± 4.9% and RPP 140.4 ± 1.4% of the respective baseline values. Heart rate was not significantly altered across the addition of 10μM 8-Br. At the end of the washout period following 10μM 8-Br, LVDP and RPP fell below the initial baseline value to 72.3 ± 2.8% and 75.6 ± 3% respectively. Treatment with the lower concentration of 5μM 8-Br did not increase LVDP, HR or RPP significantly, however a decrease in LVDP and RPP compared to baseline was observed during the washout period (Figure 7-8).

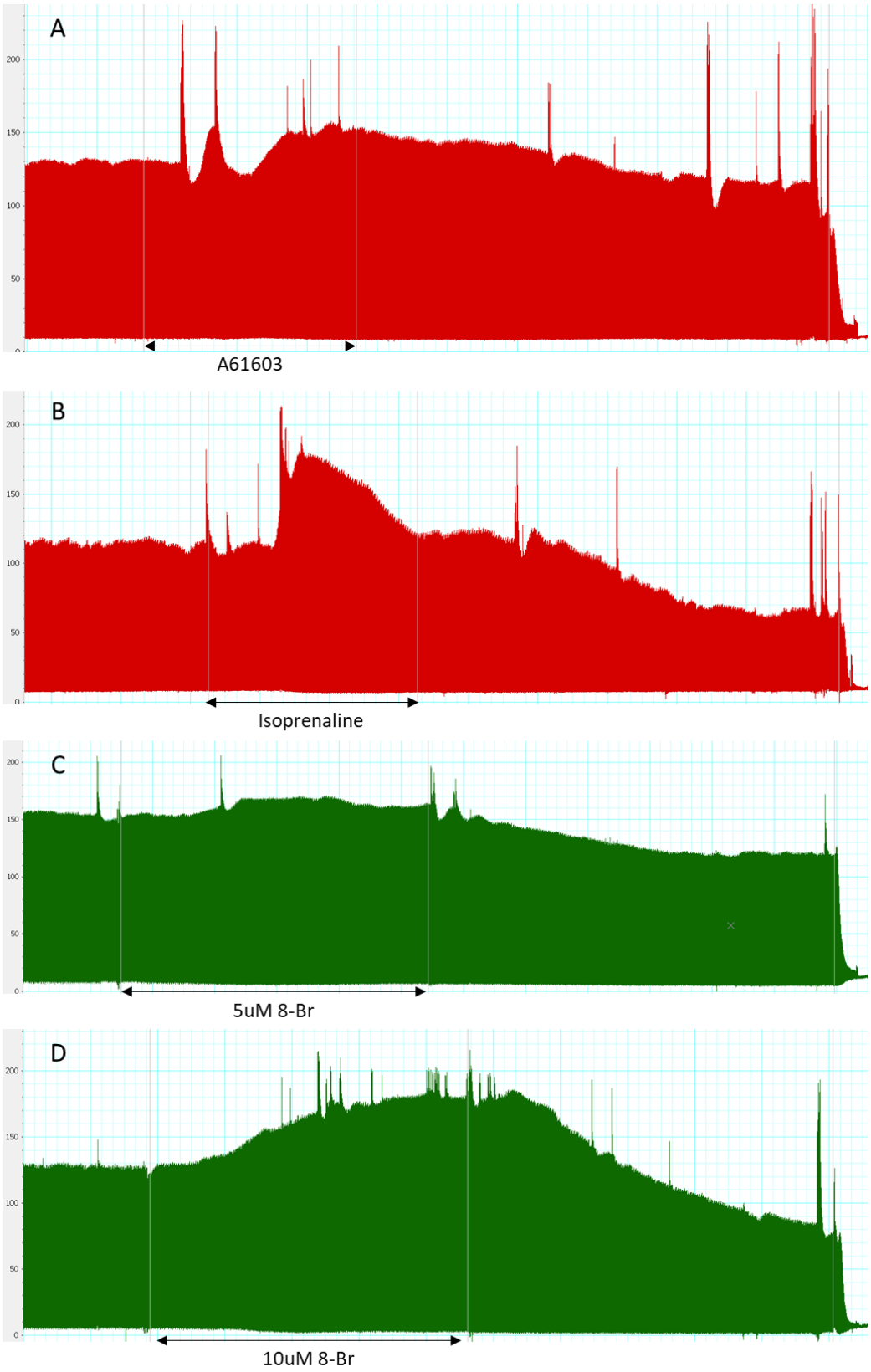

Figure 7-7 Example LabChart traces of drug addition

Representative pressure traces from the LV prior, during and after treatment with (A) A61603, (B) Isoprenaline, (C) 5μM 8-Br and (D) 10μM 8-Br.

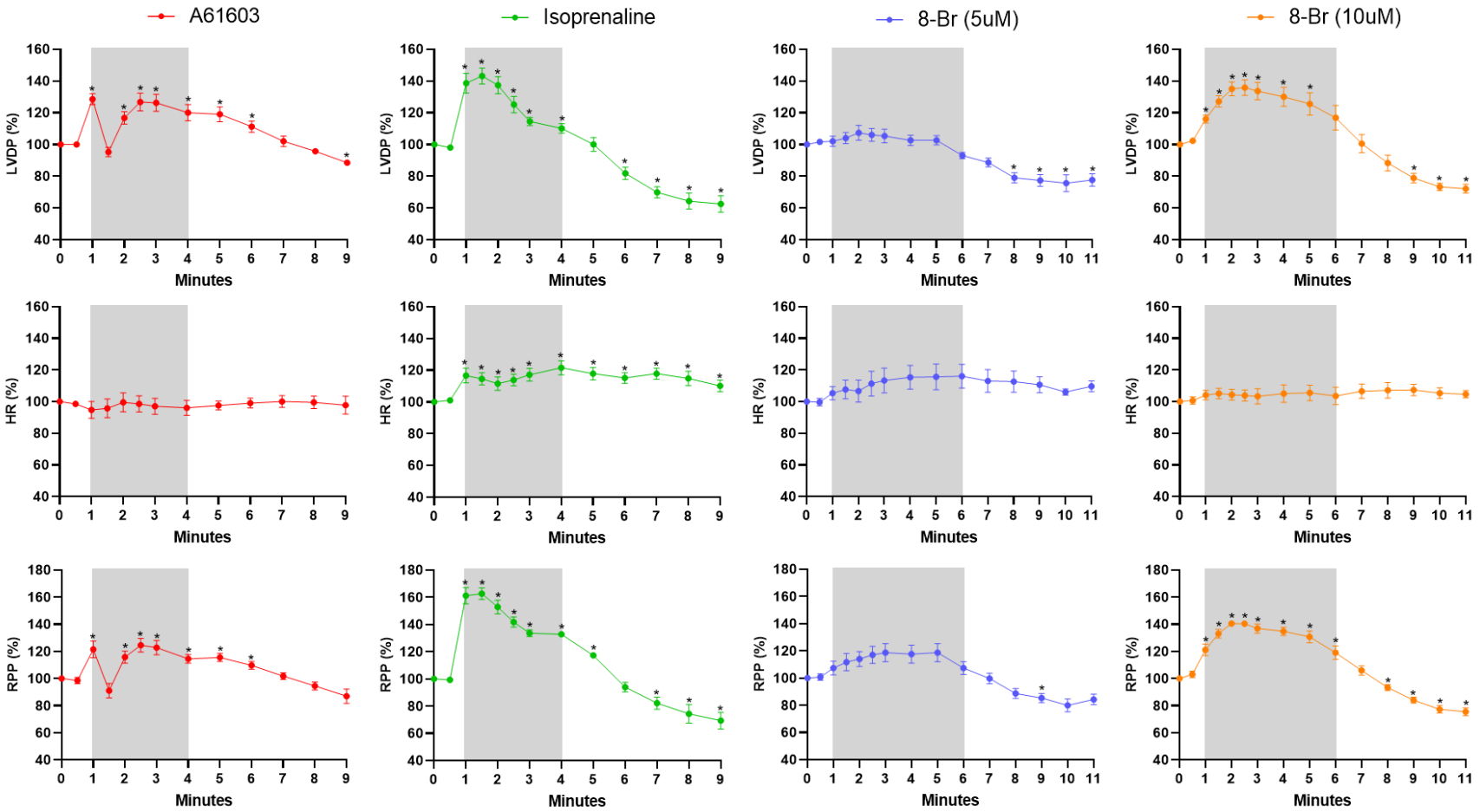

Figure 7-8 Effect of drug perfusion on heart function

*Left ventricle function during (shaded area) and after treatment with drugs targeting the adrenergic pathways (A61603 - red, Isoprenaline - green, 5μM 8-Br - blue and 10μM 8-Br -orange), expressed as a percentage of baseline value. Top row – left ventricular developed pressure (LVDP), middle row – heart rate (HR), bottom row – rate pressure product (RPP). Analysed by one-way repeated measures ANOVA with post-hoc comparison of each time-point to time 0 (*p<0.05).*

7.4.2.3 Effect of drug pre-conditioning on cardioplegic arrest

The time for the heart to arrest following cardioplegia perfusion was not significantly different following pre-conditioning with any of the drugs tested (Figure 7-9).

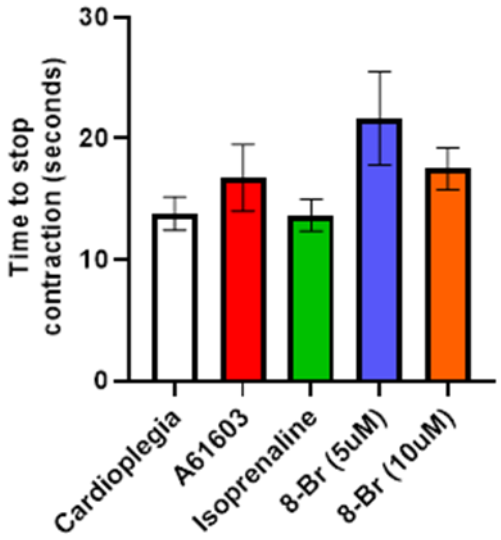

Figure 7-9 Cardioplegic arrest following drug treatment

Time taken for contraction to cease following the start of cardioplegic ischemic arrest, with or without adrenergic drug pre-conditioning, analysed by one-way ANOVA ($p>0.05$).

7.4.2.4 Effect of drug pre-conditioning on ischemic contracture

During ischemia the heart undergoes contracture which can be measured via the pressure balloon inserted in the LV. Contracture of the heart during ischemia is altered by pre-conditioning strategies (Figure 7-10A). The time to onset of contracture was decreased following pre-conditioning with Iso, 8-Br (5μM) or 8-Br (10μM) (14.07 ± 1.08, 10.49 ± 0.9 or 10.53 ± 0.3 minutes, respectively) compared to cardioplegia alone (20.34 ± 0.5 minutes) (Figure 7-10B). Peak contracture during ischemia is also significantly altered by the pre-conditioning drug treatments targeting adrenergic pathways (Figure 7-10C). Peak contracture (mmHg) was greater during ischemia following pre-conditioning with isoprenaline, 5μM 8-Br or 10μM 8-Br (87.7 ± 6.5, 104 ± 10.8 and 100.8 ± 4.4 respectively) compared to cardioplegia alone (60.1 ± 2.9). In the A61603 treatment group, onset of contracture and peak contracture did not differ from cardioplegia alone.

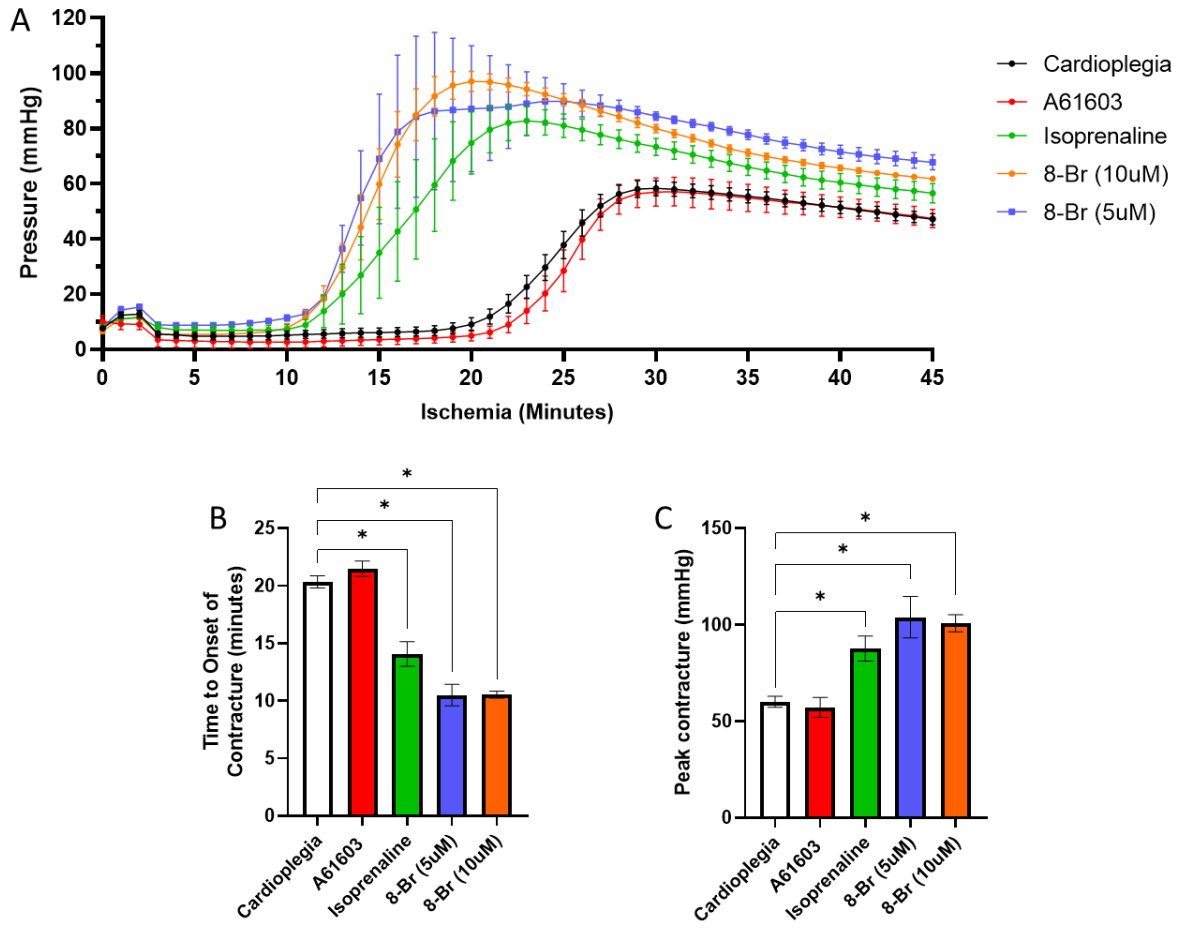

Figure 7-10 Ischemic contracture

*(A) Profile of contracture in the heart across 45 minutes ischemic cardioplegic arrest with/without adrenergic drug pre-conditioning. (B) Time to the onset of contracture and (C) Peak contracture during ischemia were measured, analysis by one-way ANOVA with Tukey's post-hoc, *p<0.05 vs cardioplegia.*

7.4.2.5 Effect of drug pre-conditioning on extent of I/R injury

7.4.2.5.1 Functional recovery

The recovery of LVDP, RPP and max dP/dt across reperfusion is affected by drug pre-conditioning, indicated by a significant interaction of drug treatment group and time. Pre-conditioning with Iso or 8-Br improved functional recovery across reperfusion, whereas recovery was reduced in the A61603 group (Figure 7-11). At the end of 2 hours reperfusion LVDP was significantly increased in the 10μM 8-Br treatment group compared to cardioplegia alone (51.47 ± 1.8 vs. 35.23 ± 3.2 mmHg) (Figure 7-11A). RPP was significantly increased in the Iso treatment group at 2 hours reperfusion (Figure 7-11B).

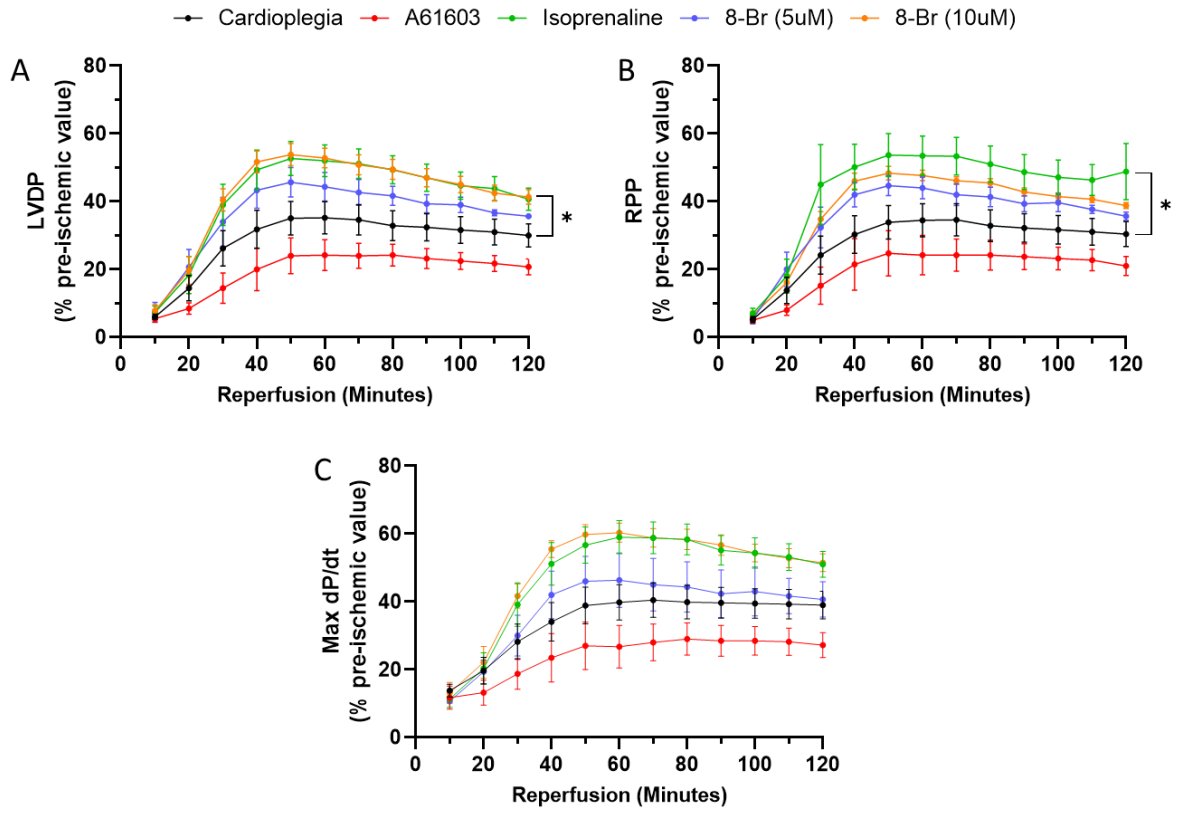

Figure 7-11 Functional recovery across reperfusion

*Recovery of LVDP (A), RPP (B) and Max dP/dt (C) across reperfusion following 45 minutes cardioplegic arrest with/without adrenergic drug pre-conditioning. Analysed by two-way repeated measures ANOVA, significant interaction of group*time, post-hoc analysis comparing treatment groups at 60 minutes reperfusion displayed, *p<0.05*

7.4.2.5.2 LDH release

LDH release is a marker of cardiac injury and can be measured across reperfusion, with activity levels peaking at 1 minute of reperfusion before a reduction and plateau (Figure 7-12A). LDH release across reperfusion, measured by the area under the curve, was significantly affected by pre-treatment with adrenergic drugs (Figure 7-12B). Release of LDH was significantly reduced in the 10µM 8-Br treatment group compared to cardioplegia alone (AUC: 1060 ± 67.5 vs 1670 ± 153). LDH release was also reduced in the isoprenaline treatment group compared to cardioplegia (AUC: 1233 ± 102 vs 1670 ± 153), but this was not a significant reduction. LDH release in the A61603 treatment group was slightly higher compared to cardioplegia alone, however LDH release was not significantly changed by pre-treatment with 5µM 8-Br or A61603 (AUC: 1629 ±177 and 2352 ± 192 respectively).

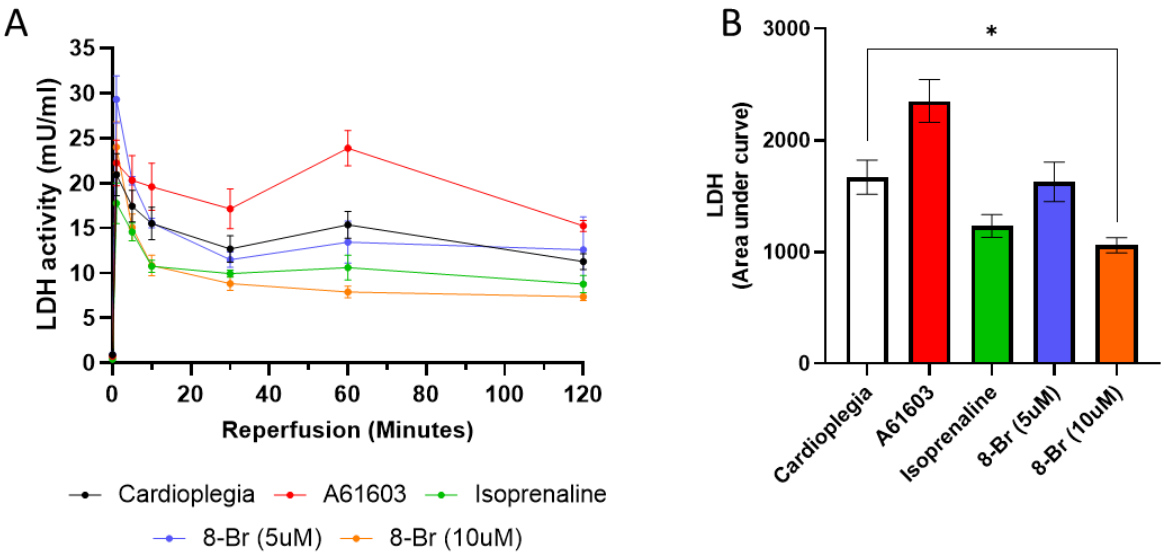

Figure 7-12 LDH release during reperfusion

*Lactate dehydrogenase (LDH) release was measured across 2 hours of reperfusion following 45 minutes cardioplegic arrest, with/without adrenergic drug pre-treatment. (A) Profile of LDH release across reperfusion in each treatment group, (B) area under the curve (AUC) was measured for each group, analysed by one-way Welch's ANOVA ($p<0.05$) with Games Howell post-hoc analysis, *$p<0.05$ vs cardioplegia.*

7.4.2.5.3 Injury sustained in the myocardium at the end of reperfusion

TTC staining of the heart at the end of reperfusion allows visualisation of injured tissue (stained in white), representative images form the 5 treatment groups can be seen in Figure 7-13A. Percentage injury was reduced in 8-Bromo hearts. The extent of injury at the end of reperfusion was different across the 5 groups, injury significantly decreased following treatment with isoprenaline (11 ± 1.7%), 5μM 8-Br (9.67 ± 1.5%) or 10μM 8-Br (9.33 ± 1.5%) in comparison to cardioplegia alone (31.7 ± 4.5%) (Figure 7-13B). Pre-treatment with A61603 did not reduce the extent of injury, percentage injury was increased although not to a significant level (51.5 ± 6.9 vs 31.7 ± 4.5%).

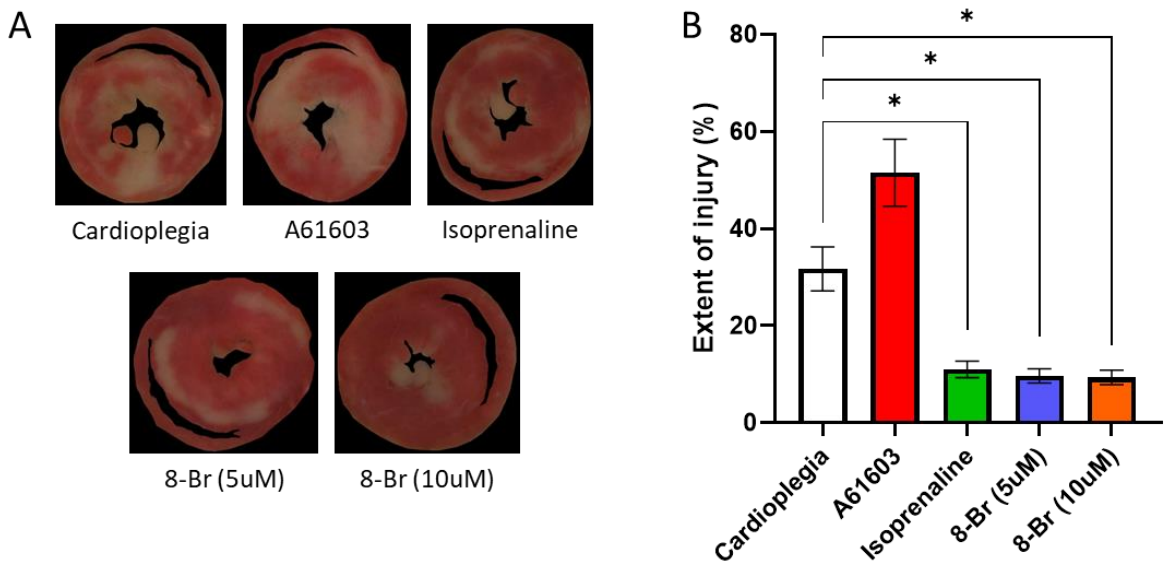

Figure 7-13 Extent of cardiac injury at the end of reperfusion

*TTC staining to assess the extent of injury at the end of 2 hours reperfusion following 45 minutes cardioplegic arrest, with/without adrenergic drug pre-treatment. (A) Representative images from each treatment group, injured tissue is stained white. (B) Percentage injury calculated for each treatment group, analysed by one-way Welch's ANOVA ($p<0.05$) with Games Howell post-hoc analysis, *$p<0.05$ vs cardioplegia.*

7.4.3 Mitochondrial swelling

7.4.3.1 The effect of cardioplegia on mitochondrial swelling

Maximal rate of mitochondrial swelling was reduced in mitochondria isolated from hearts subjected to cardioplegic ischemic arrest compared to control ischemia. Extent of swelling was reduced in cardioplegic group but not to a significant level. Addition of MPTP blocker CsA (2μM) to the isolated mitochondria attenuated the swelling response in both groups (Figure 7-14).

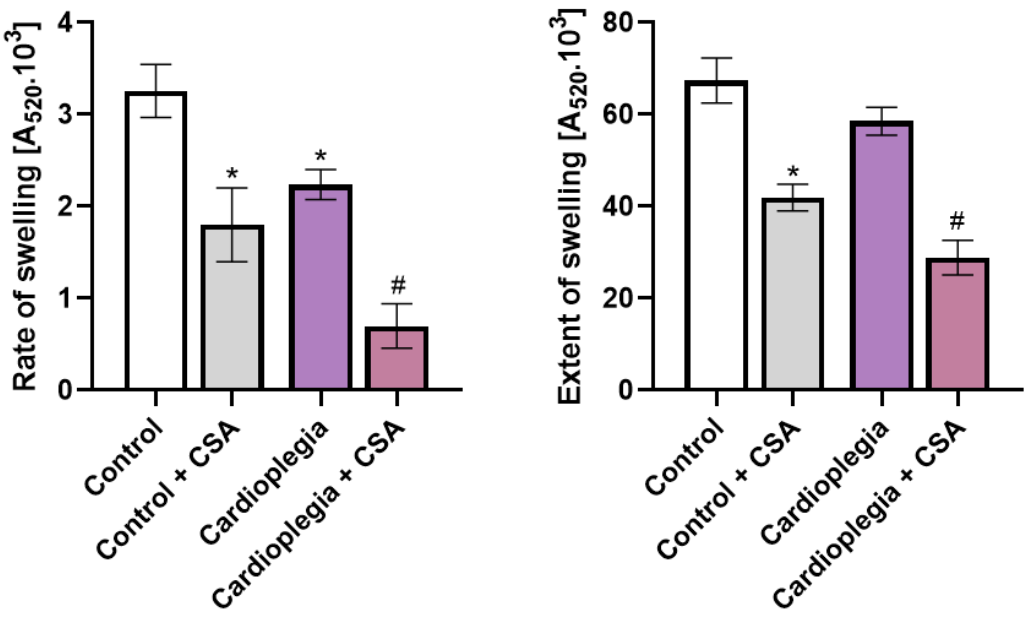

Figure 7-14 Effect of cardioplegia on mitochondrial swelling

*Maximal rate of swelling and maximal extent of swelling in mitochondria isolated from hearts subjected to control ischemia (30 minutes) and cardioplegic ischemic arrest (45 minutes). Cyclosporin A (CsA) was added to the isolated mitochondria to inhibit the MPTP. Analysed by one-way ANOVA, *p<0.05 vs control, #p<0.05 vs cardioplegia.*

7.4.3.2 The effect of 8-Br pre-conditioning on mitochondrial swelling

Maximal rate of swelling was reduced in mitochondria isolated from hearts pre-conditioned with 10μM 8-Br prior to cardioplegic ischemic arrest compared to cardioplegia alone. Extent of mitochondrial swelling was reduced in the 8-Br pre-conditioned group compared to cardioplegia alone, but not to a significant level (0.063). The addition of MPTP inhibitor CsA to the isolated mitochondria attenuated the extent of swelling in the cardioplegia + 8-Br group (Figure 7-15).

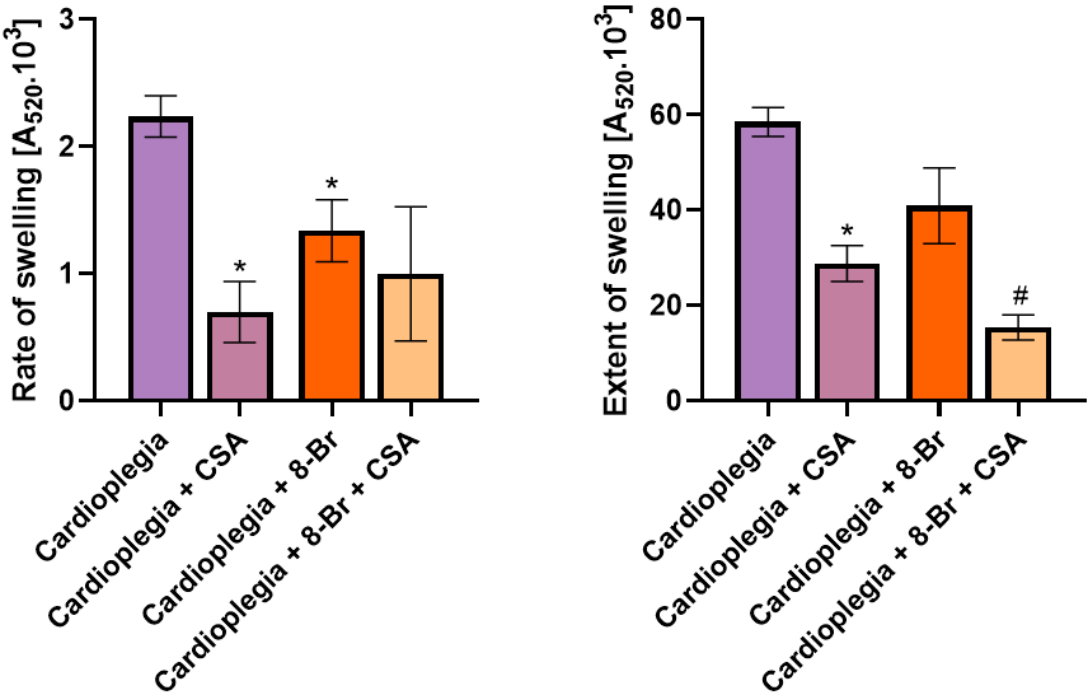

Figure 7-15 Effect of pre-conditioning with 8-Br prior to cardioplegic arrest on mitochondrial swelling

*Maximal rate of swelling and maximal extent of swelling in mitochondria isolated from hearts subjected to cardioplegic ischemic arrest (45 minutes) with and without pre-conditioning with 10μM 8-Br. Cyclosporin A (CsA) was used to inhibit the MPTP. Analysed by one-way ANOVA, *p<0.05 vs cardioplegia, #p<0.05 vs cardioplegia + 8-Br.*

7.5 Discussion

7.5.1 Key findings

- Cardioplegia reduces the extent of injury in the heart allowing for extended ischemic time, this is partly mediated by reduced mitochondrial swelling.
- Pre-conditioning with 8-Br or isoprenaline was cardioprotective against cardioplegic ischemic arrest and reperfusion in healthy rat hearts.
- 8-Br pre-conditioning reduced mitochondrial swelling upon reperfusion following cardioplegic ischemic arrest
- Despite showing cardioprotective efficacy against I/R injury in the absence of cardioplegia (Chapter 6) 10nM A61603 did not confer protection to the heart against I/R injury in combination with cardioplegia.

7.5.2 Cardioplegia is protective against I/R injury

Cardioplegic arrest is widely used in cardiac surgery, the heart is depolarised using high potassium solution to arrest the heart in diastole (Chambers and Fallouh 2010; Dobson et al. 2013). Rapid arrest of the heart preserves energy substrates in the heart, improving recovery upon reperfusion (Hearse et al. 1974). As expected, the use of cardioplegia in this study conferred protection against I/R injury in the heart. Cardioplegia facilitated an increase in ischemic time compared to control ischemia, with a similar level of injury sustained. It was important to consider the length of the ischemic period with cardioplegia to obtain a level of injury that allowed for the investigation of protective strategies. Maintaining the ischemic time at 30 minutes with cardioplegia would not produce enough injury to measure further protection when testing pre-conditioning strategies. Equally it is important not to induce injury so great that any effect of cardioprotective strategies cannot be observed (Bell et al. 2011). Testing cardioprotective strategies in combination with cardioplegic arrest is important for translation into a clinical setting. As cardioplegia already offers protection against I/R injury, cardioprotective strategies need to be additive to this effect.

7.5.2.1 Cardioplegia delays onset of ischemic contracture

The onset of ischemia contracture was delayed with the use of cardioplegia, as has been previously described, and this effect is due to a delay in the reduction of ATP (Hearse et al. 1977). Contracture of the heart occurs during ischemia due to formation of cross-bridges in the arrested heart creating an increase in tension. Modulation of the

ischemic contracture profile may have some indication on the protection against I/R injury, however pre-conditioning strategies have been shown to have the opposite effect on contracture, shortening the time to onset, and still afforded the same level of protection to cardioplegia (Kolocassides et al. 1996a; Kolocassides et al. 1996b).

7.5.2.2 Cardioplegia reduced mitochondrial swelling

This study has shown for the first time that cardioplegia reduces mitochondrial swelling. Mitochondrial swelling is reduced upon reperfusion following cardioplegic arrest in comparison to control ischemia, despite a similar extent of injury sustained. This suggests that cardioplegia protection is partly mediated by reduced opening of the MPTP. Calcium loading within the cell and ROS production are central to triggering MPTP opening (Suleiman et al. 2001). Calcium loading and ROS production may be reduced during cardioplegic arrest due to preservation of ATP.

7.5.3 Pre-conditioning with Iso or 8-Br is protective against I/R in combination with cardioplegia

In this work, three drugs targeting the α and β adrenergic pathways or downstream targets were investigated in combination with cardioplegic arrest. Isoprenaline and 8-Br have previously been shown to protect against I/R injury in the absence of cardioplegia, and A61603 is also cardioprotective against I/R injury as shown in the chapter above. The cAMP analogue 8-Br conferred the greatest protection to the heart against I/R injury, with improved recovery of function, reduced LDH release and a reduction in injury sustained in the myocardium. Stimulating the β-ARs prior to ischemia with isoprenaline was also protective against I/R injury, whilst targeting the α1A-ARs using A61603 did not protect the heart when used in combination with cardioplegic arrest.

7.5.4 Inotropic response to adrenergic stimulation

All the drug interventions tested triggered a positive inotropic response in the heart prior to ischemia. With 8-Br, the inotropic response was only initiated with the higher concentration of 10μM. Iso and 8-Br both act through increased cAMP signalling, isoprenaline through the β-ARs and 8-Br directly. cAMP is primarily associated with the downstream target of PKA, which phosphorylates proteins associated with calcium handling and excitation-contraction coupling mediating the positive inotropic response (Figure 1-4A). Activation of Epac is also inotropic, the response to 8-Br is likely to have

involved activation of PKA and Epac (Khaliulin et al. 2017). Epac modulates calcium signalling through downstream activation of PKC (Cazorla et al. 2009; Oestreich et al. 2007). A61603, targeting the α1A-ARs, also initiates an inotropic response through a PKC mediated pathway (Figure 1-4B) (J et al. 2008).

As discussed in Chapter 6, one implication of a positive inotropic response prior to ischemia is the depletion of glycogen stores which is considered a potential contributing factor to cardioprotection. Previous studies have measured glycogen reduction during β-AR pre-conditioning by isoprenaline (Khaliulin et al. 2010). Although glycogen was not measured in this study, based on this previous finding and the inotropic response induced, it is likely both isoprenaline and 8-Br may have reduced glycogen content.

7.5.5 Is there a role for glycogen depletion in cardioprotection following cardioplegic arrest and I/R?

During ischemia anaerobic glycolysis is the primary source of ATP production, however lactate is produced as a by-product creating acidosis within the cell. The consequence of this is intracellular changes leading to calcium loading which is detrimental to the cell (Murphy and Steenbergen 2008a). By having a depleted glycogen level at the beginning of ischemia, less anaerobic glycolysis can occur, subsequently producing less lactate. This will result in less Na+/H+ exchange and the intracellular increase in sodium will be less, in turn leading to less calcium loading within the cell. Reduced capacity for anaerobic glycolysis will result in an earlier reduction in ATP which initiates early ischemic contracture, an observation associated with improved outcomes from I/R injury (Cross et al. 1996). In this work, all pre-conditioning drug treatments that shortened the time to onset of contracture improved at least one marker of cardiac injury on reperfusion. With reduced levels of glycogen available, the production of ATP will decline quicker resulting in an earlier onset of contracture. This was the case in the 8-Br and isoprenaline groups, suggesting the treatment of these drugs may have reduced glycogen content. Although, a shift in the onset of contracture earlier in ischemia was also seen with the lower concentration of 8-Br (5μM) that did not produce any significant increases in LVDP or RPP. Furthermore, A61603 treatment did significantly increase LVDP and RPP prior to ischemia but had no effect on the

profile of ischemic contracture and did not protect the heart in combination with cardioplegia.

Therefore, an increase in cardiac workload, and potential decrease in glycogen, prior to ischemia is clearly not the only contributing factor to early initiation of ischemic contracture or the subsequent afforded protection against I/R injury. Particularly given the differentially findings on ischemic contracture with two doses of A61603 in the previous chapter. Aside from ATP level, contracture may also be modulated by calcium which is central to the formation of actin-myosin complexes. Calcium-free solutions delayed onset of contracture, however this is potentially linked to the preservation of ATP by rapid cardiac arrest (Hearse et al. 1977). It may be possible pre-conditioning strategies interact with calcium signalling altering the profile of contracture.

7.5.6 Signalling pathways involved in pre-conditioning by Iso and 8-Br

The signalling pathways activated by the pre-conditioning interventions play an important contribution to the protection against I/R injury. Both 8-Br and isoprenaline were protective against cardioplegic arrest and reperfusion. The common pathway activated by both interventions is PKA signalling, which has been shown to contribute to cardioprotection (Inserte et al. 2004; Khaliulin et al. 2017). The cAMP analogue 8-Br additionally activates Epac downstream pathways, this combination activating Epac in addition to PKA has shown to provide optimal protection against I/R in a non-cardioplegia model (Khaliulin et al. 2017). Downstream signalling from Epac activates PKC, which is cardioprotective, additionally isoprenaline has been previously shown to increase PKC contributing to the cardioprotective effect. The combination of PKA and PKC activation provides greater protection (Khaliulin et al. 2010; M. Lewis et al. 2018)

7.5.7 Involvement of the MPTP – protection with 8-BR reduces swelling

Mitochondrial swelling reflects opening of the MPTP opening, confirmed by the reduction in swelling in the presence of pore blocker CsA. A key mediator of I/R injury is opening of the MPTP upon reperfusion (Halestrap and Richardson 2015; Ong et al. 2015). As discussed previously, glycogen depletion is associated with reduced opening of the MPTP through reduced dissociation of hexokinase II from the outer mitochondrial membrane (Halestrap et al. 2015). In a study looking at regional ischemia, in which 8-Br conferred protection when given as a pre- or post-conditioning strategy, mitochondrial swelling was measured after 8-Br treatment prior to ischemia and mitochondrial

swelling was reduced with hexokinase II binding increased (Khaliulin et al. 2021). The reduction in mitochondrial swelling in hearts pre-conditioned with 8-Br is also observed upon reperfusion (M. J. Lewis et al. 2022). The findings in this study confirm the reduction in swelling upon reperfusion, indicative of reduced MPTP opening, with 8-B pre-conditioning when used in combination with cardioplegic arrest. Modulation of MPTP opening by pre-conditioning may be the result of changes in conditions which initiate MPTP opening, such as ROS, rather than direct effects on the pore itself.

7.5.8 Pre-conditioning with A61603 was not protective in combination with cardioplegia

Despite promising results of A61603 pre-conditioning being protective in both healthy and failing hearts against I/R injury, in the situation of cardioplegic ischemic arrest and reperfusion this protection was not seen. The cardioprotection of 10nM A61603 was blunted by the use of cardioplegia, the mechanisms involved in cardioplegic arrest may have interacted with the protective signalling of A61603. A61603 specifically targets the α1A-ARs, which have been shown to be present on only 60% of cardiac myocytes whereas the β-ARs targeted by isoprenaline are ubiquitously expressed on all myocytes (Myagmar et al. 2017). This may contribute to the reduced effectiveness of A61603 in comparison to the other cardioprotective drugs. However, only the 10nM concentration of A6103 was tested in combination with cardioplegia, further work is needed to test different concentration.

7.5.9 Summary

This work shows pre-conditioning strategies targeting the β-AR pathways is cardioprotective when used in combination with cardioplegic arrest. Working in combination with cardioplegia is promising for the translatability into a clinical setting where use of cardioplegia is standard practice. Furthermore, by targeting cAMP directly and bypassing the receptors, this may have greater potential in disease settings where receptor desensitisation has occurred. This work has also highlighted the need to investigate the mechanism of these protective strategies further beyond an inotropic response leading to glycogen depletion.

8 Overall summary, limitations and future directions

8.1 Overall Summary

8.1.1 Temporal changes in cardiac remodelling following MI

This work has comprehensively investigated the cardiac remodelling process over time following MI in rat hearts, assessing functional, structural, molecular, and metabolic changes. In doing so, this has added to the understanding of the cardiac remodelling process, which can hopefully help in the development of novel therapeutic strategies. Manipulation of the cardiac remodelling process could help to prevent the decline in cardiac function and progression into heart failure.

The early 3-day time-point appears to be a critical time in the remodelling process. Cardiac function has declined but end systolic and diastolic volumes have not yet increased. Cellular infiltration is ongoing in the infarcted area, with evidence of immune cells still present and increased numbers of fibroblasts, suggesting ongoing immune response alongside ECM deposition. Cardiomyocytes are still evident, with an ongoing apoptotic response and mitochondrial disruption. In addition to the ongoing changes in the infarcted area, during the early stage of remodelling molecular changes were identified in non-infarcted tissue. There was significant upregulation of proteins related to cell death, antioxidants, and ECM components, whereas proteins related to mitochondria, calcium handling and fatty acid metabolism were decreased. Post-translational modification of calcium handling proteins was increased during this period. Downregulation of β-AR signalling was observed early post-MI. At this time-point there were changes identified in circulating metabolites, with increased metabolites relating to anaerobic metabolism and ischemia (lactate, succinate and alanine).

Comparatively to 3-days, at 2-weeks and 4-weeks there are greater structure changes with wall thinning and LV dilation more evident and a further decline in cardiac function. Within the infarct area fibroblasts are present and collagen deposition increases to stabilise the LV wall. Other cell types including telocytes are identified in the infarct area, which are potentially important in the cardiac remodelling process. The remodelling process appears relatively stable from the 2-week time-point, the changes to 4-weeks post-MI are more subtle. Changes in the cardiac proteome and phospho-proteome identified 4-weeks post-MI were reduced compared to the early time-point. At the late stage of remodelling a decline in β-AR function and changes in metabolism

were identified, as well as alterations in structural proteins. Fatty acid β-oxidation was identified as an inhibited pathway, and increased circulating lipids were measured, suggesting changes in substrate utilisation.

8.1.2 The importance of sham surgery groups

Sham surgery groups are utilised within animal studies to determine any effects of the stress of the surgical procedure itself. Sham surgery resulted in changes in the cardiac proteome and phospho-proteome, particularly at the early time-point. Additionally changes in circulating metabolites were identified. The changes observed in sham groups compared to naïve did not translate to impairment in cardiac function as measured through echocardiography. These findings in sham hearts are contradicting to previous work investigating the sham environment following MI in mice which reported no significant changes in sham hearts during the first week post-surgery (Iyer et al. 2016). The discrepancy in these findings may further highlight the need to assess the sham response when establishing an animal model due to differences in technique and protocols between researchers. It may also reflect species differences which is an important consideration.

8.1.3 Cardioprotective efficacy of targeting adrenergic receptors against I/R injury

Cardioprotective strategies that can be applied prior to ischemia offer potential to be used during CPB surgery where the ischemic insult is planned. Patients undergoing heart surgery may have pre-existing pathology, therefore it is important to consider the effectiveness of any cardioprotective strategy in disease settings. During heart failure, it is well established that β-ARs are desensitised, supported in this work by the downregulation of β-AR signalling highlighted in the proteomic analysis. Therefore, cardioprotective strategies that do not require interaction with β-ARs could be preferable. This thesis assessed two approaches to this, targeting the α1-ARs which are reportedly unaffected in failing hearts, or by-passing the β-ARs targeting the second messenger with cAMP analogue 8-Br.

The α1A-AR has been previously shown to have cardioprotective potential in cardiac disease, this work used the specific agonist A61603 as a pre-conditioning strategy against I/R injury. Pre-conditioning with A61603 successfully reduced cardiac injury sustained from I/R in healthy hearts, highlighting A61603 as a promising pre-conditioning strategy. Further work is needed to evaluate the effectiveness of A61603

pre-conditioning in the failing heart model and in combination with cardioplegic arrest, including testing the higher concentration of A61603 in these models.

Pre-conditioning the heart with the cAMP analogue 8-Br had been previously shown to protect against I/R injury, but this had not been tested in combination with use of cardioplegic arrest. This work shows that 8-Br confers additional protection to the heart when using cardioplegia and confirmed previous findings that the MPTP was involved in the mechanism of protection. Testing cardioprotection in combination with cardioplegia is important to develop clinically translatable strategies.

8.2 Limitations

8.2.1 Animal work

One limitation of this work is the use of a chronic ischemic insult, rather than an ischemia reperfusion model which may be considered more clinically relevant. However, timely reperfusion of an ischemic insult is not always possible, and reperfusion after long periods of ischemic does not salvage tissue with irreversible damage induced. Reperfusion of an infarct is associated with greater variations in injury, with less damaged caused. Therefore, there is a benefit to complete chronic occlusion, in that the injury induced is sufficiently large enough to study the remodelling changes (Lindsey et al. 2018).

All work in this thesis has been completed using only male adult rats. Gender variations are an important consideration for translatability. There are known differences in the response to cardiac pathology in male vs female, therefore this is a limitation throughout this study.

8.2.2 Langendorff perfusion

The use of Langendorff ex vivo perfusion is well established but it is not without sources of variation and limitations. The use of organs isolated from animals provides a source of biological variation, however this was controlled to the best of my ability by utilising the same sex and strain of animals sourced from the same company. I found large fluctuations in body weight to have an impact of the extent of I/R injury, therefore it was also important to maintain small weight ranges for animals in each set of experiments. Accurate and timely cannulation of the heart is an important factor for a successful Langendorff experiment, particularly when assessing I/R injury. Any damage to the aortic valve when cannulating can prevent adequate retrograde coronary perfusion, whilst taking too long to cannulate may inadvertently precondition the heart. Due to good technical ability for cannulation this was not a common problem, but poor cannulation due to either factor was a reason for exclusion.

The Langendorff setup used was a constant flow setup, rather than constant pressure. The use of constant flow prevents any autoregulation mechanisms to adjust coronary flow, the flow rate is not adjusted in response to changes in cardiac workload or in the presence of ischemic tissue which may have compromised vasculature (Bell et al. 2011). The Langendorff setup does not provide any filling pressure to simulate

preload or afterload triggering external work from the hearts, this can only be achieved by use of a working heart perfusion model.

8.2.3 Functional analysis

There was variability in echocardiography measurements in some animals due to the presence of the stitches and muscle closure interfering, this made obtaining clear echocardiography recordings more difficult in the early time-points. Only M-mode recordings were made for the majority of animals, preventing extra analysis including strain analysis being completed.

8.2.4 Tissue sampling to study remodelling

The sample collection protocol used in this study allowed multiple analysis to be completed for each heart, utilising the tissue in the most efficient way. Tissue for proteomics, histology and EM analysis was collected from each heart. The limitation to this protocol is that defined sections were taken for each analysis, preventing comparisons from different regions which may create bias. Cross-sectional areas were taken for histology and EM to try and account for this, allowing infarcted and non-infarcted areas to be evaluated. The limitations this had on proteomic analysis is discussed below (8.2.6.1).

8.2.5 Structural analysis

One limitation to the electron microscopy work is the need for relaxed myocardium to make accurate observations. Morphology of mitochondria, and other cardiac structures, are sometimes distorted in contracted tissue which could be mistaken for damage.

8.2.6 Proteomics

8.2.6.1 Tissue sampling

The use of tissue from the apex of the hearts for proteomic analysis does not allow for comparison of changes in the left and right side of the heart. Studies have shown differentially effects in the LV and RV of cardiac diseases such as MI, by taking apical tissue this could not be done. Given the sample collection protocol used in this study, taking LV and RV biopsies for proteomics would have compromised the tissue samples for histological and EM analysis. Taking tissue from the apex, without infarct tissue being included, gives an understanding into the changes within the border zone.

However, it does not reflect the changes in the infarct area, for example the changes in collagen proteins and other ECM components present in the scar tissue. For example, this may be why no differences in collagen content were observed at 4-weeks post-MI between sham and LAD occlusion groups, which would be expected if infarct tissue was sampled.

Hearts terminated at the 3-day time-point were cannulated on a modified perfusion setup so tissue collection could be completed within the animal facility. Due to some technical issues, the clearance of blood from these tissue samples was not as complete as in the later time-points. This meant there was several proteins associated with blood that were identified in the 3-day time-point. Blood proteins did not appear in greater number in the 3-day LAD/3-day Sham comparison suggesting it was an equal effect in the sham and LAD hearts and these proteins were not adjusted in the LAD group. However, it was a confounding factor when looking at the 3-day Sham to naïve comparison, several of the proteins identified as DEPs may have been blood proteins inflating the overall number of significant DEPs.

8.2.6.2 Proteomics analysis and validation

One limitation to the proteomic analysis is the need to provide cut-offs for FDR and inclusion criteria such as proteins only identified in every sample of each group in a given comparison. This will mean that not every protein in the cardiac proteome is analysed in this work. However, it provides more confidence in the proteins that are identified and included in the analysis. Another limitation is the lack of validation of proteins identified by proteomic analysis. This can be achieved by Western Blot analysis but was not completed for any proteins identified in this study. Previous work within the research group has shown strong correlation between western blotting for selected proteins and the proteomic results giving some confidence in the validity of the proteomic analysis ((Littlejohns et al. 2014) and recent unpublished work by Dr Skeffington).

8.2.7 Metabolomics

An unbiased approach to metabolomics allows the detection of all metabolites in a sample, however one of the major challenges is metabolite identification (McGarrah et al. 2018). The metabolites discussed in this thesis are metabolites that are well characterised and could be identified through previous reports. Identification of peaks

with a high level of confidence was limited by the availability of software for comprehensive analysis. To definitively confirm the identification of any of the metabolites of interest spiking experiments would be required.

Identification of circulating biomarkers that can be correlated to the extent of injury would be ideal, to provide further information on the severity of disease. Correlations between metabolite levels and either function or infarct size were limited in this study due to small sample sizes. Additionally, as this was a surgical induction of MI the injury extent was relatively similar between animals and did not provide a great range of injury levels. In the human setting the variation in injury would be a lot greater. The n numbers used in this study were relatively small, particularly for the earlier time-points and naïve groups. This may explain why some metabolites with a fold change between groups did not reach the significance level of <0.05.

8.2.8 Ischemia reperfusion experiments

One limitation to this work is the use of young, healthy animals which do not express the co-morbidities often present in people undergoing CPB surgery. Presence of pathology can impact the effectiveness of cardioprotective strategies, therefore future studies testing these interventions in diseased heart models would be interesting. Particularly in the case of 8-Br, which doesn't require activation of the receptors, future work to assess this strategy in failing hearts which may have receptor desensitisation would be important.

In addition, the use of warm cardioplegia does not fully represent the clinical situation as cold-cardioplegic solution is also used. Giving cold solutions on the Langendorff setup is technically harder to manage and maintain throughout ischemia, it would also require greater time for ischemia due to the protection afford by hypothermia.

Another limitation is the lack of measurements of glycogen depletion following the inotropic stimulation in these hearts, given the potential link to the potential protective mechanism. Given the findings in the previous chapter also, the measurement of glycogen would help to understand the contribution of this factor to the early onset of ischemic contracture and the differential effect observed.

8.3 Future work

8.3.1 Assessment of functional and structural changes post-MI

To add to the functional analysis in future additional echo views could be recorded to provide greater information, including measurements such as the E/A ratio to assess diastolic function. Further analysis could be performed using the Vevolab software such as strain analysis with additional recordings in B-mode.

To further the investigation into structural changes at different time-points post-MI, future work could involve more specific histological assessment. Further staining could be completed to identify the cellular types present in the areas of infiltration early after MI, specific collagen subtypes, components of the ECM of interest. As well as to assess presence of fibroblasts and telocytes, to determine if the number is increased in the infarcted area in comparison to healthy myocardium. To further the EM work looking at ultrastructure, quantitative analysis of mitochondrial morphology should be completed. Investigation of structural changes in the RV was not completed in this thesis and could be assessed in future work.

8.3.2 Proteomics

Analysis of the proteomic/phospho-proteomic data is ongoing given the vast number of proteins identified that were significantly differentially expressed. Following completion of this, future work would be to validate any identified proteins of interest using Western blot analysis. Further to this, the role of any protein of interest in the remodelling process could be explored further, with potential development of interventions to target the protein or signalling pathway. The ideal way to test any intervention strategy would be within the MI model, assessing any improvement in function, reduction in extent of injury or attenuation of adverse remodelling.

8.3.3 Metabolomics

Future work regarding metabolomic assessment is needed to identify the remaining peaks that I have not yet been able to identify. Further to this, spiking experiments could be performed to conclusively identify metabolites. Future work could involve performing metabolomic analysis on cardiac tissue samples from corresponding time-points to identify if the circulating metabolites are correlated to metabolite changes in the heart itself.

8.3.4 Ischemia reperfusion injury experiments

All the cardioprotective strategies triggered an inotropic response in the heart prior to ischemia, therefore measuring glycogen depletion following intervention would be interesting. This could help understand any involvement of glycogen depletion in the mechanism of protection and help understand the differential responses of ischemic contracture following different inotropic interventions.

ARs are also present on the vasculature in the heart and as an isolated heart setup was used in these experiments, further work may look to investigate the effects in isolated myocytes to differentiate from the vascular influence in protection.

Regarding the A61603 cardioprotection work, further work should be focussed on understanding the mechanism of action, this could include assessing mitochondrial swelling and any involvement of the MPTP. A61603 did protect the heart when given prior to cardioplegic arrest, albeit the n number was small, which may warrant further investigation. Future work could test the higher concentration of A61603 in combination with cardioplegia to confirm. Future work regarding 8-Br which had positive results in combination with cardioplegia could involve testing with cold cardioplegia, or more clinically relevant cardioplegia protocols. Additionally, testing this strategy in a large animal model of CPB surgery.

9 References

Abdul-Ghani, S., et al. (2022), 'Effect of cardioplegic arrest and reperfusion on left and right ventricular proteome/phosphoproteome in patients undergoing surgery for coronary or aortic valve disease', *International Journal of Molecular Medicine,* 49 (6).

Ahmed, M. S., et al. (2003), 'Induction of myocardial biglycan in heart failure in rats - an extracellular matrix component targeted by AT(1) receptor antagonism', *Cardiovascular Research,* 60 (3), 557-68.

Aladag, N., et al. (2021), 'Oxidants and antioxidants in myocardial infarction (MI): Investigation of ischemia modified albumin, malondialdehyde, superoxide dismutase and catalase in individuals diagnosed with ST elevated myocardial infarction (STEMI) and non-STEMI (NSTEMI)', *J Med Biochem,* 40 (3), 286-94.

Alex, L. and Frangogiannis, N. G. (2018), 'The Cellular Origin of Activated Fibroblasts in the Infarcted and Remodeling Myocardium', *Circ Res,* 122 (4), 540-42.

--- (2019), 'Pericytes in the infarcted heart', *Vasc Biol,* 1 (1), H23-H31.

Andersson, D. C. and Marks, A. R. (2010), 'Fixing ryanodine receptor Ca leak - a novel therapeutic strategy for contractile failure in heart and skeletal muscle', *Drug Discov Today Dis Mech,* 7 (2), e151-e57.

Asimakis, G. K., et al. (1994), 'Transient Beta-Adrenergic Stimulation Can Precondition the Rat-Heart against Postischemic Contractile Dysfunction', *Cardiovascular Research,* 28 (11), 1726-34.

Bai, H., et al. (2020), 'Proteomic and metabolomic characterization of cardiac tissue in acute myocardial ischemia injury rats', *PLoS One,* 15 (5), e0231797.

Baines, C. P. (2009), 'The mitochondrial permeability transition pore and ischemia-reperfusion injury', *Basic Res Cardiol,* 104 (2), 181-8.

Baudino, T. A., et al. (2006), 'Cardiac fibroblasts: friend or foe?', *Am J Physiol Heart Circ Physiol,* 291 (3), H1015-26.

Bell, R. M., Mocanu, M. M., and Yellon, D. M. (2011), 'Retrograde heart perfusion: the Langendorff technique of isolated heart perfusion', *J Mol Cell Cardiol,* 50 (6), 940-50.

Bereczki, E. and Santha, M. (2008), 'The role of biglycan in the heart', *Connective Tissue Research,* 49 (3-4), 129-32.

Bereczki, E., et al. (2007), 'Overexpression of biglycan in the heart of transgenic mice: An antibody microarray study', *Journal of Proteome Research,* 6 (2), 854-61.

Bers, D. M. (2002), 'Cardiac excitation-contraction coupling', *Nature,* 415 (6868), 198-205.

--- (2007), 'Going to cAMP just got more complicated', *J Physiol,* 583 (Pt 2), 415-6.

BHF (2022), 'UK Factsheet'.

Bond, A. R., et al. (2019), 'The cardiac proteome in patients with congenital ventricular septal defect: A comparative study between right atria and right ventricles', *J Proteomics,* 191, 107-13.

Bristow, M. R., et al. (1986), 'Beta 1- and beta 2-adrenergic-receptor subpopulations in nonfailing and failing human ventricular myocardium: coupling of both receptor subtypes to muscle contraction and selective beta 1-receptor down-regulation in heart failure', *Circ Res,* 59 (3), 297-309.

Burchfield, J. S., Xie, M., and Hill, J. A. (2013), 'Pathological ventricular remodeling: mechanisms: part 1 of 2', *Circulation,* 128 (4), 388-400.

Cahill, T. J. and Kharbanda, R. K. (2017), 'Heart failure after myocardial infarction in the era of primary percutaneous coronary intervention: Mechanisms, incidence and identification of patients at risk', *World J Cardiol,* 9 (5), 407-15.

Cazorla, O., et al. (2009), 'The cAMP binding protein Epac regulates cardiac myofilament function', *Proc Natl Acad Sci U S A,* 106 (33), 14144-9.

Chambers, D. J. and Fallouh, H. B. (2010), 'Cardioplegia and cardiac surgery: pharmacological arrest and cardioprotection during global ischemia and reperfusion', *Pharmacol Ther,* 127 (1), 41-52.

Chandrashekhar, Y., et al. (2004), 'Long-term caspase inhibition ameliorates apoptosis, reduces myocardial troponin-I cleavage, protects left ventricular function, and attenuates remodeling in rats with myocardial infarction', *J Am Coll Cardiol,* 43 (2), 295-301.

Chen, C., et al. (2016), 'Integrins and integrin-related proteins in cardiac fibrosis', *J Mol Cell Cardiol,* 93, 162-74.

Chen, L., et al. (2009), 'Mitochondrial OPA1, apoptosis, and heart failure', *Cardiovasc Res,* 84 (1), 91-9.

Chen, Y. R. and Zweier, J. L. (2014), 'Cardiac Mitochondria and Reactive Oxygen Species Generation', *Circulation Research,* 114 (3), 524-37.

Chew, D. S., et al. (2018), 'Change in Left Ventricular Ejection Fraction Following First Myocardial Infarction and Outcome', *JACC Clin Electrophysiol,* 4 (5), 672-82.

Chouchani, E. T., et al. (2014), 'Ischaemic accumulation of succinate controls reperfusion injury through mitochondrial ROS', *Nature,* 515 (7527), 431-35.

Cieniewski-Bernard, C., et al. (2008), 'Proteomic analysis of left ventricular remodeling in an experimental model of heart failure', *J Proteome Res,* 7 (11), 5004-16.

Clarke, S. J., et al. (2008), 'Inhibition of mitochondrial permeability transition pore opening by ischemic preconditioning is probably mediated by reduction of oxidative stress rather than mitochondrial protein phosphorylation', *Circulation Research,* 102 (9), 1082-90.

Cleutjens, J. P., et al. (1995), 'Collagen remodeling after myocardial infarction in the rat heart', *Am J Pathol,* 147 (2), 325-38.

Cohn, J. N., Ferrari, R., and Sharpe, N. (2000), 'Cardiac remodeling--concepts and clinical implications: a consensus paper from an international forum on cardiac remodeling. Behalf of an International Forum on Cardiac Remodeling', *J Am Coll Cardiol,* 35 (3), 569-82.

Crompton, M., Ellinger, H., and Costi, A. (1988), 'Inhibition by cyclosporin A of a Ca2+-dependent pore in heart mitochondria activated by inorganic phosphate and oxidative stress', *Biochem J,* 255 (1), 357-60.

Cross, H. R., et al. (1996), 'Is a high glycogen content beneficial or detrimental to the ischemic rat heart? A controversy resolved', *Circ Res,* 78 (3), 482-91.

Dahl, E. F., et al. (2019), 'ERK mediated survival signaling is dependent on the Gq-G-protein coupled receptor type and subcellular localization in adult cardiac myocytes', *J Mol Cell Cardiol,* 127, 67-73.

Darbandi Azar, A., et al. (2014), 'Echocardiographic evaluation of cardiac function in ischemic rats: value of m-mode echocardiography', *Res Cardiovasc Med,* 3 (4), e22941.

de Lucia, C., Eguchi, A., and Koch, W. J. (2018), 'New Insights in Cardiac beta-Adrenergic Signaling During Heart Failure and Aging', *Front Pharmacol,* 9, 904.

de Rooij, J., et al. (1998), 'Epac is a Rap1 guanine-nucleotide-exchange factor directly activated by cyclic AMP', *Nature,* 396 (6710), 474-7.

DeLeon-Pennell, K. Y., et al. (2017), 'Matrix Metalloproteinases in Myocardial Infarction and Heart Failure', *Prog Mol Biol Transl Sci,* 147, 75-100.

Dobaczewski, M., Gonzalez-Quesada, C., and Frangogiannis, N. G. (2010), 'The extracellular matrix as a modulator of the inflammatory and reparative response following myocardial infarction', *J Mol Cell Cardiol,* 48 (3), 504-11.

Dobson, G. P., et al. (2013), 'Hyperkalemic cardioplegia for adult and pediatric surgery: end of an era?', *Front Physiol,* 4, 228.

Doenst, T., Nguyen, T. D., and Abel, E. D. (2013), 'Cardiac metabolism in heart failure: implications beyond ATP production', *Circ Res,* 113 (6), 709-24.

Dridi, H., et al. (2020), 'Intracellular calcium leak in heart failure and atrial fibrillation: a unifying mechanism and therapeutic target', *Nat Rev Cardiol,* 17 (11), 732-47.

Du, X. J., et al. (2006), 'Transgenic alpha1A-adrenergic activation limits post-infarct ventricular remodeling and dysfunction and improves survival', *Cardiovasc Res,* 71 (4), 735-43.

Esmaeili, R., et al. (2017), 'Echocardiographic assessment of myocardial infarction: comparison of a rat model in two strains', *Iran J Vet Res,* 18 (1), 30-35.

Estigoy, C. B., et al. (2009), 'Intercalated discs: multiple proteins perform multiple functions in non-failing and failing human hearts', *Biophys Rev,* 1 (1), 43.

Faussone Pellegrini, M. S. and Popescu, L. M. (2011), 'Telocytes', *Biomol Concepts,* 2 (6), 481-9.

Ferdinandy, P., Schulz, R., and Baxter, G. F. (2007), 'Interaction of cardiovascular risk factors with myocardial ischemia/reperfusion injury, preconditioning, and postconditioning', *Pharmacol Rev,* 59 (4), 418-58.

Fishbein, M. C., Maclean, D., and Maroko, P. R. (1978), 'Experimental myocardial infarction in the rat: qualitative and quantitative changes during pathologic evolution', *Am J Pathol,* 90 (1), 57-70.

Fowler, M. B., et al. (1986), 'Assessment of the beta-adrenergic receptor pathway in the intact failing human heart: progressive receptor down-regulation and subsensitivity to agonist response', *Circulation,* 74 (6), 1290-302.

Fraccarollo, D., Galuppo, P., and Bauersachs, J. (2012), 'Novel therapeutic approaches to post-infarction remodelling', *Cardiovasc Res,* 94 (2), 293-303.

Frangogiannis, N. G. (2017), 'The extracellular matrix in myocardial injury, repair, and remodeling', *J Clin Invest,* 127 (5), 1600-12.

Gaemperli, O., et al. (2010), 'Myocardial beta-adrenoceptor down-regulation early after infarction is associated with long-term incidence of congestive heart failure', *Eur Heart J,* 31 (14), 1722-9.

Gomez-Mendoza, D. P., Lara-Ribeiro, A. C., and Verano-Braga, T. (2021), 'Pathological cardiac remodeling seen by the eyes of proteomics', *Biochim Biophys Acta Proteins Proteom,* 1869 (6), 140622.

Griffiths, E. J. and Halestrap, A. P. (1993), 'Protection by Cyclosporin A of ischemia/reperfusion-induced damage in isolated rat hearts', *J Mol Cell Cardiol,* 25 (12), 1461-9.

--- (1995), 'Mitochondrial non-specific pores remain closed during cardiac ischaemia, but open upon reperfusion', *Biochem J,* 307 (Pt 1), 93-8.

Guo, Y., et al. (2017), 'Proteomics of acute heart failure in a rat post-myocardial infarction model', *Mol Med Rep,* 16 (2), 1946-56.

Halestrap, A. P. (2009), 'What is the mitochondrial permeability transition pore?', *J Mol Cell Cardiol,* 46 (6), 821-31.

Halestrap, A. P. and Richardson, A. P. (2015), 'The mitochondrial permeability transition: a current perspective on its identity and role in ischaemia/reperfusion injury', *J Mol Cell Cardiol,* 78, 129-41.

Halestrap, A. P., Pereira, G. C., and Pasdois, P. (2015), 'The role of hexokinase in cardioprotection - mechanism and potential for translation', *Br J Pharmacol,* 172 (8), 2085-100.

Hara, A., et al. (2020), 'Galectin-3: A Potential Prognostic and Diagnostic Marker for Heart Disease and Detection of Early Stage Pathology', *Biomolecules,* 10 (9).

Hashmi, S. and Al-Salam, S. (2015), 'Galectin-3 is expressed in the myocardium very early post-myocardial infarction', *Cardiovascular Pathology,* 24 (4), 213-23.

Hausenloy, D. J., Boston-Griffiths, E. A., and Yellon, D. M. (2012), 'Cyclosporin A and cardioprotection: from investigative tool to therapeutic agent', *Br J Pharmacol,* 165 (5), 1235-45.

Hausenloy, D. J., et al. (2005), 'Ischemic preconditioning protects by activating prosurvival kinases at reperfusion', *Am J Physiol Heart Circ Physiol,* 288 (2), H971-6.

Hearse, D. J., Stewart, D. A., and Chain, E. B. (1974), 'Recovery from cardiac bypass and elective cardiac arrest. The metabolic consequences of various cardioplegic procedures in the isolated rat heart', *Circ Res,* 35 (3), 448-57.

Hearse, D. J., Garlick, P. B., and Humphrey, S. M. (1977), 'Ischemic contracture of the myocardium: mechanisms and prevention', *Am J Cardiol,* 39 (7), 986-93.

Henderson, C. A., et al. (2017), 'Overview of the Muscle Cytoskeleton', *Compr Physiol,* 7 (3), 891-944.

Hollander, J. M., Thapa, D., and Shepherd, D. L. (2014), 'Physiological and structural differences in spatially distinct subpopulations of cardiac mitochondria: influence of cardiac pathologies', *Am J Physiol Heart Circ Physiol,* 307 (1), H1-14.

Hostiuc, S., et al. (2018), 'Cardiac telocytes. From basic science to cardiac diseases. II. Acute myocardial infarction', *Ann Anat,* 218, 18-27.

Huang, Y., et al. (2007), 'An alpha1A-adrenergic-extracellular signal-regulated kinase survival signaling pathway in cardiac myocytes', *Circulation,* 115 (6), 763-72.

Inserte, J., et al. (2004), 'Ischemic preconditioning attenuates calpain-mediated degradation of structural proteins through a protein kinase A-dependent mechanism', *Cardiovascular Research,* 64 (1), 105-14.

Isobe, K., et al. (2010), 'Inhibition of endostatin/collagen XVIII deteriorates left ventricular remodeling and heart failure in rat myocardial infarction model', *Circ J,* 74 (1), 109-19.

Iyer, R. P., et al. (2016), 'Defining the sham environment for post-myocardial infarction studies in mice', *Am J Physiol Heart Circ Physiol,* 311 (3), H822-36.

J, O. Uchi, et al. (2008), 'Interaction of alpha1-adrenoceptor subtypes with different G proteins induces opposite effects on cardiac L-type Ca2+ channel', *Circ Res,* 102 (11), 1378-88.

Janssen, P. M. L., et al. (2018), 'Human Myocardium Has a Robust alpha1A-Subtype Adrenergic Receptor Inotropic Response', *J Cardiovasc Pharmacol,* 72 (3), 136-42.

Javadov, S. A., et al. (2003), 'Ischaemic preconditioning inhibits opening of mitochondrial permeability transition pores in the reperfused rat heart', *J Physiol,* 549 (Pt 2), 513-24.

Jenca, D., et al. (2021), 'Heart failure after myocardial infarction: incidence and predictors', *ESC Heart Fail,* 8 (1), 222-37.

Jennings, R. B. and Reimer, K. A. (1991), 'The cell biology of acute myocardial ischemia', *Annu Rev Med,* 42, 225-46.

Jensen, B. C., O'Connell, T. D., and Simpson, P. C. (2014), 'Alpha-1-adrenergic receptors in heart failure: the adaptive arm of the cardiac response to chronic catecholamine stimulation', *J Cardiovasc Pharmacol,* 63 (4), 291-301.

Kamato, D., et al. (2015), 'Structure, Function, Pharmacology, and Therapeutic Potential of the G Protein, Galpha/q,11', *Front Cardiovasc Med,* 2, 14.

Khaliulin, I., Parker, J. E., and Halestrap, A. P. (2010), 'Consecutive pharmacological activation of PKA and PKC mimics the potent cardioprotection of temperature preconditioning', *Cardiovasc Res,* 88 (2), 324-33.

Khaliulin, I., et al. (2021), 'Preconditioning or Postconditioning with 8-Br-cAMP-AM Protects the Heart against Regional Ischemia and Reperfusion: A Role for Mitochondrial Permeability Transition', *Cells,* 10 (5).

Khaliulin, I., et al. (2007), 'Temperature preconditioning of isolated rat hearts--a potent cardioprotective mechanism involving a reduction in oxidative stress and inhibition of the mitochondrial permeability transition pore', *J Physiol,* 581 (Pt 3), 1147-61.

Khaliulin, I., et al. (2014), 'Clinically-relevant consecutive treatment with isoproterenol and adenosine protects the failing heart against ischaemia and reperfusion', *J Transl Med,* 12, 139.

Khaliulin, I., et al. (2017), 'Functional and cardioprotective effects of simultaneous and individual activation of protein kinase A and Epac', *Br J Pharmacol,* 174 (6), 438-53.

Kielty, C. M., Sherratt, M. J., and Shuttleworth, C. A. (2002), 'Elastic fibres', *J Cell Sci,* 115 (Pt 14), 2817-28.

Kim, M. A., et al. (2010), 'Effects of ACE2 inhibition in the post-myocardial infarction heart', *J Card Fail,* 16 (9), 777-85.

Kimura, T., et al. (2019), 'Tenascin-C accelerates adverse ventricular remodelling after myocardial infarction by modulating macrophage polarization', *Cardiovascular Research,* 115 (3), 614-24.

Knepper, S. M., et al. (1995), 'A-61603, a potent alpha 1-adrenergic receptor agonist, selective for the alpha 1A receptor subtype', *J Pharmacol Exp Ther,* 274 (1), 97-103.

Knowlton, A. A., et al. (1992), 'Rapid Expression of Fibronectin in the Rabbit Heart after Myocardial-Infarction with and without Reperfusion', *Journal of Clinical Investigation,* 89 (4), 1060-68.

Kohlhauer, M., et al. (2018), 'Metabolomic Profiling in Acute ST-Segment-Elevation Myocardial Infarction Identifies Succinate as an Early Marker of Human Ischemia-Reperfusion Injury', *J Am Heart Assoc,* 7 (8).

Kolocassides, K. G., Galinanes, M., and Hearse, D. J. (1996a), 'Dichotomy of ischemic preconditioning: improved postischemic contractile function despite intensification of ischemic contracture', *Circulation,* 93 (9), 1725-33.

Kolocassides, K. G., et al. (1996b), 'Paradoxical effect of ischemic preconditioning on ischemic contracture? NMR studies of energy metabolism and intracellular pH in the rat heart', *J Mol Cell Cardiol,* 28 (5), 1045-57.

Kolodziej, A. R., et al. (2019), 'Prognostic Role of Elevated Myeloperoxidase in Patients with Acute Coronary Syndrome: A Systemic Review and Meta-Analysis', *Mediators Inflamm,* 2019, 2872607.

Konstandin, M. H., et al. (2013), 'Fibronectin Is Essential for Reparative Cardiac Progenitor Cell Response After Myocardial Infarction', *Circulation Research,* 113 (2), 115-25.

Kostin, S. (2016), 'Cardiac telocytes in normal and diseased hearts', *Semin Cell Dev Biol,* 55, 22-30.

Kostin, S., et al. (2003), 'Gap junction remodeling and altered connexin43 expression in the failing human heart', *Mol Cell Biochem,* 242 (1-2), 135-44.

Kovacs, H. A., et al. (2021), 'Characterization of the Proprotein Convertase-Mediated Processing of Peroxidasin and Peroxidasin-like Protein', *Antioxidants (Basel),* 10 (10).
Lal, A., et al. (2005), 'Prevention of cardiac remodeling after myocardial infarction in transgenic rats deficient in brain angiotensinogen', *J Mol Cell Cardiol,* 39 (3), 521-9.
Lazzeri, C., et al. (2015), 'Clinical significance of lactate in acute cardiac patients', *World J Cardiol,* 7 (8), 483-9.
Levick, J.R. (2010), *An introduction to Cardiovascular Physiology* (Fifth edn.).
Lewis, M., et al. (2018), 'Consecutive Isoproterenol and Adenosine Treatment Confers Marked Protection against Reperfusion Injury in Adult but Not in Immature Heart: A Role for Glycogen', *Int J Mol Sci,* 19 (2).
Lewis, M. J., et al. (2022), 'Cardioprotection of Immature Heart by Simultaneous Activation of PKA and Epac: A Role for the Mitochondrial Permeability Transition Pore', *Int J Mol Sci,* 23 (3).
Lezoualc'h, F., et al. (2016), 'Cyclic AMP Sensor EPAC Proteins and Their Role in Cardiovascular Function and Disease', *Circ Res,* 118 (5), 881-97.
Li, M., et al. (2023), 'Development and prevention of ischemic contracture ("stone heart") in the pig heart', *Front Cardiovasc Med,* 10, 1105257.
Li, R., et al. (2019a), 'Time Series Characteristics of Serum Branched-Chain Amino Acids for Early Diagnosis of Chronic Heart Failure', *J Proteome Res,* 18 (5), 2121-28.
Li, Y. F., et al. (2019b), 'The whole transcriptome and proteome changes in the early stage of myocardial infarction', *Cell Death Discovery,* 5.
Lindsey, M. L. and Zamilpa, R. (2012), 'Temporal and spatial expression of matrix metalloproteinases and tissue inhibitors of metalloproteinases following myocardial infarction', *Cardiovasc Ther,* 30 (1), 31-41.
Lindsey, M. L., et al. (2018), 'Guidelines for experimental models of myocardial ischemia and infarction', *Am J Physiol Heart Circ Physiol,* 314 (4), H812-H38.
Lips, D. J., et al. (2004), 'MEK1-ERK2 signaling pathway protects myocardium from ischemic injury in vivo', *Circulation,* 109 (16), 1938-41.
Littlejohns, B., et al. (2014), 'The effect of disease on human cardiac protein expression profiles in paired samples from right and left ventricles', *Clin Proteomics,* 11 (1), 34.
Liu, T. T., et al. (2014), 'Mitochondrial proteome remodeling in ischemic heart failure', *Life Sciences,* 101 (1-2), 27-36.
Lochner, A., et al. (1999), 'Ischemic preconditioning and the beta-adrenergic signal transduction pathway', *Circulation,* 100 (9), 958-66.
Lohse, M. J., Engelhardt, S., and Eschenhagen, T. (2003), 'What is the role of beta-adrenergic signaling in heart failure?', *Circ Res,* 93 (10), 896-906.
Lopaschuk, G. D., et al. (2010), 'Myocardial fatty acid metabolism in health and disease', *Physiol Rev,* 90 (1), 207-58.
Lopaschuk, G. D., et al. (2021), 'Cardiac Energy Metabolism in Heart Failure', *Circulation Research,* 128 (10), 1487-513.
Luo, D. L., et al. (2007), 'Receptor subtype involved in alpha 1-adrenergic receptor-mediated Ca2+ signaling in cardiomyocytes', *Acta Pharmacol Sin,* 28 (7), 968-74.
Luther, D. J., et al. (2012), 'Absence of type VI collagen paradoxically improves cardiac function, structure, and remodeling after myocardial infarction', *Circ Res,* 110 (6), 851-6.
Mahmood, A., Ahmed, K., and Zhang, Y. (2022), 'beta-Adrenergic Receptor Desensitization/Down-Regulation in Heart Failure: A Friend or Foe?', *Front Cardiovasc Med,* 9, 925692.

Manole, C. G., et al. (2011), 'Experimental acute myocardial infarction: telocytes involvement in neo-angiogenesis', *J Cell Mol Med,* 15 (11), 2284-96.

Matsumura, K., et al. (2000), 'Protein kinase C is involved in cardioprotective effects of ischemic preconditioning on infarct size and ventricular arrhythmia in rats in vivo', *Mol Cell Biochem,* 214 (1-2), 39-45.

Matsumura, S., et al. (2005), 'Targeted deletion or pharmacological inhibition of MMP-2 prevents cardiac rupture after myocardial infarction in mice', *J Clin Invest,* 115 (3), 599-609.

Matsushita, T., et al. (1999), 'Remodeling of cell-cell and cell-extracellular matrix interactions at the border zone of rat myocardial infarcts', *Circ Res,* 85 (11), 1046-55.

McCudden, C. R., et al. (2005), 'G-protein signaling: back to the future', *Cell Mol Life Sci,* 62 (5), 551-77.

McGarrah, R. W., et al. (2018), 'Cardiovascular Metabolomics', *Circ Res,* 122 (9), 1238-58.

McIlwain, D. R., Berger, T., and Mak, T. W. (2013), 'Caspase functions in cell death and disease', *Cold Spring Harb Perspect Biol,* 5 (4), a008656.

McKirnan, M. D., et al. (2019), 'Metabolomic analysis of serum and myocardium in compensated heart failure after myocardial infarction', *Life Sci,* 221, 212-23.

Meagher, P. B., et al. (2021), 'Cardiac Fibrosis: Key Role of Integrins in Cardiac Homeostasis and Remodeling', *Cells,* 10 (4).

Mizuno, T., et al. (2005), 'Elastin stabilizes an infarct and preserves ventricular function', *Circulation,* 112 (9 Suppl), I81-8.

Mocanu, M. M., Baxter, G. F., and Yellon, D. M. (2000), 'Caspase inhibition and limitation of myocardial infarct size: protection against lethal reperfusion injury', *Br J Pharmacol,* 130 (2), 197-200.

Montgomery, M. D., et al. (2017), 'An Alpha-1A Adrenergic Receptor Agonist Prevents Acute Doxorubicin Cardiomyopathy in Male Mice', *PLoS One,* 12 (1), e0168409.

Muller, O. J., et al. (2019), 'Comprehensive plasma and tissue profiling reveals systemic metabolic alterations in cardiac hypertrophy and failure', *Cardiovasc Res,* 115 (8), 1296-305.

Murphy, E. and Steenbergen, C. (2008a), 'Mechanisms underlying acute protection from cardiac ischemia-reperfusion injury', *Physiol Rev,* 88 (2), 581-609.

--- (2008b), 'Ion transport and energetics during cell death and protection', *Physiology (Bethesda),* 23, 115-23.

Murry, C. E., Jennings, R. B., and Reimer, K. A. (1986), 'Preconditioning with ischemia: a delay of lethal cell injury in ischemic myocardium', *Circulation,* 74 (5), 1124-36.

Myagmar, B. E., et al. (2019), 'Coupling to Gq Signaling Is Required for Cardioprotection by an Alpha-1A-Adrenergic Receptor Agonist', *Circulation Research,* 125 (7), 699-706.

Myagmar, B. E., et al. (2017), 'Adrenergic Receptors in Individual Ventricular Myocytes: The Beta-1 and Alpha-1B Are in All Cells, the Alpha-1A Is in a Subpopulation, and the Beta-2 and Beta-3 Are Mostly Absent', *Circ Res,* 120 (7), 1103-15.

Nasa, Y., Yabe, K., and Takeo, S. (1997), 'Beta-adrenoceptor stimulation-mediated preconditioning-like cardioprotection in perfused rat hearts', *J Cardiovasc Pharmacol,* 29 (4), 436-43.

Neubauer, S. (2007), 'The failing heart--an engine out of fuel', *N Engl J Med,* 356 (11), 1140-51.

Nielsen, S. H., et al. (2019), 'Understanding cardiac extracellular matrix remodeling to develop biomarkers of myocardial infarction outcomes', *Matrix Biol,* 75-76, 43-57.

Njegic, A., Wilson, C., and Cartwright, E. J. (2020), 'Targeting Ca(2 +) Handling Proteins for the Treatment of Heart Failure and Arrhythmias', *Front Physiol,* 11, 1068.

O'Reilly, J., Lindsey, M. L., and Baugh, J. A. (2018), 'Physiological proteomics of heart failure', *Current Opinion in Physiology,* 1, 185-97.

Oestreich, E. A., et al. (2007), 'Epac-mediated activation of phospholipase C(epsilon) plays a critical role in beta-adrenergic receptor-dependent enhancement of Ca2+ mobilization in cardiac myocytes', *J Biol Chem,* 282 (8), 5488-95.

Omran, M. M., et al. (2018), 'Role of myeloperoxidase in early diagnosis of acute myocardial infarction in patients admitted with chest pain', *J Immunoassay Immunochem,* 39 (3), 337-47.

Ong, S. B., et al. (2015), 'The mitochondrial permeability transition pore and its role in myocardial ischemia reperfusion injury', *J Mol Cell Cardiol,* 78, 23-34.

Palm, D. C., Rohwer, J. M., and Hofmeyr, J. H. (2013), 'Regulation of glycogen synthase from mammalian skeletal muscle--a unifying view of allosteric and covalent regulation', *FEBS J,* 280 (1), 2-27.

Park, I. H., et al. (2021), 'Clinical Significance of Serum Lactate in Acute Myocardial Infarction: A Cardiac Magnetic Resonance Imaging Study', *J Clin Med,* 10 (22).

Patel, M. S. and Korotchkina, L. G. (2001), 'Regulation of mammalian pyruvate dehydrogenase complex by phosphorylation: complexity of multiple phosphorylation sites and kinases', *Exp Mol Med,* 33 (4), 191-7.

Pendergrass, K. D., et al. (2011), 'Temporal effects of catalase overexpression on healing after myocardial infarction', *Circ Heart Fail,* 4 (1), 98-106.

Perez, D. M. (2021), 'Current Developments on the Role of alpha(1)-Adrenergic Receptors in Cognition, Cardioprotection, and Metabolism', *Front Cell Dev Biol,* 9, 652152.

Peterson, J. T., et al. (2000), 'Evolution of matrix metalloprotease and tissue inhibitor expression during heart failure progression in the infarcted rat', *Cardiovasc Res,* 46 (2), 307-15.

Popescu, L. M. and Faussone-Pellegrini, M. S. (2010), 'TELOCYTES - a case of serendipity: the winding way from Interstitial Cells of Cajal (ICC), via Interstitial Cajal-Like Cells (ICLC) to TELOCYTES', *J Cell Mol Med,* 14 (4), 729-40.

Porter, K. E. and Turner, N. A. (2009), 'Cardiac fibroblasts: at the heart of myocardial remodeling', *Pharmacol Ther,* 123 (2), 255-78.

Pouralijan Amiri, M., et al. (2019), 'Metabolomics in early detection and prognosis of acute coronary syndrome', *Clin Chim Acta,* 495, 43-53.

Prabhu, S. D. and Frangogiannis, N. G. (2016), 'The Biological Basis for Cardiac Repair After Myocardial Infarction: From Inflammation to Fibrosis', *Circ Res,* 119 (1), 91-112.

Psychogios, N., et al. (2011), 'The human serum metabolome', *PLoS One,* 6 (2), e16957.

Ramachandra, C. J. A., et al. (2020), 'Myeloperoxidase As a Multifaceted Target for Cardiovascular Protection', *Antioxid Redox Signal,* 32 (15), 1135-49.

Remondino, A., et al. (2000), 'Altered expression of proteins of metabolic regulation during remodeling of the left ventricle after myocardial infarction', *J Mol Cell Cardiol,* 32 (11), 2025-34.

Richardson, W. J., et al. (2015), 'Physiological Implications of Myocardial Scar Structure', *Compr Physiol,* 5 (4), 1877-909.

Richter, M. and Kostin, S. (2015), 'The failing human heart is characterized by decreased numbers of telocytes as result of apoptosis and altered extracellular matrix composition', *Journal of Cellular and Molecular Medicine,* 19 (11), 2597-606.

Rodriguez, P., Jackson, W. A., and Colyer, J. (2004), 'Critical evaluation of cardiac Ca2+-ATPase phosphorylation on serine 38 using a phosphorylation site-specific antibody', *J Biol Chem,* 279 (17), 17111-9.

Rorabaugh, B. R., et al. (2005), 'alpha1A- but not alpha1B-adrenergic receptors precondition the ischemic heart by a staurosporine-sensitive, chelerythrine-insensitive mechanism', *Cardiovasc Res,* 65 (2), 436-45.

Salie, R., Lochner, A., and Loubser, D. J. (2017), 'The significance of the washout period in preconditioning', *Cardiovasc Ther,* 35 (3).

Sanada, S., Komuro, I., and Kitakaze, M. (2011), 'Pathophysiology of myocardial reperfusion injury: preconditioning, postconditioning, and translational aspects of protective measures', *Am J Physiol Heart Circ Physiol,* 301 (5), H1723-41.

Santos-Ribeiro, D., et al. (2018), 'The integrated stress response system in cardiovascular disease', *Drug Discov Today,* 23 (4), 920-29.

Shamhart, P. E. and Meszaros, J. G. (2010), 'Non-fibrillar collagens: key mediators of post-infarction cardiac remodeling?', *J Mol Cell Cardiol,* 48 (3), 530-7.

Skeffington, K. L., et al. (2020), 'Changes in inflammation and oxidative stress signalling pathways in coarcted aorta triggered by bicuspid aortic valve and growth in young children', *Exp Ther Med,* 20 (5), 48.

Soininen, P., et al. (2009), 'High-throughput serum NMR metabonomics for cost-effective holistic studies on systemic metabolism', *Analyst,* 134 (9), 1781-5.

Sowton, A. P., Griffin, J. L., and Murray, A. J. (2019), 'Metabolic Profiling of the Diabetic Heart: Toward a Richer Picture', *Front Physiol,* 10, 639.

Steenbergen, C., et al. (1990), 'Correlation between cytosolic free calcium, contracture, ATP, and irreversible ischemic injury in perfused rat heart', *Circ Res,* 66 (1), 135-46.

Stenemo, M., et al. (2019), 'The metabolites urobilin and sphingomyelin (30:1) are associated with incident heart failure in the general population', *ESC Heart Fail,* 6 (4), 764-73.

Stepanov, A. V., Baidyuk, E. V., and Sakuta, G. A. (2017), 'The features of mitochondria of cardiomyocytes from rats with chronic heart failure', *Cell and Tissue Biology,* 11 (6), 458-65.

Sugiyama, A., et al. (2018), 'Endostatin Stimulates Proliferation and Migration of Myofibroblasts Isolated from Myocardial Infarction Model Rats', *Int J Mol Sci,* 19 (3).

Suleiman, M. S., Halestrap, A. P., and Griffiths, E. J. (2001), 'Mitochondria: a target for myocardial protection', *Pharmacol Ther,* 89 (1), 29-46.

Suleiman, M. S., et al. (2011), 'Cardioplegic strategies to protect the hypertrophic heart during cardiac surgery', *Perfusion,* 26 Suppl 1, 48-56.

Suleiman, M. S., et al. (1998), 'Metabolic differences between hearts of patients with aortic valve disease and hearts of patients with ischaemic disease', *J Mol Cell Cardiol,* 30 (11), 2519-23.

Sun, Y. and Weber, K. T. (1996), 'Angiotensin converting enzyme and myofibroblasts during tissue repair in the rat heart', *J Mol Cell Cardiol,* 28 (5), 851-8.

Surendran, A., Aliani, M., and Ravandi, A. (2019), 'Metabolomic characterization of myocardial ischemia-reperfusion injury in ST-segment elevation myocardial infarction patients undergoing percutaneous coronary intervention', *Sci Rep,* 9 (1), 11742.

Sutton, M. G. and Sharpe, N. (2000), 'Left ventricular remodeling after myocardial infarction: pathophysiology and therapy', *Circulation,* 101 (25), 2981-8.

Takagawa, J., et al. (2007), 'Myocardial infarct size measurement in the mouse chronic infarction model: comparison of area- and length-based approaches', *J Appl Physiol (1985),* 102 (6), 2104-11.

Tong, H., et al. (2005), 'The role of beta-adrenergic receptor signaling in cardioprotection', *FASEB J,* 19 (8), 983-5.

Tougaard, R. S., et al. (2022), 'Remodeling after myocardial infarction and effects of heart failure treatment investigated by hyperpolarized [1-(13) C]pyruvate magnetic resonance spectroscopy', *Magn Reson Med,* 87 (1), 57-69.

Wang, J., et al. (2013), 'Metabolomic identification of diagnostic plasma biomarkers in humans with chronic heart failure', *Mol Biosyst,* 9 (11), 2618-26.

Wang, X., et al. (2017), 'Metabolic Characterization of Myocardial Infarction Using GC-MS-Based Tissue Metabolomics', *Int Heart J,* 58 (3), 441-46.

Wei, S., et al. (1999), 'Left and right ventricular collagen type I/III ratios and remodeling post-myocardial infarction', *J Card Fail,* 5 (2), 117-26.

Werner, Christina, Doenst, Torsten, and Schwarzer, Michael (2016), 'Chapter 4 - Metabolic Pathways and Cycles', in Michael Schwarzer and Torsten Doenst (eds.), *The Scientist's Guide to Cardiac Metabolism* (Boston: Academic Press), 39-55.

White, H. D., et al. (1987), 'Left ventricular end-systolic volume as the major determinant of survival after recovery from myocardial infarction', *Circulation,* 76 (1), 44-51.

Willems, I. E. M. G., Arends, J. W., and Daemen, M. J. A. P. (1996), 'Tenascin and fibronectin expression in healing human myocardial scars', *Journal of Pathology,* 179 (3), 321-25.

Wu, Y., et al. (2011), 'Acute myocardial infarction in rats', *J Vis Exp,* (48).

Yamanishi, A., et al. (1998), 'Sequential changes in the localization of the type IV collagen alpha chain in the infarct zone: immunohistochemical study of experimental myocardial infarction in the rat', *Pathol Res Pract,* 194 (6), 413-22.

Yang, F., et al. (2002), 'Myocardial infarction and cardiac remodelling in mice', *Exp Physiol,* 87 (5), 547-55.

Yang, L., et al. (2017), 'Quantitative Proteomics and Immunohistochemistry Reveal Insights into Cellular and Molecular Processes in the Infarct Border Zone One Month after Myocardial Infarction', *J Proteome Res,* 16 (5), 2101-12.

Yarbrough, W. M., et al. (2010), 'Caspase inhibition modulates left ventricular remodeling following myocardial infarction through cellular and extracellular mechanisms', *J Cardiovasc Pharmacol,* 55 (4), 408-16.

Yokota, T., et al. (2020), 'Type V Collagen in Scar Tissue Regulates the Size of Scar after Heart Injury', *Cell,* 182 (3), 545-62 e23.

Ytrehus, K., Liu, Y., and Downey, J. M. (1994), 'Preconditioning protects ischemic rabbit heart by protein kinase C activation', *Am J Physiol,* 266 (3 Pt 2), H1145-52.

Zacchigna, S., et al. (2021), 'Towards standardization of echocardiography for the evaluation of left ventricular function in adult rodents: a position paper of the ESC Working Group on Myocardial Function', *Cardiovasc Res,* 117 (1), 43-59.

Zhang, J., Simpson, P. C., and Jensen, B. C. (2021), 'Cardiac alpha1A-adrenergic receptors: emerging protective roles in cardiovascular diseases', *Am J Physiol Heart Circ Physiol,* 320 (2), H725-H33.

Zhao, B., et al. (2013), 'Cardiac telocytes were decreased during myocardial infarction and their therapeutic effects for ischaemic heart in rat', *J Cell Mol Med,* 17 (1), 123-33.

Zhao, X., et al. (2015), 'Overexpression of Cardiomyocyte alpha1A-Adrenergic Receptors Attenuates Postinfarct Remodeling by Inducing Angiogenesis Through Heterocellular Signaling', *Arterioscler Thromb Vasc Biol,* 35 (11), 2451-9.

Zhou, J., et al. (2019), 'Comprehensive metabolomic and proteomic analyses reveal candidate biomarkers and related metabolic networks in atrial fibrillation', *Metabolomics,* 15 (7), 96.

Zhu, M. R., et al. (2019), 'The value of serum metabolomics analysis in predicting the response to cardiac resynchronization therapy', *J Geriatr Cardiol,* 16 (7), 529-39.

Zuurbier, C. J., et al. (2020), 'Cardiac metabolism as a driver and therapeutic target of myocardial infarction', *J Cell Mol Med,* 24 (11), 5937-54.

10 Appendix

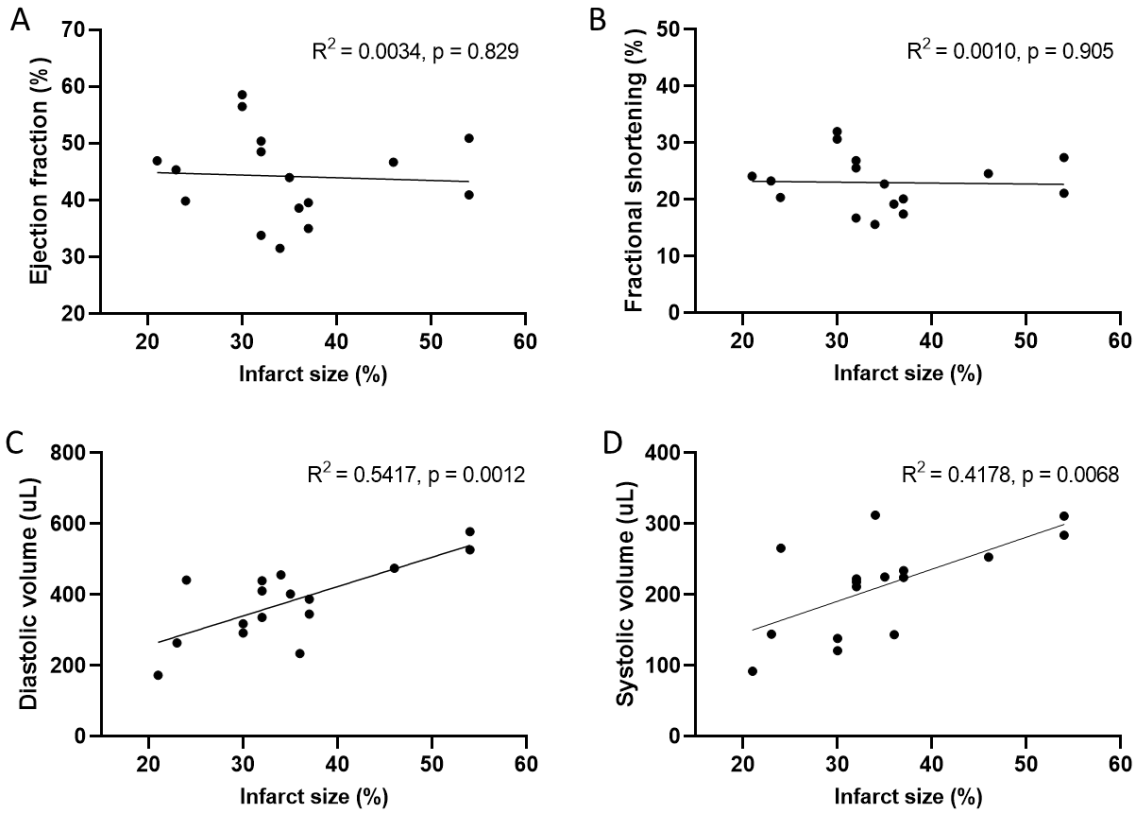

Figure 10-1 Relationship between echocardiography parameters and infarct size

Ejection fraction (A), fractional shortening (B), diastolic volume (C) and systolic volume (D) measured by echocardiography 4-weeks post-MI, against the infarct size measured from TTC staining in hearts on the I/R protocol (n=16). Analysed by linear regression, R^2 and p-value for each displayed.